Étude de la résistance de Plasmodium falciparum et des phénotypes de dormance induite par l'artémisinine : du patient à la cellule

Lucien Platon

Thèse de Doctorat
Étude de la résistance de *Plasmodium falciparum* et des phénotypes de dormance induite par l'artémisinine : du patient à la cellule.

Par Lucien Platon

Thèse réalisée en vue de l'obtention du grade universitaire de Docteur en microbiologie et immunologie.

Directeur de thèse : Didier Ménard

Affiliations :

- École doctorale ED515 CDV «Complexité du Vivant»; Sorbonne Université ; 15-21 rue de l'École de Médecine, 75006 Paris.
- Département « Parasites and Insect vectors » ; Unité « Malaria Genetic and Resistances » ; Institut Pasteur ; INSERM U1201 ; 25-28 rue du Dr Roux ; 75724 Paris Cedex 15.

Thèse soutenue le 29 mars 2023.

Devant les jurys :

Sandrine Houzé – Présidente du Jury et Rapporteur
Didier Leroy – Rapporteur
Didier Ménard – Directeur de thèse

Olivier Silvie – Examinateur et représentant de Sorbonne Université
Carlo Severini – Examinateur
David Fidock – Examinateur
Odile Puijalon – Examinateur
Pascal Millet – Examinateur

À la mémoire de Christophe Platon
(1963 - 2013)

À ta mémoire, papa, je te dédie cette thèse.

Sommaire

Remerciements

Pour toutes les personnes qui ont été impliquées, qui m'ont soutenus, qui ont rendu cette thèse possible.

Je souhaiterais exprimer mes plus sincères remerciements à Didier Ménard. Tu m'as accordé ta confiance, tu m'as permis de cheminer intellectuellement pendant ces trois ans, me permettant d'avoir une vraie démarche de chercheur. Merci pour tout.

J'aimerais témoigner mes remerciements à l'ensemble de mes collaborateurs locaux et internationaux. Particulièrement les personnel des plateformes CBUtech, ICAREB, BIOMICS et le Hub bio-informatique de l'Institut Pasteur dont les services et l'expertise ont été indispensables à la conduite de mes travaux. Je tiens à remercier plus particulièrement Stéphan Fischer et Laurence Ma pour leur investissement et le précieux soutien bio-informatique fourni.

Je remercie chaleureusement Jun Cao du *Jiangsu Institute of Parasitic Disease* et toute son équipe pour les collaborations menées durant cette thèse.

Merci à Olivier Silvie, Rémy Durand et Mohamed-Ali Hakimi pour avoir accepté d'intégrer mon comité de suivi, vos conseils et remarques m'ont été d'une aide précieuse.

Merci l'ensemble des membres du jury pour avoir accepté de prendre de votre temps pour juger de ce travail de thèse.

Je remercie chaleureusement les équipes BIHP et BAP de l'Institut Pasteur, avec qui j'ai pu avoir de nombreuses interactions, déterminantes dans ma formation de chercheur.

Je remercie Éric Legrand pour les nombreuses discussions et sa participation à ma formation durant la thèse.

Une petite dédicace à mon estimé camarade Alexandre Francq, dont la pédanterie n'a d'égale que ses connaissances en philosophie. Nos nombreuses discussions m'ont permis d'avoir un recul critique sur la pratique des sciences et de la construction de nos savoirs. Il me tarde de te voir aller en thèse à ton tour !

Il m'est impossible de ne pas remercier ma moitié. Mon cher Vincent, c'est ton soutien qui m'aura permis de tenir dans les moments les plus difficiles.

À ma mère et ma grand-mère, je souhaite exprimer mes plus chaleureux remerciements, votre soutien indefectible aura lui aussi été indispensable.

À tous mes amis, de l'Ile de France ou de Montpellier, impossible de ne pas vous témoigner un minimum de gratitude quant à votre soutien et votre présence. Merci de me supporter comme vous le faites.

À toi Mylène, immenses merci pour tous ces bons moments hors du temps passés (et à venir), plus puissant que n'importe quel anxiolytique.

Je souhaite remercier l'administration de l'école doctorale CDV "Complexité Du vivant". Vous avez été un fil rouge important, distillant efficacement toutes les informations durant les moments critiques de la thèse, comme les inscriptions, les rapports d'activités et la soutenance.

Je remercie également les assistantes administratives avec qui j'ai pu travailler durant ma thèse, à savoir Carina Tomasso Deverge, Anne Cozanet, Maryse Brandt et Gladys Elisabeth. Votre réactivité et votre efficacité m'ont permis de franchir les épreuves administratives de la thèse comme les réinscriptions et autre demande de remboursement. Vous êtes la preuve que l'administration française, **des fois**, ça marche.

Je souhaite remercier le professeur David Baker, de la *London School of Hygiene and Tropical Medicine* pour sa participation à mon travail et son aide technique précieuse, avec l'envoi du réactif ML10 qui m'a permis de faire de grandes économies de temps.

Je remercie Alexandra Elbakyan et lui témoigne mon soutien inflexible. Créatrice de Sci-Hub, c'est grâce à elle et à son outil de diffusion gratuite des connaissances scientifique que cette thèse a été rendue possible.

Je remercie le restaurant de l'Institut Pasteur et son personnel. Mention spéciale pour la crème brûlée du vendredi (qui serait selon des études sérieuses, la raison principale de pourquoi les chercheurs souhaitent obtenir un CDI à Pasteur).

J'aimerais également manifester ma sympathie pour les salariés de la RATP et SNCF n'ayant PAS fait grève et qui ont continués d'assurer leur mission de service public malgré les pressions syndicales. Ce travail de thèse vous est en partie due, car sans vous, je n'aurais pas pu aller bien loin (littéralement).

À tous ceux qui ont continué de travailler pendant les confinements, caissier, personnel médical, etc...Vous avez mon respect éternel.

Enfin, je remercie chaleureusement le COVID-19 ainsi que Olivier Véran, dont l'action conjointe m'aura permis d'obtenir 6 mois de plus pour conduire et terminer la thèse de façon sereine.

Non-Remerciements

Parce que la thèse c'est aussi des difficultés, qu'il convient d'honorer comme il se doit.

Pour toi, *Plasmodium falciparum*, tu m'auras plombé mes nuits, tu t'es accaparé toutes mes pensées, t'immisçant jusqu'à devenir une quasi-obsession. Et pourtant, tu auras aussi été source de joie et d'excitation (intellectuelle) durant cette thèse.

Pour tous les grévistes de la RATP et SNCF... Vos blocages fin 2019 m'ont privé de 2 mois de travail. Certaines de vos revendications sont justes, mais de vouloir préserver vos privilèges au détriment de la qualité de vie du prolétaire rendrait ce cher Marx très fier de vous (Sarcasme*).

J'adresse mes sincères non-remerciements aux RH de proximité de Sorbonne Université pour leur extrême lenteur et le manque de communication que j'ai subi durant ces trois ans.

À l'administration en général, et surtout aux managers en charge de structurer le système, vous m'avez coûté un temps considérable, des mois de perdus en paperasse futile pour expédier des échantillons importants pour ma thèse. Des procédures sont encore en cours au moment où ces lignes sont écrites, et à cause de vous, des données cruciales ne seront pas présentes dans ce manuscrit.

Je ne remercie pas la présidente de la région Ile-de-France. Le Navigo à 84€, je m'en serais bien passé.

Aux décisionnaires ayant annoncé les confinements / déconfinements / reconfinements... Vos actions ont eu des répercussions lourdes sur le déroulé de mes travaux (et de l'Institut Pasteur en général) que l'on peut encore ressentir dans ce manuscrit, notamment certains travaux expérimentaux n'ayant pu être finalisés en temps et en heure à cause des pénuries de matériel ou de reports de formations.

Cher Lecteur, cher Lectrice, il ne me reste qu'à vous souhaiter une bonne lecture (et bon courage).

Lexique et abréviation

- **ADN :** *(molécule)* Acide Désoxyribonucléique.
- **ARN :** *(molécule)* Acide ribonucléique.
- **ATP :** *(molécule)* Adénosine triphosphate.
- **DHA :** *(molécule)* Dihydroartémisnine.
- **DHFR :** *(protéine)* Dihydrofolate reductase.
- **DHPS :** *(protéine)* Dihydropteroate synthetase.
- **DID :** Dormance induite par les drogues.
- **DMSO :** *(molécule)* Diméthylsulfoxide.
- **Drogue :** *(anglosaxon)* Petite molécule thérapeutique.
- **EXP1 :** *(protéine)* Exported protein 1.
- **GTP :** *(molécule)* Guanosine triphosphate.
- **HRP2/3 :** *(protéine)* Histidin-rich protein 2 / 3.
- **H2O2 :** *(molécule)* Peroxyde d'hydrogène.
- **kDa :** *(unité de mesure)* KiloDalton.
- **NADH :** *(molécule)* Nicotinamide adénine dinucléotide.
- **OMS :** Organisation mondiale de la santé.
- ***Pfcrt* :** *(gène) Plasmodium falciparum Chloroquine Resistance Transporter.*
- ***Pfkelch13* :** *(gène) Plasmodium falciparum Kelch-13.*
- ***Pfmdr1* :** *(gène) Plasmodium falciparum Multidrugs Resistance.*
- ***qPCR :*** *(technique) Quantitative Polymerase Chain Reaction.*
- **RPMI :** Roswell Park Memorial Institute Medium.
- **RSA :** *(technique)* Ring-Stage Survival Assay.
- **SCS :** Surnageant de Culture Stressée.
- **TCA :** Thérapies combinées à l'Artémisinine.
- **TLR :** *(protéine)* Toll-like receptor.
- **UMI :** Unique Molecular Identifier.
- **WT :** Wild-Type.

Résumé

Plasmodium falciparum est l'agent pathogène responsable des formes les plus graves de paludisme. *P. falciparum* a été responsable de 619 0000 décès et 247 millions de cas de paludisme dans le monde en 2022. Le parasite possède un cycle de vie complexe qui se déroule chez les moustiques du genre *Anopheles* et les hôtes humains. L'artémisinine et ses dérivés, associés à des médicaments partenaires, constituent les thérapies combinées à base d'artémisinine (TCA) et sont les traitements les plus efficaces actuellement disponibles. Malheureusement, depuis plus de 15 ans, des souches de *P. falciparum* originaire d'Asie du Sud-est présentent une résistance partielle à l'artémisinine et menacent les efforts de lutte contre le paludisme. Cette résistance partielle a pu être associée à la présence de mutations au sein du gène *Pfkelch13* mais également à un retard de croissance (dormance) induit par l'artémisinine, permettant à une partie des parasites de survivre à la drogue. Cette thèse a pour objectif de mieux comprendre les mécanismes sous-jacents à la résistance à l'artémisinine. Elle s'articule autour de trois axes incluant la compréhension de l'épidémiologie de la résistance en Afrique, l'amélioration des outils permettant de détecter la résistance et l'étude des mécanismes moléculaires et cellulaires.

La première partie décrit l'émergence en Erythrée d'un double mutant *Pfkelch13* résistant à l'artémisinine grâce à la mutation R622I mais indétectable par les tests de diagnostic rapide car dépourvu des gènes *Pfhrp2* et *Pfhrp3*. Ces données s'inscrivent dans un récent contexte d'émergence de la résistance de *P. falciparum* à l'artémisinine à travers le continent africain et soulignent l'urgence de mettre en place de nouvelles stratégies de contrôle.

Dans la seconde partie de ce travail, une version optimisée du Ring-Stage Survival Assay, un outil de diagnostic clé pour détecter les souches de *P. falciparum* résistantes à l'artémisinine, a été développée. Cette optimisation du test permet la synchronisation simultanée de plusieurs souches de *P. falciparum* avec des profils de croissance *in vitro* différents, permettant de réaliser en parallèle de manière fiable et reproductible, des tests RSA sur plusieurs souches.

La troisième partie s'est concentrée sur l'étude de la dormance induite par l'artémisinine en tant que mécanisme de résistance. Nous avons pu mettre en évidence des changements importants dans le métabolisme des stades rings dormants, basés sur le catabolisme des acides aminés.

De plus, nous avons pu faire la lumière sur l'inductibilité de la dormance, chez les parasites au stade ring, par des signaux de stress extracellulaires libérés lors de la mort de parasites matures.

Enfin, des données préliminaires d'analyse transcriptomique à l'échelle de l'individu a révélé l'existence d'une étonnante diversité parmi les stades rings synchrones et issus d'une souche clonale. Finalement, l'ensemble des données présentées ici suggèrent que la dormance est un mécanisme constitutif chez le stade ring de *P. falciparum*, dépendant de l'exposition à des signaux extracellulaire de nature et concentration inconnue, indépendant du génotype *Pfkelch13*. Nous sommes convaincus que ces travaux peuvent servir de base au développement de nouvelle stratégie thérapeutique, basée sur la perturbation des communications extracellulaires du parasite, l'inhibition de l'entrée en dormance et le maintien du parasite dans un état de susceptibilité à l'artémisinine.

Abstract

Plasmodium falciparum is the causative agent of the most severe form of malaria. In 2022, the disease was responsible for 619,000 deaths and 247 million cases worldwide. *P. falciparum* has a complex life cycle in the mosquito vector and in the human host. Artemisinin and its derivatives are used in combination with partner drugs. Artemisinin-based combination therapies (ACT) are currently the most effective treatment available. Unfortunately, efforts to control malaria are threatened by mutations in the *Pfkelch13* gene of *P. falciparum*, which confer partial resistance to artemisinin. This resistance to artemisinin is also associated with a drug-induced dormancy phenotype, which allows a proportion of parasites to survive exposure to the drug.

This thesis focuses on artemisinin resistance and drug-induced dormancy through a multidisciplinary approach. It combines public health, technical optimisation and basic research.

As part of the public health work, we have detected the emergence of a new double mutant *Pfkelch13-R622I* resistant to artemisinin in patients in Eritrea. This mutant is associated with deletions in the *Pfhrp2* and *Pfhrp3* genes, reducing the performances of HRP2-based rapid diagnostic tests. These data highlight the urgency of developing new control strategies in the context of the emergence of artemisinin resistance across the African continent.

An optimised version of the Ring-Stage Survival Assay, the main diagnostic tool used to detect artemisinin-resistant *P. falciparum* parasites, was developed. This optimisation allows the simultaneous synchronisation of several *P. falciparum* strains with different genetic backgrounds, thus enabling multiple RSA tests to be performed in parallel in a reliable and reproducible manner.

Finally, basic research focused on studying drug-induced dormancy as a mechanism of artemisinin resistance. We were able to demonstrate important changes in the metabolism of dormant ring stage parasites based on amino acid catabolism. We have also shown that dormancy can be induced by extracellular stress signals released by dying mature stage parasites. Finally, our data indicate that the synchronous early ring stage of a clonal parasite population exhibits high transcriptional diversity. All the data presented suggest that dormancy is a constitutive mechanism at *P. falciparum* ring stage, mediated by extracellular signals of an unknown nature and concentration, independent of *Pfkelch13* genotypes. We are convinced this work may provide a basis for developing a new therapeutic strategy based on interfering with the parasite's extracellular communications.

Partie I

Synthèse bibliographique et introduction générale

1) Le paludisme: généralités et vue d'ensemble

A) Biologie et cycle du parasite.

Plasmodium falciparum est un micro-organisme eucaryote unicellulaire appartenant à l'embranchement des *Apicomplexes*, découvert en 1880 par Alphonse Laveran (Laveran, 1880). C'est un parasite intracellulaire obligatoire de 1 à 20 µm, agent étiologique du paludisme et transmis par les moustiques du genre Anopheles. *P. falciparum* possède un génome haploïde constitué de 23 mégabases réparties en 14 chromosomes pour un total de 5 300 gènes dont la majorité ont une fonction inconnue ou putative (Gardner *et al.*, 2002). Le parasite possède un cycle de vie complexe (figure 1) se déroulant successivement dans le vecteur puis dans l'hôte humain ; respectivement dans le foie et la circulation sanguine.

Durant le repas sanguin, le moustique injecte par sa salive des sporozoïtes dans la circulation sanguine de l'hôte (Rosenberg *et al.*, 1990). Ces sporozoïtes migrent jusque dans le foie, où ils envahissent les hépatocytes. Le parasite s'y développe en trophozoïte puis en schizonte, et relâche des mérozoïtes dans la circulation sanguine après multiplication asexuée et lyse de l'hépatocyte infecté (Mazier *et al.*, 1985). Les mérozoïtes envahissent les érythrocytes, débutant le cycle sanguin (Mazier *et al.*, 1985). Le parasite passe par plusieurs étapes de développement intraérythrocytaires, avec en premier lieu le stade ring durant les 20 premières heures. Durant le stade ring, le parasite aménage le globule rouge par la mise en place de plusieurs structures caractéristiques telles que les Knobs ou les structures de Maurer (Trager *et al.*, 1966 ; Raventos-Suarez *et al.*, 1985), permettant respectivement la cytoadhésion à l'endothelium vasculaire et l'échange de protéines entre le milieu extracellulaire, le cytoplasme du globule rouge et la vacuole du parasite (Raventos-Suarez *et al.*, 1985 : Lanzer *et al.*, 2005). Le ring mature en stade trophozoïte, durant lequel la digestion de l'hémoglobine est la plus intense (Moore *et al.*, 2006). La digestion de l'hémoglobine dans la vacuole digestive du parasite libère de l'hème, cofacteur ferreux hautement toxique sous sa forme soluble (Rosenthal et Meshnick, 1996). L'hème est neutralisé par cristallisation en hémozoïne inerte, visible par microscopie sous la forme d'un pigment brunâtre dans le cytoplasme du parasite (Pagola *et al.*, 2000). La multiplication de la quantité d'ADN marque le début du stade schizonte, durant lequel de nouveaux mérozoïtes sont produits puis relâchés dans la circulation sanguine par éclatement du globule rouge infecté. L'ensemble des étapes allant de l'invasion jusqu'à l'éclatement du globule rouge dure en moyenne 48h (Trager et Jensen, 1976). Une partie des rings peuvent se différencier en cellules sexués mâle (♂) et femelle (♀), nommés gamétocytes (Bruce *et al.*, 1990). Le prélèvement des gamétocytes par le moustique débute la partie du cycle se déroulant dans le vecteur. La fusion des gamétocytes mâle (♂) et femelle (♀) produit un zygote au niveau du tube

digestif du moustique, maturant en ookinète puis en oocyste (Beier, 1998). L'oocyste mature dans les glandes salivaires et se différencie en sporozoïte, prêt à être injecté dans le flux sanguin de l'hôte au prochain repas du moustique, terminant ainsi le cycle de *P. falciparum*.

P. falciparum est donc un micro-organisme particulièrement complexe à appréhender, de par ses nombreuses étapes de croissance, changements morphologiques et transcriptionnels spécifiques à chaque stade (Kappe *et al.*, 2001 ; Young *et al.*, 2005 ; Smith *et al.*, 2020). L'ensemble de la lutte contre le paludisme consiste donc à interrompre le cycle du parasite en ciblant les différentes étapes de développement, comme nous allons le voir dans la section suivante.

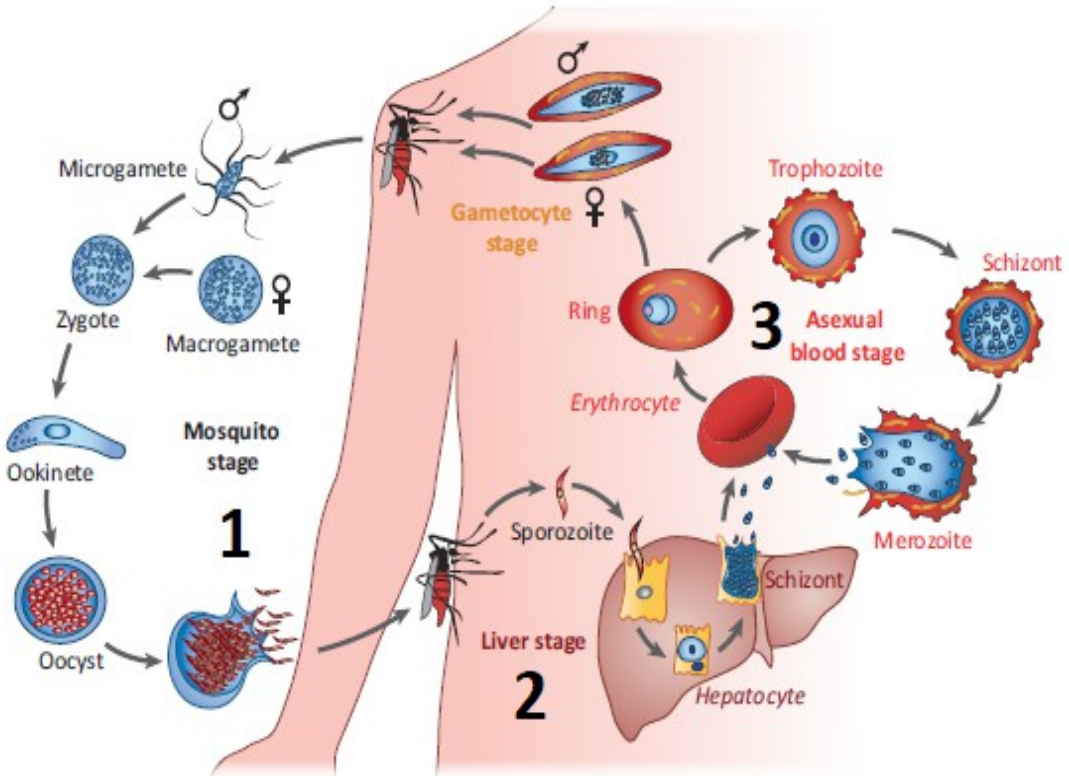

Figure 1 : Cycle de vie de *P. falciparum*

1) Cycle sexué (hôte: vecteur *Anopheles*), les gamétocytes (♂ et ♀) sont prélevés durant le repas sanguin puis fécondent dans le tube digestif du moustique. Les sporozoïtes matures migrent dans les glandes salivaires du vecteur.

2) Transmission des sporozoïtes par la salive du vecteur durant le repas sanguin, début du cycle hépatique (hôte: humain)

3) Invasion des érythrocytes par les mérozoïtes issus de la multiplication hépatique du parasite. Les parasites se multiplient de manière asexuée ou peuvent se différencier en gamétocytes mâles et femelles.

Référence : figure adaptée de Maier *et al.*, 2018

B) Aspect clinique du paludisme : distribution, pathologie et traitements

Distribution

P. falciparum est distribué dans la majorité de l'hémisphère Sud de la planète (rapport de l'OMS 2022 ; figure 2). Le parasite est présent en Afrique, en Asie du Sud-Est ainsi qu'en Amérique du Sud. D'autres espèces de *Plasmodium* d'intérêt clinique telles que *P. vivax*, *P. ovale*, *P. malariae* et *P. knowlesi* partagent également son aire de répartition (données OMS). Les espèces d'anophèles vectrices pouvant varier d'une région du monde à l'autre (Sinka *et al.*, 2012). Cette grande diversité de vecteur ainsi que leur large distribution géographique exposent la moitié de la population globale au paludisme et est l'objet d'une lutte anti-vectorielle intense (Rapport de l'OMS 2022). La majorité des cas (95%) de paludisme à *P. falciparum* se retrouvent sur le continent africain, notamment en Afrique subsaharienne (Rapport de l'OMS 2022) avec pour principal vecteur *Anopheles gambiae* (Sinka *et al.*, 2012 ; Malaria Atlas Project). On dénombre 247 millions de cas et 619 000 morts du paludisme pour l'année 2021, en augmentation par rapport aux années précédentes (Rapport de l'OMS 2022). *P. falciparum* a néanmoins été éliminé avec succès dans plusieurs pays, comme la Chine, l'Iran, la Turquie, le Salvador et la Malaisie, où aucun cas de paludisme n'a été détecté depuis 2019 (Rapport de l'OMS 2022). La diffusion du parasite dépend d'une multitude de facteurs biotiques, abiotiques et sociaux. Le premier facteur est la présence du vecteur, dépendante de la densité en hôtes humain à proximité et de l'accès à l'eau comme site de ponte. En effet, la présence des anophèles et la transmission du paludisme diminuent durant la saison sèche dans les pays sous climat tropical (Coulibaly *et al.*, 2013). Un autre paramètre jouant sur la présence du vecteur est la température, étroitement impliquée dans le développement larvaire du moustique (Christiansen-Jucht *et al.*, 2014). Les principaux paramètres sociaux sont la stabilité géopolitique et les fonds disponibles, jouant directement sur l'accès aux soins, au diagnostic, c'est-à-dire la qualité générale de la prise en charge des patients (Rapport de l'OMS 2022). La distribution de *P. falciparum* reste donc majoritairement médiée depuis le XXe siècle par des facteurs tels que la lutte anti-vectorielle, la qualité du diagnostic, des soins (impliquant la découverte de nouvelles molécules thérapeutiques) et de la prise en charge des patients, la stabilité géopolitique des pays impaludés et dans une moindre mesure, des facteurs climatiques (Rapport OMS 2022 ; Gething *et al.*, 2010).

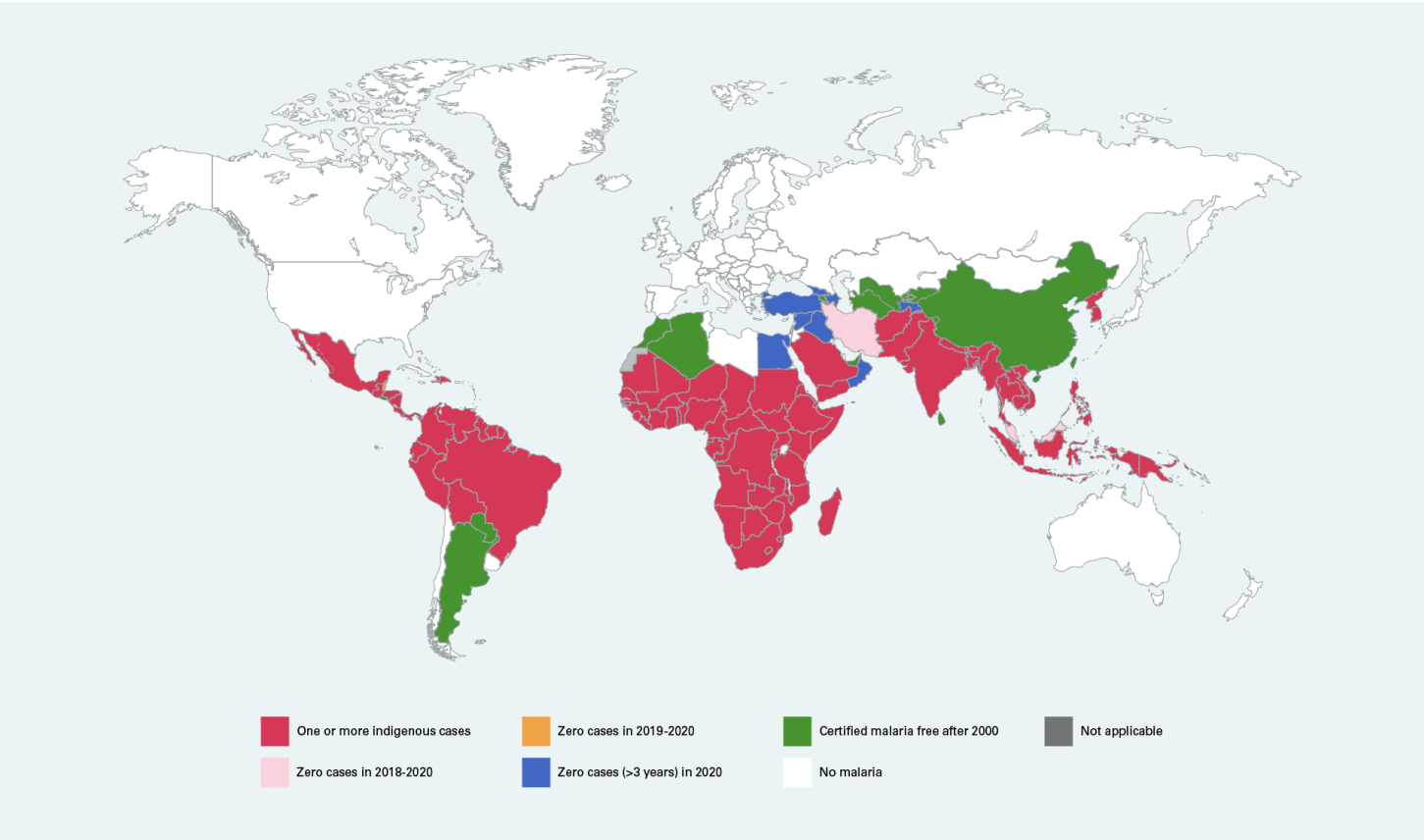

Figure 2: Situation globale de la distribution des cas de paludisme dans le monde en 2021.

Référence : Rapport de l'OMS 2022.

Pathologie

Le paludisme est une zoonose complexe ayant une symptomatologie dépendante du stade des parasites infectant l'hôte. L'infection des hépatocytes par le parasite est asymptomatique pour le patient (figure 1), bien que des cas rares d'hépatite grave aient été rapportés chez des patients impaludés notamment en Inde (Joshi *et al.*, 1986 ; Kochar *et al.*, 2003). C'est durant le cycle sanguin que le paludisme se déclare cliniquement, avec des symptômes tels qu'une fièvre modérée à forte (>39°C), une anémie causée par la lyse des érythrocytes infectés (pouvant entraîner des complications comme la nécrose des tissus par manque d'oxygénation), une splénomégalie, des céphalées et des myalgies (Rapport OMS 2022). La périodicité des fièvres palustres est causée par la libération dans la circulation sanguine de molécules hautement inflammatoire comme l'hémozoïne et des déchets métaboliques issus de la digestion de l'hémoglobine par le parasite au moment de l'éclatement de l'érythrocyte infecté (Parroche *et al.*, 2004 ; Dostert *et al.*, 2009). Cette inflammation est en outre induite par l'exposition des récepteurs TLR9 des macrophages et des cellules dendritiques circulantes à l'ADN du parasite, associé à l'hémozoïne (Parroche *et al.*, 2004). Pour les cas les plus graves, le paludisme peut évoluer vers une forme cérébrale appelée

neuropaludisme (Idro *et al.*, 2005). Cette forme de la maladie est provoquée par la rétention des érythrocytes infectés dans les capillaires sanguins irriguant l'encéphale. En effet, par les modifications opérées par le parasite sur la membrane érythrocytaire, celui-ci est capable d'adhérer à l'endothélium vasculaire, conduisant à l'obstruction des capillaires sanguin et causant la mort par asphyxie des tissus en aval (Idro *et al.*, 2005). La mortalité du paludisme est la plus élevée chez les jeunes enfants (< 5 ans) et l'immunité développée à la suite de l'infection dépend grandement de l'âge, du statut immunitaire et du taux de transmission de la zone géographique considérée (Rapport OMS 2022 ; White et Watson, 2018 ; Rodriguez-Barraquer *et al.*, 2018). Des stratégies de luttes ont été mises en place par l'OMS afin de diminuer l'exposition au vecteur, ainsi que des moyens préventifs et prophylactiques pour protéger les populations (Rapport OMS 2022).

Molécules antipaludiques

Les traitements contre le paludisme sont connus depuis des millénaires, par l'usage de préparations thérapeutiques à base de plantes notamment (Alebie *et al.*, 2017 ; Cock *et al.*, 2019). De nos jours, la science moderne a permis l'isolement et le développement de composés présentant des activités antipaludiques, devenant partie intégrante de notre arsenal thérapeutique. Ces molécules ciblent différentes étapes de développement du cycle parasitaire (figure 1) en s'attaquant à des structures ou à des mécanismes cellulaires vitaux (voir tableau 1).

- Les 4-aminoquinoléines (chloroquine, amodiaquine, pipéraquine et pyronaridine) et les aryl-amino-alcools (quinine, méfloquine et la luméfantrine) sont des familles de molécules ayant un mode d'action similaire (peu décrit dans le cas de la luméfantrine). Les données de la littérature décrivent leurs modes d'action comme de puissants inhibiteurs de la cristallisation de l'hème durant le stade trophozoïte du cycle sanguin (figure 1 ; Slater *et al.*, 1992 ; Combrinck *et al*., 2013 ; Olafson *et al.*, 2015 ; Sullivan *et al.*, 2017). Cette inhibition de la cristallisation de l'hème provoque la mort du parasite par l'accumulation d'hème libre toxique suite à la protéolyse de l'hémoglobine dans la vacuole digestive. Toutefois, des études *in vitro* récentes révèlent que la chloroquine possède la propriété d'interagir avec la double hélice d'ADN comme agent intercalant, avec des conséquences cytotoxiques pour les cellules notamment en bloquant la réplication de l'ADN (Costa *et al.*, 2022). La méfloquine est un des principaux antipaludiques (Rapport de l'OMS 2022). Sa cible est le stade schizonte du cycle sanguin, mais dont le mécanisme moléculaire est actuellement contesté. Une étude *in vitro* suggère que la méfloquine cible spécifiquement le site catalytique à activité GTPase localisé dans la sous-unité 80S des ribosomes du parasite, inhibant la synthèse des protéines (Wong *et al.*, 2017). Une autre étude, infirme ces résultats et indique que la méfloquine n'a

aucune activité *in vitro* au niveau de la sous-unité 80S du ribosome et n'inhibe donc pas la synthèse des protéines chez *P. falciparum* (Sheridan *et al.*, 2018). La question du mode d'action de la méfloquine reste donc ouverte.

- La primaquine (8-aminoquinoléine) est utilisée pour l'élimination des stades hépatiques. La molécule est réduite par la P450 NADH-oxydoréductase humaine, libérant du peroxyde d'hydrogène H2O2 comme sous-produit de la réaction (Camarda *et al.*, 2019). Cette libération de H2O2 provoque un stress oxydatif létal pour les stades hépatiques.
- Les molécules appartenant aux sulfadoxines et aux pyriméthamines sont des antifolates importants en raison de leur efficacité contre les parasites résistant à la chloroquine, ainsi que leur innocuité chez la femme enceinte (Peters *et al.*, 2007). Ces antifolates inhibent la dihydrofolate réductase (DHFR) et la dihydroptéorate synthétase (DHPS), enzymes de *P. falciparum* clés dans le métabolisme des folates, responsables de la biosynthèse des acides nucléiques (Peterson *et al.*, 1988 ; Basco *et al.*, 1995).
- L'atovaquone est un antipaludique agissant sur la mitochondrie du parasite. La molécule bloque sélectivement le cytochrome *bc1* de la chaîne respiratoire, inhibant *in fine* la synthèse d'ATP (Mather *et al.,* 2005). L'atovaquone entraîne donc un arrêt létal du métabolisme énergétique du parasite.
- L'artémisinine et ses dérivés (artésunate, dihydroartéminsinine et artéméther) sont des antipaludiques puissants à action rapide et temps de demi-vie court. Leur utilisation conjointe avec une drogue partenaire à demi-vie longue constitue le principal traitement recommandé par l'OMS, nommée thérapie combinée à base d'artémisinine (TCA) (Rapport de l'OMS 2022 ; Nosten et White 2007, figure 3). L'artémisinine est chimiquement activée par oxydation via l'hème libéré durant la digestion de l'hémoglobine, et provoque l'alkylation non-spécifique des biomolécules du parasite comme les lipides, les protéines ou encore l'ADN (Ying-Zi *et al.*, 1994 ; Klonis *et al.*, 2011 ; Wang *et al.*, 2015). Ce mode d'action particulier permet à l'artémisinine d'éliminer rapidement l'ensemble des stades sanguins du parasite et cette propriété fait donc des TCA le traitement le plus efficace actuellement disponible (Rapport OMS 2022).

En dépit des avancées significatives réalisées en matière de lutte contre le paludisme lors de ces dernières décennies, l'émergence de résistance contre les antipaludiques est un problème critique dans la stratégie de lutte globale mise en place par l'OMS et fait l'objet d'une recherche intense.

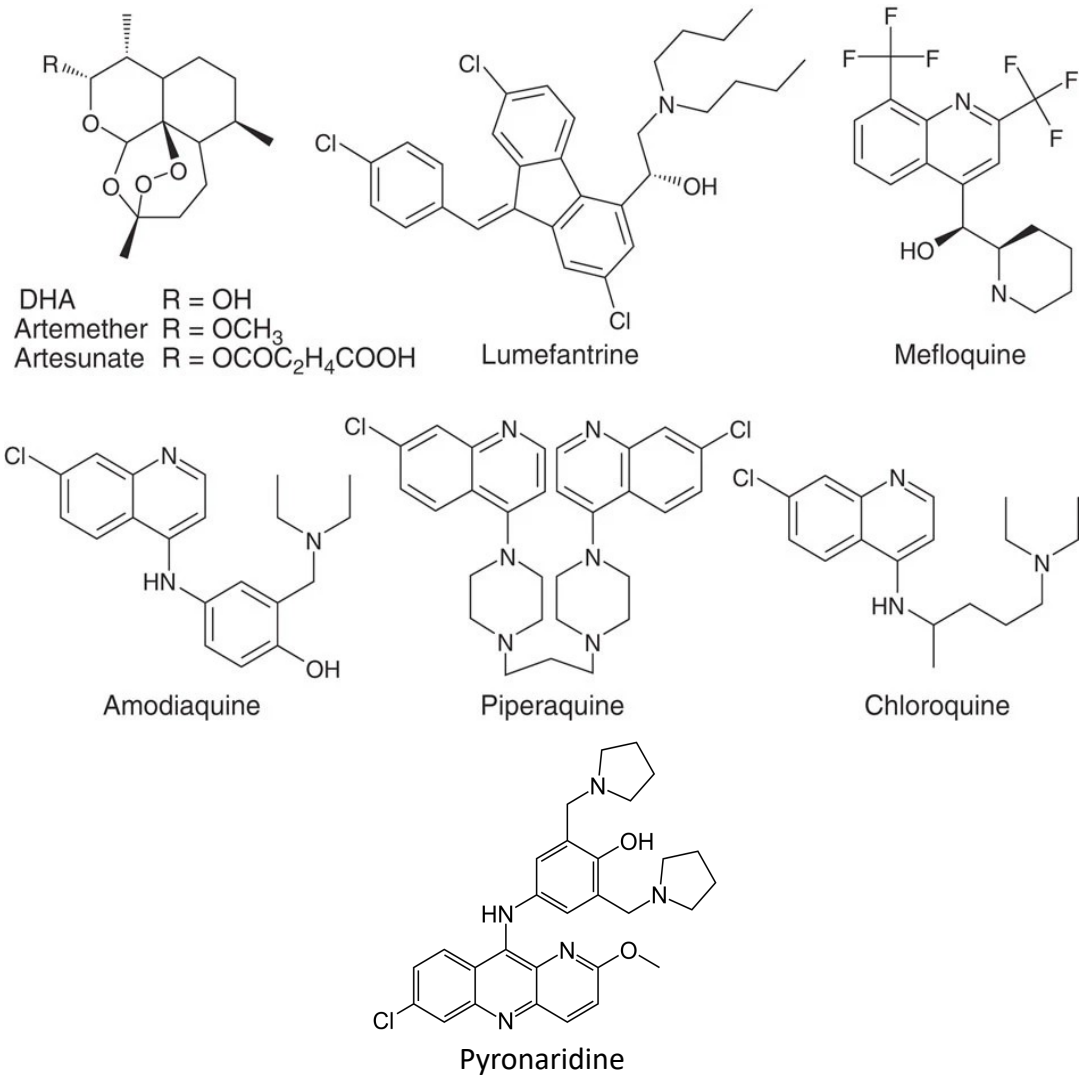

Figure 3 : Principaux antipaludiques employés dans les thérapies combinées à l'artémisinine.

Dérivés de l'artémisinine : DHA (Dihydroartémisinine) ; Artéméther et Artésunate.

Drogue partenaire : Luméfantrine ; Méfloquine ; Amodiaquine ; Pipéraquine ; Chloroquine ; Pyronaridine.

Référence : Adapté de Veiga *et al.*, 2016

C) Émergence des résistances aux antipaludiques chez *P. falciparum*

Malheureusement, *P. falciparum* a acquis des résistances à la plupart des antipaludiques au fil du temps en raison de leur usage en monothérapie, se propageant dans le monde et menaçant nos efforts de lutte. Plusieurs mécanismes de résistances ont été découverts tels que l'acquisition de mutations, la variation du nombre de copie de certains gènes ou encore des phénotypes d'arrêt de croissance. Ces mécanismes de résistances sont détaillés dans cette section (voir tableau 1).

- La résistance à la chloroquine est dépendante de mutations au sein du gène *Pfcrt*, codant pour une protéine fonctionnant comme une pompe à efflux dans la membrane de la vacuole digestive (Fidock *et al.*, 2000). Ces mutations permettent à la protéine de pomper la chloroquine de la vacuole

digestive vers le cytoplasme, préservant ainsi la réaction de cristallisation de l'hème durant la digestion de l'hémoglobine (Fidock *et al.*, 2000).

- La résistance à la piperaquine est associée à des variations du nombre de copie des gènes codants pour les plasmepsines 2 et 3, notamment au Cambodge (Witkowski *et al.*, 2017). Des mutations dans le gène *pfcrt* ont également été rapportées sur des parasites au Cambodge, avec les mutations H97Y, F145I, M343L et G353V associées à un phénotype de résistance à la pipéraquine (Duru et *al.,* 2015 ; Ross *et al.*, 2018 ; Dhingra *et al.*, 2019).
- L'amplification du nombre de copie du gène *Pfmdr1* est également impliquée dans la résistance à la méfloquine chez *P. falciparum* (Wilson *et al.*, 1989 ; Price *et al.*, 2004). Plus récemment, des mutations dans la sous-unité 80S des ribosomes du parasite ont été associées à une résistance à la méfloquine *in vitro* (Wong *et al.*, 2017). Cette résistance est due à des mutations localisées dans le site d'interaction entre le ribosome et la méfloquine, empêchant la molécule de se lier à sa cible (Wong *et al.*, 2017). Ce mécanisme d'action doit cependant être démontré *in vivo,* sachant que des études complémentaires ont infirmés l'implication de la méfloquine dans l'inhibition de la synthèse des protéines *in vitro* (Sheridan *et al.*, 2018).
- La résistance à l'atovaquone est médiée par des modifications structurales de la cible de la molécule, le cytochrome *bc1* mitochondrial du parasite (Srivastava *et al.*, 1999 ; Korsinczki *et al.*, 2000 ; Fisher *et al.*, 2012). Ces modifications sont causées par des mutations localisées sur le site d'interaction de l'enzyme, réduisant l'affinité du cytochrome *bc1* pour l'atovaquone, préservant le potentiel de membrane mitochondrial et la production d'ATP (Srivastava *et al.*, 1999 ; Korsinczki *et al.*, 2000 ; Fisher *et al.*, 2012). La mutation Y268S réduit la stabilité du cytochrome *bc1* et son affinité pour l'atovaquone, conférant un phénotype de résistance chez les parasites mutés (Fischer *et al.*, 2012).
- L'accumulation de mutations dans les gènes codants les enzymes DHFR et DHPS chez le parasite sont associées à la résistance contre la sulfadoxine et la pyriméthamine (Cowman *et al.*, 1988 ; Wang *et al.*, 1997 ; Plowe *et al.*, 1997 ; Nzila *et al.*, 2000). La résistance est obtenue par une combinaison de mutations dans les enzymes DHFR et DHPS, avec notamment des doubles mutants A437G et K540E pour la DHPS associés avec trois mutations dans DHFR sur les résidus S108N, N51I et C59R détectés sur des parasites au Kenya (Nzila *et al.*, 2000). Les modifications structurales provoquées par ces mutations dans DHFR et DHPS sont localisées dans le site d'interaction des sulfadoxines et pyriméthamines, réduisant l'affinité des enzymes pour ces molécules (Peterson *et al.*, 1988).
- Enfin, le premier cas de résistance à l'artémisinine chez *P. falciparum* a été rapporté dans les années 2000 en Asie du Sud-Est (Noedl *et al.*, 2008 ; Dondorp *et al.*, 2009), puis plus récemment en

Afrique, notamment au Rwanda (Uwimana *et al.*, 2020) et en Ouganda (Balikagala *et al.*, 2021). Des mutations dans la région codante du domaine propeller du gène *Pfkelch13* ont été directement liées à un phénotype de résistance partielle à l'artémisinine, avec une sous-population de parasite capable de survivre à l'exposition brève à l'artémisinine (Ariey *et al.*, 2014 ; Straimer *et al.*, 2015). La mutation C580Y est la plus répandue au Cambodge, multipliant par un facteur 5 le taux de survie du parasite après exposition à l'artémisinine en comparaison avec des parasites sauvages *Pfkelch13-WT* (Straimer *et al.*, 2015). Ce phénotype de résistance partielle à l'artémisinine est caractérisé par un délai de clairance parasitaire après traitement chez les patients ainsi qu'un retard de croissance affectant la transition du stade ring au trophozoïte sanguin (Witkowski *et al.*, 2010 et 2012). Ce phénotype de retard de croissance a été désigné comme étant une dormance induite par les drogues (DID), et n'a été rapporté que chez le stade ring du cycle sanguin après exposition à l'artémisinine, tandis que les stades avancés comme les trophozoïtes et les schizontes sont éliminés (Witkowski *et al.*, 2010). En tant que biomarqueur de la résistance à l'artémisinine, *Pfkelch13* a été étudié extensivement afin d'en caractériser la fonction biologique ; des implications ont été rapportés dans l'activation du protéasome (Tilley *et al.*, 2016), la consommation de l'hémoglobine (Yang *et al.*, 2019) et les mécanismes d'endocytoses (Birnbaum *et al.*, 2020). En dépit d'une compréhension incomplète, il est actuellement suggéré que la résistance à l'artémisinine conférée par les mutations dans *Pfkelch13* soit causée par une activation limitée de l'artémisinine via une réduction de l'endocytose de l'hémoglobine depuis la cellule hôte (Birnbaum *et al.*, 2020).

Tableau 1 : Liste des principaux antipaludiques, de leurs modes d'actions et marqueurs de résistances associés (adapté de Ross et Fidock, 2019).

Classe	Nom	Utilisation clinique	Cible	Marqueur de résistance
Endopéroxydes	Artémisinine, Dihydroartémisinine, Artésunate et Artéméther	Traitement de première intention (TCA), traitement du paludisme sévère	Pléiotropes, Alkylations non spécifique des protéines et lipides	Mutations dans *Pfkelch13*
4-Aminoquinoléines	Chloroquine	Traitement du paludisme non *falciparum*	Inhibition de la détoxification de l'hème dans la vacuole digestive	Mutations dans *pfcrt* et *pfmdr1*
	Amodiaquine	Drogue partenaire TCA		
	Pipéraquine	Drogue partenaire TCA		Amplification du nombre de copies des plasmepsines II et III, mutations dans *pfcrt*
	Pyronaridine	Drogue partenaire TCA		Inconnu
Aryl-Amino-Alcool	Quinine	Traitement du paludisme sévère	Potentielle inhibition de l'importation d'hémoglobine et détoxification de l'hème	Amplification dans *pfcrt* et *pfmdr1*
	Luméfantrine	Drogue partenaire TCA		
	Méfloquine	Drogue partenaire TCA		
Antifolates	Pyriméthamine et Sulfadoxine	Usage en combinaison, traitement de prévention	Inhibition du métabolisme des folates	Mutations dans *dhfr* et *dhps*
	Proguanil	Usage en combinaison Atovaquone + Proguanil		
Naphtoquinones	Atovaquone		Inhibition du transport d'électron dans la chaîne respiratoire mitochondriale	Mutations dans *cytb*
8-Aminoquinoléines	Primaquine	Traitement radical pour *P. vivax* et *P. ovale*, effet gamétocide chez *P. falciparum*	Inconnu	Inconnu
	Tafenoquine	Traitement radical, effect gamétocide chez *P. vivax* et *P. falciparum*	Inconnu	Inconnu

Comme revue dans cette section, la résistance aux antipaludiques est un événement commun, basé sur des modifications génomique et/ou un phénotype de dormance. La lutte contre le paludisme reposant sur la découverte de nouvelles molécules thérapeutiques est directement menacée par l'émergence de ces parasites résistants. Ainsi, l'émergence et la diffusion des parasites résistant à l'artémisinine, mutés sur *Pfkelch13*, représente un enjeu de santé publique majeur.

D) La protéine K13 et la résistance à l'artémisinine

Fonction(s) de la protéine K13

Le gène *Pfkelch13* localisé sur le chromosome 13 de *P. falciparum* code pour la protéine K13, constituée de 726 acides aminés (Coppée *et al.*, 2019). La structure tertiaire de la protéine comporte une séquence N-terminale peu conservée et spécifique à *P. falciparum*, un domaine BTB putatif ainsi qu'un domaine propeller en C-terminal (Coppée *et al.*, 2019). La majorité des mutations sur *Pfkelch13* conférant la résistance à l'artémisinine se situent sur ce domaine propeller (Ariey *et al.*, 2014 ; Straimer *et al.*, 2015). La protéine K13 de *P. falciparum* fait l'objet de nombreuses recherches. Sa fonction est encore vivement débattue, mais des études récentes suggèrent une implication de K13 dans plusieurs mécanismes cellulaires. Des recherches proposent que K13 soit une protéine adaptatrice, permettant le recrutement par son domaine BTB des ubiquitines ligases E2 et E3, impliquées dans la réponse au stress et l'inhibition du protéasome (Tilley *et al.*, 2016). Dans ce modèle, K13 serait en interaction avec un facteur de transcription via son domaine propeller, qui serait ubiquitiné et dégradé par le protéasome en condition physiologique ; en condition de stress, le facteur de transcription est libéré, permettant l'expression de gènes impliqués dans la réponse aux stress (Tilley *et al.*, 2016). Une implication de K13 dans l'endocytose de l'hémoglobine depuis le cytoplasme du globule rouge, a également pu être mise en évidence *in vitro* (Yang *et al.*, 2019 ; Birnbaum *et al.*, 2020). En effet, le génotype *Pfkelch13-C580Y* conférant une résistance partielle à l'artémisinine (Straimer *et al.*, 2015) induit une diminution en quantité de protéine K13 disponible ainsi qu'une endocytose de l'hémoglobine plus faible qu'une souche non mutée (Birnbaum *et al.*, 2020). De plus, une douzaine de protéines partenaires en interaction avec K13 ont pu être détectées durant le processus d'endocytose de l'hémoglobine, suggérant que K13 serait une protéine adaptatrice permettant la formation de ce complexe (Birnbaum *et al.*, 2020 ; Gnädig *et al.*, 2020 ; Mok *et al.*, 2021). Néanmoins, le rôle des mutations dans K13 conférant la résistance à l'artémisinine dans ces mécanismes cellulaires doit être élucidé. Une étude récente *in silico* suggère que l'ensemble des mutations conférant la résistance à l'artémisinine se situeraient dans des sites d'interactions protéine-protéine conservés au niveau du domaine propeller de K13 (Coppée *et al.*, 2019). Plus particulièrement, les mutations C580Y et R539T déstabiliseraient le domaine propeller

de K13 *in silico* (Coppée *et al.*, 2019). L'hypothèse est que cette déstabilisation de K13 par ces mutations provoquerait une réduction en quantité de K13 fonctionnelle disponible pour le parasite, diminuant sa capacité à endocyter l'hémoglobine, lui conférant alors une résistance partielle à l'artémisinine (Yang *et al.*, 2019 ; Birnbaum *et al.*, 2020). Ainsi, la fonction exacte de K13 reste hypothétique et notre compréhension du lien fonctionnel entre le domaine propeller et la diversité des mutations de *Pfkelch13* présente chez les parasites résistants à l'artémisinine est limitée.

La diversité des génotypes de Pfkelch13 conférant la résistance à l'artémisinine

K13 est le principal biomarqueur de la résistance à l'artémisinine (Ariey *et al.*, 2014). Plusieurs génotypes aboutissant à la résistance à l'artémisinine ont été détectés chez *Pfkelch13* au Cambodge, avec notamment les mutants C580Y; R539T; I543T; Y493H (Straimer *et al*., 2015 ; figure 4). Curieusement, chaque mutation confère un niveau différent de résistance à l'artémisinine (exprimé par la proportion de parasites viables après exposition de 6 heures à 700 nM de DHA *in vitro*), et contre-intuitivement, la mutation conférant le plus de survie à face à l'artémisinine, c'est-à-dire la mutation *Pfkelch13-I543T*, n'est pas celle qui s'est le plus propagée (Straimer *et al*., 2015 ; Ménard *et al*., 2016 ; Iwagami *et al*., 2018 ; figure 4). En effet, la mutation C580Y qui confère une survie modérée du parasite en comparaison à d'autres mutations (Straimer *et al*., 2015) s'est rapidement propagée dans l'ensemble de l'Asie du Sud-Est (figure 4), suggérant l'existence d'un coût en fitness de ces mutations pour le parasite. Par la suite, des travaux ont pu mettre en évidence que les parasites résistants à l'artémisinine subissent des carences nutritionnelles, compensées par la mise en place de mécanismes d'importations d'acides aminés depuis le sérum de l'hôte (Mesen-Ramirez *et al.*, 2021). La sélection d'un mutant *Pfkelch13* résistant à l'artémisinine implique donc un équilibre entre le coût en fitness d'une mutation donnée, et la capacité du parasite à survivre. En Afrique, les mutants résistants porteurs des mutations R561H (Rwanda) ainsi que C469Y et A675V (Ouganda) ont été détectés et confirmés comme étant d'origine locale et non pas importés d'Asie (Uwimana *et al.*, 2020 ; Balikagala *et al.*, 2021), indiquant la capacité inquiétante de *P. falciparum* à résister à l'artémisinine quel que soit son origine.

En dehors des études cliniques, la surveillance génomique des génotypes *Pfkelch13* et le Ring Stage Survival Assay (RSA) font partie des outils de diagnostic développés pour la détection et la validation de la résistance à l'artémisinine chez *P. falciparum.*

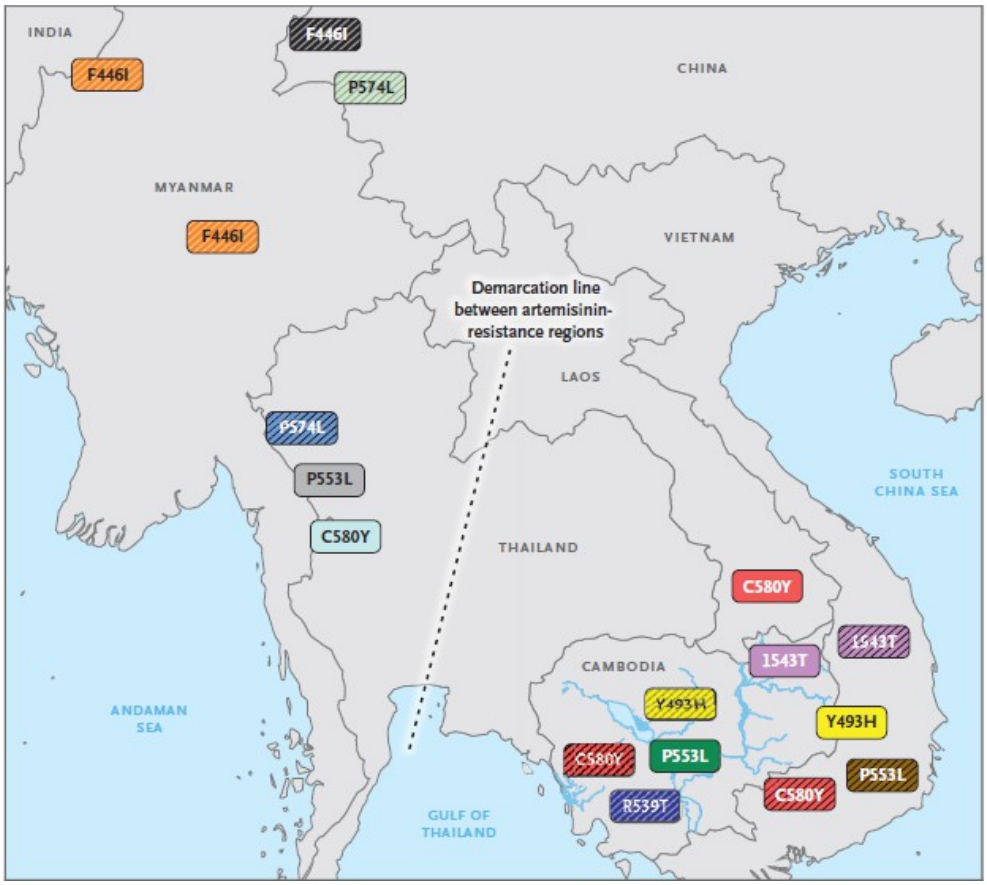

Figure 4: Carte de la distribution des mutations au sein du gène *Pfkelch13* conférant la résistance à l'artémisinine, en Asie du Sud-Est.

Référence : Ménard *et al.*, 2016

Le Ring-stage Survival Assay (RSA) comme outil de détection in vitro des souches résistantes à l'artémisinine.

Dans un contexte de diffusion des parasites résistant à l'artémisinine, la détection des souches mutées est un élément central dans la lutte contre le paludisme. Le Ring-stage Survival Assay (RSA) a été mis au point pour répondre à ce besoin, il s'agit d'un test *in vitro* consistant à comparer l'exposition durant 6h à des doses cliniques d'artémisinine (700 nM) de parasites au stade ring (0-3h après invasion) avec des parasites non-exposés (Witkowski *et al.*, 2013). Le taux de survie des parasites est mesuré par microscopie à 72h post exposition à l'artémisinine, et comparé au taux de survie des parasites non-exposés. On considère une souche comme étant résistante à l'artémisinine si le taux de survie RSA est supérieur à 1%. Ainsi, le test RSA permet de mesurer efficacement la susceptibilité à l'artémisinine d'une souche donnée et par extension, de valider si une mutation au sein du gène *Pfkelch13* confère la résistance (Witkowski *et al.*, 2013). Depuis, le

test RSA a été décliné en plusieurs variantes, faisant appel à des techniques comme la qPCR pour mesurer le taux d'accroissement entre parasites traités ou non traités à l'artémisinine (Davis *et al*., 2020) ou encore la cytométrie en flux pour s'affranchir des comptages par microscopie (Amaratunga *et al.*, 2014).

Cependant, le RSA présente plusieurs limites. La mise en place du RSA nécessite de connaître précisément le temps de progression du cycle sanguin de la souche testée afin d'obtenir des schizontes matures en quantité suffisante. Cela représente un problème important car il a été démontré que le temps de progression dans le cycle sanguin varie significativement d'une souche à l'autre, pouvant aller de 36 à 54 heures (Smith *et al.*, 2020 ; Wockner *et al.*, 2020). Cela rend donc l'application du test RSA difficile quand plusieurs souches sont testées simultanément. De plus, le RSA mesure le taux de survie des parasites sur la base d'une seule exposition à l'artémisinine, alors que le traitement TCA donné chez l'homme s'étale sur 3 jours et que le parasite est exposé à 3 doses successives. Les taux de survie mesurés par le RSA ne permettent donc pas d'établir si la souche testée est capable ou non de survivre *in vivo* en condition réelle. Enfin, le taux de survie que mesure le RSA chez une souche résistante à l'artémisinine peut varier de manière significative en fonction du fond génétique pour une même mutation dans *Pfkelch13* (Stokes *et al.*, 2021), démontrant l'implication de facteurs additionnels dans la survie des parasites.

Le phénotype des mutants K13 résistant à l'artémisinine

Le phénotype des parasites résistant à l'artémisinine se caractérise chez les patients par un délai de clairance des parasites au cours des 3 jours de traitement (Noedl *et al.*, 2008 ; Dondorp *et al.*, 2009). Classiquement, l'artémisinine élimine rapidement les schizontes et les trophozoïtes, car l'activation de la drogue par l'hème est la plus importante du fait de la digestion intense de l'hémoglobine durant ces stades (Moore *et al.*, 2006). Il a été mis en évidence la capacité des stades ring à stopper temporairement leur croissance en réponse à l'exposition à l'artémisinine. Ce phénotype d'arrêt de croissance des stades ring est possiblement associé à une recrudescence des parasites, jusqu'à plusieurs semaines à l'exposition à la drogue (Witkowski *et al.*, 2010 ; Teuscher *et al.*, 2010). Il a également été rapporté que les parasites mutants K13 ont un délai de transition du stade ring au stade trophozoïte plus long que chez les souches sauvages, possiblement causé par une endocytose réduite de l'hémoglobine (Birnbaum *et al.*, 2020 ; Mok *et al.*, 2021).

2) La dormance induite chez *P. falciparum*

A) La dormance comme stratégie de survie

La première observation de la dormance remonte à 1944, sur des bactéries du genre *Staphylococcus aureus* ayant un phénotype décrit comme un arrêt de croissance à la suite d'une exposition à un antibiotique, la pénicilline (Bigger 1944). La dormance est définie comme un phénotype d'arrêt de croissance temporaire et réversible d'un organisme lorsque les conditions environnementales sont défavorables. La dormance est une stratégie ubiquiste dans le vivant et a été décrite dans de nombreux modèles, comme les plantes avec la germination des graines (Li et Foley, 1997 ; Soltani *et al.*, 2021) ; la sporulation et la persistance chez les bactéries et les champignons (Bigger 1944 ; Cochrane 1974 ; Tommerup 1983 ; Lewis 2010) ; la diapause chez les insectes (Diniz *et al.*, 2017) ou encore la quiescence cellulaire dans les modèles de cellules souches ou cancéreuses (Li et Bhatia 2011 ; Recasens et Munoz 2018). Ces phénotypes possèdent une grande diversité sémantique, avec l'emploi de termes variés comme dormance ; latence ; quiescence ; hibernation ; persistance ou encore diapause, utilisés pour décrire un arrêt de croissance temporaire chez un modèle particulier. Néanmoins, nous nous cantonnerons ici à l'usage des termes "dormance" et "arrêt de croissance temporaire" par soucis de clarté.

La dormance se caractérise donc par un arrêt de croissance d'une durée variable, entre plusieurs jours à plusieurs semaines, selon le modèle biologique considéré. Chez les bactéries, un environnement appauvri en nutriments déclenche une réponse cellulaire dans une partie de la population, qui entre en dormance jusqu'à la levée du stress nutritif afin de préserver la population. (Kaprelyants *et al.*, 1993 ; Kim *et al.*, 2022). Dans le cas des plantes, la levée de dormance des graines n'est réalisée que lorsque les conditions physico-chimiques du sol deviennent favorables, déclenchant la germination (Née *et al.*, 2017). Contre-intuitivement, la dormance n'implique pas qu'un ralentissement du métabolisme ou des processus biologiques, mais également un changement du profil transcriptionnel, distinct de la population générale (Lemons *et al.*, 2010 ; Vega *et al.*, 2012 ; Keroack et Duraisingh, 2022). Ces données indiquent donc que la dormance est une réponse induite de l'organisme à la suite de signaux détectés dans l'environnement, entraînant un changement de l'état transcriptionnel d'une partie de la population. Ce mécanisme de survie permet ainsi le maintien dans l'environnement sur de longues périodes d'individus dans un milieu donné.

Chez les *Apicomplexes*, la dormance a été décrite chez *Toxoplasma gondii*, capable de différencier une partie de sa population en bradyzoïtes, des cellules enkystées capable de survivre sur de longues périodes dans l'hôte humain (Lyons *et al.*, 2002). On retrouve également des formes dormantes chez *P. vivax* ou encore *P. cynomolgi* sous forme d'hypnozoïtes hépatiques, mais également dans d'autres espèces de *Plasmodium* (tableau 2), constituant un réservoir durable de

parasites chez l'hôte (Krotoski *et al.*, 1985 ; Deye *et al.*, 2012 ; Pasini *et al.*, 2017). Dans le cas de *P. falciparum*, la dormance est principalement décrite au stade ring (Witkoswki *et al.*, 2013 ; tableau 2). Ainsi, la dormance constitue une stratégie de survie capable de maintenir durablement une population d'individus dans un milieu défavorable. Dans le cas d'agents infectieux comme *P. falciparum*, la dormance permettrait l'échappement au système immunitaire de l'hôte ainsi qu'une tolérance aux antipaludiques (Teuscher *et al.*, 2010 ; Peatey *et al.*, 2020).

Tableau 2 : Phénotype de dormance décrit chez *Plasmodium*.

Espèce	Dormance décrite ?	Hôte	Stade	Référence
P. falciparum	Oui	Humain	Oocyste (vecteur) ; Ring (stade sanguin)	Witkoswki 2013 ; Habtewold 2021
P. vivax	Oui	Humain	Hypnozoïte (stade hépatique)	Krotoski 1985
P. berghei	Oui	Rongeur	Oocyste (vecteur)	Habtewold 2021
P. cynomolgi	Oui	Primate	Hypnozoïte (stade hépatique)	Deye 2012 ; Pasini 2017
P. knowlesi	Non décrit	Primate & Humain	----------	----------
P. malariae	Non décrit	Humain	----------	----------
P. ovale	Suspectée	Humain	Possiblement Hypnozoïte (stade hépatique)	Richter 2010
P. chabaudi	Non décrit	Rongeur	----------	----------
P. yoelii	Non décrit	Rongeur	----------	----------
P. vinckei	Oui	Rongeur	Ring (stade sanguin)	LaCrue 2011

B) La dormance induite des stades sanguins de *P. falciparum*

Découverte

Les recherches sur la dormance chez *P. falciparum* sont relativement récentes. L'existence de stades sanguins capables de dormance a été rapportée pour la première *in vitro* en 1995 sur des cultures sensibles à la pyriméthamine et recrudescentes après traitement (Nakazawa *et al*., 1995). Ces observations aboutirent à la conclusion qu'il existe dans la population générale de *P. falciparum*, une sous-population de parasite capable de stopper temporairement leur croissance pour survivre au traitement. Un argument supplémentaire était que ces parasites dormants conservent une sensibilité au traitement après leur réveil, indiquant l'absence de sélection d'un quelconque mutant résistant (Nakazawa *et al.*, 1995). Ces observations *in vitro* furent reproduites en contexte d'exposition à l'artémisinine, révélant des stades rings en arrêt temporaire de croissance et reprenant leur cycle immédiatement après la levée du stress (Teuscher *et al.*, 2010 ; Witkowski *et al.*, 2010 et 2012). Ce phénotype d'arrêt de croissance fût plus tard considéré comme étant une cause sous-estimée de recrudescence et d'échec thérapeutique chez les patients traités par TCA , montrant que l'étude de la dormance induite est un champ de recherche aux implications cliniques considérables

(Teuscher *et al.*, 2010 ; Peatey *et al.*, 2020).

Phénotype, durée de dormance et détection

La DID a été décrite comme un ralentissement du stade ring dans sa progression dans le cycle sanguin, avec un retard pouvant aller jusqu'à 24h sous pression à l'artémisinine (Witkowski *et al.*, 2012). D'autres études, ont montré des temps de dormance pouvant aller jusqu'à plusieurs jours, voire plusieurs semaines (Teuscher *et al.*, 2010 ; Cheng *et al.*, 2012 ; Grobler *et al.*, 2014 ; Peatey *et al.*, 2015 ; Gray *et al.*, 2016 ; Holmes *et al.*, 2017 ; Reyser *et al.*, 2020 ; Peatey *et al.*, 2020 ; Connelly *et al.*, 2021 ; Mok *et al.*, 2021). Ces données diffèrent du phénotype de DID initialement décrit, consistant en un arrêt temporaire de croissance du stade ring suivit d'une reprise immédiate à la levée de la pression par l'artémisinine (Witkowski *et al.*, 2012). Il est à noter que de nombreux termes sont employés pour qualifier ces phénotypes d'arrêt de croissance chez le stade ring de *P. falciparum*, avec la dormance, la latence ou encore la quiescence (Chen *et al.*, 2014 ; Holmes *et al.*, 2017 ; Reyser *et al.*, 2020). Il est difficile d'établir si ces phénotypes ont une réalité biologique, où s'il s'agit du même mécanisme de dormance mais sous différentes appellations. De plus, la comparaison des résultats de ces études sur la dormance est limitée par leurs différences dans les variables expérimentales, comme les souches testées (fonds génétiques et génotypes *Pfkelch13*), la synchronisation des parasites, la concentration d'artémisinine utilisée et la durée d'exposition, ou encore les critères morphologiques employés pour dénombrer les parasites dormants. En effet, il n'existe pas de critères morphologiques précis pour différencier un stade ring dormant d'un parasite mort ou d'un autre stade ring, pouvant conduire à différentes interprétations durant l'examen par microscopie. D'autres stratégies utilisant la fluorescence et la détection du potentiel de membrane mitochondrial sont à l'étude quant à la détection des parasites en stade ring dormants par cytométrie en flux, révélant que ces parasites conserveraient une activité mitochondriale (Peatey *et al.*, 2015). La détection des stades rings en dormance est par conséquent actuellement limitée en raison du manque de biomarqueur spécifique.

Activité métabolique

Les parasites dormants conservent une activité métabolique, notamment au niveau de la mitochondrie par le maintien du potentiel de membrane mitochondrial (Peatey *et al*., 2015), mais également au niveau de l'apicoplaste (Chen *et al.*, 2014). En effet, il a été rapporté que des parasites sous pression d'artémisinine conservent un métabolisme actif du pyruvate et de la synthèse des acides gras, avec une répression active du métabolisme de la glycolyse et du cycle de Krebs (Chen *et al.*, 2014). Ces données supportent l'idée que la dormance repose sur un métabolisme spécifique,

distinct du métabolisme basal.

La dormance induite : principales questions et hypothèses

De nombreuses questions sur la dormance sont encore en suspens, notamment sur l'implication de *Pfkelch13* dans la dormance. Aucun lien clair n'est établi entre DID et les mutations de K13 conférant la résistance à l'artémisinine. Cependant, des parasites *Pfkelch13-WT* exposés à l'artémisinine conservent une sous-population de parasite survivant, de l'ordre de 0,1-0,5% (Straimer *et al.*, 2015). Il est possible que la survie de ces parasites sensibles à l'artémisinine puisse s'expliquer par la dormance, si l'on considère qu'il s'agit d'un mécanisme constitutif, et non pas acquis, comme les mutations dans K13.

La cinétique de la dormance chez *P. falciparum* est mal connue, mais peut être divisée en trois événements successifs : l'induction, le maintien et le réveil. Peu de travaux ont été menés chez *P. falciparum* sur la cinétique de la dormance, néanmoins, des résultats récents suggèrent que des signaux extracellulaires pourraient moduler la durée de dormance du parasite (Duvalsaint et Kyle, 2018). Curieusement, l'acide gibbérellique et l'acide abscissique, deux phytohormones impliquées dans la signalisation du stress chez les plantes, accélèrent le réveil des stades rings en dormance jusqu'à 48h en comparaison avec l'artémisinine seule *in vitro* (Duvalsaint et Kyle, 2018). Ces données mettent en évidence la nature modulable de la dormance par des signaux extracellulaires.

L'induction de la dormance reste peu documentée, cependant, la dormance semble être un mécanisme mis en place uniquement par une sous-population de rings durant une exposition à la DHA, pour une raison inconnue (Witkowski *et al.*, 2012). L'exposition à un environnement appauvri en acides aminés induit également un phénotype d'arrêt de croissance temporaire chez *P. falciparum* (Babbitt *et al.*, 2012), suggérant que ce phénotype serait provoqué par un environnement défavorable au sens large. Ainsi, il est envisageable que la dormance puisse être une réponse induite par l'environnement, potentiellement par l'intervention de signaux extracellulaires, mais cet axe de recherche est actuellement peu exploré chez *P. falciparum*.

La dormance induite chez *P. falciparum* est donc une stratégie de survie importante et d'un grand intérêt clinique dans la lutte contre le paludisme mais pour laquelle nous n'avons, paradoxalement, que peu de connaissances.

C) Des perspectives de mieux comprendre la dormance

La dormance représente donc un mécanisme de résistance à part entière, dont les implications cliniques sont difficilement quantifiables du fait de la difficulté à détecter efficacement les cellules en arrêt de croissance, notamment chez les porteurs asymptomatiques. Des recherches

suggèrent que la fréquence des parasites en dormance est largement sous-estimée chez les patients, et serait une stratégie de maintien dans l'hôte durant la saison sèche des pays endémiques à transmission saisonnière (Andrade *et al.*, 2020). Ce mécanisme de survie permet un maintien durable du parasite dans l'hôte, lui permettant d'échapper au système immunitaire et aux traitements antipaludiques, et pourrait possiblement être à l'origine d'échecs thérapeutiques et de recrudescence. (Teuscher *et al*., 2010 ; Peatey *et al.*, 2020).

Aucun traitement efficace n'existe à ce jour pour inhiber l'entrée en dormance de *P. falciparum*, et l'artémisinine ne permet pas toujours l'élimination complète du parasite, comme observé *in vitro*, où des recrudescences ont été observées plusieurs jours post-traitement (Teuscher *et al.*, 2010 ; Grobler *et al.,* 2014 ; Chen *et al.*, 2014). La compréhension des mécanismes d'induction et de levée de dormance pourrait permettre à terme de développer des stratégies de type "wake-up and kill', afin de bloquer la dormance et de maintenir le parasite dans un état susceptible à l'artémisinine. Les mécanismes moléculaires gouvernant la dormance restent à découvrir, notamment restent à définir les implications potentielles des mutations au sein du gène *Pfkelch13* et des signaux extracellulaires. Ainsi, il semble difficile d'envisager l'élimination du paludisme sans prendre en considération le rôle de la dormance comme mécanisme de survie du parasite chez l'hôte humain.

3) Objectifs de la thèse

L'ensemble de mon travail de thèse s'est concentré sur trois axes, différents mais complémentaires, visant à étudier la résistance de *P. falciparum* aux dérivés de l'artémisinine. Le premier axe était une approche appliquée à la santé publique, visant à étudier la résistance à l'artémisinine en Afrique et plus particulièrement en Érythrée. Ce premier objectif visait à détecter la présence de parasites mutants K13 dans des isolats de *P. falciparum* prélevés au cours d'études cliniques mesurant l'efficacité des antipaludiques. Le second volet de ma thèse, en lien avec le premier, avait pour objectif d'optimiser la méthodologie du test RSA, principal outil de diagnostic utilisé dans la détection de la résistance *in vitro* de *P. falciparum* à l'artémisinine. Enfin, le dernier axe de ma thèse consistait à explorer les mécanismes impliqués dans la résistance *P. falciparum* aux dérivés de l'artémisinine, notamment la dormance, à l'échelle de la population et de l' individu. Ce dernier axe s'est appuyé sur des techniques telles que le séquençage ARN à l'échelle individuelle (single-cell RNA-seq), la culture cellulaire et la cytométrie. Cette approche avait pour objectif de caractériser des biomarqueurs de la dormance induite chez *P. falciparum*, de déterminer le rôle de l'environnement extracellulaire dans l'induction de la dormance (ainsi que l'implication des mutations *Pfkelch13*). L'ensemble de ces travaux a été rendu possible grâce à l'expertise et au parc technologique disponible à l'Institut Pasteur.

Partie II

Travaux de recherche

Axe 1 : Veille épidémiologique de la résistance à l'artémisinine en Érythrée, dans la corne de l'Afrique.

Article 1 : Augmentation du paludisme résistant à l'artémisinine et HRP2-négatif en Érythrée 'Increasing Artemisinin-resistant HRP-2 negative malaria in Eritrea.'

Ce travail a été réalisé en collaboration avec les autorités Érythréennes, associant une approche clinique à la biologie moléculaire. Les études cliniques visant à évaluer l'efficacité des TCA menées depuis 2016 ont permis de détecter un nombre croissant de cas de paludisme résistant à l'artémisinine et à détecter des souches de *P. falciparum* possédant une nouvelle mutation *Pfkelch13* jamais décrite jusqu'à présent. Cette mutation, *Pfkelch13-R622I*, a été associée à une résistance *in vitro* modérée à l'artémisinine d'après les tests RSA réalisés sur des souches éditées (3D7 et DD2). L'analyse des séquences complètes des parasites mutants et wild type (WT) ont confirmé l'origine locale et indique que la mutation *Pfkelch13-R622I* serait une mutation apparue spontanément dans la population générale de parasites, qui se serait fixée au cours du temps. De plus, nous avons démontré qu'une fraction des parasites mutants (~17%) présentaient également des délétions des gènes *Pfhrp2* et *Pfhrp3*, codant pour des protéines utilisées comme cibles par les tests de diagnostic rapides. Ainsi, le cas de l'Érythrée est extrêmement préoccupant, dans la mesure où cette combinaison de mutation *Pfkelch13* et délétions HRP2-HRP3 confère au parasite à la fois une résistance partielle à l'artémisinine (pour laquelle il n'existe pas à l'heure actuelle d'alternative thérapeutique viable), mais lui permet également de ne pas être détecté par les tests de diagnostic rapides. Les implications cliniques et épidémiologiques sont sérieuses, avec notamment le risque de diffusion rapide de ces parasites mutés dans les pays limitrophes comme l'Éthiopie, le Soudan ou encore Djibouti. Enfin, ces données impliquent que les cas de paludisme résistant à l'artémisinine en Érythrée seraient possiblement sous-évalués. Ce travail s'inscrit donc dans un contexte d'émergence de la résistance à l'artémisinine en Afrique, faisant écho aux cas du Rwanda et de l'Ouganda, où des mutations *Pfkelch13* (R561H, C469Y et A675V) conférant une résistance partielle à l'artémisinine ont également été rapportées récemment. Les données présentées ont été soumises pour publication dans un journal à comité de lecture et sont actuellement en cours de révision.

Increasing Artemisinin-Resistant HRP2-Negative Malaria in Eritrea

Selam Mihreteab*, B.Sc.,

Lucien Platon*, M.Sc.,

Araia Berhane, M.D., M.Sc.,

Barbara H. Stokes, Ph.D.,

Marian Warsame, M.D.,

Pascal Campagne, Ph.D.,

Alexis Criscuolo, Ph.D.,

Laurence Ma, B.S.,

Nathalie Petiot, B.S.,

Cécile Doderer-Lang, M.Sc.,

Eric Legrand, Ph.D.,

Lydia Arnoux, B.S.,

Kurt E. Ward, Ph.D.,

Assefash Zehaie Kassahun, M.D., M.Sc.,

Pascal Ringwald, M.D., Ph.D.,

David A. Fidock, Ph.D.,

Didier Ménard, Pharm.D., Ph.D.

* Dr. Selam Mihreteab and Lucien Platon contributed equally to this manuscript

National Malaria Control Program, Ministry of Health, Asmara, Eritrea (S.M.); Institut Pasteur, INSERM U1201, Malaria Genetic and Resistance Unit, F-75015 Paris, France (L.P., N.P., E.L., D.M.); Sorbonne Université, Collège doctoral ED 515 Complexité du Vivant, F-75015 Paris, France (L.P.); Communicable Diseases Control Division, Ministry of Health, Asmara, Eritrea (A.B.); Columbia University Irving Medical Center, Department of Microbiology & Immunology, New York,

NY 10032, USA (B.H.S., K.W., D.A.F.); Gothenburg University, School of Public Health and Social Medicine, Gothenburg, Sweden (M.W.); Université de Strasbourg, Institute of Parasitology and Tropical Diseases, UR7292 Dynamics of Host-Pathogen Interactions, F-67000 Strasbourg, France (C.L-D., L. A., D.M.); CHU Strasbourg, Laboratory of Parasitology and Medical Mycology, F-67000 Strasbourg, France (D.M.); Institut Pasteur, Université Paris Cité, Bioinformatics and Biostatistics Hub, F-75015 Paris, France (P.C., A.C.); World Health Organization office, Asmara, Eritrea (A. Z. K.); Institut Pasteur, Biomics Platform, C2RT, F-75015 Paris, France (L.M.) ; Global Malaria Programme, World Health Organization, Geneva, Switzerland (P.R.); Columbia University Irving Medical Center, Center for Malaria Therapeutics and Antimicrobial Resistance. Division of Infectious Diseases. Department of Medicine, New York, NY 10032, USA (D.A.F.).

Address reprint requests to Dr. Didier Ménard at the Institut Pasteur, Paris 25-28 Rue du Dr Roux 75724 Paris Cedex 15 or at dmenard@pasteur.fr or dmenard@unistra.fr and Dr. Selam Mihreteab National Malaria Control Program, Ministry of Health, Asmara, Eritrea or at smuqubay@gmail.com.

Short title: Artemisinin-Resistant HRP2-Negative Malaria in Eritrea

Abstract word count: 250

Manuscript word count: 2698

Key words: Malaria, *P. falciparum*, antimalarial treatment, artemisinin resistance, *Pfkelch13*, HRP2-based rapid diagnostic test, *hrp2* deletion, Horn of Africa, Eritrea,

Abstract.

Background. While the clinical efficacy of artemisinin-based combination therapies (ACTs) in Africa remains high, the recent emergence of artemisinin partial resistance (ART-R) on the continent is concerning, given the lack of alternative treatments.

Methods. Using drug efficacy studies conducted in 2016-19 to evaluate artesunate-amodiaquine or artemether-lumefantrine treatment for uncomplicated falciparum malaria in Eritrea, we estimated the proportion of patients with persistent parasitaemia at day3 (D3+) and assayed parasites for mutations in the *Pfkelch13* gene as predictive markers of ART-R. We also screened for deletions in *hrp2/hrp3* that result in variable performance of HRP2-based malaria rapid diagnostic tests (RDTs).

Results. We noted increased proportions of D3+ patients from 2016 (0.4%, 1/273) to 2017 (1.9%, 4/209) and 2019 (4.2%, 15/359, p=0.002). A novel *Pfkelch13* R622I variant, detected in 109/818 isolates prior to treatment, similarly showed a marked rise in prevalence from 2016 (24/278) to 2019 (69/329, p=0.01) and was the main predictor of the D3+ rate by multivariable analysis (OR 6.4, 95% CI 2.3-17.6, p=0.0003). *In vivo* ART-R was confirmed in Eritrea, with >5% of D3+ patients <15 years old harboring *Pfkelch13* 622I mutant parasites. *In vitro*, the 622I variant conferred low-level ART-R when edited into *P. falciparum* NF54 and Dd2 parasite lines. A large proportion (16.9%) of *Pfkelch13* 622I parasites carried double *hrp2/hrp3* deletions, rendering these parasites likely undetectable by HRP2-based RDTs.

Conclusions. The emergence and spread of *P. falciparum* lineages with both *Pfkelch13*-mediated ART-R and deletions in *hrp2/hrp3* genes in Eritrea threaten to compromise regional malaria control and elimination campaigns.

Introduction

Artemisinin-based combination therapies (ACTs), which combine fast-acting and potent artemisinin derivatives with long-acting partner drugs, are essential first-line treatments for uncomplicated *Plasmodium falciparum* malaria.[1,2] Over the last fifteen years, *P. falciparum* parasites have developed artemisinin partial resistance (ART-R) in the Greater Mekong Subregion, manifested as delayed parasite clearance or persistence of parasites on day 3 (D3+) following ACT treatment due to decreased susceptibility of intraerythrocytic ring-stage parasites.[2-7] This Subregion has witnessed increasing rates of ACT treatment failure as parasites also acquire resistance to the partner drugs piperaquine or mefloquine.[8]

Although the clinical efficacy of ACTs in African settings is presently high, the recent emergence of ART-R is of major concern, specifically in Rwanda and Uganda.[2,9-15] Molecular studies have confirmed the presence of nonsynonymous mutations in *Pfkelch13* (PF3D7_1343700), the primary determinant of ART-R.[16,17] These mutations include R561H in Rwanda, and C469Y and A675V in Uganda. All three variants, associated with delayed parasite clearance and/or D3+, have displayed increasing prevalence over time (7.8% in 2015 to 12.8% in 2018 in Rwanda, and 3.9% in 2015 to 19.8% in 2019 in Uganda).[11,13] *Ex vivo* and *in vitro* assays measuring survival rates of *Pfkelch13* R561H and C469Y parasites (either gene-edited lines or field isolates) support these mutations as markers of *in vitro* ART-R.[11,12] Genomic analyses have demonstrated the independent emergence and local expansion of these *Pfkelch13* mutants.[11-13]

In Eritrea, artesunate-amodiaquine (ASAQ), first introduced in 2007 as treatment for uncomplicated falciparum malaria, is now available free of charge both at health facilities and the community level. In 2015, a single dose of primaquine was added to ASAQ as a

transmission-blocking agent.[15] Artemether-lumefantrine (AL) was implemented in 2019 at health facilities as an alternative first-line treatment for uncomplicated malaria (all *Plasmodium* species).

Here, we describe the results of therapeutic efficacy studies conducted between 2016-2019 at five sites in Eritrea evaluating ASAQ and AL treatment for uncomplicated falciparum malaria. We assessed the proportion of D3+ patients and assayed parasites for molecular signatures of ART-R. We also screened for deletions in *hrp2* and *hrp3* that result in variable performance of HRP2-based malaria rapid diagnostic tests (RDTs).

Methods

Study design, areas and population

Open-label, single-arm, multi-site clinical drug efficacy studies were designed to assess clinical ART-R in Eritrea, as determined by the proportion of D3+ patients after a 3-day ACT treatment with ASAQ or AL. These are recommended in Eritrea as first- and second-line treatments, respectively, for uncomplicated falciparum malaria.[2] Studies were conducted in 2016, 2017 and 2019 at health centers or regional hospitals at five sites in western Eritrea. Patient were at least six months old, and eligibility was determined according to WHO inclusion and exclusion criteria (***Supplementary Information***).

Treatment, follow-up procedure and outcomes

Patients who consented to participate were assigned a supervised standard 3-day course of ASAQ (2016 and 2019) or AL (2017) and monitored clinically throughout. Thick and thin blood smears were obtained by finger prick upon recruitment (day0), and during follow up visits on days 1, 2, 3, 7, 14, 21 and 28 to screen for *P. falciparum* and estimate parasite

density. Additional follow up visits were scheduled if further symptoms occurred. Samples of dried blood spots (DBS) on filter papers were used for molecular studies. The primary outcome was the proportion of D3+ patients, as assessed by microscopic examination of thick blood smears after 3-day ACT treatment. [2] We also evaluated, as a secondary outcome, the PCR-adjusted clinical response to the designated treatment on day28 (***Supplementary Information***).

DNA extraction and molecular analysis

Parasite DNA was extracted from pre- and post-treatment (in case of recurrence) DBS using the QIAamp DNA Blood Mini Kit (Qiagen). Genotyping was carried out by PCR and post treatment infections were either classified as recrudescence (same genotype as day0) or new infections (different genotype) using the polymorphic genetic markers *msp1*, *msp2,* and *polyα*.[18]

Paired DNA samples (day0 and day of recurrence) were analyzed for mutations in the propeller domain of *Pfkelch13* (codons 430-720) and in *pfcrt*, *pfmdr-1, dhfr* and *dhps*, which are associated with decreased parasite susceptibility to artemisinin derivatives, 4-aminoquinolines (notably piperaquine and chloroquine), amino-alcohols (including mefloquine and lumefantrine), pyrimethamine, and sulfadoxine, respectively.[19] We also screened for *hrp2* and *hrp3* deletions that can cause false-negative results with HRP2-based rapid diagnostic tests (RDTs).[20]

Whole-genome sequencing was performed by Illumina paired-end sequencing after selective amplification of parasite DNA.[21] Read alignments against the 3D7 genome (v45) were used to infer a phylogenetic tree. The Genome Analysis Toolkit was used to identify SNPs, genotype isolates, and assess the genetic identity of *Pfkelch13* mutants from Eritrea. Principal

158 Coordinate Analysis (PCoA), hierarchical clustering as well as AMOVA (Analysis of
159 Molecular Variance) were performed based on pairwise Euclidean genetic distances between
160 samples (***Supplementary Information***).
161
162 **Generation of gene-edited lines and *in vitro* susceptibility assays.**
163 The *Pfkelch13* R622I mutation was introduced into African (NF54) and Asian (Dd2) parasite
164 lines by CRISPR/Cas9-mediated gene editing. *In vitro* ART susceptibilities of edited parasites
165 and wild-type controls were assessed using the Ring Stage Survival Assay ($RSA_{0–3h}$) [22]
166 (***Supplementary Information***).
167
168 **Statistical analysis**
169 Experimental data were analyzed with GraphPad Prism 9.3.1 (GraphPad Software). Mann–
170 Whitney U tests (two-sided) were used for non-parametric comparisons. Chi-squared or
171 Fisher's exact tests (one-sided) were used for frequency data (expressed as percentages with
172 95% confidence intervals). Associations between clinical outcomes and genotypes were
173 assessed using Fisher's exact test and multiple regression analysis. Odds ratios were estimated
174 using the Cochran–Mantel–Haenszel test. Two-sided *p*-values lower than 0.05 were
175 considered to indicate statistical significance.
176
177 ## Results
178 **Participants and study design.**
179 A total of 852 patients with uncomplicated falciparum malaria were enrolled (***Table 1***). Of
180 these, 841 (98.7%) and 825 (96.8%) were assessed for D3+ rate and clinical efficacy
181 outcome, respectively. Remaining patients either withdrew consent (n=10) or were lost to
182 follow-up (n=17) (***Fig. S1***).

Day3 positivity rate (D3+).

Twenty patients (2.4%, 20/841) from Guluj, Shambuko and Tokombia remained parasitemic on day3 post treatment (***Table S1, Fig. 1A***). D3+ rates significantly increased from 2016 (0.4%, 1/273) to 2019 (4.2%, 15/359, p=0.002, chi-squared for trend). The highest D3+ rates were seen at Tokombia (10.2%) and Shambuko (5.7%) in 2019. A total of 825/852 (96.8%) participants reached the study endpoints ***(Table S2***). Of the 27 recurrent infections, 17 were classified as recrudescent. PCR-corrected per-protocol and Kaplan-Meier estimates of ASAQ and AL treatment efficacies were >94%, above the threshold recommended by the WHO for treatment policy change (90%) (***Tables S3-S5)***.

Pfkelch13 **genotyping.**

Of the 828 available pre-treatment samples, 818 (98.8%) were successfully genotyped. Twelve *Pfkelch13* non-synonymous mutations were detected in 120 samples (***Table 1***). The *Pfkelch13* R561H mutation, a validated marker for ART-R, was observed in one isolate (Shambuko, 2019).[12,13] A novel *Pfkelch13* R622I mutation was detected at high frequency (13.3%, 109/818). The prevalence of this variant markedly increased from 2016-2017 (24/278, 8.6% and 16/211, 7.6%, respectively) to 2019 (69/329, 21.0%, p=0.01) (***Fig. 1B-1C, Table S6***). In 2019, the prevalence was 8.1% in Shambuko, 21.9% in Guluj, 26.2% in Akordat, and 29.1% in Tokombia.

Validation of the *Pfkelch13* R622I mutation as a novel marker of ART-R.

Association with delayed parasite clearance (D3+). The proportion of the *Pfkelch13* 622I variant prior to treatment was significantly higher in D3+ patients (9/20, 45%) compared to D3- patients (97/787, 12.3%, p=0.0004). *In vivo* ART-R was confirmed in Eritrea as the

proportion of D3+ patients (aged <15 years) harboring *Pfkelch13* 622I mutant parasites at day0 was >5% in Tokombia (7.0% in 2019) and Shambuko (5.4% in 2017) (***Table S7***).[23] The *Pfkelch13* 622I variant was found to be a major predictor of D3+ by multivariable analysis (OR 6.4, 95% CI 2.3-17.6, p=0.0003) (***Table 2***).

While ASAQ treatment failure rates were similar between patients with *Pfkelch13* 622I mutant and wild-type parasites in day0 isolates (2/87, 2.3% vs. 15/495, 3.0%, p=1.0), *Pfkelch13* genotyping of paired isolates from day0 and the day of recrudescence indicated selection of the 622I mutant following ASAQ administration (4.4-fold increase from 12% at day0 to 53% at day of recrudescence, p=0.02). Using amplicon deep sequencing, we detected the presence of *Pfkelch13* 622I genotypes in minor proportions (1.4%-3.2%) in 7 of 9 day0 samples previously classified as wild-type, providing evidence of intra-host selection after administration of ASAQ (***Table S8***).

In vitro survival rate of the Pfkelch13 622I mutant. The *Pfkelch13* R622I mutation was edited into NF54 (African) and Dd2 (Asian) parasites, and recombinant clones were tested in the $RSA_{0–3h}$ that measures the survival of early ring-stage parasites exposed to 700 nM DHA for 6 hr. Survival >1% (relative to mock-treated parasites) after 3 days indicates *in vitro* ART-R. Results showed that the *Pfkelch13* R622I mutation conferred low-level ART-R in $NF54^{R622I}$ parasites compared to the isogenic wild-type (WT) control line (3.3% versus 0.6%, p<0.0001, Mann–Whitney U-test). *In vitro* resistance was borderline in the $Dd2^{R622I}$ line (1.5% in the mutant versus 0.7% in the isogenic control, p=0.28). In NF54 parasites, the R622I mutation conferred somewhat lower levels of resistance than the C580Y mutation that predominates across Southeast Asia ($RSA_{0–3h}$ survival rate of 4.3%, p=0.001) (***Fig. 2***).

Origins of the *Pfkelch13* 622I genotype. We compared whole-genome sequences of 291 samples, including 128 Eritrean *P. falciparum* sequences generated for this study, 162 publicly available sequences, and the 3D7 reference genome from Africa (***Table S9***). A maximum-likelihood phylogenetic tree showed that the *Pfkelch13* 622I mutants were scattered within East African wild-type isolates (***Fig. 3***).

We then explored haplotype diversity in the genomic regions flanking the R622I mutation. A PCoA based on a pairwise genetic distance matrix indicated a shared genetic background between Eritrean 622I mutants and wild-type isolates (***Fig. S2-S3***). Haplotype similarity in a ~300 kb region around the mutation pointed to a shared ancestry among mutants found across different sites (***Fig. S4***). In the absence of accurate estimates of recombination rates in populations of *P. falciparum*, the age of the R622I mutation could not be properly assessed. Nevertheless, the limited segment of haplotype homozygosity, as well as the lack of space/time structure in the distribution of haplotypes, do not suggest a recent clonal expansion of the *Pfkelch13* R622I mutation (***Fig. S5-S6, Table S10***).

Genetic backgrounds of Eritrean *Pfkelch13* 622I variants. We investigated the genetic background of Eritrean *Pfkelch13* 622I mutants by profiling both mutant and wild-type parasites at known antimalarial drug resistance loci, and by measuring the frequency of *hrp2* and *hrp3* gene deletions, a genomic feature previously observed in Eritrean *P. falciparum* (***Table S11***).[24]

We assessed 67 *Pfkelch13* 622I and 311 wild-type parasite samples for mutations in four genes. Significant differences were observed in the *pfcrt* and *dhfr* genes, whose variants can confer resistance to chloroquine/piperaquine and pyrimethamine, respectively.[25] Most of the

Pfkelch13 622I mutants carried PfCRT M74I/N75E/K76T mutations (present in 92.5% of the 622I mutants vs. 66.9% of *Pfkelch13* wild-type parasites, p=0.0001), and N51I/S108N DHFR mutations (74.6% of mutants *vs.* 49.5% of wild-type parasites, p=0.0001).

We evaluated 29 *Pfkelch13* 622I and 139 wild-type parasites for amplification of *plasmepsin2* or *multidrug resistance-1*, as these are considered markers of reduced susceptibility to piperaquine and lumefantrine/mefloquine, respectively.[25] No parasites had *pfmdr-1* amplification, and the proportion of isolates harboring ≥ 2 copies of *plasmepsin-2* was similar in both mutant (31.0%) and wild-type (32.4%, *p=0.3*) parasites.

We also tested for deletions in the *hrp2* and *hrp3* genes amongst 65 *Pfkelch13* 622I mutant and 280 wild-type parasites. The majority (69.2%, 45/65) of *Pfkelch13* 622I parasites had an *hrp3* deletion (vs. 22.5%, 63/280 in wild-type parasites, $p<10^{-4}$). More worryingly, we detected a substantial proportion of 622I mutant parasites with both *hrp2* and *hrp3* deletions (16.9%, 9/65 vs. 21.8%, 61/280 for wild-type parasites, p=0.3), potentially threatening the efficacy of HRP2-based RDTs. No *Pfkelch13* 622I mutant parasites had only *hrp-2* gene deletions (vs. 5.7%, 16/280 for wild-type parasites, p=0.05).

Discussion

P. falciparum partial resistance to artemisinin is now firmly established in Africa. While to date ART-R has only been confirmed in Central (Rwanda) and East (Uganda) Africa,[11-13] here we provide evidence of an additional hotspot of ART-R in the Horn of Africa.[23] More worryingly, the emergence and spread of a novel *Pfkelch13* 622I mutant lineage was accompanied by deletions in the *hrp2/hrp3* genes in a substantial proportion of parasites (16.9%), rendering these parasites likely undetectable by HRP2-based RDTs.

In vivo ART-R in Eritrea was evidenced by the significant increase over time in the proportion of D3+ patients following ACT treatment (from 0.4% in 2016 to 4.2% in 2019). We also witnessed a substantial rise in the proportion of *Pfkelch13* 622I mutant parasites (from 8.6% in 2016 to 21.0% in 2019). We confirmed that this mutation, which has not been observed previously in Southeast Asia, confers *in vitro* ART-R in the African parasite strain NF54, at slightly lower levels than the C580Y mutation that predominates in Southeast Asia (mean $RSA_{0\text{-}3h}$ survival rate of 3.3% vs. 4.3%, respectively). The R622I mutation conferred only low-level survival (1.5%) in Dd2 parasites (an Asian reference strain), consistent with prior evidence that *Pfkelch13* mutations do not afford resistance across all strains, and that ART-R levels can be substantially modulated by the parasite genetic background.[26] We also documented significant intra-host selection of the *Pfkelch13* 622I mutation in recrudescent infections following ASAQ treatment (from 12% at day0 to 53% at day28, a 4.4-fold increase). These findings validate the *Pfkelch13* 622I mutation as a molecular marker of ART-R.

Eritrean *Pfkelch13* 622I mutants were phylogenetically closely related to other African parasites. They clustered with both Eritrean and Ethiopian wild-type isolates. Hallmarks of the spread of a newly arisen mutation would be expected to include extended haplotype homozygosity in the genomic region flanking the *Pfkelch13* 622I mutation. By contrast, we observed a limited identity of core haplotypes among mutants. This might reflect the spread of a pre-existing *Pfkelch13* resistance allele in *P. falciparum* populations from the Horn of Africa. This finding is supported by previous reports of low frequency detection of the *Pfkelch13* 622I variant in Eritrea and neighbouring countries (0.8% in Eritrea in 2013-14, 2.4% in Ethiopia in 2013-14, 0.7% in Somalia in 2016-17, and 0.3% in Zambia in 2012)[27-30], and in Chinese travellers returning from Mozambique or Somalia (2016-18).[31]

Although recent data on treatment efficacy at sites with high prevalence of *Pfkelch13* mutants are limited in Eritrea,[32-34] we observed high cure rates with both ASAQ and AL for uncomplicated falciparum malaria (> 94%), presumably attributable to the continued efficacy of the partner drugs amodiaquine and lumefantrine. These data are concordant with recent reports in Rwanda for AL.[13] Lower efficacy rates for AL (<90%), recently reported in some free ART-R areas (Angola,[35] the Democratic Republic of the Congo[36] and East central Uganda[37]), remain highly questionable as the methodological deviation from WHO standard genotyping protocol might have potentially underestimated the efficacy of AL.

Our study also reports that a substantial proportion (16.9%) of *Pfkelch13* 622I mutant parasites had deletions in both the *hrp2* and *hrp3* genes (a similar proportion to *Pfkelch13* wild-type parasites), potentially resulting in false-negative results in HRP2-based RDTs.[20] This genomic trait, frequently observed in Eritrea[38] with prevalences ranging from 7% in Shambuko up to 81% in Ghindae[24] resulted in a policy switch to pLDH-based RDTs in 2016. This emphasizes the need to conduct further research to evaluate the performance of pLDH-based RDTs for detecting *Pfkelch13* 622I mutant with dual *hrp2/3* deletions.

Over the past two decades, Eritrea has achieved substantial reductions in malaria morbidity and mortality through active leadership at all levels of government and effective implementation of Insecticide-Treated Nets (ITNs), Indoor Residual Spraying (IRS), larvicidal activities and malaria case management.[39,40] However, decreased malaria prevalence may in turn have favored the emergence and spread of artemisinin-resistant parasites by reducing parasite genetic diversity and naturally acquired immunity, and increasing per-patient drug pressure as fewer infections are naturally cleared and therefore

require treatment.[41] These data suggest that in settings where strategies to reduce malaria transmission are efficiently implemented, surveillance of the emergence and spread of drug resistance must be prioritized.

Our findings confirm *P. falciparum* ART-R along with *hrp2/hrp3* gene deletions in parasite populations from Eritrea. Strategies to contain the spread of these lineages across the Horn of Africa are urgently needed, as the potential occurrence of partner drug resistance could lead to high treatment failure rates and uncontrolled expansion of *P. falciparum hrp2/hrp3*-deleted parasites out of this region. Genomic-based surveillance of *Pfkelch13* mutations and *hrp2/hrp3* deletions must be sustained and strengthened to avoid a catastrophic scenario.

Contributions

S.M., A.B., A.Z.K., P.R., D.A.F. and D.M. contributed to study design. SM, AB and AZK, M.W. supervised the clinical drug studies, collected clinical samples and data.
L.P., N.P., E.L., C. D-L, L.A. and D.M. prepared the DNA. C. D-L, L.A., N.P., L.M., P.C., A.C. and D.M. performed the sequencing and sequence analyses.
B.H.S., K.E.W, D.A.F., L.P., E.L. and D.M. performed genome-editing and in vitro assays.
S.M., A.B., A.Z.K., P.C., A.C., P.R., D.A.F. and D.M. analyzed data. D.M wrote the first draft of the manuscript, with contributions from D.A.F, K.E.W., B.H.S., P.R., M.W., S.M. and A.B. All authors reviewed and approved the manuscript. S.M., A.B., A.Z.K., D.A.F, P.R., and D.M decided to publish the paper.

Acknowledgments

We thank all patients who contributed samples and their guardians in the communities of Akordat, Ghindae, Guluj, Shambuko and Tokombia, and all team members in the health

centers. We are also grateful to the members of the national Malaria Control Programme in Eritrea for their support. We acknowledge the help HPC Core Facility of the Institut Pasteur for this work as well as the Biomics Platform, C2RT, Institut Pasteur, Paris, France (supported by France Génomique, ANR-10-INBS-09 and IBISA). We are grateful to ICAReB team of the CTS (Center for Translational Science) and CRBIP (BioResource Center of Institut Pasteur) for providing blood samples from healthy volunteers, to Hélène Laude, Laurence Arowas, Ayla Zayoud and Marie Noelle Ungeheuer for managing the participants' visits, to the healthy volunteers for their participation in the study, and to Emmanuel Roux, Alain Li, Dorian Cheval, Sophie Vacant, Sophie Chaouche, Elsa Lievin for preparing the blood samples from donors. We thank Aurélie Claës (Biology of Host-Parasite Interactions Unit, INSERM U1201, Institut Pasteur, Paris, France) for providing advice on *P. falciparum* genome editing.

Funding

Funding was obtained from the Bill and Melinda Gates Foundation through the World Health Organization (grant no. OPP1209843). The study was also supported by the Institut Pasteur, Paris, the French Government (Agence Nationale de la Recherche), Laboratoire d'Excellence (LabEx) "French Parasitology Alliance for Health Care" (ANR-11-15 LABX-0024-PARAFRAP), and the University of Strasbourg through the Programme IdEX 2022 (Attractivité - Dotation d'accueil des professeurs d'université recrutés en 2021) to DM. DAF gratefully acknowledges funding from the US National Institutes of Health (R01 AI109023).

Conflict of Interest

None of the authors declared a conflict of interest or any agreements concerning confidentiality of the data between the sponsor and the authors, or the institutions named in

the funding section. P.R. and A.Z.K. are staff members of the World Health Organization. The authors alone are responsible for the views expressed in this publication and they do not necessarily represent the decisions, policies, or views of the World Health Organization.

References

1. Bhatt S, Weiss DJ, Cameron E, et al. The effect of malaria control on *Plasmodium falciparum* in Africa between 2000 and 2015. Nature 2015;526:207-11.

2. World Health Organization. Report on antimalarial drug efficacy, resistance and response: 10 years of surveillance (2010–2019). 2020.

3. Ashley EA, Dhorda M, Fairhurst RM, et al. Spread of artemisinin resistance in *Plasmodium falciparum* malaria. N Engl J Med 2014;371:411-23.

4. Dondorp AM, Nosten F, Yi P, et al. Artemisinin resistance in *Plasmodium falciparum* malaria. N Engl J Med 2009;361:455-67.

5. Noedl H, Socheat D, Satimai W. Artemisinin-resistant malaria in Asia. N Engl J Med 2009;361:540-1.

6. Imwong M, Suwannasin K, Srisutham S, et al. Evolution of multidrug resistance in *Plasmodium falciparum*: a longitudinal study of genetic resistance markers in the Greater Mekong Subregion. Antimicrob Agents Chemother 2021;65:e0112121.

7. Jacob CG, Thuy-Nhien N, Mayxay M, et al. Genetic surveillance in the Greater Mekong subregion and South Asia to support malaria control and elimination. Elife 2021;10.

8. van der Pluijm RW, Imwong M, Chau NH, et al. Determinants of dihydroartemisinin-piperaquine treatment failure in *Plasmodium falciparum* malaria in Cambodia, Thailand, and Vietnam: a prospective clinical, pharmacological, and genetic study. Lancet Infect Dis 2019;19:952-61.

9. Assefa DG, Yismaw G, Makonnen E. Efficacy of dihydroartemisinin-piperaquine versus artemether-lumefantrine for the treatment of uncomplicated *Plasmodium falciparum* malaria among children in Africa: a systematic review and meta-analysis of randomized control trials. Malar J 2021;20:340.

10. Asua V, Conrad MD, Aydemir O, et al. Changing prevalence of potential mediators of aminoquinoline, antifolate, and artemisinin resistance across Uganda. J Infect Dis 2021;223:985-94.

11. Balikagala B, Fukuda N, Ikeda M, et al. Evidence of artemisinin-resistant malaria in Africa. N Engl J Med 2021;385:1163-71.

12. Uwimana A, Legrand E, Stokes BH, et al. Emergence and clonal expansion of *in vitro* artemisinin-resistant *Plasmodium falciparum kelch13* R561H mutant parasites in Rwanda. Nat Med 2020;26:1602-8.

13. Uwimana A, Umulisa N, Venkatesan M, et al. Association of *Plasmodium falciparum kelch13* R561H genotypes with delayed parasite clearance in Rwanda: an open-label, single-arm, multicentre, therapeutic efficacy study. Lancet Infect Dis 2021;21:1120-8.

14. White NJ. Malaria parasite clearance. Malar J 2017;16:88.

15. World Health Organization. World malaria report 2021. 2021.

16. Ariey F, Witkowski B, Amaratunga C, et al. A molecular marker of artemisinin-resistant *Plasmodium falciparum* malaria. Nature 2014;505:50-5.

17. Straimer J, Gnadig NF, Witkowski B, et al. Drug resistance K13-propeller mutations confer artemisinin resistance in *Plasmodium falciparum* clinical isolates. Science 2015;347:428-31.

18. World Health Organization. Informal consultation on methodology to distinguish reinfection from recrudescence in high malaria transmission areas: report of a virtual meeting, 17–18 May 2021. 2021.

19. Menard D, Dondorp A. Antimalarial drug resistance: a threat to malaria elimination. Cold Spring Harb Perspect Med 2017;7.

20. World Health Organization. False-negative RDT results and implications of new reports of *P. falciparum histidine-rich protein 2/3* gene deletions. 2017.

21. Oyola SO, Ariani CV, Hamilton WL, et al. Whole genome sequencing of *Plasmodium falciparum* from dried blood spots using selective whole genome amplification. Malar J 2016;15:597.

22. Witkowski B, Amaratunga C, Khim N, et al. Novel phenotypic assays for the detection of artemisinin-resistant *Plasmodium falciparum* malaria in Cambodia: in-vitro and ex-vivo drug-response studies. Lancet Infect Dis 2013;13:1043-9.

23. World Health Organization. Artemisinin and artemisinin-based combination therapy resistance. 2016.

24. Mihreteab S, Anderson K, Pasay C, et al. Epidemiology of mutant *Plasmodium falciparum* parasites lacking *histidine-rich protein 2/3* genes in Eritrea 2 years after switching from HRP2-based RDTs. Sci Rep 2021;11:21082.

25. Wicht KJ, Mok S, Fidock DA. Molecular mechanisms of drug resistance in *Plasmodium falciparum* malaria. Annu Rev Microbiol 2020;74:431-54.

26. Stokes BH, Dhingra SK, Rubiano K, et al. *Plasmodium falciparum* K13 mutations in Africa and Asia impact artemisinin resistance and parasite fitness. Elife 2021;10.

27. Bayih AG, Getnet G, Alemu A, Getie S, Mohon AN, Pillai DR. A Unique *Plasmodium falciparum* K13 gene mutation in northwest Ethiopia. Am J Trop Med Hyg 2016;94:132-5.

28. L'Episcopia M, Kelley J, Patel D, et al. Targeted deep amplicon sequencing of *kelch 13* and *cytochrome b* in *Plasmodium falciparum* isolates from an endemic African country using the Malaria Resistance Surveillance (MaRS) protocol. Parasit Vectors 2020;13:137.

29. Menard D, Khim N, Beghain J, et al. A worldwide map of *Plasmodium falciparum* K13-propeller polymorphisms. N Engl J Med 2016;374:2453-64.

30. Warsame M, Hassan AM, Hassan AH, et al. High therapeutic efficacy of artemether-lumefantrine and dihydroartemisinin-piperaquine for the treatment of uncomplicated falciparum malaria in Somalia. Malar J 2019;18:231.

31. Wang X, Ruan W, Zhou S, et al. Molecular surveillance of *Pfcrt* and *k13* propeller polymorphisms of imported *Plasmodium falciparum* cases to Zhejiang Province, China between 2016 and 2018. Malar J 2020;19:59.

32. Mohammed AO, Tewolde S, Estifanos D, Tekeste Y, Osman MH. Therapeutic efficacy of artesunate - amiodaquine for treating uncomplicated falciparum malaria at Ghindae Zonal Referral Hospital, Eritrea. Acta Trop 2018;177:94-6.

33. Ghebremeskel T. Therapeutic efficacy of sulfadoxine/pyrimethamine plus chloroquine and artesunate plus amodiaquine for the treatment of uncomplicated flaciparum malaria. J Eritrean Med Assoc 2007; 2, 14–16. .

34. Mihreteab M, Berhane A, Berhane D, Zehaie A, Araia A, Banteyrga L. Therapeutic efficacy study on artesunate + amodiaquine (AS + AQ) for the treatment of uncomplicated *Plasmodium falciparum* (Pf) malaria in Eritrea. . J Eritrean Med Assoc 2014;1, 9–12.

35. Dimbu PR, Horth R, Candido ALM, et al. Continued low efficacy of artemether-lumefantrine in Angola in 2019. Antimicrob Agents Chemother 2021;65.

36. Moriarty LF, Nkoli PM, Likwela JL, et al. Therapeutic efficacy of artemisinin-based combination therapies in Democratic Republic of the Congo and investigation of molecular markers of antimalarial resistance. Am J Trop Med Hyg 2021;105:1067-75.

37. Ebong C, Sserwanga A, Namuganga JF, et al. Efficacy and safety of artemether-lumefantrine and dihydroartemisinin-piperaquine for the treatment of uncomplicated *Plasmodium falciparum* malaria and prevalence of molecular markers associated with artemisinin and partner drug resistance in Uganda. Malar J 2021;20:484.

38. Berhane A, Anderson K, Mihreteab S, et al. Major threat to malaria control programs by *Plasmodium falciparum* lacking histidine-rich protein 2, Eritrea. Emerg Infect Dis 2018;24:462-70.

39. Barat LM. Four malaria success stories: how malaria burden was successfully reduced in Brazil, Eritrea, India, and Vietnam. Am J Trop Med Hyg 2006;74:12-6.

40. Nyarango PM, Gebremeskel T, Mebrahtu G, et al. A steep decline of malaria morbidity and mortality trends in Eritrea between 2000 and 2004: the effect of combination of control methods. Malar J 2006;5:33.

41. Scott N, Ataide R, Wilson DP, et al. Implications of population-level immunity for the emergence of artemisinin-resistant malaria: a mathematical model. Malar J 2018;17:279.

Figure legends

Fig. 1. Evidence of delayed parasite clearance associated with the expansion of the mutant *Pfkelch13* 622I in Eritrea (A) Proportions of D3+ rate per site and year. Day3 parasitemia cases were not observed in Akordat (2016, 2017 and 2019), Ghindae (2017, no data were available in 2016 and 2019), Guluj (2016 and 2017), and Tokombia ((2016 and 2017). (B) Allele frequency of *P. falciparum kelch13* 622I mutant parasites per site and year. Only *Pfkelch13* wild-type parasites were observed in Akordat and Ghindae in 2017 (no data were available in 2016 and 2019). (C) Distribution of *Pfkelch13* genotypes per site and year. The proportions of each *Pfkelch13* allele are shown per year in pie charts (except for Ghindae where only 2017 data were available). The frequency for the *Pfkelch13* wild type allele is shown in dark blue, the *Pfkelch13 622I* allele is in red and the other *Pfkelch13* mutants are in yellow. The size of the pie chart is proportional to the sample size. The study sites colored in green correspond to areas where no D3+ case was observed. The study sites where D3+ cases where detected are colored in red (Guluj, Tokombia, and Shambuko).

Fig. 2. *Pfkelch13* R622I mediates low-level artemisinin resistance in *P. falciparum* parasites. Results show the percentage of early ring-stage parasites (0–3 hours post-invasion) that survived a 6-hour pulse of 700 nM DHA, relative to DMSO-treated parasites assayed in parallel. Percent survival values are shown as means ± SEM. Results were obtained from two ($Dd2^{WT}$) to three ($NF54^{WT}$, $Dd2^{R622I}$, $NF54^{R622I}$ and $NF54^{C580Y}$) independent experiments, each performed in duplicate ($Dd2^{WT}$ and $Dd2^{R622I}$) or triplicate ($NF54^{WT}$, $NF54^{R622I}$ and $NF54^{C580Y}$). p-values were determined by unpaired t-tests and were calculated for *Pfkelch13* mutant lines relative to their isogenic wild-type lines and relative to $NF54^{C580Y}$ for $NF54^{R622I}$. ** $p<0.01$; *** $p<0.001$; **** $p<0.0001$.

Fig. 3. Genome-wide phylogenetic tree. This maximum-likelihood tree is based on 128 *P. falciparum* Eritrean isolates (red), together with 163 isolates collected worldwide (Africa, Asia and South America). Labels of Eritrean isolates include the year of collection. The non-Eritrean isolates were sourced from the MalariaGEN *P. falciparum* Community Project (https://www.malariagen.net/apps/pf/4.0) and are labelled with their accession identifier. Each leaf represents one sample and is colored according to the country of collection (bottom). Eritrean parasites carrying the *Pfkelch*13 622I mutation are identified by filled red stars at the tip. Eritrean *Pfkelch*13 622I mutants are closely related to *Pfkelch*13 wild type parasites originating from East African countries. Scale bar, 0.00005 nucleotide substitutions per character.

585 **Table 1.** Characteristics of the participants with measured D3+ rate and detected *Pfkelch13*
586 genotypes from blood samples collected prior to artemisinin-based combination therapy
587 according by study year.

		2016	2017	2019	Total
Baseline characteristics					
Study period		Jan-Dec	Sept-Dec	Aug-Nov	-
No. of patients		280	211	361	852
Antimalarial treatment		ASAQ	AL	ASAQ	-
Site	Akordat	58	19	88	165
	Ghindae	-	15	-	15
	Guluj	73	25	97	195
	Shambuko	73	64	88	225
	Tokombia	76	88	88	252
Median age, years (IQR)		13.0 (8.0-19.0)	13.0 (9.0-22.7)	17.5 (12.0-29.0)	15.0 (10.0-25.0)
Gender ratio (Female/Male)		120/160	82/129	119/242	321/531
Median temperature, °C (IQR)		38.0 (38.0-39.0)	38.0 (38.0-38.3)	38.0 (38.0-38.5)	38.0 (38.0-39.0)
Median parasite density, µL (IQR)		7,530 (2,736-18,036)	7,900 (2,677-22,335)	9,312 (2,720-23,933)	8,280 (2,715-21,902)
Day3 positivity (D3+) rate, no. (%)					
Site	Akordat	0/54 (0)	0/19 (0)	0/88 (0)	0/161 (0)
	Ghindae	-	0/15 (0)	-	0/15 (0)
	Guluj	0/71 (0)	0/23 (0)	**1/95 (1.1)**	1/189 (0.5)
	Shambuko	**1/73 (1.4)**	**4/64 (6.2)**	**5/88 (5.7)**	10/225 (4.4)
	Tokombia	0/75 (0)	0/88 (0)	**9/88 (10.2)**	9/251 (3.6)
Total		1/273 (0.4)	4/209 (1.9)	15/359 (4.2)	20/841 (2.4)
Pfkelch13 genotype, no. (%)					
Missing samples		0/280 (0)	0/211 (0)	23/352 (6.5)	23/852 (2.7)
Missing data		2/280 (0.7)	0/211 (0)	9/352 (2.5)	11/852 (1.3)
WT		251/278 (90.3)	193/211 (91.4)	254/329 (77.2)	698/818 (85.3)
Mutant	503 (K>W)		1/211 (0.5)		1/818 (0.1)
	515 (R>G)		1/211 (0.5)		1/818 (0.1)
	520 (V>A)	1/278 (0.3)			1/818 (0.1)
	532 (C>W)			1/329 (0.3)	1/818 (0.1)
	533 (G>N)			1/329 (0.3)	1/818 (0.1)
	543 (I>V)			1/329 (0.3)	1/818 (0.1)
	548 (G>C)			1/329 (0.3)	1/818 (0.1)
	556 (E>K)			1/329 (0.3)	1/818 (0.1)
	561 (R>H)			**1/329 (0.3)**	**1/818 (0.1)**
	591 (G>N)	1/278 (0.3)			1/818 (0.1)
	622 (R>I)	**24/278 (8.6)**	**16/211 (7.6)**	**69/329 (21.0)**	**109/817 (13.3)**
	658 (K>E)	1/278 (0.3)			1/817 (0.1)

588

589

590

591

592

593

Table 2. Multiple regression analysis for D3+ rate among 840 cases, Eritrea, 2016-2019.

Variable	Coefficient	Std. Error	Wald	P-value	Odds ratio (95% CI)
Age	0.0036136	0.016711	0.04676	0.82	-
Sex (Male)	0.17415	0.50965	0.1168	0.73	-
Initial parasitemia	0.000012578	0.0000067282	3.4948	0.06	-
Site= Ghindae	1.64848	29881.92895	3.043324611027^{E}-9	1.00	-
Site=Guluj	19.00567	8204.66536	0.000005366	0.99	-
Site=Shambuko	21.88580	8204.66531	0.000007115	0.99	-
Site=Tokombia	21.30438	8204.66531	0.000006742	0.99	-
Year	0.63193	0.22607	7.8138	**0.005**	**1.9 (1.2-2.9)**
Pfkelch13 622I	1.85559	0.51749	12.8576	**0.0003**	**6.4 (2.3-17.6)**

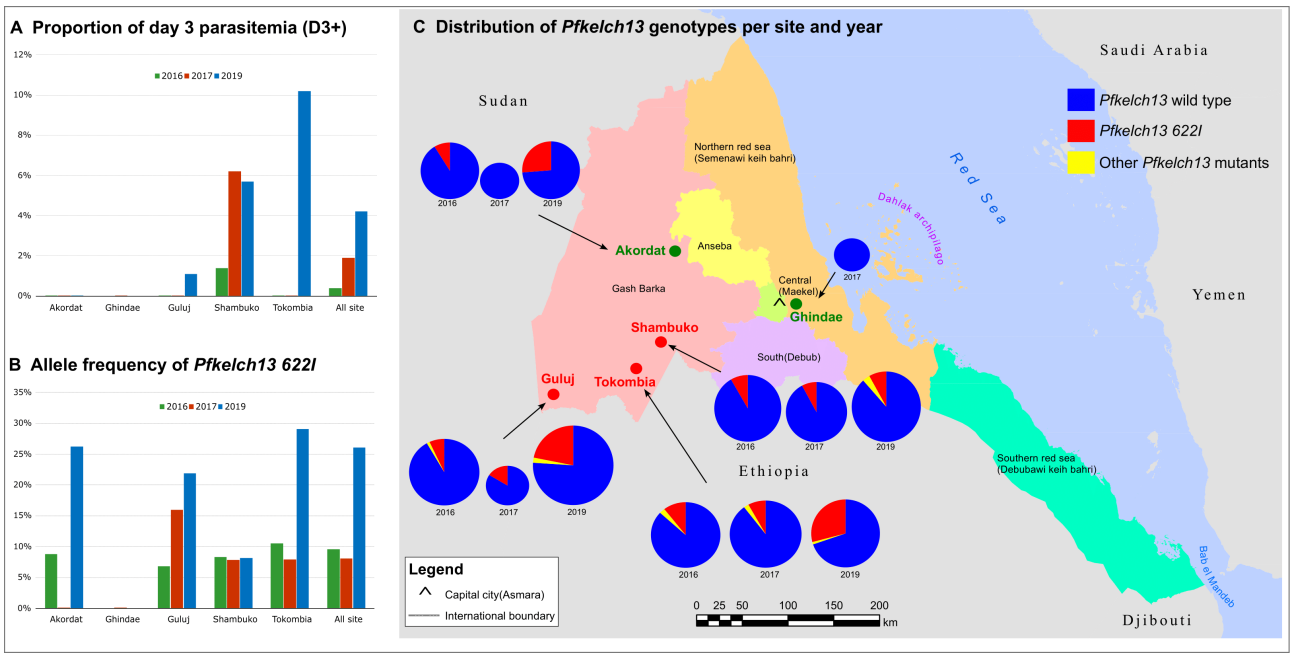

Figure 1

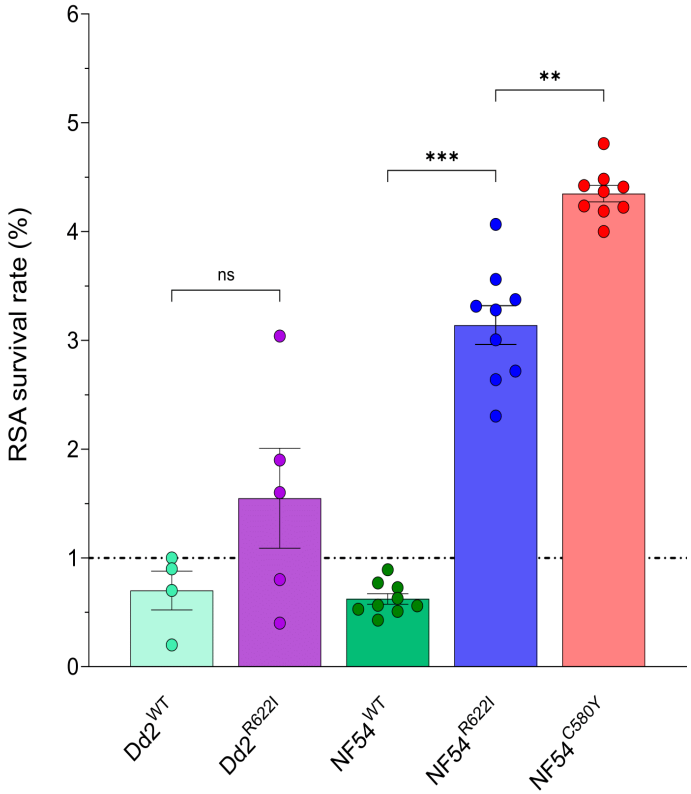

Figure 2

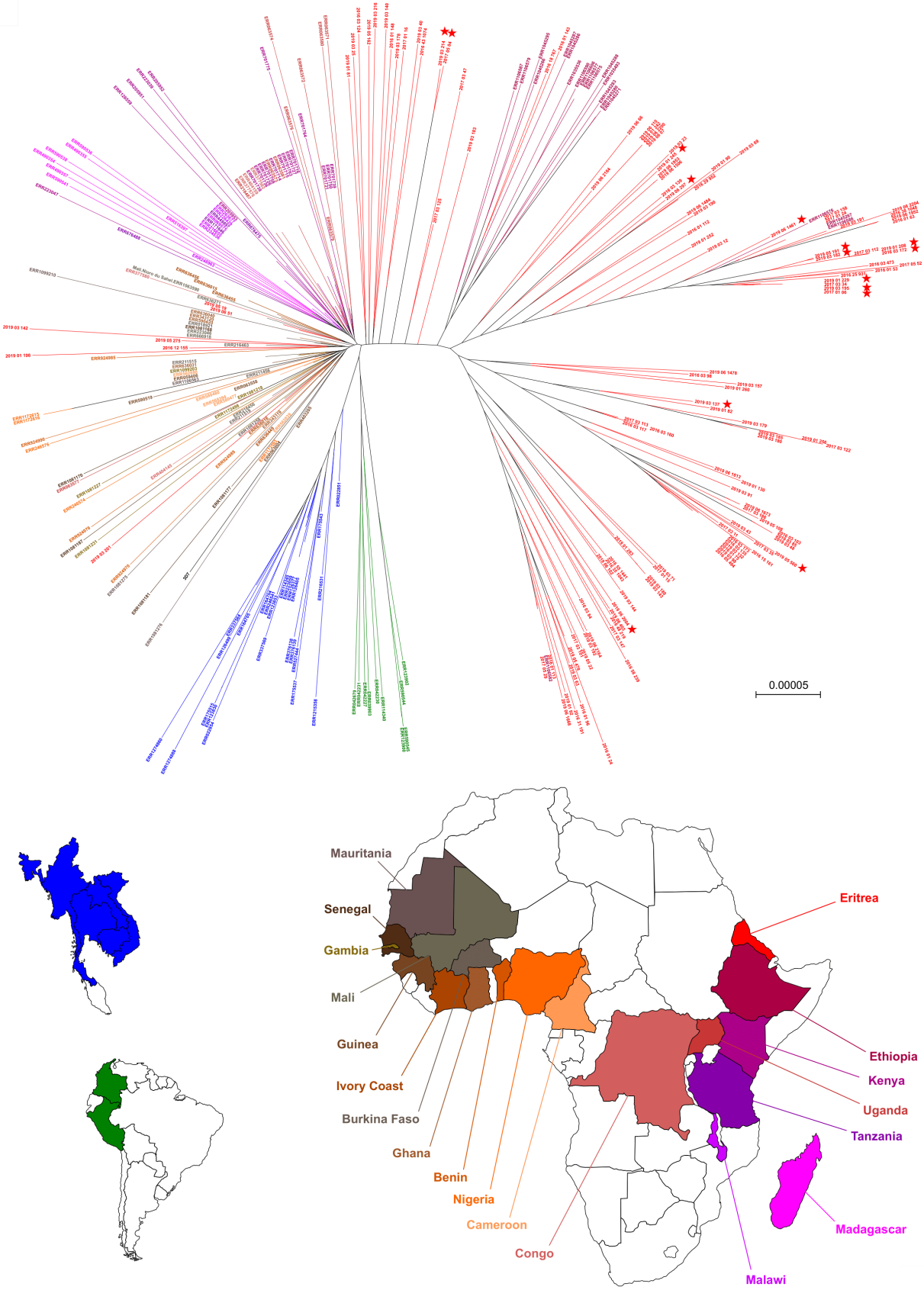
0.00005
Mauritania
Senegal
Gambia
Mali
Guinea
Ivory Coast
Burkina Faso
Ghana
Benin
Nigeria
Cameroon
Congo
Eritrea
Ethiopia
Kenya
Uganda
Tanzania
Madagascar
Malawi

Figure 3

Axe 2 : Optimisation du RSA, principal outil de détection des souches de *P. falciparum* résistantes à l'artémisinine.

Article 2 : Ring-stage Survival Assay de *Plasmodium falciparum* modifié avec l'inhibiteur de kinase ML10.

'Modified *Plasmodium falciparum* Ring-stage Survival Assay with ML10 kinase inhibitor.'

Ce travail avait pour objectif d'optimiser le test RSA, principal outil de diagnostic *in vitro* des souches de *P. falciparum* résistantes à l'artémisinine. En effet, une des limites du test RSA provient de la nécessité d'obtenir des parasites au stade schizonte en quantité suffisante. Les variations de vitesse de progression du cycle asexué du parasite entre les souches de *P. falciparum* rendent la réalisation du test RSA délicate quand plusieurs souches doivent être testées simultanément. L'utilisation du ML10, un inhibiteur de kinase impliqué dans l'éclosion des stades schizontes, permet d'obtenir une synchronisation étroite des parasites. Cette propriété du ML10 a été mise en application pour faciliter la réalisation du test RSA. Nos données indiquent que l'ajout de ML10 n'altère pas le résultat final du test RSA et permet une synchronisation simultanée de souches dont la vitesse de progression du cycle diffère. L'ajout du traitement ML10 à la procédure globale du RSA permet ainsi de tester simultanément la résistance *in vitro* à l'artémisinine de plusieurs souches de façon reproductible et fiable, sans ajouter de manipulation laborieuse supplémentaire. Cette étude a été réalisée en collaboration avec la *London School of Hygiene and Tropical Medicine*. Un article au format court a été soumis dans un journal à comité de lecture, et est actuellement en relecture.

Title: Modified *Plasmodium falciparum* Ring-stage Survival Assay with ML10 kinase inhibitor

Running title: Modified RSA

Lucien Platon[1,2,3], David A. Baker[4], Didier Ménard[1,3,5,6]

[1]Institut Pasteur, Université Paris Cité, Malaria Genetics and Resistance Unit, INSERM U1201, F-75015 Paris, France.

[2]Sorbonne Université, Collège doctoral ED 515 Complexité du Vivant, F-75015 Paris, France.

[3] Institut Pasteur, Université Paris Cité, Malaria Parasite Biology and Vaccines Unit, F-75015 Paris, France.

[4]Faculty of Infectious and Tropical Diseases, London School of Hygiene & Tropical Medicine, London WC1E 7HT, UK.

[5]Université de Strasbourg, Institute of Parasitology and Tropical Diseases, UR7292 Dynamics of Host-Pathogen Interactions, F-67000 Strasbourg, France.

[6]CHU Strasbourg, Laboratory of Parasitology and Medical Mycology, F-67000 Strasbourg, France

Corresponding author: Lucien Platon (lucien.platon@pasteur.fr)

Abstract 75 words

The Ring-stage Survival Assay is the reference assay to measure *in-vitro Plasmodium falciparum* artemisinin partial resistance. The main challenge of the standard protocol is to generate 0-3 hours post-invasion ring-stages (the stage least susceptible to artemisinin) from schizonts obtained by sorbitol treatment and percoll gradient. We report here, a modified protocol facilitating the production of synchronized schizonts when multiple strains are tested simultaneously, by using ML10 a protein kinase inhibitor that reversibly blocks merozoite egress.

Main text 1249 words

Plasmodium falciparum malaria is a vector-borne parasite disease, responsible for 627,000 deaths and 241 million cases in 2021, predominantly in Sub-Saharan Africa (1). Artemisinin-based combination therapies (ACTs), that include a fast and potent artemisinin derivative (ART) and a long half-life companion drug to kill persistent parasites that may survive after ART is metabolized, are currently recommended by the World Health Organization (WHO) as the front-line treatment of uncomplicated *falciparum* malaria (1, 2). Unfortunately, *P. falciparum* partial resistance to artemisinin (ART-R), that emerged in Southeast Asia in 2006-2007 (3, 4) has been detected recently in Africa (5, 6). ART-R, defined as delayed parasite clearance in patients treated with artemisinin monotherapy or 3-days ACT course, is due to the decreased susceptibility of ring-stage parasites to ART. The decreased susceptibility of ring-stage parasites to ART can be measured *in vitro* using the Ring-stage Survival Assay (RSA^{0-3h}) and single point mutations in the gene coding for the propeller domain of the Kelch13 protein (*Pfkelch13,* PF3D7_1343700) strongly correlate with ART-R (7-10).

The most challenging step in performing the standard RSA^{0-3h} is to obtain tightly synchronized ring-stage parasites (0-3 h post-invasion) by sequential use of sorbitol and percoll solutions (9, 11). The subsequent steps, which involve pulsing ring-stages with 700 nM dihydroartemisinin (DHA, the active metabolite of all artemisinin derivatives) for 6 h, washing them and culturing them for 66 h, are straightforward. The survival rate of the assayed parasites (from *ex vivo* isolates or *in vitro* culture-adapted strains) is then calculated relative to dimethyl sulfoxide (DMSO, the vehicle used to dissolve DHA)-exposed parasites (***Figure 1***). While effective, this protocol is laborious, and time-consuming and requires multiple steps over many hours. Moreover, although *in vivo P. falciparum* infection suggests a 48-hour periodicity, *in vitro* and transcriptomic studies showed that *P. falciparum* isolates

can have different period lengths that can vary substantially from 48 hours (from 36 to 54 hours) (12, 13). This difference, genetically controlled, between strains represents a major challenge when multiple strains are tested simultaneously. ML10 is a specific inhibitor of the cGMP-dependent protein kinase that arrests *P. falciparum* growth immediately prior to merozoite egress (14). This compound allows parasite cultures to be synchronized so that all parasites are within a window of development of several minutes, with a simple washing step. As this compound is of unquestionable interest for enrichment of tightly synchronized schizonts required for the RSA^{0-3h}, we developed a modified RSA protocol facilitating simultaneous synchronization of different *P. falciparum* strains.

We tested first the effectiveness of different concentrations of ML10 for blocking merozoite egress. Two parasite lines (3D7-K13-wild-type, an African laboratory strain and a culture-adapted Cambodian strain, Cam1-K13-wild-type) were used (see table S1 for the detailed strain list). The asynchronous cultures were firstly treated with 5%-sorbitol to achieve 0-12h ring-stage synchronization. The cells were cultivated for 20 hours to reach 20-32h trophozoite stage and later exposed to 50, 100, 150 and 200 nM of ML10 or complete RPMI culture medium (RPMI, used as control) for 17h in order to obtain ML10-treated mature 37-49h parasites, when the merozoite egress is happening. This range of concentrations was used to validate the ML10 safety and ensure schizonts tight synchronization necessary for the RSA. Red blood cells were then collected to prepare Giemsa-stained blood smears. Microscopic examination showed that the proportions of RPMI-treated 3D7-K13-wild-type and Cam1-K13-wild-type schizonts were 7.5% and 20.5%, respectively, most of the other blood stages being ring stages. For ML10-treated 3D7-K13-wild-type and Cam1-K13-wild-type parasites, the proportions of schizonts were significantly higher (~3 to 16-fold) compared to RPMI-treated lines, regardless of the concentrations of ML10: 83% and 78.5% at 50 nM, 92% and 84% at 100 nM, 89.5% and 78.5% at 150 nM and 95% and 79.5% at 200 nM, for the 3D7-K13-wild-type and the Cam1-K13-wild-type respectively. ML10 treatment, regardless of the concentrations used, was highly effective at increasing the proportion of schizonts in both strains (***Figure 2***). ML10 was used at 200 nM in the following experiments as it provides satisfactory schizont yield in all strains tested without visible toxicity to parasites.

Next, we estimated the range of the exposure time of ML10 (from 17h to 24h) allowing the schizonts to remain viable when treated at 200 nM. Two parasite lines (3D7-K13-wild-type and Cam2-K13-C580Y), treated with 5%-sorbitol, were cultivated for 20 hours and exposed to ML10 200 nM for 17, 20, 22 or 24 hours, respectively. After ML10 exposure, parasites were isolated using 75%-percoll gradient, washed, placed in culture flasks at 37°C in 5% O2,

5% CO2, and 90% N2 for 3h to allow for re-invasion, treated with 5%-sorbitol to remove residual mature forms and cultivated for additional 24h. Red blood cells were then collected to prepare Giemsa-stained blood smears to estimate the parasite density. All experiments were carried out in duplicate. Viable parasites were detected in all tested conditions (***Figure 3A***). As expected, we noticed a decrease of the parasitaemia from 17h to 24h exposure for both strains. The observed decrease was associated with schizont death caused by prolonged egress inhibition, notably beyond 20 hours exposure to ML10. Of note, we observed in any conditions, all ML10-treated parasites were highly synchronous (at trophozoite-stage) for both strains. Our data suggest that ML10 treatment (from 17h to 20h pulse) is a practical step to produce large amounts of synchronized schizonts, especially when multiple strains are assayed simultaneously.

Lastly, we estimated whether the ML10 pulse had an impact on the survival rates expressed in the RSA^{0-3h}. To this end, both 3D7-K13-wild-type (ART-sensitive) and Cam2-K13-C580Y (ART-resistant) were assayed in triplicate and processed simultaneously using the standard (RPMI) or the modified protocol (ML10 at 200 nM for 17h). We found similar survival rates between both protocols, consistent with previous published data for these *Pfkelch13* genotypes ***(7)***. For the 3D7-K13-wild-type strain, the mean survival rates (±SEM) were 0.20%±0.10% (standard) vs. 0.26% ±0.10% (modified) (p=0.65, Mann-Whitney test) and for the Cam2-K13-C580Y strain, 8.50%±1.10% (standard) vs. 7.80%±0.80% (modified) (p=1.0, Mann-Whitney test) (***Figure 3B***). The laboratory strains Dd2 and NF54 and three additional field isolates from Cambodia were used to validate our modified RSA protocol. The *Pfkelch13* genotypes tested were the wild type as well as three mutations known to confer moderate and high levels of resistance to DHA, including C580Y, R622I and R539T. As shown in Figure S1, the survival rates of the different parasitic lines assayed were consistent with those expected from previous observations based on the Pfkelch13 genotype. To confirm that the viability is maintained not only for 72 hours after DHA but also through successive cycles, we also followed the parasitaemia of two ART-resistant strains (3D7-K13-C580Y and Cam2-K13-C580Y). Both strains remain viable and reach >2% parasitemia in 8 and 12 days for 3D7-K13-C580Y and Cam2-K13-C580Y respectively (see Figure S2). All of these results confirm that ML10 does not alter the survival rate obtained with RSA0-3h and can be successfully used to test a variety of strains simultaneously compared to the standard protocol.

We show here that the use of ML10 can improve the standard RSA protocol for assessing ART-resistance, by facilitating tight 0-3 h ring stage synchronization when multiple strains that might have different period length are tested simultaneously (12, 13). ML10 treatment is

simple to handle and does not add complex steps to the procedure, making it a convenient tool (14). This protocol constitutes a new addition to the other improvements already published regarding the RSA procedure (15-17) (see supplementary table S2 for detailed comparisons). However, additional research is required for assessing its potential impacts on cell signaling, gene transcriptions, metabolomics, and epigenetic regulation.

Acknowledgment.

We would like to thank Simon Osborne from LifeArc for supplying ML10. ML10 is available at MR4 (BEI Resources) https://www.beiresources.org/Collection/54/MR4-Malaria-Resources.aspx?f_displaysearchname=Proteins%23%7E%23Monoclonal%2BAntibodies&page=1

References

1. World Health Organization. 2021. World Malaria Report 2021.

2. Nosten F, White NJ. 2007. Artemisinin-based combination treatment of falciparum malaria. Am J Trop Med Hyg 77:181-92.

3. Dondorp AM, Nosten F, Yi P, Das D, Phyo AP, Tarning J, Lwin KM, Ariey F, Hanpithakpong W, Lee SJ, Ringwald P, Silamut K, Imwong M, Chotivanich K, Lim P, Herdman T, An SS, Yeung S, Singhasivanon P, Day NP, Lindegardh N, Socheat D, White NJ. 2009. Artemisinin resistance in *Plasmodium falciparum* malaria. N Engl J Med 361:455-67.

4. Noedl H, Se Y, Schaecher K, Smith BL, Socheat D, Fukuda MM, Artemisinin Resistance in Cambodia 1 Study C. 2008. Evidence of artemisinin-resistant malaria in western Cambodia. N Engl J Med 359:2619-20.

5. Balikagala B, Fukuda N, Ikeda M, Katuro OT, Tachibana SI, Yamauchi M, Opio W, Emoto S, Anywar DA, Kimura E, Palacpac NMQ, Odongo-Aginya EI, Ogwang M, Horii T, Mita T. 2021. Evidence of Artemisinin-Resistant Malaria in Africa. N Engl J Med 385:1163-1171.

6. Uwimana A, Legrand E, Stokes BH, Ndikumana JM, Warsame M, Umulisa N, Ngamije D, Munyaneza T, Mazarati JB, Munguti K, Campagne P, Criscuolo A, Ariey F, Murindahabi M, Ringwald P, Fidock DA, Mbituyumuremyi A, Menard D. 2020. Emergence and clonal expansion of in vitro artemisinin-resistant *Plasmodium falciparum* kelch13 R561H mutant parasites in Rwanda. Nat Med 26:1602-1608.

7. Kite WA, Melendez-Muniz VA, Moraes Barros RR, Wellems TE, Sa JM. 2016. Alternative methods for the *Plasmodium falciparum* artemisinin ring-stage survival assay with increased simplicity and parasite stage-specificity. Malar J 15:94.

8. Straimer J, Gnadig NF, Witkowski B, Amaratunga C, Duru V, Ramadani AP, Dacheux M, Khim N, Zhang L, Lam S, Gregory PD, Urnov FD, Mercereau-Puijalon O, Benoit-Vical F,

179 Fairhurst RM, Menard D, Fidock DA. 2015. Drug resistance. K13-propeller mutations confer
180 artemisinin resistance in *Plasmodium falciparum* clinical isolates. Science 347:428-31.

181 9. Witkowski B, Amaratunga C, Khim N, Sreng S, Chim P, Kim S, Lim P, Mao S, Sopha C,
182 Sam B, Anderson JM, Duong S, Chuor CM, Taylor WR, Suon S, Mercereau-Puijalon O,
183 Fairhurst RM, Menard D. 2013. Novel phenotypic assays for the detection of artemisinin-
184 resistant *Plasmodium falciparum* malaria in Cambodia: in-vitro and ex-vivo drug-response
185 studies. Lancet Infect Dis 13:1043-9.

186 10. Zhang J, Feng GH, Zou CY, Su PC, Liu HE, Yang ZQ. 2017. Overview of the
187 improvement of the ring-stage survival assay-a novel phenotypic assay for the detection of
188 artemisinin-resistant *Plasmodium falciparum*. Zool Res 38:317-320.

189 11. Lambros C, Vanderberg JP. 1979. Synchronization of *Plasmodium falciparum*
190 erythrocytic stages in culture. J Parasitol 65:418-20.

191 12. Smith LM, Motta FC, Chopra G, Moch JK, Nerem RR, Cummins B, Roche KE, Kelliher
192 CM, Leman AR, Harer J, Gedeon T, Waters NC, Haase SB. 2020. An intrinsic oscillator
193 drives the blood stage cycle of the malaria parasite *Plasmodium falciparum*. Science
194 368:754-759.

195 13. Wockner LF, Hoffmann I, Webb L, Mordmuller B, Murphy SC, Kublin JG, O'Rourke P,
196 McCarthy JS, Marquart L. 2020. Growth Rate of *Plasmodium falciparum*: Analysis of
197 Parasite Growth Data From Malaria Volunteer Infection Studies. J Infect Dis 221:963-972.

198 14. Ressurreicao M, Thomas JA, Nofal SD, Flueck C, Moon RW, Baker DA, van Ooij C.
199 2020. Use of a highly specific kinase inhibitor for rapid, simple and precise synchronization
200 of *Plasmodium falciparum* and *Plasmodium knowlesi* asexual blood-stage parasites. PLoS
201 One 15:e0235798.

202 15. Amaratunga, C., Neal, A. T. & Fairhurst, R. M. 2014. Flow Cytometry-Based Analysis of
203 Artemisinin-Resistant *Plasmodium falciparum* in the Ring-Stage Survival Assay. Antimicrob
204 Agents Chemother 58, 4938–4940.

205 16. Kite, W. A., Melendez-Muniz, V. A., Moraes Barros, R. R., Wellems, T. E. & Sá, J. M.
206 2016. Alternative methods for the *Plasmodium falciparum* artemisinin ring-stage survival
207 assay with increased simplicity and parasite stage-specificity. Malar J 15, 94.

208 17. Davis, S. Z., Singh, P. P., Vendrely, K. M., Shoue, D. A., Checkley, L. A., McDew-White,
209 M., Button-Simons, K. A., Cassady, Z., Sievert, M. A. C., Foster, G. J., Nosten, F. H.,
210 Anderson, T. J. C., Ferdig, M. T. 2020. The Extended Recovery Ring-Stage Survival Assay
211 Provides a Superior Association with Patient Clearance Half-Life and Increases Throughput.
212 Malar J, 19, 54.

213

214

215

216

217

Figure legends

Figure 1: Overview of the Ring-stage Survival Assay. 1) Parasites were cultivated to reach 1% parasitaemia (all blood stages); 2) Parasites were treated with 5%-sorbitol to eliminate mature parasites and preserving ring-stages (~0 to 12 hours post invasion); 3) Parasites were cultivated for 20 hours to reach 20-32h trophozoites and exposed to ML10 at 200 nM for 17 to 20 hours; 4) Schizonts (~37-49h) were isolated using 75%-percoll gradient. Red blood cells were then washed to remove ML10 and cultivated with fresh blood cell for 3 hours for reinvasion; 5) Synchronous 0-3 h ring-stages were recovered and pulsed with 5%-sorbitol to eliminate any remaining schizonts; 6) Parasites were treated for 6 h with 700 nM dihydroartemisinin (DHA) or 0,1% Dimethyl sulfoxide (DMSO) (control), then washed and cultivated for additional 66 h (72 h total); 7) Red blood cells were collected and used to prepared Giemsa-stained blood smears. The mean survival was then calculated as following: $(Parasitemia\ DHA) \ / \ (Parasitemia\ DMSO) \ * 100$

Figure 2. Effectiveness of different concentrations of ML10 for blocking merozoite egress.

Panel A. Proportion of the parasite stages (schizonts vs. other blood stages) detected at 37 h post 5%-sorbitol treatment for the 3D7-K13-wild-type and Cam1-K13-wild-type strains after 17 h pulse complete RPMI culture medium (control) or ML10 at 50 nM, 100 nM, 150 nM and 200 nM (data from biological duplicate, data are available in Table S3).

Panel B. Upper. Giemsa-stained blood smears of 3D7-K13-wild-type complete RPMI culture medium-treated and ML10-treated. Lower. Giemsa-stained blood smears of Cam1-K13-wild-type complete RPMI culture medium-treated and ML10-treated. Each image is representative of the culture, the concentration used for ML10 treated parasites is 150 nM.

Figure 3: Impact of ML10 treatment on schizont availability. *Panel A*. Impact of the exposure time of ML10 (from 17 h to 24 h) on schizonts viability. Parasitaemia of 3D7-K13-wild-type and Cam2-K13-C580Y are expressed as percentage compared to 17 hours pulse exposure time (biological duplicates). *Panel B*. Impact on the survival rates expressed in the $RSA^{0\text{-}3h}$. Data present the survival rates (proportion of viable parasites) of 3D7-K13-wild-type (ART-S) and Cam2-K13-C580Y (ART-R) strains exposed for 17 h to complete RPMI culture medium (standard protocol) and 200 nM ML10 (modified protocol) (biological triplicates).

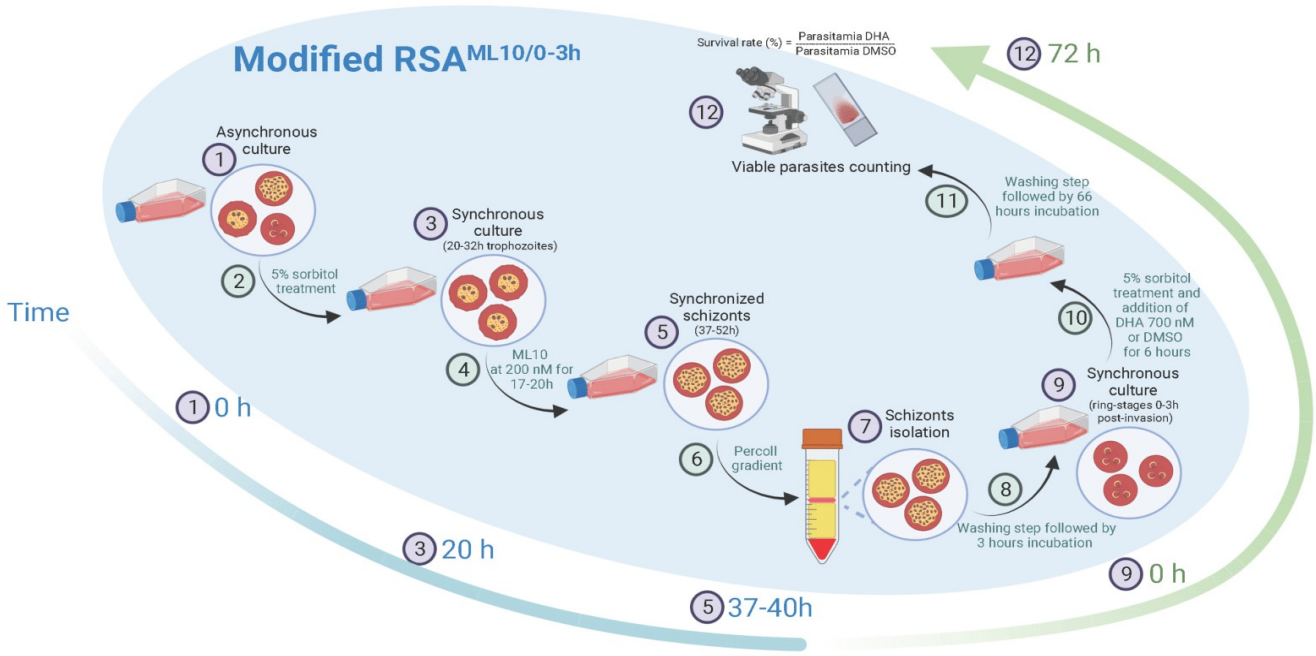
Modified RSA ML10/0-3h
Survival rate (%) = Parasitamia DHA / Parasitamia DMSO
12 72 h
12
Viable parasites counting
11
Washing step followed by 66 hours incubation
10
5% sorbitol treatment and addition of DHA 700 nM or DMSO for 6 hours
9
Synchronous culture
(ring-stages 0-3h post-invasion)
8
Washing step followed by 3 hours incubation
7
Schizonts isolation
6
Percoll gradient
5
Synchronized schizonts
(37-52h)
4
ML10 at 200 nM for 17-20h
3
Synchronous culture
(20-32h trophozoites)
2
5% sorbitol treatment
1
Asynchronous culture
Time
1 0 h
3 20 h
5 37-40h
9 0 h

Figure 1

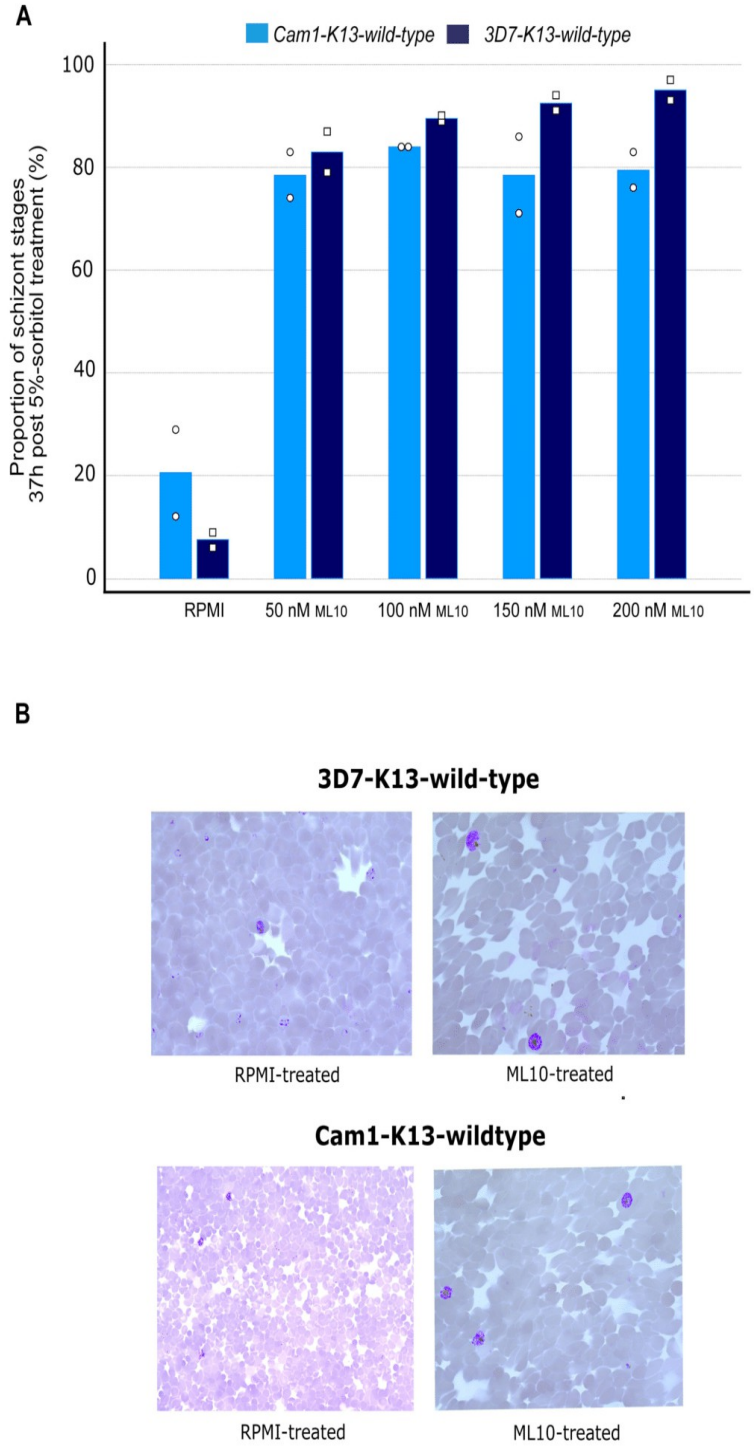
A
Cam1-K13-wild-type
3D7-K13-wild-type
Proportion of schizont stages 37h post 5%-sorbitol treatment (%)
100
80
60
40
20
0
RPMI
50 nM ML10
100 nM ML10
150 nM ML10
200 nM ML10
B
3D7-K13-wild-type
RPMI-treated
ML10-treated
Cam1-K13-wildtype
RPMI-treated
ML10-treated

Figure 2

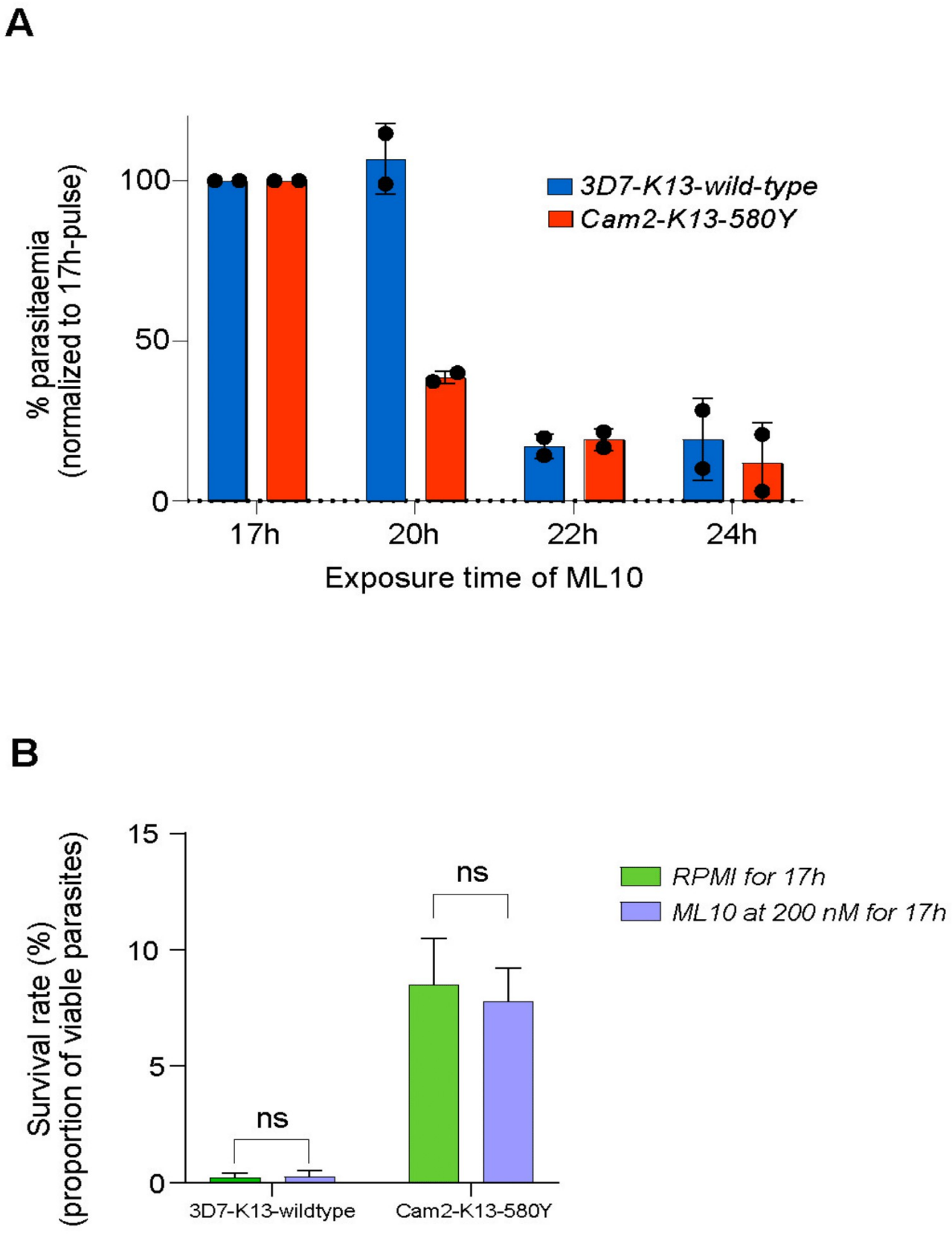
A
% parasitaemia
(normalized to 17h-pulse)
100
50
0
3D7-K13-wild-type
Cam2-K13-580Y
17h
20h
22h
24h
Exposure time of ML10
B
Survival rate (%)
(proportion of viable parasites)
15
10
5
0
ns
ns
RPMI for 17h
ML10 at 200 nM for 17h
3D7-K13-wildtype
Cam2-K13-580Y

Figure 3

Axe 3 : Résistance à l'artémisinine et caractérisation de la dormance induite comme mécanisme de tolérance aux antipaludiques chez *P. falciparum*.

Article 3 : Mécanismes de compensation de la résistance à l'artémisinine chez *P. falciparum*. 'Compensating *P. falciparum* artemisinin resistance.'

Nous avons rédigé un article de synthèse (previews) présentant une étude explorant la capacité des parasites résistant à l'artémisinine à assurer leur apport en acides aminés durant le cycle sanguin. En effet, il a été montré que la résistance à l'artémisinine liée aux mutations au sein du gène *Pfkelch13* entraîne un coût en fitness pour le parasite, du fait de sa croissance ralentie à la suite de la diminution de la digestion de l'hémoglobine. Pour compenser ce coût en fitness, les données présentées montrent que le parasite surexprime EXP1, une protéine assurant la fonction de pore dans la membrane parasitophore, et permettant le passage d'acides aminés (notamment l'isoleucine, pour laquelle *P. falciparum* est auxotrophe) provenant du sérum de l'hôte. De plus, il est présenté que EXP1 facilite le passage de molécules antipaludiques comme la chloroquine, la méfloquine, l'amodiaquine, et la dihydroartémisinine. Ces travaux mettent donc clairement en lumière un nouveau mécanisme moléculaire par lequel le parasite s'adapte aux traitements et pose de nouvelles perspectives de recherches quant aux mécanismes d'actions des antipaludiques et de leurs associations.

CellPress

Cell Host & Microbe
Previews

Compensating *P. falciparum* artemisinin resistance

Lucien Platon,[1,2] Jun Cao,[3,4] and Didier Ménard[1,5,6,*]
[1]Malaria Genetics and Resistance Unit, INSERM U1201, Paris, France
[2]ED515 Complexité du Vivant, Sorbonne Université, Paris, France
[3]Jiangsu Institute of Parasitic Diseases, Wuxi, China
[4]Center for Global Health, School of Public Health, Nanjing Medical University, Nanjing, China
[5]Institute of Parasitology and Tropical Diseases, UR7292 Dynamics of Host-Pathogen Interactions, Federation of Translational Medicine, University of Strasbourg, Strasbourg, France
[6]Laboratory of Parasitology and Medical Mycology, Strasbourg University Hospital, Strasbourg, France
*Correspondence: dmenard@unistra.fr
https://doi.org/10.1016/j.chom.2021.11.007

Amino acid deprivation from reduced hemoglobin degradation in *Pfkelch13* artemisinin-resistant parasites reduces fitness. In this issue of *Cell Host & Microbe*, Mesén-Ramírez et al. decipher the role of nutrient permeable channel activity within the parasitophorous vacuolar membrane to compensate for this fitness cost in asexual blood-stage *Plasmodium falciparum* parasites.

Malaria, caused by the protozoan parasite *Plasmodium falciparum,* is a major public health issue and a potentially fatal disease in tropical regions. Currently, strategies for malaria control and treatment rely on mosquito vector control and the prompt and effective management of malaria cases. However, *P. falciparum* resistance to antimalarial drugs remains a permanent threat that jeopardizes efforts and gains made in reducing the global burden of malaria. This "sword of Damocles" seems to be an inevitable outcome of the drugs' widespread use (White, 2004). Over the last century, nearly all the antimalarial drugs deployed worldwide have led to the selection and spread of drug-resistant parasites. This is the case for artemisinin derivatives, the most potent antimalarial drug and the cornerstone of current first-line artemisinin-based combination therapies (ACTs) (Menard and Dondorp, 2017). Although artemisinins are active against a large range of intraerythrocytic developmental stages, their usefulness is curtailed by ring-stage resistance (Mok et al., 2015).

Seminal genetic studies have demonstrated that *P. falciparum* resistance to antimalarial drugs (i.e., chloroquine, antifolates, mefloquine, or piperaquine) is associated with the spontaneous arising of mutations in genes or changes in the copy number of genes encoding proteins affecting drug influx/efflux or drug binding affinity (Ross and Fidock, 2019). With regard to artemisinins, mutations in a *kelch* gene located on chromosome 13 (*Pfkelch13*) have been shown to be a major determinant of both *in vitro* and *in vivo* artemisinin resistance (Ariey et al., 2014; Straimer et al., 2015). These mutations mediate artemisinin resistance via a reduced hemoglobin endocytosis and catabolism in rings (the youngest blood-stage parasite), resulting in lowered levels of free ferrous-protoporphyrin IX [Fe(II) PPIX] available to activate artemisinin and an enhanced parasite capacity to remove damaged proteins. As a consequence, artemisinin-resistant *Pfkelch13* mutant parasites are reported to be less fit compared with wild-type parasites (Ross and Fidock, 2019).

In this issue of *Cell Host & Microbe*, Mesén-Ramírez and colleagues unveil a role for the activity of nutrient permeable channels (NPC) located in the parasite vacuole membrane (PVM), an enveloping membrane that surrounds the parasite (Mesén-Ramírez et al., 2021). The NPC activity modulates the acquisition of nutrients (including glucose and amino acids from the host's serum) and in some cases, apparently, the passage of antimalarial drugs. NPC activity also appears to compensate for fitness costs associated with artemisinin resistance.

Based on engineered parasites expressing different levels of EXP1(Mesén-Ramírez et al., 2019), this study provides compelling evidence that EXP1 is a major contributor to NPC activity. EXP1 expression, already active in the ring stages when artemisinin resistance occurs, directly influences the access of nutrients through the NPC. Using *in vitro* susceptibility assays with parasites expressing reduced versus normal levels of EXP1, these authors also assessed whether NPC could regulate the access of antimalarial drugs into the parasite. Results provided evidence that the NPC might act as a conduit for several antimalarial drugs, depending on their physicochemical properties. Small water-soluble molecules appeared to reach the parasite via the NPC, whereas hydrophobic or bulky molecules appeared to cross the PVM independent of the NPC. NPC activity was observed to facilitate the access of the 4-aminoquinolines (4-AQ) chloroquine, amodiaquine, and mefloquine, as well as the endoperoxide dihydroartemisinin. The amount of drug reaching the parasite also correlated with the level of activity of EXP1. However, for some other antimalarial drugs like lumefantrine (an aryl amino alcohol), the passage through the PVM was not influenced by the level of EXP1 expression.

Of interest, Mesén-Ramírez et al. noted that, in contrast to the other tested 4-AQs, parasites expressing low levels of EXP1 were highly susceptible to piperaquine (a companion drug combined with dihydroartemisinin in an ACT), suggesting that piperaquine reaches the parasite independent of the NPC. Further analysis confirmed that elevated NPC activity increased amino acid availability from the host's serum rather than the passage of piperaquine, highlighting the dual mode of action of this molecule: inhibition of hemozoin formation as observed with other 4-AQs, and the inhibition of hemoglobin proteolysis leading to a reduced acquisition of hemoglobin-derived amino acids. This finding might suggest that defining

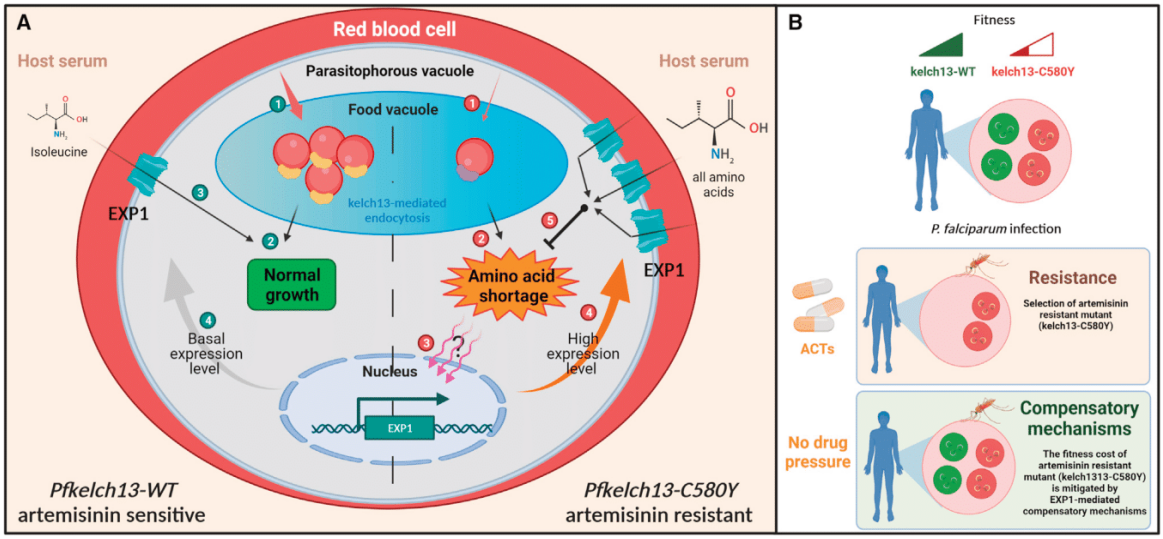

Figure 1. Compensatory mechanism in *P. falciparum* artemisinin resistance: Mechanisms and consequences

(A) Biological mechanisms (individual level). *Pfkelch13*-WT (left side): (1) hemoglobin uptake is mediated by Pfkelch13-WT protein by endocytosis; (2) hemoglobin digestion provided amino acids to sustain continuous and optimal growth (optimal transition rate from ring- to trophozoite-stages); and (3 and 4) isoleucine and nutrients are obtained from the host's serum through the nutrient permeable channel activity (basal production of EXP1 protein). *Pfkelch13*-C580Y (right side): (1) hemoglobin uptake is reduced in *Pfkelch13*-C580Y mutant parasites; (2) amino acid deprivation from the reduced hemoglobin degradation drives a fitness cost; (3) in response to amino acid shortage, EXP1 is highly expressed under the control of unknown regulatory factors; (4) increased production of EXP1 proteins increases the supply of amino acids from the host's serum through the nutrient permeable channel located in the parasitophorous vacuolar membrane; and (5) increased nutrient permeable channel activity mitigates the fitness cost associated with artemisinin resistance in asexual blood stage *Plasmodium falciparum* parasites.

(B) Epidemiological consequences (population level). *P. falciparum* infections treated with ACT lead to the selection of artemisinin resistant parasites. Only *Pfkelch13*-C580Y mutant parasites are capable to survive to the drug exposure despite its reduced fitness compared to *Pfkelch13*-WT parasites. When parasites are not exposed to artemisinin (like asymptomatic infections), change in expression of EXP1 in *Pfkelch13*-C580Y mutant parasites compensate for the fitness cost caused by hemoglobin-derived amino acid restriction. This natural compensatory mechanism allows *Pfkelch13*-C580Y mutant parasites population to compete with *Pfkelch13*-WT parasites population and secure the transmission of its gametocytes (sexual blood stages) to new hosts.

whether antimalarial drugs can passage through the NPC should be taken into account in the selection of lead compounds and designing new combinations such as triple ACTs (van der Pluijm et al., 2021).

Finally, Mesén-Ramírez et al. provide convincing data on how *P. falciparum* ring stages resistant to artemisinin manage the shortage of hemoglobin-derived amino acids that is a consequence of mutant *Pfkelch13* causing reduced hemoglobin endocytosis. Their data suggest that compensatory mechanisms in artemisinin-resistant parasites might involve the increased expression of EXP1 and thus the supply of amino acids through the NPC. Increased EXP1 expression was found to restore the growth of artemisinin-resistant parasites to levels observed with isogenic *Pfkelch13* wild-type parasites (Figure 1A). This mechanism is reminiscent of how parasites respond to low amino acid conditions. Transcriptomic and proteomic analyses of field samples obtained from Southeast Asian malaria patients with known artemisinin resistance provided further evidence that the change in expression of EXP1 might be a natural mechanism to compensate for the fitness cost caused by hemoglobin-derived amino acid restriction. This might have facilitated the rapid spread of *Pfkelch13* C580Y mutant parasites in the Greater Mekong Subregion over the last decade (Figure 1B; Imwong et al., 2020).

This study sheds light on how *P. falciparum* malaria parasites can acquire effective compensatory mechanisms that counterbalance fitness costs linked to genetic changes associated with drug resistance. This work also raises several core questions. Which regulatory factors control the expression of EXP1 (i.e. a transcriptional regulator, DNA methylation, or post-translational modification), and how? Is EXP1 expression adaptive or heritable? Do other biological pathways such as autophagy, eukaryotic initiation factor 2α(eIF2α), or PfMAF1-associated nutrient and stress response pathways participate in reducing the fitness cost of artemisinin resistance? Understanding mechanisms that mitigate the fitness cost associated with artemisinin resistance might help define further strategies aiming at extending the usefulness of artemisinin or developing a better rationale for combining partner drugs with artemisinin in triple ACTs with the ultimate intent of eliminating malaria.

REFERENCES

Ariey, F., Witkowski, B., Amaratunga, C., Beghain, J., Langlois, A.C., Khim, N., Kim, S., Duru, V., Bouchier, C., Ma, L., et al. (2014). A molecular marker of artemisinin-resistant Plasmodium falciparum malaria. Nature *505*, 50–55.

Imwong, M., Dhorda, M., Myo Tun, K., Thu, A.M., Phyo, A.P., Proux, S., Suwannasin, K., Kunasol, C., Srisutham, S., Duanguppama, J., et al. (2020). Molecular epidemiology of resistance to antimalarial drugs in the Greater Mekong subregion: an observational study. Lancet Infect. Dis. *20*, 1470–1480.

Menard, D., and Dondorp, A. (2017). Antimalarial Drug Resistance: A Threat to Malaria Elimination. Cold Spring Harb. Perspect. Med. *7*, 7.

Mesén-Ramírez, P., Bergmann, B., Tran, T.T., Garten, M., Stäcker, J., Naranjo-Prado, I., Höhn, K., Zimmerberg, J., and Spielmann, T. (2019). EXP1 is critical for nutrient uptake across the parasitophorous vacuole membrane of malaria parasites. PLoS Biol. *17*, e3000473.

Mesén-Ramírez, P., Bergmann, B., Elhabiri, M., Zhu, L., von Thien, H., Castro-Peña, C., Gilberger, T.-W., Davioud-Charvet, E., Bozdech, Z., Bachmann, A., and Spielmann, T. (2021). The parasitophorous vacuole nutrient channel is critical for drug access in malaria parasites and modulates the fitness cost of artemisinin resistance. Cell Host & Microbe *29*, 1774–1787.

Mok, S., Ashley, E.A., Ferreira, P.E., Zhu, L., Lin, Z., Yeo, T., Chotivanich, K., Imwong, M., Pukrittayakamee, S., Dhorda, M., et al. (2015). Drug resistance. Population transcriptomics of human malaria parasites reveals the mechanism of artemisinin resistance. Science *347*, 431–435.

Ross, L.S., and Fidock, D.A. (2019). Elucidating Mechanisms of Drug-Resistant Plasmodium falciparum. Cell Host Microbe *26*, 35–47.

Straimer, J., Gnädig, N.F., Witkowski, B., Amaratunga, C., Duru, V., Ramadani, A.P., Dacheux, M., Khim, N., Zhang, L., Lam, S., et al. (2015). Drug resistance. K13-propeller mutations confer artemisinin resistance in Plasmodium falciparum clinical isolates. Science *347*, 428–431.

van der Pluijm, R.W., Amaratunga, C., Dhorda, M., and Dondorp, A.M. (2021). Triple Artemisinin-Based Combination Therapies for Malaria - A New Paradigm? Trends Parasitol. *37*, 15–24.

White, N.J. (2004). Antimalarial drug resistance. J. Clin. Invest. *113*, 1084–1092.

Article 4 : Arrêt de croissance du stade Ring : Bases métaboliques de la tolérance à l'artémisinine chez *Plasmodium falciparum*.

'Ring-stage growth arrest : Metabolic basis of artemisnin tolerance in *Plasmodium falciparum*.'

Nous avons cherché dans cette étude à déterminer l'état métabolique des stades rings en arrêt de croissance après une exposition à l'artémisinine. Pour cela, plusieurs souches présentant des génotypes *Pfkelch13* différents (WT, C580Y et Y493H) ont été utilisées. La première étape de ce travail de recherche a été de développer une technique permettant l'isolement des parasites au stade ring afin de pouvoir ensuite étudier leurs profils métabolomiques, tout en s'affranchissant du bruit généré par la présence des globules rouges non infectés. La technique SLOPE qui associe une lyse des globules rouges non infectés par un traitement à la Streptolysine-O et une centrifugation différentielle sur gradient de Percoll a permis l'isolement, la purification et un enrichissement significatif des stades rings.

La seconde partie de l'étude a permis d'établir le profil métabolomique par spectrométrie de masse des stades rings en arrêt de croissance après exposition à la DHA. Les données obtenues indiquent que la glycolyse, le cycle de Krebs, la voie des porphyrines ainsi que la phosphorylation oxydative sont modifiés par l'exposition à la DHA. Les parasites mutants *Pfkelch13* C580Y et Y493H présentent un métabolisme énergétique principalement basé sur la dégradation des acides aminés et une inhibition de la glycolyse. Ces données fournissent donc un nouvel éclaircissement sur la plasticité métabolique des stades rings et leur capacité à survivre à la DHA par un arrêt de croissance temporaire. Ce travail de recherche est pionnier en matière d'exploration métabolique sur les stades jeunes de *P. falciparum*, en raison des difficultés techniques dans la séparation des cellules infectées et non infectées. Ce travail, publié dans la revue *iScience* en 2022, est le fruit d'une collaboration avec le *Jiangsu Institute of Parasitic Disease* situé à Wuxi en Chine.

iScience

CellPress
OPEN ACCESS

Article

Ring-stage growth arrest: Metabolic basis of artemisinin tolerance in *Plasmodium falciparum*

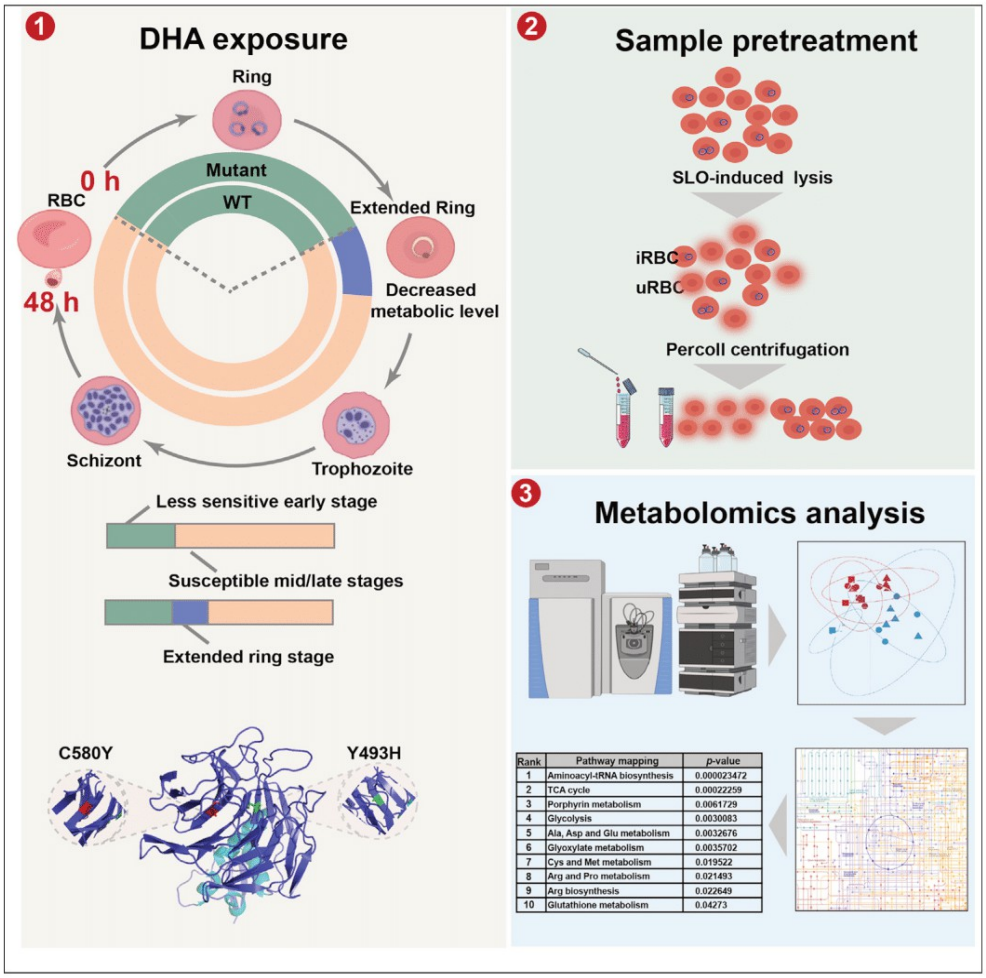

Xinyu Yu, Changhong Wang, Yuemeng Zhao, ..., Didier Ménard, Qingfeng Zhang, Jun Cao

jipdzhu@hotmail.com (G.Z.)
qfzhang@tongji.edu.cn (D.M.)
didier.menard@pasteur.fr (Q.Z.)
caojun@jipd.com (J.C.)

Highlights

Typical *PfKelch13* mutant parasite lines confer to ART resistance have been constructed

Modified SLOPE protocol allows for the enrichment of early ring-stage parasites

Metabolomics screening points to altered energy metabolism with metabolic plasticity

Altering metabolic flow or chemical inhibition confirms the screening results

Yu et al., iScience ■■, 105725
■■, 2022 © 2022 The Authors.
https://doi.org/10.1016/j.isci.2022.105725

Please cite this article in press as: Yu et al., Ring-stage growth arrest: Metabolic basis of artemisinin tolerance in *Plasmodium falciparum*, iScience (2022), https://doi.org/10.1016/j.isci.2022.105725

iScience

CellPress
OPEN ACCESS

Article

Ring-stage growth arrest: Metabolic basis of artemisinin tolerance in *Plasmodium falciparum*

Xinyu Yu,[1,2,3] Changhong Wang,[4] Yuemeng Zhao,[4] Jianxia Tang,[2,3] Meng Zhu,[3] Lucien Platon,[5,6] Richard Culleton,[7] Guoding Zhu,[2,3,*] Didier Ménard,[5,8,9,*] Qingfeng Zhang,[4,*] and Jun Cao[2,3,10,*]

SUMMARY

The emergence and spread of artemisinin-tolerant malaria parasites threatens malaria control programmes worldwide. Mutations in the propeller domain of the Kelch13 protein confer *Plasmodium falciparum* artemisinin resistance (ART-R). ART-R is linked to the reduced susceptibility of temporary growth-arrested ring-stage parasites, but the metabolic mechanisms remain elusive. We generated two *PfKelch13* mutant lines via CRISPR-Cas9 gene editing which displayed a reduced susceptibility accompanied by an extended ring stage. The metabolome of ART-induced ring-stage growth arrest parasites carrying *PfKelch13* mutations showed significant alterations in the tricarboxylic acid (TCA) cycle, glycolysis, and amino acids metabolism, pointing to altered energy and porphyrin metabolism with metabolic plasticity. The critical role of these pathways was further confirmed by altering metabolic flow or through chemical inhibition. Our findings uncover that the growth arrestment associated with ART-R is potentially attributed to the adaptative metabolic plasticity, indicating that the defined metabolic remodeling turns out to be the trigger for ART-R.

INTRODUCTION

Malaria remains one of the most important tropical diseases and causes significant morbidity and mortality, especially in sub-Saharan Africa. In 2020, the world health organization (WHO) reported 241 million cases of malaria worldwide, resulting in 627,000 deaths.[1] Currently, the two main strategies for the control of malaria are vector control (long-lasting insecticide-treated nets and indoor residual spraying) and management of malaria cases (malaria rapid diagnostic tests and artemisinin-based combination therapies[ACTs]).[2,3] First-line treatments for managing uncomplicated *falciparum* malaria, recommended globally by the WHO, are based on ACT, combining a potent but short-lived artemisinin (ART) derivative and a slower-acting companion drug that increases the effectiveness of treatment and reduces the risk of recrudescence and the development of resistance.[4–6]

Plasmodium falciparum parasites' partial resistance/tolerance to ART (ART-R) has, however, emerged less than a decade ago following the use of ACT in Southeast Asia.[7–9] Clinical and biological investigations have demonstrated that ART-R was associated with an increased number of ring stages capable of undergoing growth arrest.[10,11] Mutations in the propeller domain of a *kelch* gene located on chromosome 13 *(Pfkelch13)*, *e.g.*, C580Y, Y493H, R539T, I543T, R561H, *etc,* are a major determinant of both *in vitro* and *in vivo* ART-R.[12–17] To date, the exact mechanism by which mutations in *Pfkelch13* enhance tolerance to ART remains controversial.[18,19] *P. falciparum* susceptibility to ART is, however, closely associated with the altered temporal responses of parasites at various stages.[20,21]

Growth arresting or quiescent states are an effective survival mechanism in a wide range of microorganisms, plants, and insects. This response is triggered by environmental stress causing cell cycle development arrest in order to enhance survival when facing unfavorable conditions.[22–24] So far, the clearest example of this phenomenon in malaria parasites is the hypnozoite stage of *Plasmodium vivax* and related species.[25] Upon exposure to ART, synchronized *P. falciparum* parasites exhibit stage-dependent susceptibility profiles correlated with hemoglobin digestion.[19,26] Interestingly, parasites at the early ring stage (2–4 h post invasion) displayed higher sensitivity in evaluation of the resistance level, which was developed as an *in vitro* ART assay, *i.e.*, ring-stage survival assay ($RSA^{0–3h}$).[27,28]

[1]Medical College of Soochow University, Suzhou, China

[2]National Health Commission Key Laboratory of Parasitic Disease Control and Prevention, Jiangsu Provincial Key Laboratory on Parasite and Vector Control Technology, Jiangsu Institute of Parasitic Diseases, Wuxi, China

[3]Center for Global Health, School of Public Health, Nanjing Medical University, Nanjing, China

[4]Laboratory of Molecular Parasitology, Key Laboratory of Spine and Spinal Cord Injury Repair and Regeneration of Ministry of Education, Tongji Hospital; Clinical Center for Brain and Spinal Cord Research, School of Medicine, Tongji University, Shanghai 200092, China

[5]Institut Pasteur, Université Paris Cité, INSERM U1201, Malaria Genetics and Resistance Unit, 75015 Paris, France

[6]Sorbonne Université, Ecole Doctorale ED515 Complexité du Vivant, 75005 Paris, France

[7]Division of Molecular Parasitology, Proteo-Science Centre, Ehime University, Matsuyama, Ehime 790-8577, Japan

[8]Institute of Parasitology and Tropical Diseases, UR7292 Dynamics of Host-Pathogen Interactions, Federation of Translational Medicine, University of Strasbourg, Strasbourg, France

[9]Laboratory of Parasitology and Medical Mycology, Strasbourg University Hospital, Strasbourg, France

[10]Lead contact

*Correspondence: jipdzhu@hotmail.com (G.Z.), qfzhang@tongji.edu.cn (D.M.), didier.menard@pasteur.fr (Q.Z.), caojun@jipd.com (J.C.)

https://doi.org/10.1016/j.isci.2022.105725

Please cite this article in press as: Yu et al., Ring-stage growth arrest: Metabolic basis of artemisinin tolerance in *Plasmodium falciparum*, iScience (2022), https://doi.org/10.1016/j.isci.2022.105725

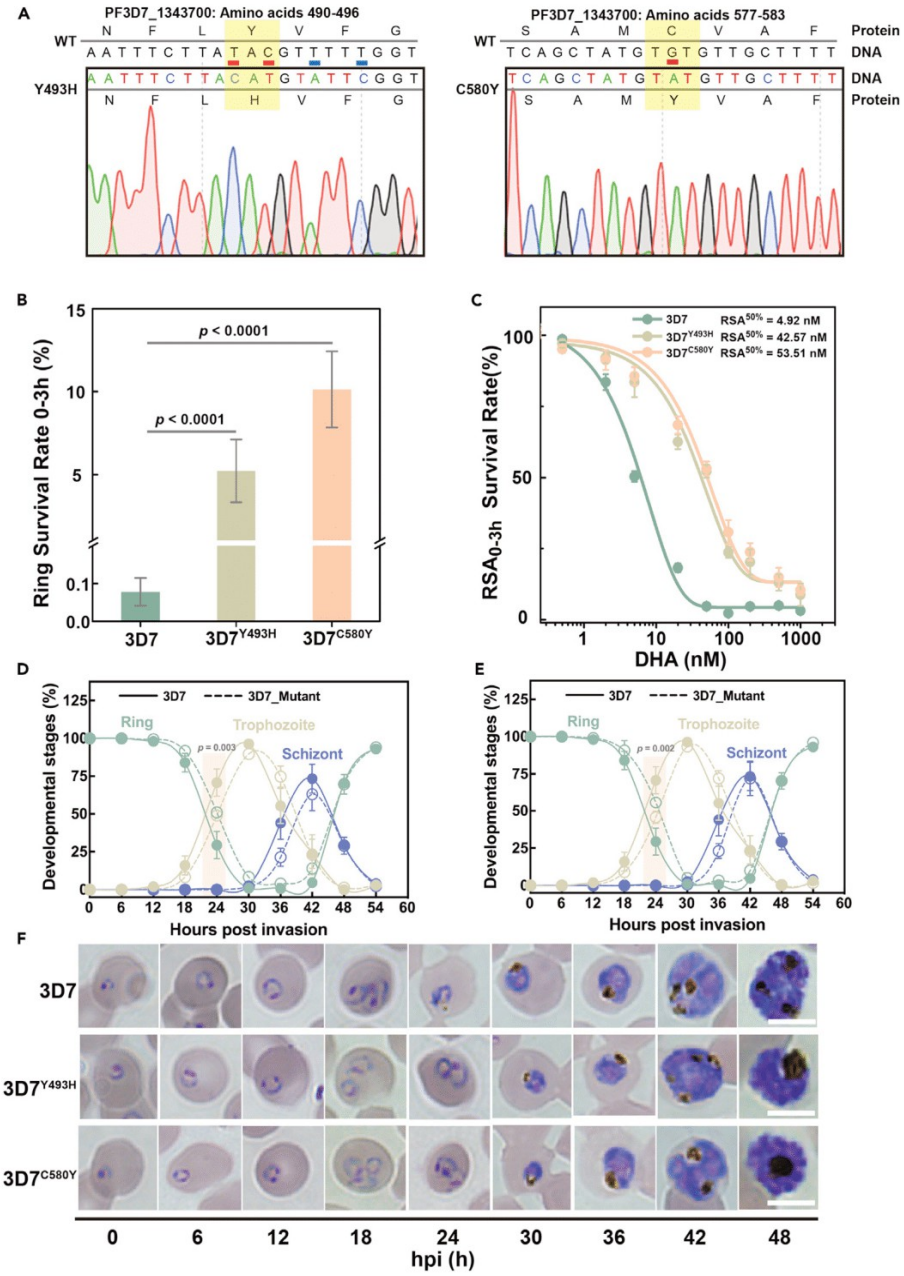

Figure 1. *Pfkelch13* 3D7^{Y493H} and 3D7^{C580Y} mutant parasites exhibits reduced susceptibility to DHA and prolonged ring stage

(A) Alignment of the mutated region of *Pfkelch13*.

(B) 0-3 h ring-stage survival assay (RSA_{0-3h}) determination for transfection control with the WT *Pfkelch13* gene (3D7^{WT}) and 3D7-*Pfkelch13* engineered mutant lines (3D7^{Y493H} and 3D7^{C580Y}). Survival rates for each parasite line were calculated by dividing the number of surviving DHA-treated parasites by the number of DMSO-treated parasites and expressed in percentage. p value indicate statistical comparisons of survival rate between the control and mutant parasites by Holm-Bonferroni method adjusted two-sided t test (n = 3). Data are represented as mean ± SD.

Please cite this article in press as: Yu et al., Ring-stage growth arrest: Metabolic basis of artemisinin tolerance in *Plasmodium falciparum*, iScience (2022), https://doi.org/10.1016/j.isci.2022.105725

Figure 1. *Continued*

(C) $RSA_{0-3h}^{50\%}$ assay was designed to evaluate the *in vitro* susceptibility of the $3D7^{WT}$ and the mutant parasite lines against various DHA concentrations (ranging from 0.5 to 1000 nM). Tightly synchronized 0-3 h post-invasion parasites were subjected to 6 h exposure with varied DHA concentrations. The survival rates of the parasites under this treatment conditions were plotted against the drug concentration. The dose-response curve was fitted by sigmoidal model (n = 3). Data are represented as mean ± SD.

(D and E) Comparison of intraerythrocytic development patterns between *Pfkelch13* WT and mutant parasites. Purified schizonts from tightly synchronized parasite lines were used to obtain early-ring-stage parasites. Blood smears were made every 6 h, and the percentage of each stage was counted in 100 parasites. Ring, trophozoite, and schizont stages are distinguished by different colors, while WT and mutant parasites were shown as continuous and dashed lines, respectively. * *(p value < 0.05)* indicate statistical comparisons of developmental stages between WT and mutant parasites at selected time point (labeled by colored background) by Student's t test (n = 3). Data are represented as mean ± SD.

(F) Microscopic examination of Giemsa-stained blood smears revealed the ring stage for transgenic strains was ~6 h longer than WT, while prolonged ring stage along with shortened trophozoite stage contributed to a similar whole IDC life (Scale bar = 5 μM).

Previous studies have reported that *P. falciparum* early ring-stage parasites play a crucial role in the development of drug tolerance during the intraerythrocytic developmental cycle (IDC).[11,29] Early ring-stage parasites are protected from DHA by a temporary developmental arrest followed by a return to a normal developmental cycle when drug pressure is removed. However, the physiological state resulting from growth arrest along with the metabolic mechanism that leads to decreased ART susceptibility has not been fully characterized. We hypothesize that investigation of the metabolic profiles of these forms could aid understanding of how temporary ring-stage growth arrest is triggered and how that could drive the development of novel antimalarials. Although it has been previously demonstrated that parasites altered their transcriptomic and proteomic profiles after the DHA pulse,[30] the metabolic alterations and the adaptative changes that *Pfkelch13* mutant parasites undergo before developing into growth-arrested forms remain elusive.

Here, we present the results of experiments in which the metabolism-based growth-arrest profile of parasites with varying ART-R profiles were investigated. The *in vitro* DHA susceptibility phenotypes and IDC development profiles were evaluated in mutant parasite lines. As host erythrocyte contamination is known to significantly affect the reliability of metabolomic data, we developed a protocol for the generation of adequate early-stage parasite samples with sufficient quality and with reduced host cell contamination. Untargeted metabolomics screening was then performed, and a finely tuned adaptive metabolic mechanism was obtained for the first time by investigating the abundance of significantly changed metabolome corresponding to amino acid, energy, and porphyrin metabolism after DHA exposure. Taking together, we have identified that the growth arrestment-associated DHA tolerance is potentially attributed to the adaptative metabolic remolding for mutant parasite lines. We then assayed whether metabolic stimulation or chemical inhibition could protect parasites from the damage caused by DHA, indicating that the metabolic plasticity turns out to be critical for parasite survival when exposed to DHA pulse during IDC life cycle.

RESULTS

In vitro DHA susceptibility of *Pfkelch13* 493H ($3D7^{Y493H}$) and 580Y ($3D7^{C580Y}$) gene-edited parasite lines

We generated two ART-R lines using CRISPR-Cas9i gene editing,[31] through the introduction of two mutations, Y493H and C580Y, in the propeller domain of *Pfkelch13* gene in the 3D7 strain (Figure S1A). To assess the *in vitro* susceptibility of *Pfkelch13* 493H ($3D7^{Y493H}$) and 580Y ($3D7^{C580Y}$) gene-edited parasite lines and control ($3D7^{WT}$) to DHA, RSA_{0-3h} was performed on three technical replicates. Survival rates of $3D7^{Y493H}$ and $3D7^{C580Y}$ parasite lines were significantly higher (5.8 and 10.9%, respectively, $p < 10^{-3}$) compared to the $3D7^{WT}$ control line (0.078%) (Figures 1A and 1B).

As the RSA_{0-3h} reflects only the survival rates for parasites exposed to 700 nM DHA for 6 h, we extended the *in vitro* susceptibility profiles of the mutant parasite lines to various concentrations of DHA (from 0.5–1000 nM) and different exposure times (from 1–9 h). We then defined the $RSA_{0-3h}^{50\%}$ as the DHA concentration and the exposure time required to kill 50% of the viable parasites observed in the nonexposed cultures (DMSO). The $3D7^{Y493H}$ and $3D7^{C580Y}$ parasite lines displayed different dose-response curves. Upon 6 h exposure, 10-fold higher $RSA_{0-3h}^{50\%}$ survival rates (42.57 nM for $3D7^{Y493H}$ and 53.51 nM for $3D7^{C580Y}$)

Please cite this article in press as: Yu et al., Ring-stage growth arrest: Metabolic basis of artemisinin tolerance in *Plasmodium falciparum*, iScience (2022), https://doi.org/10.1016/j.isci.2022.105725

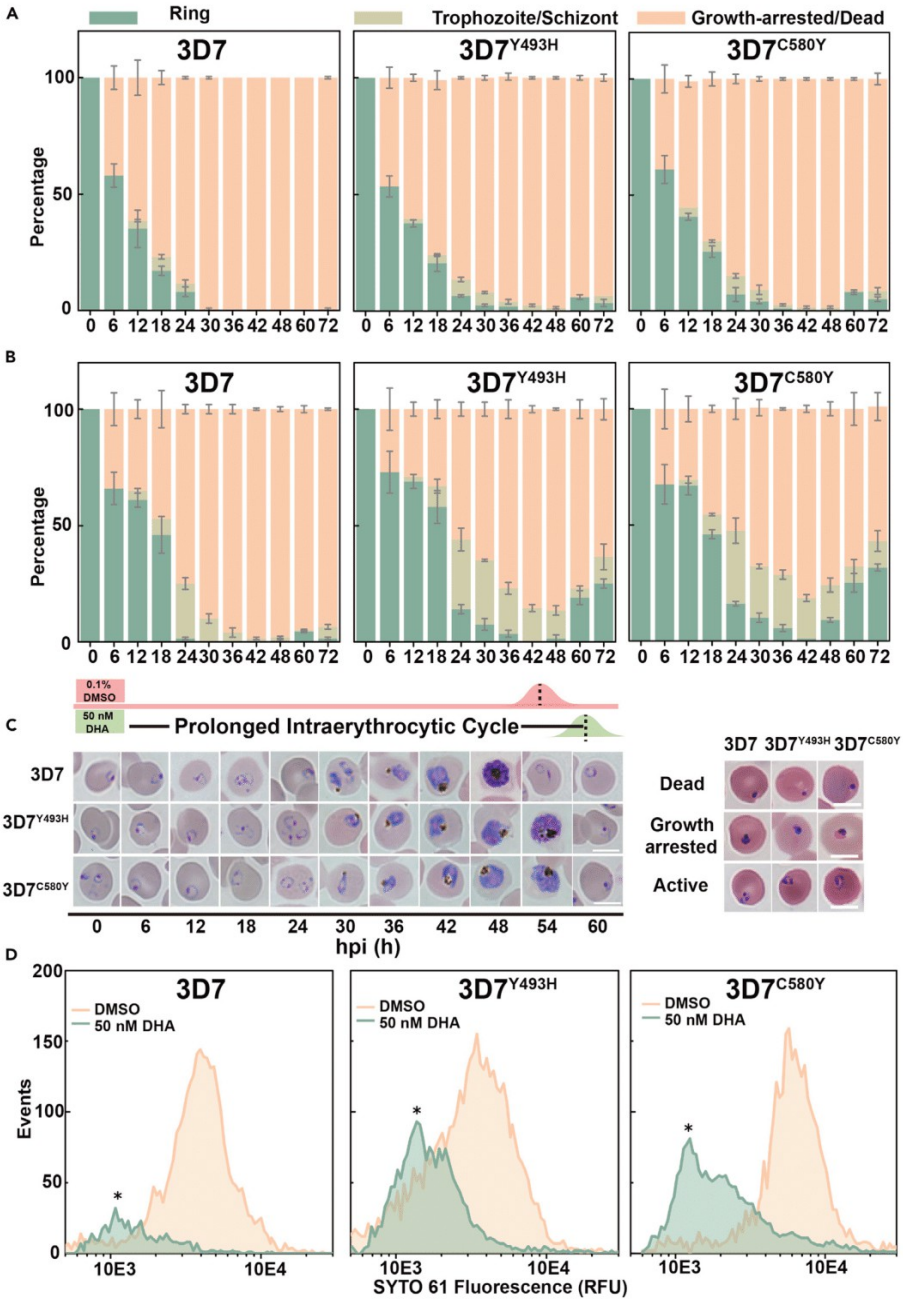

Figure 2. Delayed clearance, growth retardation, and recrudescence from DHA-induced growth arrest of *Pfkelch13*-mutated parasite

Percentage of parasites (n = 100) with different morphology after DHA exposure was monitored by microscopic examination. Parasites were morphologically categorized into ring, trophozoite/schizont, or growth-arrested/dead form at each time point. Stage distributions for parasites after vehicle or DHA treatment at 72 h.

(A) After treatment of 700 nM DHA for 6 h, no variable parasite in $3D7^{WT}$ was observed in the second life cycle whereas both ring- and mature-stage parasites were observed for $3D7^{Y493H}$ and $3D7^{C580Y}$, respectively. Data are represented as mean ± SD.

Please cite this article in press as: Yu et al., Ring-stage growth arrest: Metabolic basis of artemisinin tolerance in *Plasmodium falciparum*, iScience (2022), https://doi.org/10.1016/j.isci.2022.105725

Figure 2. *Continued*

(B) Following the exposure of 50 nM DHA for 6 h, DHA-resistant lines indicated a delayed IDC with more variable parasites than $3D7^{WT}$. Data are represented as mean ± SD.

(C) Morphological analysis of prolonged IDC development for $3D7^{Y493H}$ and $3D7^{C580Y}$ parasites after 6-h exposure of DHA exposure, and the insert indicated the representative images of dead, growth-arrested, and active forms of parasites. (Scale bar = 5 μM).

(D) Changes in the SYTO-61 staining profile of viable parasites after drug exposure for 88h. WT and 3D7 mutant parasites were subjected to 6-h DHA pulses at 50 nM and SYTO-61 signals were measured by flow cytometry when DMSO-treated parasite had progressed into mid-late stage (~40h) in the next cycle. Asterisks indicate an absolute increase in the number of early-stage parasites due to growth arrestment.

were observed compared to the $3D7^{WT}$ control line (4.92 nM) (Figures 1C and S1B). These DHA concentrations and exposure periods were then used in subsequent metabolomics experiments.

We next investigated the IDC profiles (from 0–3 h) of post-invasion ring-stages of $3D7^{WT}$, $3D7^{Y493H}$ (Figure 1D), and $3D7^{C580Y}$ (Figure 1E) in the absence of DHA. Generally, the developmental stage was based on the overall size of parasites, including the ratios of the area and diameter of the nucleus to those of the cytoplasm, and the amount of visible pigment and mature nuclei after Giemsa staining. Specifically, for late rings (~18 h) and early trophozoites (~24 h), we discriminate them from each other according to the appearance of pigment in brown as well as the filling degree of cytoplasm.

The total length of the IDC of each parasite line was approximately 48 h (from rings to trophozoites and schizonts). While the length of the whole IDC remained unchanged, the progression of $3D7^{Y493H}$ and $3D7^{C580Y}$ ring stages was delayed by ~6 h compared to $3D7^{WT}$, and the subsequent trophozoite-stage duration was shortened (Figure 1F). The ring to trophozoite transition for $3D7^{Y493H}$ and $3D7^{C580Y}$ occurred at ~24 h and ~3 h later than $3D7^{WT}$ (estimated at ~21 h), respectively. These altered IDC profiles of the $3D7^{Y493H}$ and $3D7^{C580Y}$ mutant parasites were observed in three independent biological replicates in the absence of drug treatment.

We then evaluated *in vitro* IDC growth up to 72 h under different concentrations of DHA. The proportions of the parasite stages were monitored by microscopic examination of Giemsa-stained smears. Parasites were categorized into rings, trophozoites/schizonts, or growth-arrested/dead forms at each time point. Ring-stage development was defined during the first 18 h with cytoplasm occurring in a ring shape with little to no hemozoin visible. In the following 12 h, parasites became increasingly enlarged and dense with clearly observable hemozoin deposition and accumulation. Thereafter, with the progressive accumulation of hemozoin, divided nuclei could be observed at 36 h, and hemozoin was into a granulate form before mature merozoites developed at ~46 h.

In addition to these morphologically normal parasites, growth-arrested parasites displayed a rounded morphology with retained cytoplasm and chromatin which differed from those of dead forms. Following administration of 700 nM DHA for 6 h, only a small portion (~10%) of morphologically normal $3D7^{WT}$ ring stages were observed up to 24 h while normal $3D7^{Y493H}$ and $3D7^{C580Y}$ ring and mature stages were detected up to 72 h, indicating an increased capacity to withstand DHA (Figure 2A). Likewise, following administration of 50 nM DHA for 6 h, normal $3D7^{Y493H}$ and $3D7^{C580Y}$ ring and mature stages were seen across the IDC development, and this was not observed in the $3D7^{WT}$ control line (Figure 2B). Overall, under both conditions, the $3D7^{Y493H}$ and $3D7^{C580Y}$ parasites were less susceptible to DHA exposure.

To further quantify drug-induced growth retardation during the ring to trophozoite transition of synchronized parasites (0–3 hpi) exposed to 50 nM DHA for 6 h, we monitored the morphology of the parasite stages at every 6 h over 60 h. Compared to the $3D7^{WT}$ control line, we observed a higher proportion of $3D7^{Y493H}$ and $3D7^{C580Y}$ parasites with rounded cytoplasm and condensed chromatin (defined as growth-arrested parasites), in addition to pyknotic forms with collapsed nuclei (dead parasites) (Figure 2C).

For $3D7^{Y493H}$ and $3D7^{C580Y}$ parasite lines stained with SYTO-61, corrected SYTO-61 signals referred to the median value of the viable parasite population. Examination of the population profile of SYTO-61 staining by flow cytometry indicated an absolute increase in the number of viable parasites for mutant parasites in the subsequent IDC, which was closely associated with growth retardation upon DHA exposure. (Figure 2D).

Please cite this article in press as: Yu et al., Ring-stage growth arrest: Metabolic basis of artemisinin tolerance in *Plasmodium falciparum*, iScience (2022), https://doi.org/10.1016/j.isci.2022.105725

Ring-stage parasites enrichment

Next, we have improved a protocol to enrich growth-arrested ring-stage parasites for metabolomic studies based on previously reported research.[32] The protocol was based on SLO, a pore-forming exotoxin that can selectively lyse uninfected erythrocytes. Lysis efficiency was assessed by measuring the proportions of infected and uninfected erythrocytes in bulk cultures using a range of SLO concentrations. Lysis of uninfected erythrocytes was effective at 875 U of SLO (95.9 ± 4.1%, 92.0 ± 2.9%, 92.4 ± 2.6% for $3D7^{WT}$, $3D7^{Y493H}$, and $3D7^{C580Y}$ parasites, respectively) (Figures S2A and S2B). Next, we improved the protocol by using 70% Percoll (v/v) to separate intact and lysed erythrocytes. By using this approach (named SLOPE), we obtained parasitemia for ring-stage parasites reaching 38.1 ± 1.9%, 36.4 ± 2.4%, 36.8 ± 3.1% for the $3D7^{WT}$, $3D7^{Y493H}$, and $3D7^{C580Y}$ parasite lines, respectively, resulting in a ~7-fold increase in ring-stage parasites and reduced host cell contamination. We later confirmed the removal of ghost cells by immunofluorescence (Figures S2D–S2F). Briefly, confocal microscopy using a set of antibodies (anti-CD235a, an external surface protein; anti-spectrin, an intracell protein only accessible in lysed erythrocytes) and Hoechst dye (parasite DNA staining) was performed to detect intact erythrocytes (infected and uninfected) from ghosts. The separation was achieved using the SLOPE approach, resulting in 50% intact cells with significantly increased rings. Less than 5% of cells were ghost cells according to quantification using acquired images.

Finally, we determined the impact of enrichment on viability and metabolic activity of enriched ring-stage parasites by measuring growth curve and morphological examination. We observed no significant changes in growth rates or parasite morphology between enriched and untreated parasites, indicating the feasibility of using this method to perform metabolomics analysis, as described below (Figure S2C).

Metabolomic profile of enriched parasites

To investigate whether the SLOPE method could separate parasite-specific signals from host contamination, enriched parasites were harvested and analyzed. The metabolomics profiles of untreated control and saponin-lysed parasites were almost indistinguishable in a principal-component analysis (PCA) score plot (Figures 3B–3D), suggesting relatively poor enrichment and/or a low discriminatory power for the separation of parasite-specific signals and background host contamination. In contrast, the SLOPE-pretreated preparations showed a significantly reduced ghost cell signal, consistent with the data obtained from immunofluorescence assay. SLOPE pretreatment clearly differentiated metabolomics profiles from treated and untreated parasites. First, PLS-DA score plot revealed distinct separations between groups without over fitting (Figure S3) and clearly separated metabolomics profiles from ring-stage samples. Second, we observed a significant reduction in the relative intensity of three representative host-derived metabolites (CDP ethanolamine, Valylleucine, and hypoxanthine) in SLOPE-treated parasites (Figures 3E–3G).

Untargeted metabolomic profiles of parasites following DHA treatment

Next, we applied the SLOPE protocol to define the metabolomic profile of ring-stage parasites exposed to 50 nM DHA for 6 h according to the schematic workflow (Figure 3A). At this drug concentration, either viable subpopulation which were still positive by the RSA_{0-3h} in contrast to the $3D7^{WT}$ strain (Figure 1C) or pyknotic parasites at ring stage were enriched. The untargeted metabolomics profiles revealed a total of 1,000 metabolite features of which 920 were included in subsequent analyses. A distinct separation pattern of four clusters was noticed, indicating specific metabolomics changes induced by DHA treatment (Figure 4A). The changes induced by DHA were detected by conducting a supervised PLS-DA model including a "variable important in projection" (VIP) larger than 1.5. A comparison of the metabolomics profiles measured by univariate analysis of variance from DHA-exposed and nonexposed parasites identified 124 and 146 metabolites (adjusted p value <0.05) in the wild-type (WT, $3D7^{WT}$) and mutant parasite lines ($3D7^{Y493H}$ and $3D7^{C580Y}$), respectively. As shown in Table 1, the metabolomics changes induced by DHA were deduced from compounds shared between exposed and nonexposed cultures and included the annotations of the most significant metabolites (Figure 4B). Overall, overlapped metabolic profile indicated that amino acid metabolism-, porphyrin metabolism-, and energy metabolism-related pathways belonged to highly ranked pathways (Figure 4C).

We then applied a metabolome wide association strategy to investigate associations between perturbations in the metabolome and the *in vitro* DHA susceptibility phenotypes of the three parasite lines. As shown in the heatmap (Figure 4D), alongside an increase in the abundance of glucose, hierarchical clustering analysis revealed a major cluster with decreasing intensity for relative level for most of the

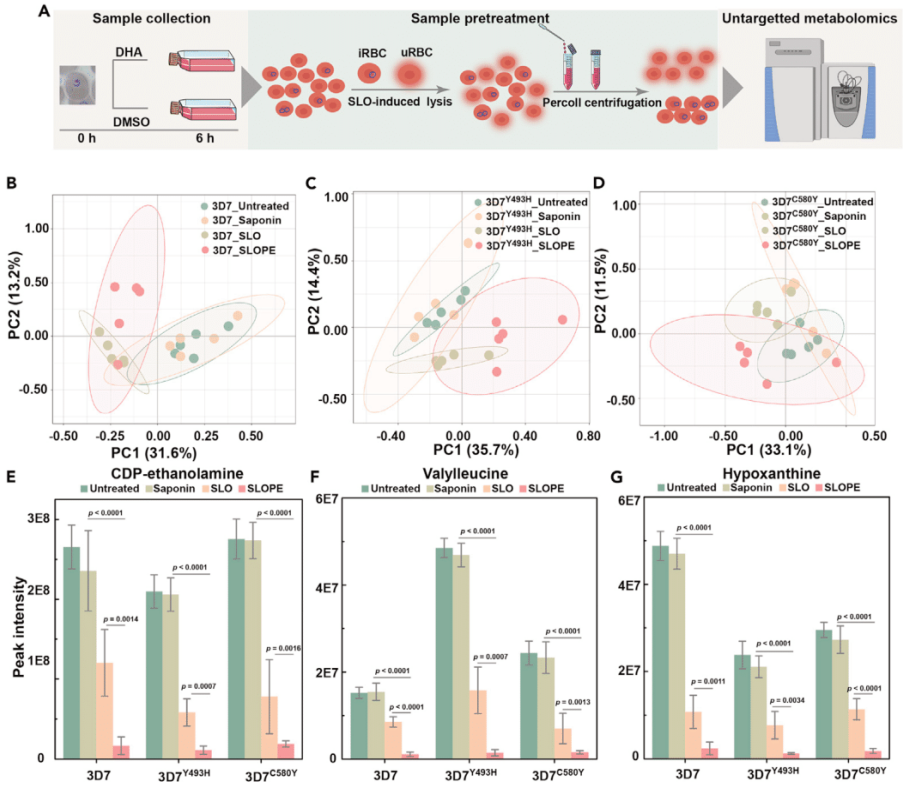

Figure 3. Metabolic profile of parasites with different treatment by untargeted metabolomics strategy

(A) Schematic workflow for the metabolomics study in which sample collection, ring-stage parasite enrichment and data acquisition are illustrated. Highly synchronized *Pfkelch13* WT and mutant parasite lines were subjected to either 50 nM DHA or 0.1% DMSO exposure for 6 h followed by thorough wash to remove remaining DHA. Cultures were treated with SLO to preferentially lyse uninfected erythrocytes and then layered on Percoll gradient to separate lysed ghosts from intact cells by centrifugation. Followed by metabolites quenching and extraction, the metabolic basis of artemisinin-induced growth-arrested parasites was investigated by through high-resolution MS-based untargeted metabolomics approach.

(B–D) PCA scatterplot for acquired metabolomes in $3D7^{WT}$, $3D7^{Y493H}$, and $3D7^{C580Y}$ parasites. The metabolic profiles of untreated control and saponin lysed parasites were hardly distinguished because of ghost contamination, while enriched ring-stage parasites treated by streptolysin-O or constructed methods showed a clear different metabolic profile (n = 5).

(E–G) Relative signal of three representative compounds which was able to reflect the host metabolic effect on classifier accuracy. Like above-acquired metabolic profile, host-derived metabolic signal was significantly reduced after sample pretreatment, indicating the feasibility of this method to reduce host contamination as well as obtain parasite-specific metabolome which was favorable for following metabolomics analysis. p value indicates statistical comparisons of the relative abundance between the control and mutant parasites by Holm-Bonferroni method adjusted two-sided t test (n = 5). Data are represented as mean ± SD.

intermediates canonically linked to tricarboxilic acid (TCA) cycle following DHA pulse. Of note, the main metabolic changes observed in ring-stage parasites exposed to DHA were significant decreases in the glycolysis pathway and the TCA cycle as well as an increased amino acids metabolism (Figures 5 and 6). These changes suggest that parasites exhibit a finely tuned adaptive metabolic mechanism upon DHA pulse. The accumulation of intermediates in glycolysis was able to enhance the activity pyruvate kinase, resulting the decrease amount of phosphoenolpyruvic acid which further regulates the gene expression in TCA cycle. Thus, the perturbation in glycolysis was capable to affect multiple processes during metabolic switching. Besides, phosphoenolpyruvic acid, a substrate in the peptidoglycan synthesis, affected metabolome including GlcNAc-P, UDP-GlcNAc, and UDP-MurNAc, suggesting a decreased carbon fluxes in glycolysis. Notably, the level of α-ketoglutaric acid, one derivative from amino acid oxidation, exhibited

Please cite this article in press as: Yu et al., Ring-stage growth arrest: Metabolic basis of artemisinin tolerance in *Plasmodium falciparum*, iScience (2022), https://doi.org/10.1016/j.isci.2022.105725

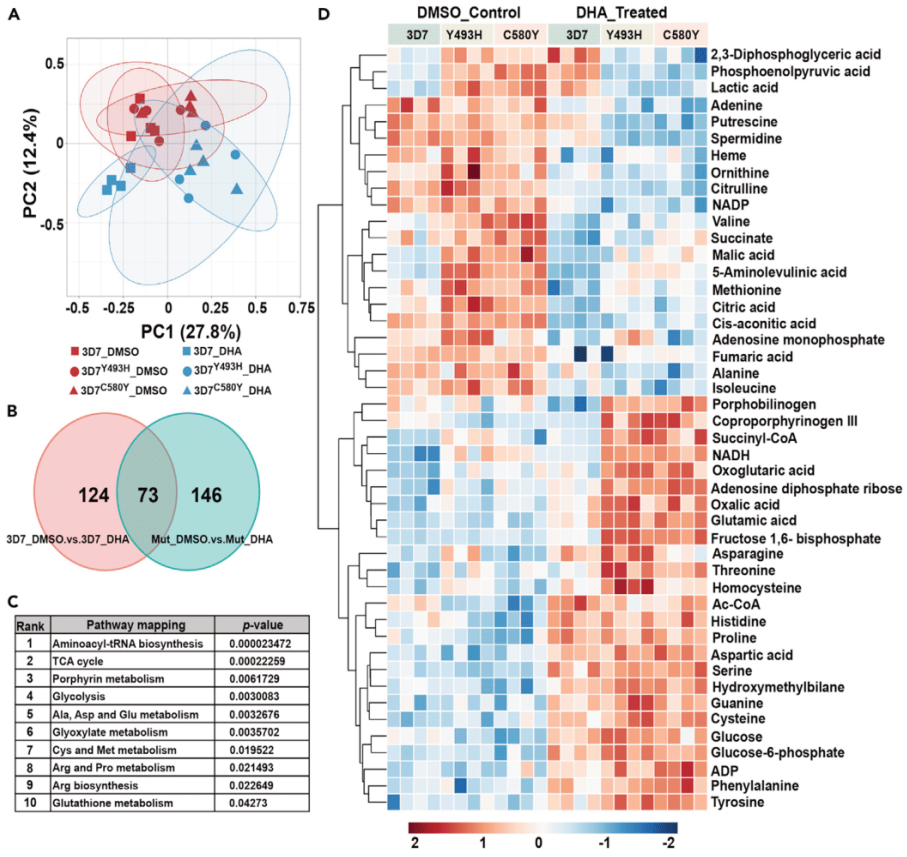

Rank	Pathway mapping	*p*-value
1	Aminoacyl-tRNA biosynthesis	0.000023472
2	TCA cycle	0.00022259
3	Porphyrin metabolism	0.0061729
4	Glycolysis	0.0030083
5	Ala, Asp and Glu metabolism	0.0032676
6	Glyoxylate metabolism	0.0035702
7	Cys and Met metabolism	0.019522
8	Arg and Pro metabolism	0.021493
9	Arg biosynthesis	0.022649
10	Glutathione metabolism	0.04273

Figure 4. Untargeted metabolomics screening of *Pfkelch13*-associated metabolome after DHA exposure and the schematic workflow is listed in Figure 3.

PCA (A) scatterplot for acquired metabolic profile in vehicle (n = 4 for each group) or DHA-treated (n = 4 for each group) $3D7^{WT}$, $3D7^{Y493H}$, and $3D7^{C580Y}$ parasites. Clearly separated clusters of DHA-resistant parasite indicated distinguishable metabolic pattern compared with $3D7^{WT}$ whereas that was similar at initial state without DHA treatment. Besides, permutation tests have validated the robustness of multivariate statistical model without over fitting. (B) Venn diagram showing significant overlap of 73 significantly alerted metabolites in pairwise comparisons between the WT and mutant lines after DHA pulse. (C) Pathway enrichment analysis of the DHA-related metabolome. Pathway enrichment analysis has been performed using a subset of metabolites listed in Table 1, indicating that amino acid metabolism, porphyrin metabolism, and energy metabolism related pathways belonged to high ranked pathways. Using a two-sided t test adjusted for multiple comparisons using the Holm-Bonferroni method (D) Heatmap of significantly changed metabolites from enriched metabolic pathways. Each line represents a detected metabolite and data were scaled and depicted on a log2 scale. Columns represent each biological replicate from four independent experiments with/without DHA exposure. Overall, metabolite abundances in DHA-treated parasites showed metabolic alterations in *Pfkelch13* WT and mutant parasite strains.

a higher abundance, suggesting a possible increase for amino acids catabolism, consistent with pathway enrich analysis. Meanwhile, as it has been proved that glutamic acid and α-ketoglutaric acid constitute a branching point for TCA cycle and amino acids, its significantly upregulated level along with its precursors (including proline, histidine, and asparagine) could suggest a metabolism shifted toward glutamic acid production. Besides, thiol-containing amino acids, known to be associated with either energy or antioxidative metabolism, were also significantly affected upon DHA exposure. As shown in Figure 6, the relative abundance for intermediates corresponding to thiol-containing amino acid metabolism (including cysteine and serine as well as their metabolic products also responsible for energy metabolism and antioxidative stress) was significantly altered. Among them, it should be noted that spermidine is responsible for cellular cycle control, strengthening our hypothesis that the IDC process is arrested.[33]

Please cite this article in press as: Yu et al., Ring-stage growth arrest: Metabolic basis of artemisinin tolerance in *Plasmodium falciparum*, iScience (2022), https://doi.org/10.1016/j.isci.2022.105725

Table 1. Different metabolites between DHA-exposed and nonexposed parasites

Upregulated metabolites

					3D7WT DMSO vs DHA		3D7Mut DMSO vs DHA	
No	Metabolite	*m/z* (amu)	RT[a] (min)	VIP[b]	FC[c]	adjusted p value	FC	adjusted p value
1	Glutamic acid	147.0533	1.39	1.56	1.515	0.0419	2.067	1.73E-07
2	Fructose 1,6- bisphosphate	339.9952	1.11	1.59	0.647	0.0040	2.414	3.63E-07
3	Serine	105.0425	1.28	1.68	2.111	0.0279	2.631	4.81E-07
4	N-Acetyl-D-Glucosamine 6-Phosphate	301.0563	10.04	1.72	1.391	0.0781	1.668	6.98E-07
5	Hydroxymethylbilane	854.2853	1.27	1.61	0.771	0.0450	1.743	7.44E-07
6	Tyrosine	181.0737	5.16	1.70	1.469	0.0274	1.810	1.90E-06
7	Glucose 6-phosphate	260.0299	10.19	1.55	1.601	0.0422	1.828	2.09E-06
8	Uridine diphosphate-N-acetylglucosamine	607.0817	14.80	1.60	1.374	0.0144	2.131	2.35E-06
9	Glycerophosphocholine	257.1028	12.99	1.53	1.677	0.0209	2.126	4.37E-06
10	Adenosine diphosphate ribose	559.0717	1.43	2.01	1.697	0.0097	2.075	5.65E-06
11	Aspartic acid	133.0351	1.20	1.67	1.332	0.0019	1.532	5.84E-06
12	Inosine	268.2263	13.74	1.75	1.742	0.0143	2.217	6.78E-06
13	Cysteine	121.0195	4.52	1.81	1.307	0.0033	1.965	1.24E-05
14	Glyoxylic acid	74.0003	8.12	1.88	0.702	0.0219	1.916	1.36E-05
15	Glucose	180.0634	9.43	1.95	1.465	0.0294	2.698	1.56E-05
16	3-Methyl-2-oxovaleric acid	130.0628	12.74	1.56	1.282	0.0354	1.989	2.19E-05
17	α-Ketoisovaleric acid	116.0471	12.48	1.52	1.153	0.0473	1.616	2.28E-05
18	Proline	115.0632	12.74	1.51	1.285	0.0180	1.444	2.48E-05
19	Putrescine	88.1002	1.39	1.64	0.768	0.0402	1.434	2.62E-05
20	Adenosine monophosphate	347.0631	1.41	1.78	1.472	0.0481	1.842	2.77E-05
21	Pantothenic Acid	219.1117	6.21	1.50	1.598	0.0247	2.123	3.47E-05
22	Citrulline	175.0955	2.10	1.64	1.239	0.0492	1.707	4.09E-05
23	Coproporphyrinogen III	660.3158	8.83	1.87	0.709	0.0038	2.484	4.20E-05
24	GDP-L-fucose	589.0818	1.26	1.77	1.502	0.0155	1.795	4.55E-05
25	Phenylalanine	165.0788	9.41	1.54	1.612	0.0402	2.151	5.42E-05
26	L-methionine	149.0512	8.77	1.64	0.570	0.0234	1.673	6.24E-05
27	Ac-CoA	809.1251	8.77	1.53	1.703	0.0194	2.379	6.99E-05
28	CDP-ethanolamine	446.0611	8.99	1.52	1.900	0.0110	2.565	7.54E-05
29	Histidine	155.0693	12.15	1.71	1.468	0.0537	1.988	9.35E-05
30	Guanine	151.0493	9.50	1.63	1.650	0.0134	1.970	1.09E-04
31	ADP	427.0294	1.43	1.83	1.251	0.0104	1.573	1.13E-04
32	Oxalic acid	89.9952	1.71	1.50	1.254	0.0324	1.937	1.17E-04
33	Galactosylsphingosine	461.3360	14.79	1.61	1.711	0.0240	3.102	1.42E-04
34	NADH	665.1244	14.88	1.65	2.192	0.0030	1.907	2.01E-04
35	Threonine	119.0582	9.98	1.51	1.289	0.0431	1.465	3.26E-04
36	Malic acid	134.0215	12.65	1.78	1.147	0.0019	1.569	3.87E-04
37	Porphobilinogen	226.0958	6.73	1.95	0.506	0.0109	1.612	4.11E-04
38	dCMP	307.0554	8.46	1.64	1.823	0.0158	1.818	8.48E-04

(*Continued on next page*)

Please cite this article in press as: Yu et al., Ring-stage growth arrest: Metabolic basis of artemisinin tolerance in *Plasmodium falciparum*, iScience (2022), https://doi.org/10.1016/j.isci.2022.105725

Table 1. *Continued*

Upregulated metabolites

No	Metabolite	*m/z* (amu)	RT[a] (min)	VIP[b]	3D7WT DMSO vs DHA FC[c]	3D7WT DMSO vs DHA adjusted p value	3D7Mut DMSO vs DHA FC	3D7Mut DMSO vs DHA adjusted p value
39	Succinyl-CoA	867.1294	14.81	1.87	1.372	0.0401	2.228	9.18E-04
40	Dodecanedioic acid	294.1859	13.47	1.60	1.381	0.0311	1.803	0.0011
41	Succinyladenosine	383.1076	6.44	1.77	1.615	0.0020	1.751	0.0029
42	Homocysteine	135.0354	1.17	1.53	1.510	0.0363	2.023	0.0067
43	Asparagine	132.0535	12.65	1.63	1.296	0.0068	1.725	0.0205
44	α-Ketoglutaric acid	146.021545	12.644	1.88	1.255	0.0361	1.553	0.0434

Downregulated metabolites

No	Metabolite	*m/z* (amu)	RT[a] (min)	VIP[b]	3D7WT DMSO vs DHA FC[c]	3D7WT DMSO vs DHA adjusted p value	3D7Mut DMSO vs DHA FC	3D7Mut DMSO vs DHA adjusted p value
1	Stearic acid	284.2722	14.79	1.72	0.521	0.0461	0.336	3.17E-11
2	*Cis*-aconitic acid	174.0165	9.38	1.75	0.636	0.0008	0.394	3.54E-08
3	Lactic acid	90.0317	12.64	1.69	1.729	0.0153	0.473	8.57E-08
4	Spermidine	145.1577	1.09	1.56	0.454	0.0662	0.211	7.30E-08
5	Oleic acid	282.2560	14.54	1.67	0.596	0.0017	0.286	1.19E-06
6	Uridine diphosphate-N-acetylmuraminate	679.1024	14.67	1.70	0.679	0.3101	0.455	7.47E-07
7	NADP	743.0754	16.00	1.71	0.471	0.0267	0.282	1.74E-06
8	Pipecolic acid	129.0788	1.84	1.60	0.395	0.0585	0.278	2.21E-06
9	Pyroglutamic acid	129.0424	6.73	1.57	0.596	0.0147	0.286	3.63E-06
10	Isoleucine	131.0945	3.07	1.83	0.742	0.0413	0.550	5.12E-06
11	Fumaric acid	116.0108	1.98	1.94	1.208	0.0093	0.363	1.76E-05
12	Valine	117.0788	9.36	1.67	0.754	0.0466	0.570	1.89E-05
13	5-Aminolevulinic acid	131.0588	1.35	1.57	0.520	0.0062	0.295	4.50E-05
14	Citric acid	192.0271	8.57	2.38	0.438	0.0036	0.317	5.60E-05
15	Citrulline	175.0957	2.10	1.64	0.486	0.0007	0.346	6.52E-05
16	Undecanedioic acid	216.1363	10.30	1.73	0.478	0.0074	0.660	7.54E-05
17	Deoxycytidine	227.0910	11.96	1.55	0.656	0.0435	0.572	1.07E-04
18	2,3-Diphosphoglyceric acid	265.9596	1.15	1.58	1.810	0.0083	0.621	1.29E-04
19	Alanine	89.0475	9.40	1.74	0.750	0.0463	0.542	1.15E-04
20	Creatine	131.0693	1.35	1.83	0.576	0.0358	0.344	3.02E-04
21	Phosphoenolpyruvic acid	167.9826	1.15	1.55	2.018	0.0011	0.155	1.76E-04
22	Succinic acid	118.0264	12.99	1.80	0.589	0.0298	0.671	4.50E-04
23	Adenine	135.0544	2.77	1.79	0.496	0.0095	0.544	4.98E-04
24	Pyridoxine	129.0788	1.84	1.60	0.511	0.0005	0.423	7.36E-04
25	Ornithine	132.0898	12.74	1.81	0.796	0.0469	0.421	0.0011
26	Inosinic acid	348.0471	1.39	1.51	0.460	0.0171	0.387	0.0015
27	Heme	616.1761	9.72	1.82	0.449	0.0274	0.408	0.0015
28	Isovaleric acid	102.0680	1.54	1.60	0.634	0.0384	0.441	0.0025
29	Mannitol 1-phosphate	262.0454	15.69	1.85	0.732	0.0158	0.612	0.0379

[a]retention time.
[b]variable important in projection.
[c]fold change.

Please cite this article in press as: Yu et al., Ring-stage growth arrest: Metabolic basis of artemisinin tolerance in *Plasmodium falciparum*, iScience (2022), https://doi.org/10.1016/j.isci.2022.105725

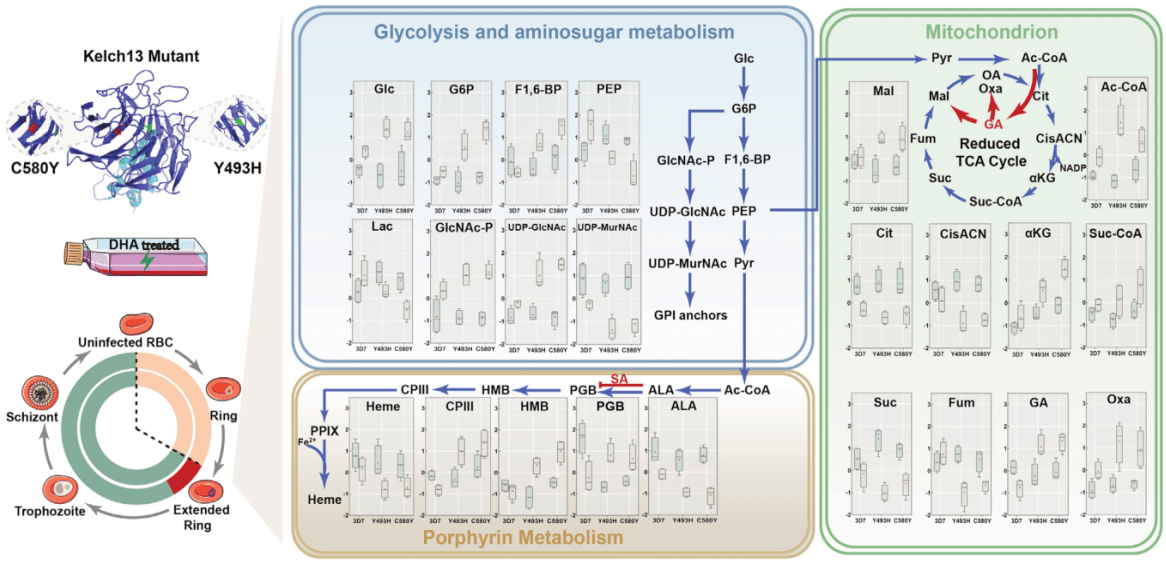

Figure 5. Proposed metabolic network of glucose metabolism, TCA, and heme biosynthetic pathways after DHA exposure

Boxplot (DMSO: light brown/DHA: green) corresponds to the relative abundance for each metabolite after normalization. Abbreviations: Glc: glucose; G6P: glucose 6-phosphate; F1,6-BP: fructose 1,6- bisphosphate; PEP: phosphoenolpyruvic acid; Lac: lactic acid; GlcNAc-P: N-acetyl-glucosamine 6-phosphate; UDP-GlcNAc: UDP-N-acetylglucosamine; UDP-MurNAc: UDP-N-acetylmuraminate; ALA: 5-Aminolevulinic acid; PGB: porphobilinogen; HMB: hydroxymethylbilane; CPIII: coproporphyrinogen III; Mal: malic acid; OA: Oxaloacetic acid; Ac-CoA: acetyl-CoA; Cit: citric acid; *Cis*-CAN: *cis*-aconitic acid; aKG: α-ketoglutaric acid; Suc-CoA: succinyl-CoA; Suc: Succinic acid; Fum: fumaric acid; GA: glyoxylic acid; Oxa: oxalic acid

To validate the relationship between decreased TCA metabolism and the temporary growth arrest of parasites exposed to DHA, we investigated the effects of glyoxylic acid (GA) on the $3D7^{WT}$, $3D7^{Y493H}$, and $3D7^{C580Y}$ lines. The effect of GA and succinyl acetone (SA) preincubation on the function of mitochondrion and generation of reactive oxygen species (ROS) as well as the growth of *Plasmodium* was monitored before subsequent analysis (Figures S4 and S5). We observed that the addition of 30 mM GA before DHA exposure promoted a decrease of DHA susceptibility to both the $3D7^{WT}$ control line and the $3D7^{Y493H}$ and $3D7^{C580Y}$ lines (Figures 7A and 7B). These results demonstrate that changes in metabolic flux have an impact on parasite susceptibility to DHA, consistent with the results from the metabolomics screening assays. This finding recalls the bacterial tolerance to antimicrobial agents that can be induced by changing the TCA metabolic flux into a glyoxylate shunt and points out that pathogens susceptibility can be metabolically tuned.[34] In addition, we revealed that exogenous supplementation with GA also elicits a protective effect against DHA-induced lethality, for currently unknown reasons.

To assess the role of porphyrin metabolism in parasite susceptibility to DHA, we examined whether its inhibition could affect the survival of parasites. We pretreated DHA-exposed parasites with SA, an inhibitor of ALAD in porphyrin metabolism, and observed a slight decrease in parasite susceptibility to DHA, especially for concentrations around EC_{50} (Figures 7A and 7B). Based on assessment of the total level of porphyrins, we confirmed that heme production was associated with changes in *in vitro* DHA susceptibility. Indeed, porphyrin levels as evaluated by fluorescence significantly decreased after SA treatment (Figure 7C), indicating that modulation of heme metabolism leads to changes in *in vitro* DHA susceptibility.

Furthermore, we also observed that mitochondrial membrane potential was significantly increased following DHA treatment in SA-exposed parasites compared to untreated parasites (Figure 7D). Oxidative stress was assessed by measuring the level of ROS (through the measurement of H_2DCFDA) caused by DHA treatment. A ~10-fold increase in ROS was detected in DHA-exposed parasites compared to nonexposed controls, indicating lethality was caused by excess oxidative stress. Meanwhile, oxidative stress caused by DHA exposure was significantly higher in $3D7^{WT}$ than in $3D7^{Y493H}$ and $3D7^{C580Y}$ ($p = 0.049$ and 0.036, respectively). Furthermore, ROS levels were slightly decreased, consistent with results from RSA, for parasites pretreated with inhibitor (Figure 7E). One of the most well-documented modes of action for DHA is

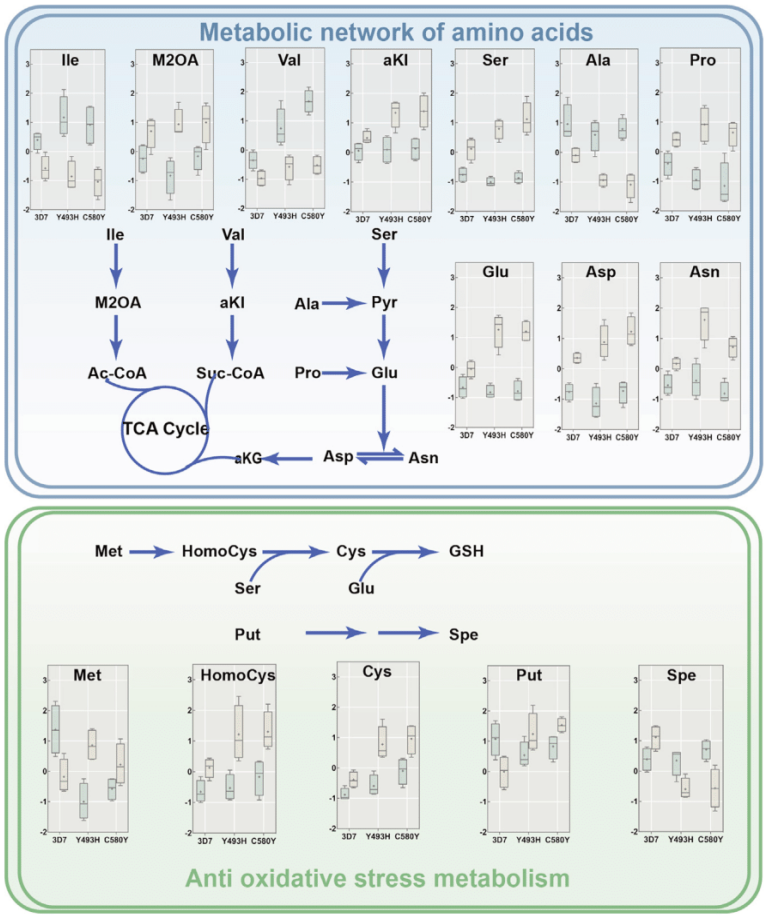

Figure 6. Metabolic network of selected amino acids and their intermediates after DHA exposure

Abbreviations: Ile: isoleucinei; M2OA: 3-methyl-2-oxovaleric acid; Ac-CoA: acetyl-CoA; TCA: tricarboxylic acid; Val: valine; aKI: α-ketoisovaleric acid; Suc-CoA: succinyl-CoA; aKG: α-ketoglutaric acid; Ser: serine; Ala: alanine; Pro: proline; Glu: glutamic acid; Asp: asparagine; Asn: Aspartic acid; Met: methionine; HomoCys: homocysteine; Cys; cysteine; GSH: Glutathione; Put: putrescine; Spe: spermidine.

through the binding of the endoperoxide with heme-related Fe^{2+} producing abundant free radicals that alkylate parasite proteins, resulting in parasite death.[35–37] ROS is also responsible for mitochondrial depolarization which impairs normal function, and excess levels of ROS can induce DNA double-strand breaks which further cause lethal effect for parasites.

DISCUSSION

In this study, we aimed at elucidating whether ring-stage growth arrest induced by DHA confers a survival benefit to *P. falciparum* parasites with mutations in the *Pfkelch13* gene. Previous metabolomics *P. falciparum* studies mainly focused on the late blood stages of life cycle; here we explored the metabolic profile of ring stages which is closely associated with growth arrest upon DHA exposure. We compared the metabolic profiles of growth-arrested ring-stage parasites in relation with their *in vitro* susceptibility to DHA as measured by the RSA.[38] Herein, we investigated the correlation of the relative abundance of altered metabolome with a metabolic process resulting from DHA pulse that parasites have to face during survival. Parasites intended to extend the less sensitive ring stage for the escape of lethal effect.

Please cite this article in press as: Yu et al., Ring-stage growth arrest: Metabolic basis of artemisinin tolerance in *Plasmodium falciparum*, iScience (2022), https://doi.org/10.1016/j.isci.2022.105725

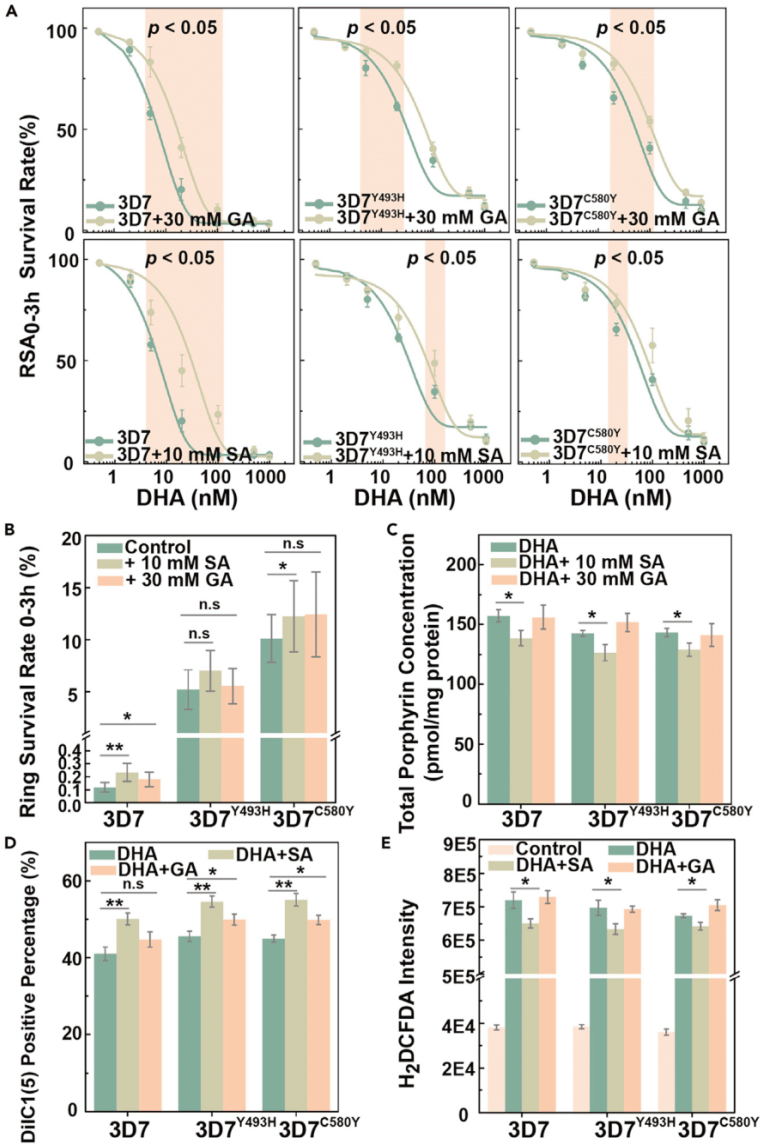

Figure 7. Affected drug susceptibility by chemical inhibition of corresponding pathway

(A) Top panel showed preincubating parasites with 30 mM for 1h GA had reduced DHA susceptibility in $3D7^{WT}$, $3D7^{Y493H}$, and $3D7^{C580Y}$ parasites; bottom panel presented preincubating parasites with 10 mM SA for 7h had reduced DHA susceptibility in $3D7^{WT}$, $3D7^{Y493H}$, and $3D7^{C580Y}$ parasites. p value indicates statistical comparisons between WT and mutant parasites at selected time point (labeled by colored background) by Student's t test.

(B) RSA_{0-3h} determination for parasites pretreated with SA or GA as a result of inhibition of TCA cycle or heme biosynthetic pathway. Changed DHA susceptibility was obtained due to the change of metabolic state.

(C) Total porphyrin levels (combination of heme and PPIX) in parasites showed a reduced porphyrin concentration due to alterations in heme biosynthetic pathways.

(D and E) DHA-dependent mitochondrial dysfunction and reactive oxygen species generation measurement. Parasites were exposed to 700 nM DHA for the evaluation of drug susceptibility with/without inhibition.

Based on a novel enrichment method (SLOPE), adaptive metabolic changes were evaluated to address the hypothesis that *Pfkelch13* WT and mutant lines constitute two different populations upon DHA pulse. The metabolome of ring-stage parasites displayed altered energy and porphyrin metabolism profiles, including changes in the TCA cycle, glycolysis, and amino acid and pyruvate metabolic pathways. We initially hypothesized that mutant parasites were capable to orchestrate a metabolic switch corresponding to energy metabolism. Considering either glucose or amino acids as the energy supply in parasites, metabolic network revealed the metabolic switch from glucose to amino acids catabolism occurs during arrested growth. Notably, perturbed porphyrin metabolism is also a metabolic feedback for hemoglobin catabolism which has been previously reported for the mode of action of DHA.[39] Meanwhile, for the corresponding antioxidative stress metabolism, previous research has reported an enhanced glutathione production by screening the biological changes, which was consistent with observed metabolic network.[40] Although the altered levels of TCA cycle has been reported by measuring level of intermediates, little is known about the adaptative metabolic plasticity that mutant parasites undergo upon DHA exposure which turns out to be critical for survival.[30] Based on the metabolomic screening results, we were able to alter the *in vitro* susceptibility to DHA by either changing metabolic flux (through exogenous supplementation with GA) or through chemical inhibition (through the addition of SA), indicating that metabolic disruption protects parasites from the damage caused by DHA exposure. Overall, this study provides metabolomics-based evidence for elucidating the role of *Pfkelch13* mutations in ART-R.

In addition to the conventional resistance phenotype measured by RSA, detailed *in vitro* stage-specific growth rates during a single IDC were determined, indicating either a ~6 h delayed growth for DHA-resistant engineered strains or the existence of growth-arrested forms of parasites following exposure to 50 nM DHA. Despite the extended ring-stage period, the overall IDC development time for engineered lines remained almost similar to the WT due to the shortened trophozoite stage period. We concluded that the altered development profile, especially concerning the extended ring-stage development, was closely related to the resistance phenotype, and this was consistent with previously reported transcriptome profiles in which a prolonged ring stage allows the upregulation of unfolded protein responses that protect the parasite from drug-induced protein damages.[41] The altered IDC profile confers the additional advantage that the most susceptible stage in asexual development receives reduced exposure. Previous studies have indicated that the late-stage parasites (trophozoite or schizont) are more sensitive to various antimalarials, and therefore based on our findings, we consider that an extended ring stage may have evolved as a protective mechanism as it reduces the exposure time for these sensitive later stages during the IDC.[20,27,42] Because ring-stage parasites are metabolically less active and less susceptible to DHA than mature stages, it is conceivable that extended ring stages would enable the parasites to better survive DHA exposure, given its relatively short *in vivo* half-life.[42,43] Some reports have shown that growth-arrested parasites resulting from drug pressure applied to ring-stage parasites can survive for several days before returning to normal development.[11,21] According to the results, we hypothesized that the extended ring stage could be an advantage in which parasites were growth-arrested with subsequent development following DHA treatment.

ART-induced arrested growth remains understudied due to the rarity of arrested parasites following drug exposure. Furthermore, most metabolomic studies focus on the parasite stages that occur late in the IDC because of the availability of efficient purification methods such as magnetic sorting which significantly reduces background noise resulting from excess uninfected erythrocytes.[30,40] For the early-stage parasites, the lack of an efficient enrichment strategy has greatly hindered attempts to investigate their metabolomics. Furthermore, recent downstream omics studies have revealed that the proteome or metabolome of early stage forms are significantly affected by host contamination due to a high ratio of host to parasite-specific signals.[44] To investigate the metabolome in arrested ring-stage-associated DHA resistance, we present here a novel enrichment method (SLOPE) to obtain ring-stage parasites by effective removal of uninfected host erythrocytes without affecting parasitic viability. Clearly separated metabolic profiles were obtained for SLOPE-enriched ring-stage samples, demonstrating its suitability for metabolic analysis. We found that the major shifts in the metabolome of parasites with DHA-resistance-associated mutations in the *Pfkelch13* gene under growth arrest involved the TCA cycle, glycolysis, and amino acid and pyruvate metabolism. In most of free-living microorganisms, the TCA cycle acts as the central wheel for carbon metabolism in which carbon-derived metabolites like pyruvate produced from glycolysis are converted into intermediate products for energy production. Previous studies have revealed that during the asexual development stages, levels of TCA cycle intermediates change periodically, indicating that the full TCA cycle

functions with mitochondrial acetyl-coenzyme A (CoA) derived from amino acid catabolism.[45] It should be noted that parasites are capable to use either glucose or amino acids as the source for energy metabolism.[46] Therefore, on the basis of metabolomics screening, significantly upregulated level of glucose as well as related amino acids indicated that either amino acids had been serving for synthesis of glucose or the intracellular glucose consumption had been arrested. Thus, we deduce that upon DHA pulse, there was a metabolic switch from glucose to amino acids consumption for fueling the energy supply in growth-arrested parasites.

Based on above-mentioned metabolomics findings, we have investigated whether inhibition of the metabolic pathways implicated above would affect DHA susceptibility. Parasites pretreated with GA or SA displayed reduced DHA susceptibility as measured by an increased survival in the $RSA_{0-3h}^{50\%}$. RSA_{0-3h} revealed a slight reduction in *in vitro* susceptibility following addition of GA or SA, demonstrating that decreased metabolism or altered metabolic flux profiles induced by growth arrest could contribute to increased DHA tolerance. Therefore, according to our metabolomics data, we hypothesize that GA may be an inducer of antibiotic tolerance through the biochemical shunting of the TCA cycle.

In conclusion, the generation of *Pfkelch13* $3D7^{493H}$ and $3D7^{580Y}$ mutants using the Cas9i system, coupled with various DHA susceptibility assays, revealed an association between *Pfkelch13* mutations and growth arrest-mediated partial resistance to DHA. Furthermore, based on a novel enrichment method, we provide metabolic evidence that DHA-induced growth arrest ring stages are associated with significantly decreased energy metabolism activity. DHA susceptibility is affected by both chemical inhibition and changes in metabolic flux. These findings could help understand how mutant parasite lines undergo adaptative changes upon drug pulse and provide useful information in understanding the critical metabolic plasticity from metabolic perspective.

Limitations of the study

The here-presented study was aimed at investigating the underlying metabolic mechanisms for *PfKelch13*-mutation-mediated ART-R in human malaria parasites by untargeted metabolic profiling. Limitations of this study included using the mix of both growth-arrested and dead parasites resulting from proposed enrichment protocol for following metabolomics analysis. Although flow cytometric sorting was not performed due to the lack of efficiency for acquiring sufficient parasites, the metabolome of dead parasites had been taken into consideration for background subtraction during data analysis which could help circumvent this problem. Therefore, we believed the unrelated metabolic signal resulting from either dead parasites or host erythrocytes could be greatly reduced, suggesting that the acquired metabolome was closely associated with growth-arrested parasites. Meanwhile, based on the primary untargeted screening analysis, more detailed targeted profiling aimed at quantitatively investigating the alterations for metabolites involved in related pathways had not been performed. Although the biological efficacy for part of proposed metabolome and pathways has been validated by either changing metabolic flow or chemical inhibition, it still remained as a comprehensive evaluation in which detailed investigation for the alterations of related metabolic pathways has to be carried out. Moreover, in spite of the fact that *PfKelch13*-mutations was closely associated with ART-R, a brief validation for results obtained from this study should be considered in more filed isolates which were unavailable due to global COVID-19 situation. Ultimately, each study has its own limitations and requirements; thus additional studies are required for detailed characterization and validation of defined metabolic pathways in more filed isolates with *PfKelch13* mutations.

STAR★METHODS

Detailed methods are provided in the online version of this paper and include the following:

- KEY RESOURCES TABLE
- RESOURCE AVAILABILITY
  - Lead contact
  - Materials availability
  - Data and code availability
- EXPERIMENTAL MODEL AND SUBJECT DETAILS
- METHOD DETAILS

- Plasmid construction
- Parasite gene transfection
- Chemical and density-based enrichment protocol
- Phenotype validation
- Biological effectiveness analysis

- QUANTIFICATION AND STATISTICAL ANALYSIS
- ADDITIONAL RESOURCES

SUPPLEMENTAL INFORMATION

Supplemental information can be found online at https://doi.org/10.1016/j.isci.2022.105725.

ACKNOWLEDGMENTS

This work was supported by National Key R&D Program of China (No. 2020YFC1200105 and 2018YFA0507300), National Natural Science Foundation of China (No. 82230077, 81971967, 82102424, 81971959, and 82172302), Natural Science Foundation of Jiangsu Province (No. BK20210061), the China Postdoctoral Science Foundation (2020M671397), the Shanghai Blue Cross Brain Hospital Co. Ltd., and Shanghai Tongji University Education Development Foundation.

AUTHOR CONTRIBUTIONS

JC, QZ, DM, and GZ conceived and designed the experiments. YZ generated transgenic parasite lines and related analysis. XY, MZ, GZ, JT, CW, and LP performed the experiments and data analysis. XY and DM wrote the manuscript with contribution from JC, QZ, and RC.

DECLARATION OF INTERESTS

The authors declare no competing interests.

Received: May 3, 2022
Revised: October 9, 2022
Accepted: November 30, 2022
Published: ■■ ■■, ■■

REFERENCES

1. World Health Organization (2021). World malaria report 2021. https://www.who.int/publications/i/item/9789240040496.

2. Bastiaens, G.J.H., Bousema, T., and Leslie, T. (2014). Scale-up of malaria rapid diagnostic tests and artemisinin-based combination therapy: challenges and perspectives in sub-Saharan Africa. PLoS Med. *11*. e1001590. https://doi.org/10.1371/journal.pmed.1001590.

3. Benelli, G., and Beier, J.C. (2017). Current vector control challenges in the fight against malaria. Acta Trop. *174*, 91–96. https://doi.org/10.1016/j.actatropica.2017.06.028.

4. Eastman, R.T., and Fidock, D.A. (2009). Artemisinin-based combination therapies: a vital tool in efforts to eliminate malaria. Nat. Rev. Microbiol. *7*, 864–874. https://doi.org/10.1038/nrmicro2239.

5. Cui, L., and Su, X.z. (2009). Discovery, mechanisms of action and combination therapy of artemisinin. Expert Rev. Anti Infect. Ther. *7*, 999–1013. https://doi.org/10.1586/eri.09.68.

6. World Health Organization (2018). Artemisinin resistance and artemisinin-based combination therapy efficacy: status report. https://apps.who.int/iris/bitstream/handle/10665/274362/WHO-CDS-GMP-2018.18-eng.pdf.

7. Breman, J.G. (2012). Resistance to artemisinin-based combination therapy. Lancet Infect. Dis. *12*, 820–822. https://doi.org/10.1016/S1473-3099(12)70226-8.

8. Tilley, L., Straimer, J., Gnädig, N.F., Ralph, S.A., and Fidock, D.A. (2016). Artemisinin action and resistance in Plasmodium falciparum. Trends Parasitol. *32*, 682–696. https://doi.org/10.1016/j.pt.2016.05.010.

9. Woodrow, C.J., and White, N.J. (2017). The clinical impact of artemisinin resistance in Southeast Asia and the potential for future spread. FEMS Microbiol. Rev. *41*, 34–48. https://doi.org/10.1093/femsre/fuw037.

10. Chen, N., LaCrue, A.N., Teuscher, F., Waters, N.C., Gatton, M.L., Kyle, D.E., and Cheng, Q. (2014). Fatty acid synthesis and pyruvate metabolism pathways remain active in dihydroartemisinin-induced dormant ring stages of Plasmodium falciparum. Antimicrob. Agents Chemother. *58*, 4773–4781. https://doi.org/10.1128/AAC.02647-14.

11. Hott, A., Ca Sandra, D., Sparks, K.N., Morton, L.C., Castanares, G.G., Rutter, A., and Kyle, D.E. (2015). Artemisinin-resistant Plasmodium falciparum parasites exhibit altered patterns of development in infected erythrocytes. Antimicrob. Agents Chemother. *59*, 3156–3167. https://doi.org/10.1128/AAC.00197-15.

12. Ariey, F., Witkowski, B., Amaratunga, C., Beghain, J., Langlois, A.-C., Khim, N., Kim, S., Duru, V., Bouchier, C., Ma, L., et al. (2014). A molecular marker of artemisinin-resistant Plasmodium falciparum malaria. Nature *505*, 50–55. https://doi.org/10.1038/nature12876.

13. Ashley, E.A., Dhorda, M., Fairhurst, R.M., Amaratunga, C., Lim, P., Suon, S., Sreng, S., Anderson, J.M., Mao, S., Sam, B., et al. (2014). Spread of artemisinin resistance in Plasmodium falciparum malaria. N. Engl. J. Med. *371*, 411–423. https://doi.org/10.1056/NEJMoa1314981.

14. Straimer, J., Gnädig, N.F., Witkowski, B., Amaratunga, C., Duru, V., Ramadani, A.P., Dacheux, M., Khim, N., Zhang, L., Lam, S.,

et al. (2015). K13-propeller mutations confer artemisinin resistance in Plasmodium falciparum clinical isolates. Science *347*, 428–431. https://doi.org/10.1126/science.1260867.

15. MalariaGEN Plasmodium falciparum Community Project (2016). Genomic epidemiology of artemisinin resistant malaria. Elife *5*. e08714. https://doi.org/10.7554/eLife.08714.

16. Haldar, K., Bhattacharjee, S., and Safeukui, I. (2018). Drug resistance in Plasmodium. Nat. Rev. Microbiol. *16*, 156–170. https://doi.org/10.1038/nrmicro.2017.161.

17. Stokes, B.H., Dhingra, S.K., Rubiano, K., Mok, S., Straimer, J., Gnädig, N.F., Deni, I., Schindler, K.A., Bath, J.R., Ward, K.E., et al. (2021). Plasmodium falciparum K13 mutations in Africa and Asia impact artemisinin resistance and parasite fitness. Elife *10*. e66277. https://doi.org/10.7554/eLife.66277.

18. Mbengue, A., Bhattacharjee, S., Pandharkar, T., Liu, H., Estiu, G., Stahelin, R.V., Rizk, S.S., Njimoh, D.L., Ryan, Y., Chotivanich, K., et al. (2015). A molecular mechanism of artemisinin resistance in Plasmodium falciparum malaria. Nature *520*, 683–687. https://doi.org/10.1038/nature14412.

19. Birnbaum, J., Scharf, S., Schmidt, S., Jonscher, E., Hoeijmakers, W.A.M., Flemming, S., Toenhake, C.G., Schmitt, M., Sabitzki, R., Bergmann, B., et al. (2020). A Kelch13-defined endocytosis pathway mediates artemisinin resistance in malaria parasites. Science *367*, 51–59. https://doi.org/10.1126/science.aax4735.

20. Murithi, J.M., Owen, E.S., Istvan, E.S., Lee, M.C.S., Ottilie, S., Chibale, K., Goldberg, D.E., Winzeler, E.A., Llinás, M., Fidock, D.A., and Vanaerschot, M. (2020). Combining stage specificity and metabolomic profiling to advance antimalarial drug discovery. Cell Chem. Biol. *27*, 158–171.e3. https://doi.org/10.1016/j.chembiol.2019.11.009.

21. Siddiqui, F.A., Boonhok, R., Cabrera, M., Mbenda, H.G.N., Wang, M., Min, H., Liang, X., Qin, J., Zhu, X., Miao, J., et al. (2020). Role of Plasmodium falciparum Kelch 13 protein mutations in P. falciparum populations from northeastern Myanmar in mediating artemisinin resistance. mBio *11*. e01134-19. https://doi.org/10.1128/mBio.01134-19.

22. De Virgilio, C. (2012). The essence of yeast quiescence. FEMS Microbiol. Rev. *36*, 306–339. https://doi.org/10.1111/j.1574-6976.2011.00287.x.

23. Rittershaus, E.S.C., Baek, S.-H., and Sassetti, C.M. (2013). The normalcy of dormancy: common themes in microbial quiescence. Cell Host Microbe *13*, 643–651. https://doi.org/10.1016/j.chom.2013.05.012.

24. Greening, C., Grinter, R., and Chiri, E. (2019). Uncovering the metabolic strategies of the dormant microbial majority: towards integrative approaches. mSystems *4*. e00107-19. https://doi.org/10.1128/mSystems.00107-19.

25. Groger, M., Fischer, H.S., Veletzky, L., Lalremruata, A., and Ramharter, M. (2017). A systematic review of the clinical presentation, treatment and relapse characteristics of human Plasmodium ovale malaria. Malar. J. *16*, 112. https://doi.org/10.1186/s12936-017-1759-2.

26. Klonis, N., Crespo-Ortiz, M.P., Bottova, I., Abu-Bakar, N., Kenny, S., Rosenthal, P.J., and Tilley, L. (2011). Artemisinin activity against Plasmodium falciparum requires hemoglobin uptake and digestion. Proc. Natl. Acad. Sci. USA *108*, 11405–11410. https://doi.org/10.1073/pnas.1104063108.

27. Klonis, N., Xie, S.C., McCaw, J.M., Crespo-Ortiz, M.P., Zaloumis, S.G., Simpson, J.A., and Tilley, L. (2013). Altered temporal response of malaria parasites determines differential sensitivity to artemisinin. Proc. Natl. Acad. Sci. USA *110*, 5157–5162. https://doi.org/10.1073/pnas.1217452110.

28. Witkowski, B., Amaratunga, C., Khim, N., Sreng, S., Chim, P., Kim, S., Lim, P., Mao, S., Sopha, C., Sam, B., et al. (2013). Novel phenotypic assays for the detection of artemisinin-resistant Plasmodium falciparum malaria in Cambodia: in-vitro and ex-vivo drug-response studies. Lancet Infect. Dis. *13*, 1043–1049. https://doi.org/10.1016/S1473-3099(13)70252-4.

29. Duvalsaint, M., and Kyle, D.E. (2018). Phytohormones, isoprenoids, and role of the apicoplast in recovery from dihydroartemisinin-induced dormancy of Plasmodium falciparum. Antimicrob. Agents Chemother. *62*. e01771-17. https://doi.org/10.1128/AAC.01771-17.

30. Mok, S., Stokes, B.H., Gnädig, N.F., Ross, L.S., Yeo, T., Amaratunga, C., Allman, E., Solyakov, L., Bottrill, A.R., Tripathi, J., et al. (2021). Artemisinin-resistant K13 mutations rewire Plasmodium falciparum's intra-erythrocytic metabolic program to enhance survival. Nat. Commun. *12*, 530–615. https://doi.org/10.1038/s41467-020-20805-w.

31. Zhao, Y., Wang, F., Wang, C., Zhang, X., Jiang, C., Ding, F., Shen, L., and Zhang, Q. (2020). Optimization of CRISPR/Cas system for improving genome editing efficiency in Plasmodium falciparum. Front. Microbiol. *11*, 625862. https://doi.org/10.3389/fmicb.2020.625862.

32. Brown, A.C., Moore, C.C., and Guler, J.L. (2020). Cholesterol-dependent enrichment of understudied erythrocytic stages of human Plasmodium parasites. Sci. Rep. *10*, 4591–4615. https://doi.org/10.1038/s41598-020-61392-6.

33. González, N.S., Huber, A., and Algranati, I.D. (2001). Spermidine is essential for normal proliferation of trypanosomatid protozoa. FEBS Lett. *508*, 323–326. https://doi.org/10.1016/s0014-5793(01)03091-5.

34. Meylan, S., Porter, C.B.M., Yang, J.H., Belenky, P., Gutierrez, A., Lobritz, M.A., Park, J., Kim, S.H., Moskowitz, S.M., and Collins, J.J. (2017). Carbon sources tune antibiotic susceptibility in Pseudomonas aeruginosa via tricarboxylic acid cycle control. Cell Chem. Biol. *24*, 195–206. https://doi.org/10.1016/j.chembiol.2016.12.015.

35. Robert, A., Benoit-Vical, F., and Meunier, B. (2005). The key role of heme to trigger the antimalarial activity of trioxanes. Coord. Chem. Rev. *249*, 1927–1936. https://doi.org/10.1016/j.ccr.2004.12.022.

36. Meunier, B., and Robert, A. (2010). Heme as trigger and target for trioxane-containing antimalarial drugs. Acc. Chem. Res. *43*, 1444–1451. https://doi.org/10.1021/ar100070k.

37. Cui, L., Wang, Z., Miao, J., Miao, M., Chandra, R., Jiang, H., Su, X.z., and Cui, L. (2012). Mechanisms of in vitro resistance to dihydroartemisinin in Plasmodium falciparum. Mol. Microbiol. *86*, 111–128. https://doi.org/10.1111/j.1365-2958.2012.08180.x.

38. Harding, C.R., Sidik, S.M., Petrova, B., Gnädig, N.F., Okombo, J., Herneisen, A.L., Ward, K.E., Markus, B.M., Boydston, E.A., Fidock, D.A., and Lourido, S. (2020). Genetic screens reveal a central role for heme metabolism in artemisinin susceptibility. Nat. Commun. *11*, 4813. https://doi.org/10.1038/s41467-020-18624-0.

39. Cobbold, S.A., Chua, H.H., Nijagal, B., Creek, D.J., Ralph, S.A., and McConville, M.J. (2016). Metabolic dysregulation induced in Plasmodium falciparum by dihydroartemisinin and other front-line antimalarial drugs. J. Infect. Dis. *213*, 276–286. https://doi.org/10.1093/infdis/jiv372.

40. Siddiqui, G., Srivastava, A., Russell, A.S., and Creek, D.J. (2017). Multi-omics based identification of specific biochemical changes associated with PfKelch13-mutant artemisinin resistant Plasmodium falciparum. J. Infect. Dis. *215*, 1435–1444. https://doi.org/10.1093/infdis/jix156.

41. Mok, S., Ashley, E.A., Ferreira, P.E., Zhu, L., Lin, Z., Yeo, T., Chotivanich, K., Imwong, M., Pukrittayakamee, S., Dhorda, M., et al. (2015). Population transcriptomics of human malaria parasites reveals the mechanism of artemisinin resistance. Science *347*, 431–435. https://doi.org/10.1126/science.1260403.

42. Witkowski, B., Khim, N., Chim, P., Kim, S., Ke, S., Kloeung, N., Chy, S., Duong, S., Leang, R., Ringwald, P., et al. (2013). Reduced artemisinin susceptibility of Plasmodium falciparum ring stages in western Cambodia. Antimicrob. Agents Chemother. *57*, 914–923. https://doi.org/10.1128/AAC.01868-12.

43. Srivastava, A., Philip, N., Hughes, K.R., Georgiou, K., MacRae, J.I., Barrett, M.P., Creek, D.J., McConville, M.J., and Waters, A.P. (2016). Stage-specific changes in Plasmodium metabolism required for differentiation and adaptation to different host and vector environments. PLoS Pathog. *12*. e1006094. https://doi.org/10.1371/journal.ppat.1006094.

Please cite this article in press as: Yu et al., Ring-stage growth arrest: Metabolic basis of artemisinin tolerance in *Plasmodium falciparum*, iScience (2022), https://doi.org/10.1016/j.isci.2022.105725

44. Carey, M.A., Covelli, V., Brown, A., Medlock, G.L., Haaren, M., Cooper, J.G., Papin, J.A., and Guler, J.L. (2018). Influential parameters for the analysis of intracellular parasite metabolomics. mSphere *3*. e00097-18. https://doi.org/10.1128/mSphere.00097-18.

45. Olszewski, K.L., Morrisey, J.M., Wilinski, D., Burns, J.M., Vaidya, A.B., Rabinowitz, J.D., and Llinás, M. (2009). Host-parasite interactions revealed by Plasmodium falciparum metabolomics. Cell Host Microbe *5*, 191–199. https://doi.org/10.1016/j.chom.2009.01.004.

46. Kumar, M., Skillman, K., and Duraisingh, M.T. (2021). Linking nutrient sensing and gene expression in Plasmodium falciparum blood-stage parasites. Mol. Microbiol. *115*, 891–900. https://doi.org/10.1111/mmi.14652.

47. Xia, J., Psychogios, N., Young, N., and Wishart, D.S. (2009). MetaboAnalyst: a web server for metabolomic data analysis and interpretation. Nucleic Acids Res. *37*, W652–W660. https://doi.org/10.1093/nar/gkp356.

48. Shang, X., Shen, S., Tang, J., He, X., Zhao, Y., Wang, C., He, X., Guo, G., Liu, M., Wang, L., et al. (2021). A cascade of transcriptional repression determines sexual commitment and development in Plasmodium falciparum. Nucleic Acids Res. *49*, 9264–9279. https://doi.org/10.1093/nar/gkab683.

49. Shang, X., Wang, C., Fan, Y., Guo, G., Wang, F., Zhao, Y., Sheng, F., Tang, J., He, X., Yu, X., et al. (2022). Genome-wide landscape of ApiAP2 transcription factors reveals a heterochromatin-associated regulatory network during Plasmodium falciparum blood-stage development. Nucleic Acids Res. *50*, 3413–3431. https://doi.org/10.1093/nar/gkac176.

Please cite this article in press as: Yu et al., Ring-stage growth arrest: Metabolic basis of artemisinin tolerance in *Plasmodium falciparum*, iScience (2022), https://doi.org/10.1016/j.isci.2022.105725

STAR★METHODS

KEY RESOURCES TABLE

REAGENT or RESOURCE	SOURCE	IDENTIFIER
Anitbodies		
PE conjugated CD235a Monoclonal Antibody	Invitrogen	Cat# MA1-19661
Mouse Anti-alpha 1 Spectrin monoclonal antibody	Abcam	Cat# ab11751
Goat Anti-Mouse IgG (Alexa Fluor® 59) antibody	Abcam	Cat# ab150116
Bacterial and virus strains		
Plasmodium.falciparum 3D7 strain	This paper	N/A
Plasmodium.falciparum 3D7-Cas9i strain	This paper	N/A
Chemicals, peptides, and recombinant proteins		
RPMI 1640	Gibco	Cat# 31800089
HEPES	Gibco	Cat# 11344041
AlbuMAX™ I	ThermoFisher	Cat# 11020088
Giemsa' stain	Sigma-Aldrich	Cat# 32884
Hypoxanthine	Sigma-Aldrich	Cat# V900452
DSM1	Sigma-Aldrich	Cat# 5333040001
WR99210 hydrochloride	Sigma-Aldrich	Cat# SML2976
Streptolysin O	Sigma-Aldrich	Cat# S5265
SYTO™ 61	Invitrogen	Cat# S11343
Methanol LC-MS grade	Merck	Cat# 1.06035
Acetonitrile LC-MS grade	Merck	Cat# 1.00029
Formic acid for LC-MS	Merck	Cat# 5.33002
Critical commercial assays		
NucleoSpin Gel and PCR Clean-up Kit	MACHEREY-NAGEL	Cat# 740609
NucleoBond Xtra Midi Plus Kit	MACHEREY-NAGEL	Cat# 740410
ClonExpressII One Step Cloning Kit	Vazyme Biotech	Cat# C112-02
MitoProbe DilC1(5) Assay Kit	ThermoFisher	Cat# M34151
H2DCFDA Assay Kit	ThermoFisher	Cat# D399
Oligonucleotides		
Primer for plasmid construction, see Table S1	This paper	N/A
Deposited data		
Raw data	This paper	Metabolights: MTBLS6388
Software and algorithms		
SIEVE	ThermoFisher	N/A
TraceFinder	ThermoFisher	N/A
MetaboAnalyst	Xia et al.,[47]	http://www.metaboanalyst.ca
GraphPad Prism8	GraphPad	https://www.graphpad.com
SIMCA-P 13.0	Umetrics	http://www.umetrics.com/products/simca

RESOURCE AVAILABILITY

Lead contact

Further information and requests for resources should be directed to and will be fulfilled by the Lead Contact, J.C (caojun@jipd.com).

Please cite this article in press as: Yu et al., Ring-stage growth arrest: Metabolic basis of artemisinin tolerance in *Plasmodium falciparum*, iScience (2022), https://doi.org/10.1016/j.isci.2022.105725

Materials availability

This study did not generate new unique reagents.

Data and code availability

The data supporting the current study have been deposited at Metabolights. Accession number is listed in the key resources table; This paper did not report any original code; Any additional information required to reanalyze the data reported in this paper is available from the lead contact upon request.

EXPERIMENTAL MODEL AND SUBJECT DETAILS

All *P. falciparum* strains were cultured with human O^+ erythrocytes (provided by Shanghai Blood Center) at 2% hematocrit in RPMI 1640 media (Thermo Fisher Scientific, MA) supplemented with 0.5% (w/v) Albumax I, 50 mg/L hypoxanthine, 25 mM $NaHCO_3$, 25 mM HEPES and 10 mg/L gentamycin as previously described.[48] Parasite cultures were maintained at 37°C under 5% O_2, 5% CO_2 and 90% N_2. Thin blood smears were prepared by methanol fixation and Giemsa's solution stain (Sigma-Aldrich, St. Louis, MO). Parasitemia was measured by bright-field microscopy with 100× oil objective and bright field image of parasite morphology was captured on an optical microscope. The experimental protocols, including parasite culture and gene transfection were reviewed and approved by the corresponding Review Committees of Jiangsu Institute of Parasitic Diseases (approval no. IRB00008756).

METHOD DETAILS

Plasmid construction

For enhancing transfection efficiency, the Cas9 endonuclease was integrated into the genome of wide type *P. falciparum* 3D7 strain for stable expression.[31] Specifically, C-terminal fragment (1219 bp) of *PfP230p* was amplified with primers P1/P2 (SI, Table S1) and cloned into *pUF1-Cas9* plasmid at the restriction sites *Eco*RI and *Avr*II. Then the blasticidin cassette was replaced with yDHODH gene with primer P3/P4 (SI, Table S1) at the restriction sites *NcoI* and *XbaI* to obtain *pUF1-DHODH-Cas9i* plasmid.

Plasmids containing *Pfkelch13* mutations were constructed based on the *pL6cs-sgRNA* plasmid (consisting of a sgRNA expression cassette and homology regions) via multiple cloning steps as previously described. Briefly, guide sequences (P5/P6) were cloned into *pL6cs-sgRNA* after annealing at the restriction sites *Avr*II and *Xho*I. Then two fragments of PF3D7_1343700 with desired mutations and corresponding donor DNA were amplified from genomic DNA 3D7 with the primers P7/P8, P9/P10, P11/P12, P13/P14 for Y493H, C580Y and homology regions, respectively (SI, Table S1). These fragments were cloned into the *pL6cs-sgRNA* plasmid using restriction sites *Asc*I and *Afl*II. The constructs were then transformed to XL10 competent cells (Vazyme Biotech Co., Ltd) for sequencing. Correctly sequenced plasmids were extracted by NucleoBond Xtra Midi Plus (Macherey-Nagel, Germany) for transfection.

Parasite gene transfection

Parasite were tightly synchronized with either 5% sorbitol or 40/70% Percoll enrichment according to protocol. Briefly, for sorbitol-synchronization, parasite pellet was collected by centrifugating at 2500 rpm for 5min followed by the addition of 10 mL sorbitol. After incubating at 37 °C for 10min, cultures were centrifuged at 2500 rom and washed for 3 times with medium. For Percoll-synchronization, parasite pellet was carefully overlayed on the gradient followed by centrifugating at 3100 rpm for 20min. After discarding the top layer of gradient, parasites were washed with medium and returned to normal culture condition.

Transfections were performed by electroporating erythrocytes infected with late-stage trophozoites with 150 μg purified plasmid DNA resuspended in Cytomix (120 mM KCl, 10 mM KH_2PO_4, 25 mM HEPES, 2 mM EGTA, 0.15 mM $CaCl_2$, 5 mM $MgCl_2$, pH 7.6) with 310V pulse voltage.[49] For construction of the Cas9i parental strain, the *pUF1-DHODH-Cas9i* plasmid was first transfected into the 3D7 strain episomally followed by 1.5 μM DSM1 drug selection to obtain integrative parental strain via single-crossover recombination.

pL6cs-sgRNA plasmids with the desired mutations were then transfected into the Cas9-integrated parental strain to obtain the corresponding *Pfkelch13* mutant parasite strains. Positive-selection was conducted by 2.5 nM WR99210 at 72h post-transfection due to co-expressed hDHFR marker and culture media with selection drug was renewed daily during first week. Cultured parasites were microscopically monitored every

Please cite this article in press as: Yu et al., Ring-stage growth arrest: Metabolic basis of artemisinin tolerance in *Plasmodium falciparum*, iScience (2022), https://doi.org/10.1016/j.isci.2022.105725

week post electroporation until the observation of viable parasites under drug selection. Sequences of *Pfkelch13* of mutant strains were validated by Sanger sequencing before experiments were initiated.

Chemical and density-based enrichment protocol

The enrichment assay was performed according to previously reported method with some modifications.[32] SLO (Sigma-Aldrich, St. Louis, MO) was activated and the hemolytic activity for each batch was evaluated in triplicate monthly. Specifically, 25,000 units of SLO was resuspended in 5 mL PBS (pH 7.4) containing 0.1% BSA and then be incubated with 5 mM dithiothreitol at 37°C for 1h. Then activated SLO was divided into aliquots and stored at −20°C for long-term application. Hemolytic units of SLO were defined as the amount required for 50% lysis of 50 μL erythrocytes at 2% hematocrit at 37°C and the hemolytic activity for each batch of SLO was evaluated in triplicate monthly. Erythrocytes were pre-incubated with complete medium at 37°C for 4h and resuspended in PBS at 2% hematocrit. Then different volumes of SLO were added into an aliquot of 50 μL erythrocytes and incubated at 37°C for 30min. The hemoglobin level was spectrophotometrically determined at 412 nm on SpectraMax iD3 microplate reader. Cell density of tightly synchronized ring stage parasite culture after two rounds of 5% sorbitol treatment was firstly adjusted to 2% parasitemia and then subjected to SLO lysis analysis. Different amounts of SLO were added into (0, 250, 375, 500, 625, 750, 875, 1000, 1250U) culture followed by thorough pipetting and incubation at 25°C for 30 min. Following the addition of 5 mL PBS, the mixture was centrifuged at 2500 rpm for 5 min and cell pellets were washed twice with PBS to remove remaining SLO. Cell pellets were then resuspended in 1 mL PBS, carefully layered onto 70% Percoll and further centrifuged at 3100 rpm for 20 min to remove permeabilizated uninfected erythrocytes. The lower layer (consisting of infected cells) was collected and washed twice with PBS to obtain ring-stage parasites.

To investigate the enrichment efficiency, lysis curves were plotted to quantitatively access the proportion of infected erythrocytes. Briefly, tightly synchronized parasites were treated with varying concentrations of SLO as described above. After staining infected cells with Hoechst for 30 min, flow cytometry was applied to evaluate the percentage of lysed uninfected cells. Total erythrocytes were gated according to their forward and side scatter parameters and uninfected cells were calculated by subtracting infected cells from total cells. The lysis percentage was calculated by comparing either the infected or uninfected cells in SLO treated samples with that in untreated controls.

Immunofluorescence assays were performed using Nikon fluorescence confocal microscopy. Either intact erythrocytes or lysed ghosts were visualized by anti-CD235a antibody which is localized on the outer surface of erythrocytes. As spectrin turned out to be a cytoskeleton-localized protein with inaccessibility for anti-spectrin antibody in intact cells, therefore lysed ghost cells without intact cytosolic member were able to be captured due to the passage of corresponding antibody and visualized as both CD235a+ and Spectrin+. Samples were fixed in 4% paraformaldehyde and blocked with 1% BSA followed by the addition of mouse anti-alpha I spectrin antibody (Abcam, Cambridge, MA) at 1:100 dilution. After washing with ice-cold PBS three times, samples were incubated with Alexa Fluor 594 conjugated goat anti mouse secondary antibody (Abcam, Cambridge, MA) at 1:2000 dilution. Following thorough washing, samples were further incubated with PE-CD235a antibody (Thermo Fisher Scientific, MA) and Hoechst (Thermo Fisher Scientific, MA) at 1:1000 and 1:10,000 dilution respectively and subjected to immunofluorescence assays.

To investigate the effect of treatment on the growth and development of parasites, purified parasites were further subjected to culture for growth curve analysis. As described above, tightly synchronized early-stage parasites were split into two parts, one for untreated control while one received treatment as above. After microscopically determining the parasitemia, fresh erythrocytes were added to the culture at 2% hematocrit and the starting parasitemia was adjusted to 0.5%. The growth curve of each sample was monitored during three complete life cycles for evaluation of whether treatment impacts on parasite growth.

Phenotype validation

Ring-stage survival assays (RSA_{0-3h} and $RSA_{0-3h}^{50\%}$)

In vitro survival assays were performed as previously described to assess resistance phenotypes.[28] Briefly, parasites were twice synchronized by 5% sorbitol at 40h intervals to narrow down the life cycle window, then 40/70% Percoll treatment was performed, and remaining parasites were cultured for 3 h with fresh erythrocytes to allow merozoite invasion. Cultures were then further synchronized with 5% sorbitol to eliminate any

remaining late-stage parasites and to obtain 0-3h ring stages. Finally, cultures were dispensed into 24-well plates at 0.5% parasitemia, 2% hematocrit. For the RSA_{0-3h} assay, parasites were exposed to 700 nM DHA or 0.1% DMSO and cultured for 6 h prior to washing twice in RPMI 1640 incomplete media to remove excess drug and returned to standard culture conditions for 66 h in new wells. Survival rates were microscopically assessed by counting the percentage of viable parasites (~10,000 erythrocytes). Survival rates were calculated as the ratios of viable parasites in DHA and DMSO treated samples, and each sample was assessed in triplicate.

Since conventional RSA_{0-3h} only measures the survival rate for parasites after single dose of DHA pulse (700 nM), $RSA_{0-3h}^{50\%}$ was further determined to evaluate the *in vitro* sensitivity as well as the required concentration and exposure period applied in metabolomics study. For $RSA_{0-3h}^{50\%}$, 0-3h ring-stage parasites were adjusted to 0.5% parasitemia and 2% hematocrit followed by the exposure of serially diluted DHA ranging from 0.5 to 1000 nM (0, 0.5, 2, 5, 20, 50, 100, 200, 500, 1000 nM) or 0.1% DMSO in opaque 96-well microplate with 200 μL culture/well. Following incubation for several periods (1h, 3h, 6h, 9h), parasites were thoroughly washed four times with 200 μL RPMI 1640 incomplete media and transferred to a new plate for ensuring the complete removal of DHA. Parasites were then returned to standard culture conditions followed by assessment of variability by measuring the parasitemia. Briefly, parasites were stained with 20 μL SYTO-61 (2 μM diluted in PBS) and incubated at room temperature for 20 min before fluorescence analysis at the excitation and emission wavelength of 628 and 645 nm, respectively. Parasite viability was calculated as the ratio of the fluorescence intensity for viable parasites in DHA-treated parasites and DMSO-treated controls after background subtraction according to the following equation, in which FLcontrol and FLkill refers to the fluorescence intensity measured in samples without drug or samples treated by constant culture with 700 nM DHA to ensure 100% parasite killing, respectively. All samples were analyzed in triplicate. $RSA_{0-3h}^{50\%}$ values were obtained by fitting data to a non-linear regression model and the value corresponding to drug concentrations producing 50% loss of parasite viability were recorded.

$$\text{Viability} = (FL - FL_{kil})/(FL_{control} - FL_{kill})$$

Proportions of growth-arrested parasites

To evaluate the propagation of different parasite stage strains, parasites were highly synchronized with 0-3h window as described above. Parasite life cycle analysis was assessed by Giemsa-stained thin-blood smears in triplicate every 6 h during 50h propagation. The percentage of parasites at different stages in three replicates were averaged and plotted against time.

Parasite propagation was further quantified following drug treatment at 700 nM or 50 nM. Thin blood smears were made daily to quantify growth-arrested, dead or other viable parasite stages according to morphology. Specifically, growth-arrested parasites had condensed chromatin surrounded by a relatively small amount of cytoplasm while dead parasites had degraded chromatin or cytoplasm.

DHA-induced growth retardation assay

It is of note that there is a portion of viable parasites could enter into a growth-arrested state after drug pulse in which they are were actually alive but unable or delayed to replicate within this period. Therefore, growth effect induced by drug pulse was assessed by labeling with SYTO-61. In this assay, highly synchronized parasites were divided in parallel for either DMSO or DHA treated while SYTO-61 labeling was performed when DMSO-treated parasite had progressed into mid-late stage (~40h) in the cycle after drug treatment (~88h after DHA treatment). It could ensure distinguishable growth alteration resulted from viable parasites and the signal of viable parasite was accessed by flow cytometry on BD FACS Verse cytometer. For the subtraction of unviable background signal, the SYTO-61 positive events at specific concentration referred to the median of viable parasites had been normalized by reducing those from killed control to obtain the SYTO-61 frequency histogram.

Metabolomic identification for proposed approach

Parasite culture samples with at least 5×10^7 infected erythrocytes (including untreated control, saponin-lysed, SLO treated and SLO+Percoll treated) were collected for evaluation to define whether the SLOPE was able to distinguish erythrocyte-based background from parasite-specific metabolome signals. Briefly, infected erythrocytes were harvested and extracted in ice-cold methanol on dry ice to quench enzymatic activity. Following quenching, samples were immediately lysed and subjected to a two-step extraction

Please cite this article in press as: Yu et al., Ring-stage growth arrest: Metabolic basis of artemisinin tolerance in *Plasmodium falciparum*, iScience (2022), https://doi.org/10.1016/j.isci.2022.105725

method to specifically profile the parasite-derived metabolome for metabolomics analyses. After aspirating the supernatant culture medium by centrifugation at 2500 rpm for 5 min, erythrocytes were immediately harvested and subjected to various treatments as quickly as possible. Following lysis or treatment, 50 μL cell pellet was carefully added into 450 μL ice-cold 100% methanol, after immediate vortex, samples were centrifuged at 2500 rpm for 5 min and returned to dry ice to remove large-molecular-weight proteins. Supernatant was carefully collected followed by the addition of 450 μL 80% methanol. Samples were subjected to sonication on ice for 15 min and then centrifuged at 12,000 rpm for 10 min. Resulting supernatants were pooled and stored at −80°C for metabolomics analyses.

Untargeted metabolomics analysis

To obtain the metabolomes of ring-stage parasites, 0–3 hpi parasites were treated with either 50 nM DHA or 0.1% DMSO for 6 h in four independent biological replicates. Infected erythrocytes were enriched as above prior to metabolome extraction. Metabolic profiling of *Pfkelch13* mutant and WT parasites were carried out in parallel for comparing metabolic states after drug treatment. Medium-based metabolites were ruled out for the subsequent data analyses. The metabolic profile of WT parasites exposed to 700 nM DHA which is composed of the signal resulted from dead parasites has been applied for background subtraction before following multivariate statistical analysis.

Untargeted metabolomics mass data was acquired on a high-resolution Q Exactive Orbitrap mass spectrometer equipped with a heated electrospray source (HESI) in both positive and negative modes simultaneously. For both positive and negative modes, the operating parameters were set as follows: a spray voltage of 3 kV, a capillary temperature of 300°C, sheath gas flow of 40 arbitrary units, auxiliary gas flow of 10 arbitrary units, sweep gas of 2 arbitrary units and S-Lens RF level of 50. In the full scan analysis (70–1050 amu), the resolution was set at 700 000 with an automatic gain control target of 1×10^6 charges and a maximum injection time of 120 ms. Chromatographic separation was performed on a UPLC Ultimate 3000 system equipped with a 1.9 mm Hypersil Gold C18 column (100 mm × 2.1 mm), and the column was maintained at 4°C. A Multi-step gradient consisting of 0.1% formic acid in water (A) and 0.1% formic acid in acetonitrile (B) was applied and the gradient operated at a flow rate of 0.4 mL min-1 by linearly increasing solvent B from 5% to 95% over 15 min, then the column was washed with 95% solvent B for 2 min and re-equilibrated in 5% solvent B. The UPLC autosampler temperature was set at 4°C and the injection volume for each sample was 5 μL. Both the UPLC and the Orbitrap mass spectrometer system were controlled by the Xcalibur 2.2 software. The quality control (QC) samples were prepared by pooling the same volume of supernatant from samples pretreated in the same manner as real samples and analyzed every 10 samples to ensure stability and repeatability. The mass spectrometry was calibrated every 24 h during the profiling to ensure the mass accuracy.

Biological effectiveness analysis

Porphyrin level analysis

Porphyrin levels were quantitatively analyzed by fluorescence spectrometry through external standard methods. Samples were collected from parasites exposed to 700 nM DHA with/without inhibition. Briefly, after washing with 10 mL PBS, pelleted parasites were resuspended in 50 μL water and quick-frozen in liquid nitrogen. Parasite lysate was incubated with 200 μL 1.5M oxalic acid at 99°C for 30 min, and fluorescence intensity was recorded on a microplate reader with the excitation and emission wavelength at 400 and 662 nm respectively. Calculated porphyrin levels were further normalized to protein concentrations obtained by BCA kits.

Mitochondrial membrane potential analysis

Mitochondrial membrane potential (MMP) assay was performed to further investigate the mitochondrial function of parasites. The MMP assay was evaluated using a MitoProbe DiIC1 kit (Thermo Fisher Scientific, MA) according to the manufacturer's instructions. Briefly, parasites exposed to 700 nM DHA were incubated with DiIC1 at 37°C for 30 min. After co-staining with Hoechst, the percentage of MMP positive cells were calculated as the ratio of DiIC1 positive cells to Hoechst positive cells on SpectraMax iD3 microplate reader using 488 and 640 nm as the excitation wavelength, respectively.

Please cite this article in press as: Yu et al., Ring-stage growth arrest: Metabolic basis of artemisinin tolerance in *Plasmodium falciparum*, iScience (2022), https://doi.org/10.1016/j.isci.2022.105725

Determination of ROS generation

Intracellular ROS levels between groups was determined as previously described. Briefly, parasites exposed to 700 nM DHA were incubated with 20 μM dichlorodihydrofluorescein diacetate at 37°C for 30 min in the dark. Then parasites were harvested and washed with PBS twice followed by saponin lysis. After thorough washing and centrifugation at 2500 rpm for 5min, cell pellets were resuspended in PBS and the fluorescence of DCF was recorded on a microplate reader.

QUANTIFICATION AND STATISTICAL ANALYSIS

Raw peak extraction and deconvolution for metabolomics data were performed by SIEVE software and metabolic data were analyzed using TraceFinder software for relative quantitative analysis of detected features. Multivariate statistical analysis including principal component analysis (PCA) and partial least squares discriminant analysis (PLS-DA) were performed by SIMCA-P 13.0 software (Umetrics, Sweden). Discriminating features were further evaluated according to the variable importance (VIP) for each metabolite in the PLS-DA model. The statistical significance was calculated using the two-tailed Student's t-test by SPSS 25.0 software (Chicago, IL, USA) and p value were further adjusted by Benjamini and Hochberg false discovery rate adjustment for multiple features comparison. Features with significant changes (q value < 0.05 and VIP >1) were selected as discriminating metabolites. Qualitative analysis was performed according to either in-house metabolite library (level 2) acquired from authentic compounds and public database including HMDB, METLIN according to the retention time and accurate mass (level 3). The mass tolerance was set as less than 5 ppm between obtained feature and database-recorded data. Pathway enrichment analysis was performed by using the website tool MetaboAnalyst 4.0 (http://www.metaboanalyst.ca).

ADDITIONAL RESOURCES

This paper did not create any additional resources.

Article 5 : Des petites molécules extracellulaires issues d'un environnement induit par un stress provoquent un arrêt de croissance temporaire chez le jeune stade ring de *Plasmodium falciparum* et réduisent *in vitro* la susceptibilité des parasites à la dihydroartémisinine.

Ce travail expérimental avait pour objectif d'explorer le rôle potentiel de l'environnement extracellulaire dans l'induction de l'arrêt de croissance des stades ring de *P. falciparum*. Pour tester cette hypothèse, nous avons mis au point un protocole de stress *in vitro* permettant de produire de manière reproductible un environnement extracellulaire défavorable. Pour cela, des parasites de la souche NF54 (souche sensible à la chloroquine) asynchrones ont été exposés pendant 20h à 200 nM de chloroquine afin d'induire un stress cellulaire et la mort des parasites. La culture a été ensuite centrifugée, puis le surnageant a été recueilli. Ce surnageant a été nommé "surnageant de culture stressée" (SCS). Nous avons ensuite incubé des stades rings très jeunes (0-3h post invasion) de souches résistantes à la chloroquine avec le SCS pendant 24h afin de mesurer l'effet de l'environnement extracellulaire stressant sur la progression du parasite dans le cycle asexué. Nos résultats ont permis de constater que l'exposition au SCS pendant 24h induit un décalage significatif de la progression du cycle asexué et mis en évidence que le stade ring stoppe temporairement sa transition vers le stade trophozoïte. Afin de tester si cet arrêt temporaire dans le développement du cycle permettait au parasite une meilleure survie à l'exposition à l'artémisinine, des rings jeunes (0-3h) ont été prétraités avec le SCS pendant 30 minutes puis exposés à une dose d'artémisinine de 700 nM pendant 6h. La proportion de parasites survivants a été calculée selon le protocole du test RSA. Nos résultats indiquaient que les stades rings 0-3h prétraités au SCS avaient en moyenne une survie deux fois supérieure à celles des stades rings 0-3h prétraités avec le milieu de culture RPMI. Ces résultats ont été observés avec des souches possédant des fonds génétiques et des génotypes *Pfkelch13* différents (WT et C580Y). Ensuite, nous avons constaté que le prétraitement des stades rings jeunes (0-3h) à des dilutions de SCS (¾ , ½ et ¼) suivie d'une exposition à une dose de 700 nM de DHA pendant 6h restaurait de manière graduelle la proportion de parasites survivants initiale comparable aux parasites prétraités avec le milieu RPMI pour toutes les souches testées, suggérant l'existence d'un seuil spécifique au signal de stress provoquant l'arrêt de croissance des parasites.
Afin de caractériser les molécules ou facteurs impliqués dans le signal de stress contenu dans le SCS, nous avons testé plusieurs filtrats de SCS sur filtre Centricon®. La filtration a permis de retenir les molécules contenues dans le SCS sur la base de leur poids moléculaire (kDa). Nos résultats montraient que les différents filtrats de SCS (< 100 kDa, < 30 kDa, < 10 kDa et < 3 kDa) induisaient toujours une augmentation de la proportion de parasites survivants après exposition à une dose de DHA (700 nM) pendant 6h, indépendamment du génotype Pfkelch13. Ceci suggérant

que les molécules ou facteurs contenu dans le SCS n'étaient pas des vésicules extracellulaires dont le diamètre est compris entre 30 et 500 nm (tailles des pores des filtres sont respectivement de 10 nm pour le filtre < 100 kDa, 3 nm pour le filtre < 30 kDa, 1 nm pour le filtre < 10 kDa et 0.3 nm pour le filtre < 3 kDa). L'ensemble de ces données a donc permis de mettre en évidence que l'arrêt de croissance est un mécanisme constitutif chez *P. falciparum*, lui conférant une meilleure survie notamment en cas de stress comme une exposition à la DHA.

Un article scientifique détaillant ces données est en cours de rédaction (voir draft ci-dessous). Il sera soumis dans un journal à comité de lecture dans quelques semaines.

Extracellular small molecules from a drug-induced stress environment mediate a temporary growth arrest of *Plasmodium falciparum* early ring-stages and reduce the *in vitro* susceptibility of parasites to dihydroartemisinin.

Lucien Platon[1, 2, 3, *], Didier Ménard[1, 3, 4, 5]

[1] Institut Pasteur, Université Paris Cité, Malaria Genetics and Resistance Unit, INSERM U1201, F-75015 Paris, France.

[2] Sorbonne Université, Collège Doctoral ED 515 Complexité du Vivant, F-75015 Paris, France.

[3] Institut Pasteur, Université Paris Cité, Malaria Parasite Biology and Vaccines Unit, F-75015 Paris, France.

[4] Université de Strasbourg, Institute of Parasitology and Tropical Diseases, UR7292 Dynamics of Host-Pathogen Interactions, F-67000 Strasbourg, France.

[5] CHU Strasbourg, Laboratory of Parasitology and Medical Mycology, F-67000 Strasbourg, France

*Correspondance : lucien.platon@pasteur.fr (Lucien Platon)

Introduction

Plasmodium falciparum malaria continues to have a significant impact on human health, despite recent efforts and progresses. In 2021, the number of *P. falciparum* infection cases was estimated to 247 million, resulting in 619,000 deaths, mainly in sub-Saharan Africa[1]. Today, artemisinin-based combination therapies (ACT) are recommended as first-line treatment in uncomplicated falciparum malaria worldwide[2]. Introduced in 2000s, ACTs have contributed significantly to reducing mortality[1]. ACTs are a combination of fast-acting artemisinin derivatives (ART) that can reduce the biomass of drug-sensitive parasites by up to 10,000-fold within 48 hr and slower-acting partner drugs such as lumefantrine, amodiaquine, mefloquine or piperaquine that decrease the selective pressure for ART resistance and clear residual parasitemia[3,4].

Unfortunately, the emergence and spread of *P. falciparum* artemisinin resistance and the decline efficacy of ACTs, first detect in 2009 in the Greater Mekong sub-region and more recently in Papua New-Guinea, Guyana and Sub-Saharan Africa (Rwanda, Uganda) are major concerns[5-9]. A better understanding of ACT modes of action and resistance mechanisms is urgently needed, not only to manage current clinical use but also to rationally design new strategies. ART-R is defined as delayed clearance of circulating asexual blood stage parasites following 3 days ACT treatment or artemisinin monotherapy[1] (half-life >5.5 hr). *In vitro*, ART-R manifests as increased survival of early ring blood-stage parasites (0–3 hr post invasion, hpi) exposed to a pulse of 700 nM dihydroartemisinin (DHA,

the active metabolite of all ARTs used clinically) 6 hr as expressed with the Ring-stage Survival Assay[10] (RSA). Later, mutations in the beta-propeller domain of the *P. falciparum* Kelch13 protein have been shown to confer *in vivo* and *in vitro* ART-R[11,12]. At present, the most prevalent K13 mutation associated with delayed clearance in the eastern part of the Greater Mekong sub region is the C580Y[12]. Recent reports suggest that *P. falciparum kelch13* mutations cause low levels of Kelch13 protein, involved in early ring-stage haemoglobin endocytosis and digestion[13,14]. Therefore, it has been postulated that the mutant parasites reduced endocytosis and catabolism of haemoglobin in young rings, resulting in reduced levels of free Fe^{2+} available for the activation of ART[15,16].
Moreover, like other organisms, *P. falciparum* can mount protective responses to sudden changes in its environment such as cell cycle temporary arrest of a fraction of the asexual ring-stage population (also called quiescence or dormancy) to increase survival under unfavourable conditions[17-18]. This has been established for some metabolic conditions (variations in sugars, amino acids, lipids and micronutrients) and for exposure to febrile temperature[19-21] but also for drugs such as ART which has been shown to induce this phenotype *in vitro*[17,22] and *in vivo*[23].

Here, we investigate whether early ring parasites can sense the environment and induce a fraction of the asexual ring population to undergo a temporary growth arrest that can withstand DHA exposure as a survival strategy. We used the NF54, $3D7^{WT}$, $3D7^{C580Y}$ as well as Cambodian *P. falciparum kelch13* wild type (WT) and mutant (C580Y) parasite lines and demonstrated that culture medium generated from CQ-killed NF54 parasites (mimicking a stressful environment) can induced delayed growth of *P. falciparum* blood-stages. Delayed growth was dependant of the genetic background of the parasite lines but independent of the *Pfkech13* genotype. Additional experiments confirmed that delayed growth of ring-stages increased the proportion of parasites that can survive a 700 nM DHA pulse. This response to signal was shown to be dose dependant; the proportion of viable parasites decreasing when the concentration of the stressful environment decreased. We also provide evidence that the signal is mediated by several molecules with different molecular weights (molecules >10 kDa and <10 kDa), excluding a role of extracellular vesicles (EVs). Finally, we demonstrate that DHA-exposed susceptible *P. falciparum* mature stages may secrete these molecules as they die. These potential molecules could thus act as danger signals of environmental stress and influence blood stage growth to optimise population survival, regardless the *Pfkelch13* genotype. This suggests that *Pfkelch13* mutations conferring artemisinin partial resistance and ring stage stress-sensing pathway are two complementary survival mechanisms. This ring stage stress sensing mechanism could have significant clinical implications in our understanding of malaria parasite drug resistance.

Results

Exposure to a culture medium collected from CQ-treated NF54 parasites culture induces delayed growth of *P. falciparum* blood-stages.

To explore the ability of *P. falciparum* parasites to sense the environment and respond to stress-induced conditions, we investigated whether a culture medium obtained from a chloroquine sensitive (CQ-S) parasite line (NF54 strain) exposed to 200 nM chloroquine (CQ) for 20 hours would affect the intraerythrocytic developmental cycle progression of the CQ-R *P. falciparum* parasite lines (***Table S1***). We produced the stress-induced environmental condition by generating a culture medium (named ***M_NF54_CQ_20h***) from an asynchronous NF54 CQ-S parasite line exposed to 200 nM CQ for 20 hours. We confirmed the killing effect of CQ on NF54 CQ-S blood stages by the microscopic examination of a Giemsa-stained blood smear (***Figures S1 and S2***). Then, we cultured 0-3h post-invasion (hpi) ring-stages of three Cambodian CQ-R *P. falciparum* parasite lines in the presence of the M_NF54_CQ20h or RPMI complete medium (as control) for 24 hours (H24 time point). After two washing steps with incomplete RPMI medium, we cultured the parasites for additional 24 hours in RPMI complete medium (H48 time point). Red blood cells were then collected at H24 and H48 and used to prepare Giemsa-stained blood smears.

We observed that blood-stages parasites exposed to RPMI complete medium (control) had a normal (but heterogenous) intraerythrocytic development cycle progression from ring-stages to trophozoite-stages (*i.e.,* average 24% for ring-stages and 76% for trophozoite-stages) at H24 and from trophozoite-stages to schizonts (*i.e.,* average 26% for trophozoite-stages and 74% for schizonts) at H48. However, a significant delayed growth was observed for the all Cambodian CQ-R *P. falciparum* parasite lines cultured in the presence of M_NF54_CQ20h. A clear shift towards younger forms were detected at H24 (*i.e.,* average 70% for ring-stages and 30% for trophozoite-stages, $p<10^{-4}$, chi-squared test) and at H48 (*i.e.,* average 8% for ring-stages, 62% for trophozoite-stages and 30% for schizonts, $p<10^{-4}$, chi-squared test) (***Figure 1***).

Although the intraerythrocytic developmental cycle progression was similar for the Cambodian parasite lines at H24 in both conditions (M_NF54_CQ20h and RPMI complete medium), at H48 in the M_NF54CQ20h-treated condition, we noted a higher proportion of younger forms for the Cambodian *Pfkelch* wild-type parasite line ($PL3^{WT}$) compared to the two other Cambodian *Pfkelch* C580Y parasite lines ($PL1^{C580Y}$ and $PL2^{C580Y}$): 21% $PL3^{WT}$ ring stages vs. 0% $PL1^{C580Y}$ and 2% $PL2^{C580Y}$ ring stages; 63% $PL3^{WT}$ trophozoite stages vs. 58% $PL1^{C580Y}$ and 65% $PL2^{C580Y}$ trophozoite stages; 17% $PL3^{WT}$ schizonts vs. 42% $PL1^{C580Y}$and 33% $PL2^{C580Y}$ schizonts ($p<10$-4, chi-squared test).

Overall, our data indicate that medium generated from CQ-killed parasites can induced delayed growth of *P. falciparum* blood-stages, similar for sugars, amino acids, lipids and nutrients depleted

culture conditions[19]. These suggest that the blood-stages growth progression could be modulated by signals released from dead or dying parasites (*i.e.,* soluble secreted factors or EVs) to enhance the survival of a fraction of receptive parasites. The difference in blood stage growth delay between parasite lines at H48 suggests that genetic background is involved in this phenotype, irrespective of *Pfkech13* genotype. We also noted a marked heterogeneity in the progression of the intraerythrocytic developmental cycle from the synchronous 0-3 hpi ring-stage populations in both conditions.

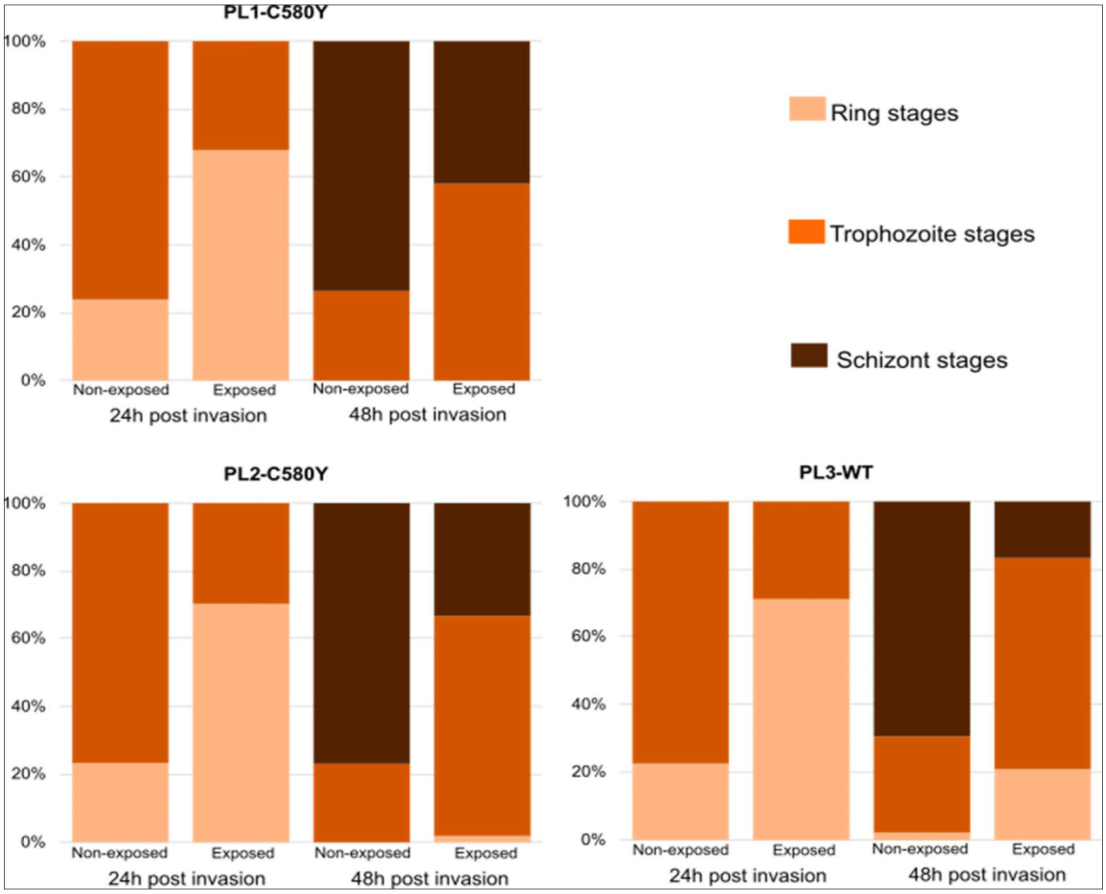

Figure 1: Exposure to a culture medium collected from CQ-treated NF54 parasites culture induces delayed growth of P. falciparum blood-stages.
The proportion of the blood-stages (rings, trophozoites and schizonts) of the three Cambodian CQ-R *P. falciparum* parasite lines at H24 and H48 are shown in each panel (microscopy examination at x1000 magnification). For each sample, roughly 20 000 erythrocytes were assessed to estimate the blood-stages proportions.

Early 0-3 hpi ring-stage parasites treated with M_NF54_CQ20h showed a decrease *in vitro* susceptibility to DHA.

We next investigated whether the *in vitro* DHA susceptibility of *P. falciparum* parasite lines, as expressed by the ring stage survival assay (RSA^{0-3h}), was affected by the delayed growth progression

induced by M_NF54_CQ20h treatment. Early 0-3 hpi ring stage parasites of the CRISPR/Cas9 edited line 3D7^{C580Y}, the parasite lines PL1^{C580Y} and PL2^{C580Y} were prepared and exposed to four different culture media for 30 minutes: complete RPMI medium (as control), M_NF54_CQ20h medium prepared as previously described, culture medium prepared from the asynchronous NF54 parasite (M_NF54) and culture medium prepared from uninfected red blood cells exposed to 200 nM CQ for 20 hours (M_RBC_CQ20h). The 3D7^{C580Y}, PL1^{C580Y} and PL2^{C580Y} parasite lines were then exposed to 700 nM DHA or 0.1% dimethyl sulfoxide (DMSO, used as a vehicle control) for 6 hr, washed three times with incomplete RPMI medium to remove the drug, transferred and cultured in complete RPMI medium for an additional 66 hr. Parasitemia was measured at 72 hr by microscopy. Parasite survival was expressed as the ratio of viable parasites in DHA- to DMSO-treated samples, as previously described. All experiments were performed in triplicate.

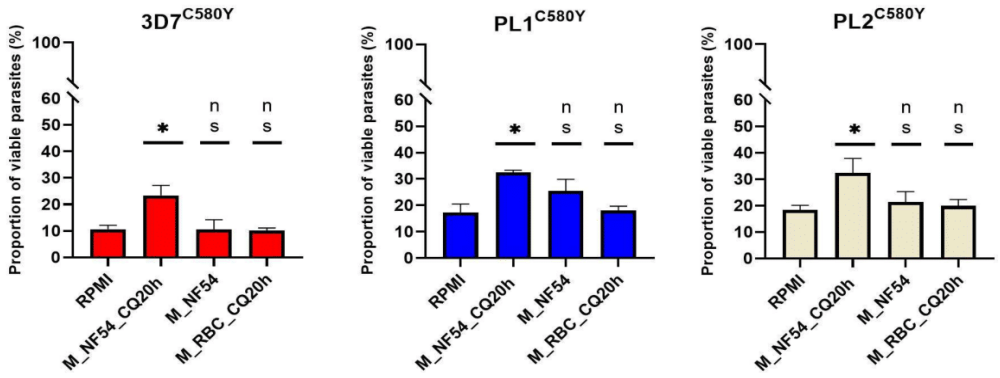

Figure 2. Early 0-3 hpi ring-stage parasites treated with M_NF54_CQ20h showed a decrease in vitro susceptibility to DHA.

Early 0-3 hpi ring stages of the 3D7^{C580Y}, PL1^{C580Y} and PL2^{C580Y} parasite lines were cultured for 30 minutes in complete RPMI medium (RPMI), in culture medium prepared from an asynchronous NF54 CQ-S parasite line exposed to 200 nM CQ for 20 hours (M_NF54_CQ20h), in culture medium prepared from the asynchronous NF54 parasite (M_NF54) and in culture medium prepared from uninfected red blood cells exposed to 200 nM CQ for 20 hours (M_RBC_CQ20h). The graphs show the proportion of viable parasites (%) as expressed by the RSA^{0-3h} for the parasite lines 3D7^{C580Y}, PL1^{C580Y} and PL2^{C580Y} in the four environmental conditions. Two-sample t-tests with equal variances were used to test for statistically significant differences between the M_NF54_CQ20h, M_NF54 or M_RBC_CQ20h conditions and the control (RPMI) conditions. For each parasite line, no statistical difference was found between M_NF54 or M_RBC_CQ20h and RPMI conditions, while survival rates in the M_NF54_CQ20h condition were significantly different (~2-fold increase) compared to the RPMI condition. The number of red blood cells counted in each RSA^{0-3h} assays was 20,000. All experiments were performed in triplicate. P-values (t-test) were ns when $p>0.05$ and * when $p<0.05$.

We found that the proportions of viable parasites of the parasite lines treated with complete RPMI medium were 10.6%, 17.3% and 18.3% for 3D7^{C580Y}, PL1^{C580Y} and PL2^{C580Y}, respectively (***Figure 2***). Similar proportions of viable parasites were detected for parasite lines treated with culture medium prepared from asynchronous NF54 parasites (M_NF54) (10.6% for 3D7^{C580Y}, p=0.8; 25.5% for PL1^{C580Y}, p=0.1 and 21.3% for PL2^{C580Y,} p=0.1, t-test) and for parasites treated with the culture medium prepared from uninfected red blood cells exposed to 200 nM CQ for 20 hours (M_RBC_CQ20h) (10.2% for the 3D7^{C580Y}, p=0.7; 18.1% for the PL1^{C580Y}, p=0.1 and 19.9% for the PL2^{C580Y}, p=0.7, t-test).

From these data we could demonstrate that i) a culture medium containing 200 nM CQ (M_RBC_CQ20h condition) did not alter the *in vitro* DHA susceptibility of the parasite lines tested, consistent with the mode of action of the 4-aminoquinoline derivatives, which acts mainly on the mature stage by inhibiting the conversion of haem to hemozoin, and ii) the culture medium prepared from an asynchronous NF54 parasite (M_NF54 condition) did not result in medium depletion or the release of signals that could affect the growth progression of the blood stages. However, we clearly observed that the proportions of viable parasites in the parasite lines treated with M_NF54_CQ20h medium were significantly increased (~2-fold) compared to the complete RPMI medium condition for all tested parasite lines. The parasite survival rates changed from 10.6% to 23.4%, p=0.01 for 3D7^{C580Y}, 17.3% to 32.5% for PL1^{C580Y}, p=0.02, and 18.3% to 32.4% for PL2^{C580Y}, p=0.02, t-test. Together, these suggest that CQ-killed parasites release a signal in the culture medium that delays the growth of CQ-R blood-stage parasites and increases the proportion of ring-stages that survives a 700 nM DHA pulse.

Dilutions of the M_NF54_CQ20h medium restore gradually initial *in vitro* DHA susceptibility phenotype of the *P. falciparum* parasite lines.

To confirm our hypothesis that a signal released by CQ-killed parasites in the culture medium can affect the growth of CQ-R blood stage parasite lines, we treated 0-3 hpi ring stage 3D7^{C580Y}, PL1^{C580Y} and PL2^{C580Y} parasites with dilutions of M_NF54_CQ20h medium (¾, ½ and ¼ dilutions) prior to assessing their *in vitro* susceptibility to DHA using the RSA^{0-3h}. The complete RPMI medium and the pure M_NF54_CQ20h medium were used as negative and positive controls, respectively. All assays were carried out in triplicate.

As previously observed, we confirmed that the proportions of viable parasites of the parasite lines treated with M_NF54_CQ20h medium were significantly increased compared to the complete RPMI medium condition, with parasite survival rates changing from 10.7% to 29.2%, p=0.002 for 3D7^{C580Y}, 11.8% to 46.7% for PL1^{C580Y}, p=0.0003, and 18.8% to 60.2% for PL2^{C580Y}, p=0.002, t-test (***Figure 3***). Significant differences in the proportions of viable parasites were found in the parasite lines that were treated with the pure M_NF54_CQ20h medium compared diluted M_NF54_CQ20h medium.

However, significant associations between dilutions and parasite survival rates of the parasite lines tested were observed (r=0.71, 95% CI: 0.19-0.91, p=0.01 for 3D7^{C580Y}; r=0.93, 95% CI: 0.71-0.98, p=0.0002 for PL1^{C580Y} and r=0.97, 95%CI: 0.78-0.99, p=0.0004 for PL2^{C580Y}), suggesting a dose-response relationship. Taken together, these data confirmed that a signal released by CQ-killed parasites diffuses into the culture medium and progressively affects the growth of an increasing number of ring stages that can survive exposure to DHA as the concentration of the signal increases.

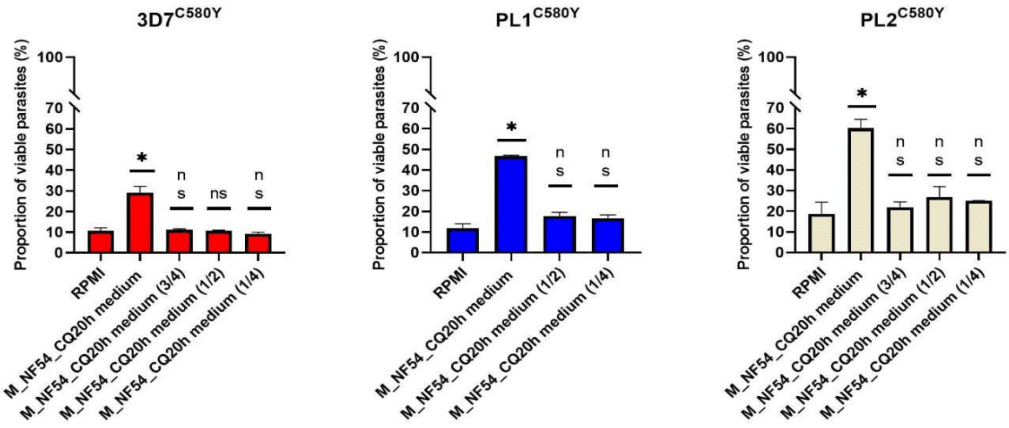

Figure 3. Dilutions of the M_NF54_CQ20h medium restore gradually initial *in vitro* DHA susceptibility of the *P. falciparum* parasite lines.

Early 0-3 hpi ring stage of the 3D7^{C580Y}, PL1^{C580Y} and PL2^{C580Y} parasite lines were exposed for 30 minutes to complete RPMI medium (RPMI, negative control) and different dilutions of the M_NF54_CQ20h medium (pure, diluted by ¾, ½ and ¼). The graphs present the proportion of viable parasites (%) as expressed by the RSA^{0-3h} for the parasite lines 3D7^{C580Y}, PL1^{C580Y} and PL2^{C580Y} in the four (PL1^{C580Y}) or five (3D7^{C580Y} and PL2^{C580Y}) experimental conditions. Two-sample t-tests with equal variances were used to test for statistically significant differences between RPMI and the M_NF54_CQ20h medium dilutions. The number of red blood cells counted in each RSA^{0-3h} assays was 20,000. All experiments were performed in triplicate. P-values (t-test) were ns when p>0.05 and * when p<0.05.

The ring-stage delayed growth and reduced *in vitro* DHA susceptibility induced by the CQ-killed parasite medium are mediated by several molecules of different molecular weight, independent of the *Pfkelch13* genotype.

The next step was to determine the molecular weight range of the molecule(s) contained in the M_NF54_CQ20h medium that was likely to be sensed by the ring stage parasites. We used Centricon centrifugal filter device and Ultracel membranes with different cut-offs to exclude molecules with molecular weights below 100 kDa (10 nm pore size), 30 kDa (3 nm pore size), 10 kDa (1 nm pore size) and 3 kDa (0.3 nm pore size) from the M_NF54_CQ20h medium (***See Material and methods***).

The M_NF54_CQ20h media were prepared, as previously described and then filtrated using Centricon equipment to obtain four M_NF54_CQ20h medium filtrates (<100 kDa; <30 kDa; <10 kDa and <3 kDa), placed later in 50 mL Falcon tubes. The early 0-3 hpi ring stages parasite line PL2^{C580Y} were then exposed to complete RPMI medium and pure unfiltered M_NF548CQ20h (control) and each of the four filtrates for 30 minutes before assessing their *in vitro* susceptibility to DHA using the RSA0-3h. All experiments were performed in triplicate.

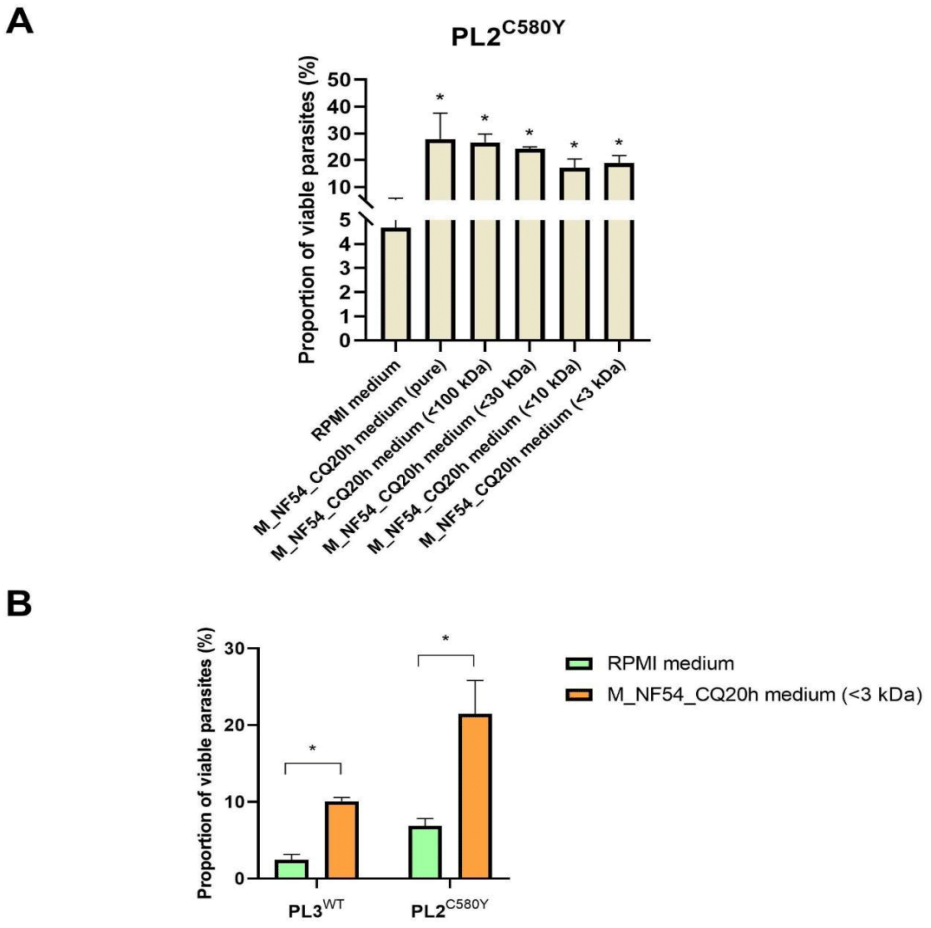

Figure 4. The ring-stage delayed growth and reduced in vitro DHA susceptibility induced by the CQ-killed parasite medium are mediated by several molecules of different molecular weight, independent of the Pfkelch13 genotype.

Panel A. Early 0-3 hpi ring stages of the PL2^{C580Y} parasite line were exposed for 30 minutes to complete RPMI medium (RPMI, negative control), pure unfiltered M_NF54_CQ20h (M_NF54_CQ20h medium (pure), positive control) and four M_NF54_CQ20h medium filtrates (<100 kDa; <30 kDa; <10 kDa and <3 kDa). The graph presents the proportion of viable parasites (%) as expressed by the RSA^{0-3h} for the parasite line PL2^{C580Y} in the six experimental conditions.

Two-sample t-tests with equal variances were used to test for statistically significant differences between RPMI and the M_NF54_CQ20h medium filtrates. The number of red blood cells counted in each RSA^{0-3h} assays was 20,000. All experiments were performed in triplicate. P-values (t-test) were ns when $p>0.05$ and * when $p<0.05$.

Panel B. Early 0-3 hpi ring stages of the $PL2^{C580Y}$ and $PL3^{WT}$ parasite lines were exposed for 30 minutes to complete RPMI medium (RPMI, negative control) and the <3 kDa M_NF54_CQ20h medium filtrate. The graph presents the proportion of viable parasites (%) as expressed by the RSA^{0-3h} for the parasite lines $PL2^{C580Y}$ and $PL3^{WT}$ in both experimental conditions. Two-sample t-tests with equal variances were used to test for statistically significant differences between RPMI and the <3 kDa M_NF54_CQ20h medium filtrate. The number of red blood cells counted in each RSA^{0-3h} assays was 20,000. All experiments were performed in triplicate. P-values (t-test) were ns when $p>0.05$ and * when $p<0.05$.

As previously observed, we confirmed that the proportion of viable parasites of the $PL2^{C580Y}$ parasite line treated with M_NF54_CQ20h medium was significantly increased compared to the complete RPMI medium condition, with parasite survival rates changing from 4.7% to 29.3%, p=0.0002, t-test. We found similar proportions of viable parasites of the $PL2^{C580Y}$ parasite line treated with <100 kDa and <30 kDa M_NF54_CQ20h filtrates (<100 kDa filter, 28.3%, p= 0,63; <30 kDa filter, 24.4%, p= 0,06, t-test) while the proportions of viable parasites of the $PL2^{C580Y}$ parasite line treated with <10 kDa and <3 kDa M_NF54_CQ20h filtrates (<10 kDa filter, 15.4%, p= 0,0016; <3 kDa filter, 17.3%, p= 0,003, t-test) were reduced. However, the reduction of the proportions of viable parasites treated with <10 kDa and <3 kDa M_NF54_CQ20h filtrates remained significantly higher than the proportion detected in the RPMI medium condition (<10 kDa filter, p= 0,0001 and <3 kDa filter, p= 0,0001, t-test) (***Figure 4A***). These results suggest that the signal involved in the delayed growth progression is mediated by multiple molecules with different molecular weights (molecules >10 kDa and <10 kDa) and exclude that the signal is mediated by extracellular vesicles (EVs) as their diameters range from 30 to 500 nm[24] (***Figure 4A***).

To confirm that small molecules < 3kDa affect the ring stage growth progression and their *in vitro* susceptibility to DHA, we exposed the $PL2^{C580Y}$ and $PL3^{WT}$ early 0-3 hpi ring-stage to the complete RPMI medium (control) and the <3 kDa M_NF54_CQ20h medium filtrate for 30 minutes before assessing *in vitro* susceptibility to DHA using the RSA^{0-3h}. Both proportions of $PL2^{C580Y}$ and $PL3^{WT}$ viable parasites treated with the <3 kDa M_NF54_CQ20h medium filtrate were significantly increased compared to the complete RPMI medium condition. The parasite survival rates changed from 6.8% to 21.5%, p=0.004 for the $PL2^{C580Y}$ parasite line and from 2.0% to 10.1%, p=0.0003 for the $PL3^{WT}$ parasite line, t-test (***Figure 4B***). We confirmed that, independent of the *Pfkelch13* genotype, molecules < 3 kDa can promote delayed ring stage growth and reduced *in vitro* susceptibility to DHA.

DHA-treated mature stage parasites release molecules into the culture medium that reduce ring-stages *in vitro* susceptibility to DHA.

We then tested whether a co-culture of *P. falciparum* ring and mature stages exposed to 700 nM DHA for 6 hours could promote delayed *P. falciparum* blood stage growth and reduced *in vitro* susceptibility to DHA. Blood stage parasites, cultured in the same medium, were physically separated by a polycarbonate membrane (upper chamber and lower compartment), using a Transwell® insert system (0.4 µm pore size).

We first exposed the parasite lines or uninfected red blood cells to 700 nM DHA or DMSO (0.1%) for 30 minutes in the upper chamber. We then seeded early 0-3 hpi ring-stages into the lower compartment which were cultured for 6 hours in the same culture medium, allowing DHA and molecules released from the upper compartment to passively diffuse into the culture medium. Parasites in the lower compartment were collected, washed twice in incomplete RPMI medium to remove the drug, transferred, and cultured in complete RPMI medium for a further 66 hours. Parasitemia was measured by microscopy after 72 hours. Parasite survival was expressed as the ratio of viable parasites in DHA- to DMSO-treated samples, as previously described. All the experiments were performed in triplicate.

We used the $3D7^{WT}$ and the $3D7^{C580Y}$ parasite lines in four experimental conditions (upper/lower compartments): 22-36 hpi mature-stages/early 0-3 hpi rings-stages, early 0-3 hpi ring-stages/early 0-3 hpi ring-stages, uninfected red blood cells/ early 0-3 hpi ring-stages and uninfected red blood cells/22-36 hpi mature-stages (***Figure S6***).

The proportions of viable parasites when $3D7^{WT}$ and $3D7^{C580Y}$ early 0-3 hpi ring stages were co-cultured with uninfected RBC were 0.5% and 3.8%, respectively (***Figure 5A***). When the $3D7^{WT}$ and $3D7^{C580Y}$ mature stages were co-cultured with uninfected RBC, the proportions of viable parasites were 0.38% and 0.39%, respectively. The significant difference observed in the *in vitro* susceptibility to DHA between $3D7^{C580Y}$ ring stages and mature stages is consistent with previous reports showing that the mature stages of the *Pfkelch13* mutant parasites are highly susceptible to DHA[25]. In addition, we provided evidence that DHA remains active when incubated with uninfected red blood cells.

As expected, we observed similar parasite survival rates (compared to the uninfected red blood cells/early 0-3 hpi ring-stages condition) from both parasite lines when $3D7^{WT}$ and $3D7^{C580Y}$ early 0-3 hpi ring stages were co-cultured with early 0-3 hpi ring stages (0.7% vs. 0.5%, p=0.34, for the $3D7^{WT}$ parasite line and 3.2% vs. 3.8%, p=0.56, for the $3D7^{C580Y}$ parasite line, t-test).

However, when early $3D7^{WT}$ and $3D7^{C580Y}$ 0-3 hpi ring stages were co-cultured with 22-36 hpi mature-stages, significant decreases in *in vitro* susceptibility to DHA for both parasite lines compared to the control condition (early 0-3 hpi ring-stages/early 0-3 hpi ring-stages) were observed. Parasite survival rates ranged from 0.5% to 2.8% (p=0.003, t-test) for parasite line $3D7^{WT}$ and from 3.8% to

13.3% (p=0.003, t-test) for parasite line 3D7^{C580Y} (***Figure 5A***).

To exclude that the decreases in *in vitro* DHA susceptibility observed for the early 0-3 hpi ring stages/22-36 hpi mature stages co-cultures were not due to a reduced concentration of DHA available in the medium as a result of DHA activation by the mature stages, we performed additional early 0-3 hpi ring stages/22-36 hpi mature stages co-cultures with the 3D7^{C580Y} parasite line in which DHA concentrations were increased up to 1400 nM and 2100 nM DHA (***Figure 5B***). We observed similar proportions of viable parasites at all concentrations (15.5% at 700 nM DHA vs. 16.5% at 1400 nM DHA, p=0.3) and 14.6% at 2100 nM DHA, p=0.6), ruling out the hypothesis of the reduced DHA availability.

These findings suggest that drug-exposed susceptible *P. falciparum* mature stages may secrete molecules as they die, that are used for population-level communication, as has been reported for bacteria and yeast. These potential molecules could thus act as danger signals of environmental stress and influence blood stage growth to optimise population survival.

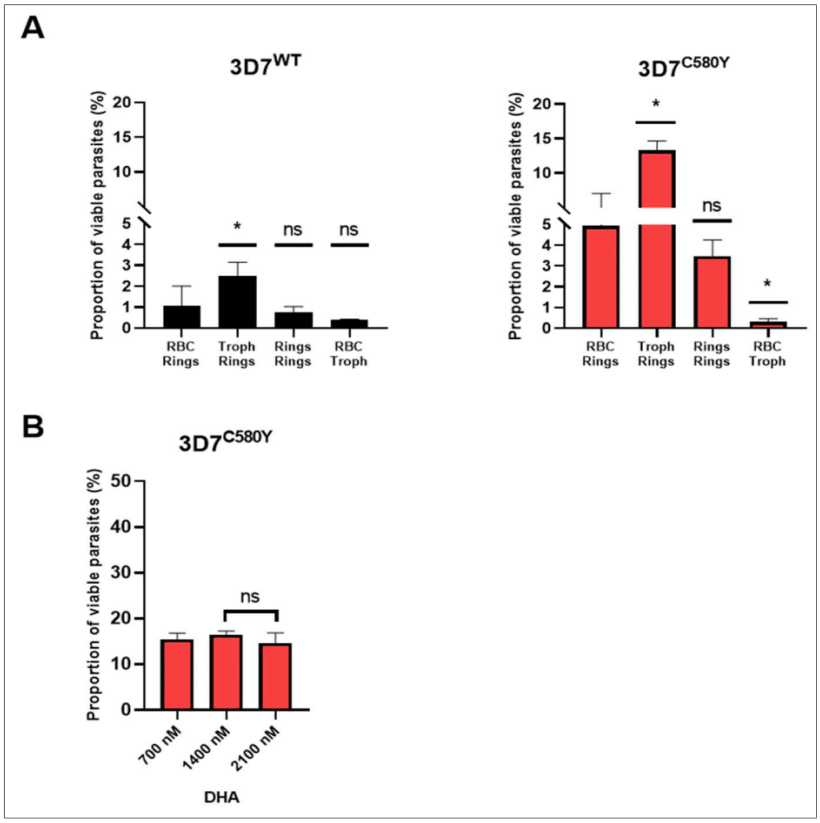

Figure 5. DHA-treated mature stage parasites release molecules into the culture medium that reduce the in vitro susceptibility of ring-stage parasites to DHA.

Panel A. The graphs present the proportion of viable parasites (%) as expressed by the RSA^{0-3h} of $3D7^{WT}$ and $3D7^{C580Y}$ 0-3 hpi early ring stages co-cultured with DHA-treated (at 700 nM for 30 minutes) uninfected red blood cells, 22-36 hpi mature-stages, early 0-3 hpi ring-stages and $3D7^{WT}$ and 22-36 hpi mature-stages co-cultured with DHA-treated uninfected red blood cells.
Two-sample t-tests with equal variances were used to test for statistically significant differences between uninfected red blood cells/early 0-3 hpi ring-stages condition and the other conditions. The number of red blood cells counted in each RSA^{0-3h} assays was 20,000. All experiments were performed in triplicate. P-values (t-test) were ns when $p>0.05$ and * when $p<0.05$. **Panel B**. The graph presents the proportion of viable parasites (%) as expressed by the RSA0-3h of $3D7^{C580Y}$ 0-3 hpi early ring stages co-cultured with DHA-treated 22-36 hpi mature-stages (at 700, 1400 and 2100 nM for 30 minutes). Two-sample t-tests with equal variances were used to test for statistically significant differences between 700 nM DHA and 1400 nM or 2100 nM. The number of red blood cells counted in each RSA^{0-3h} assays was 20,000. All experiments were performed in triplicate. P-values (t-test) were ns when $p>0.05$ and * when $p<0.05$.

Discussion

Here we report evidence that stressful extracellular environments can induce reversible growth arrest in several parasite lines independent of *Pfkelch13* genotype ***(Figure 1***). First, we show that DHA sensitivity can be reduced in a dose-dependent manner when 0-3h ring stages are briefly exposed to medium from CQ-killed CQ-S parasites (M_NF54_CQ20H). This is independent of *Pfkelch13* status (***Figures 2 and 3***). This suggests the existence of a specific signal concentration threshold required to induce the parasites to stop growing at the ring stage. The extracellular signal was found to be mediated by molecules with sizes <30 kDa (***Figure 4***). This excludes a role for extracellular vesicles. The signal was shown to be mediated by DHA-treated dying trophozoites ***(Figure 5***) in our final experiment.

The data presented here are in line with previous studies that have reported on the ability of *P. falciparum* to sense extracellular signals. For example, it has been shown that the proportion of asexual parasites committed to sexual stages can be increased by decreasing levels of lysophosphatidylcholine, a compound from the human host[26]. Other reports have suggested that *P. falciparum* is able to limit the number of parasites through quorum sensing (a density sensing mechanism) by promoting apoptosis when the parasitemia exceeds a certain threshold[27,28]. In another *Apicomplexa* model, polypeptides have been shown to be produced and secreted by Trypanosoma parasites to regulate their cell cycle[29]. Parasite growth arrest phenotypes have also been rescued by amino acid starvation[19] as well as by exposure to antimalarial drugs such as artemisinin[17] and abiotic stress such as heat[20,21]. In addition, a recent report has shown that the growth arrest of the parasite can be shortened when the parasite is exposed to phytohormones such as abscisic acid and gibberellic acid in vitro[30]. Thus, the growth arrest of *P. falciparum* at the ring stage appears to be a natural response when the parasites are exposed to adverse conditions and suggests that *P. falciparum* is able

to sense the extracellular environment and adapt accordingly. In spite of the unknown nature of the extracellular signal, our study allows us to make some hypotheses. First, we can exclude a possible role for host molecule lysophosphatidylcholine*26*. In fact, our data strongly suggest that the molecules are released from parasites that are dead or dying (***Figure 5***). Interestingly, although EVs have been shown to be involved in host-parasite communication, such as modulating the immune response and delivering cargo[31-36], their role in halting parasite growth is unlikely. EVs have sizes ranging from 30 to 500 nm[24], whereas medium from CQ-killed parasites filtered at <10 nm was fully active to mediate ring stage growth arrest and reduced *in vitro* susceptibility to DHA (***Figure 4***).

We were also able to show that the growth arrest of the ring stage was observed in both wild-type and mutant *Pfkelch13* parasites (***Figure 2-5***). From this observation, we can infer that the temporary growth arrest of the ring stage is a natural survival mechanism that is mediated by a specific but unknown factor or soluble molecule that is released from dead or dying mature stages and is sensed by the ring stages when a threshold concentration is reached. Finally, our results suggest that the growth arrest of the ring stage and the partial resistance to artemisinins mediated by *Pfkelch13* mutations are two independent but complementary survival mechanisms against artemisinins. Reduced haemoglobin degradation is thought to be central to conferring artemisinin resistance in both mechanisms. Indeed, a proportion of ~70% wild-type and mutant ring stages were detected 24 h after exposure to medium from CQ-killed parasites. This suggests that the parasites have significantly reduced their cycle progression and thus haemoglobin uptake from the host cell (***Figure 1***), as has been demonstrated for artemisinin-resistant *Pfkelch13* mutant parasites[13-14].

In conclusion, our study provides new insights into artemisinin partial resistance and provides new evidence regarding the ring stage growth phenotype and how it affects *in vitro* susceptibility to DHA. However, unravelling the signalling pathway of parasite temporary growth arrest and the nature of extracellularly released factors requires further research. We can speculate that the signalling molecule may either bind to erythrocyte surface receptor(s), as previously reported[37], or cross the erythrocyte membrane in an active (transporter protein) or passive manner. This work could serve as a basis for developing new strategies based on quenching by disrupting extracellular communication. Preventing ring stage dormancy by disrupting extracellular signalling could keep early ring stage *P. falciparum* artemisinin sensitive.

Material and Methods

P. falciparum parasite *in vitro* culture.

P. falciparum asexual blood-stage parasites were seeded in T50 flask (Falcon®) and cultured at 4% hematocrit and a parasiamia < 1% in 10 mL RPMI-1640 medium (Gibco®) supplemented with 10% Albumax (Gibco®), 0.2 mM Hypoxanthin, 2% AB human serum (heat inactivated at 56°C) and 4 µg/mL Gentamicin (complete RPMI culture medium). Parasites were maintained at 37°C in 90% N_2, 5% O_2 and 5% CO_2. Human sera were provided by the EFS (Établissement Français du Sang) and the fresh bloods from healthy donors were provided by the ICAReB platform from Institut Pasteur.

We used several parasite lines including the laboratory strains 3D7 and NF54, the CRISPR/Cas9 edited line $3D7^{C580Y}$ (as described by Ghorbal *et al.*[38]) and three culture-adapted isolates originated from Pailin (Cambodia), the $PL1^{C580Y}$ and the $PL2^{C580Y}$ (harboring the *Pfkelch13 580Y* mutation) and the PL3WT (harboring the *Pfkelch13* wild type genotype). Genotypes of the parasite lines in *P. falciparum chloroquine resistant transporter* gene (*Pfcrt*), *Plasmodium falciparum multidrug resistant protein* gene (*Pfmdr-1*) and *Plasmodium falciparum kelch* gene located on the chromosome 13 (*Pfkelch13*) were determined by whole genome sequencing and are presented in the Table S1.

Parasite synchronization and Ring-stage Survival Assay (RSA^{0-3h}).

Parasites were cultured until the parasitemia ranges from 1% to 1.5%. Synchronized parasite cultures were obtained by exposing predominantly ring-stage cultures to 5% D-Sorbitol (Sigma) for 15 min at 37°C to remove mature parasites, as previously described by Lambros *et al.*[39]. The kinase inhibitor ML10 (200 nM) was added into the culture medium at 20h (trophozoite stages) to block schizonts rupture[40].

After 37-49 hr of culture, parasite stages were controlled on Giemsa-stained blood smear. Multinucleated schizonts were collected through a differential centrifugation (8 min, 600 g, no brake) over a density gradient consisting of 75% Percoll (Sigma). Schizonts were resuspended in 10 mL of complete RPMI culture medium with 200 µL RBC and centrifuged 5 min at 2000 rpm to remove the ML10 and residual Percoll. The red blood cell pellet was resuspended in 10 mL of complete RPMI culture medium and cultures were incubated at 37°C in in 90% N_2, 5% O_2 and 5% CO_2 on a shaker plate for 3 hr. Early rings (0–3 hr post invasion, hpi) were treated with 5% D-Sorbitol to remove remaining schizonts. Blood stage parasites and parasitemia were controlled on Giemsa-stained blood smear and parasitemia were adjusted to 0.5%.

In vitro RSA^{0-3h} were conducted as previously described.[18] Briefly, tightly synchronized 0–3 hpi rings were exposed to a pharmacologically-relevant dose of 700 nM DHA or 0.1% dimethyl sulfoxide (DMSO; vehicle control) for 6 hr at 0.5% parasitemia and 4% hematocrit, washed twice with RPMI

incomplete medium to remove drug, transferred to 6-well or 12-well plates, and cultured for an additional 66 hr in drug-free medium at 4% hematocrit. Red blood cell pellets were then collected to prepare Giemsa-stained blood smears for estimating the parasitemia. The number of red blood cells counted in each RSA^{0-3h} assays was 20,000. Parasite survival was expressed as the percentage value of the parasitemia in DHA-treated samples divided by the parasitemia in DMSO-treated samples processed in parallel.

We considered any RSA mean survival rates <2% to be ART sensitive.

Statistical analysis.

Data were analysed with Microsoft Excel, MedCalc version 20 (Mariakerke, Belgium) and GraphPad Prism® (v.9.0.0). Quantitative data were expressed as mean (± SEM). Continuous variables were compared with the one-sample *t*-test. Correlations were analysed with the Spearman correlation test. We deemed significant p values of less than 0.05.

Supplementary materials

Exposure to a culture medium collected from CQ-treated NF54 parasites culture induces delayed growth of *P. falciparum* blood-stages.

We produced the stress-induced environmental condition by generating a culture medium (named M_NF54_CQ_20h) from an asynchronous NF54 CQ-S parasite line exposed to 200 nM CQ for 20 hr. We confirmed the killing effect of 200 nM CQ on NF54 CQ-S blood stages by the microscopic examination of a Giemsa-stained blood smear, as presented in Figure S1 (Panel A. NF54 parasites before addition of 200 nMCQ and Panel B. NF54 parasites after 20 hr incubation with 200 nM CQ). As negative control, uninfected RBC were also exposed to 200 nM CQ for 20 hours.

Cambodian CQ-R *P. falciparum* $PL1^{C580Y}$, $PL2^{C580Y}$ and $PL3^{WT}$ parasite lines were cultured, synchronized by exposing predominantly ring-stage cultures to 5% D-Sorbitol (Sigma) for 15 min at 37°C to remove mature parasites. Tightly synchronized 0–3 hpi rings were prepared and exposed to the M_NF54_CQ_20h culture medium or complete RPMI medium (non-exposed) for 24 hr. After two washing steps with incomplete RPMI medium, the parasite lines were cultured for additional 24 hr in RPMI complete medium (H48). Red blood cells were collected at H24 and H48 to prepare Giemsa-stained blood smears (Figure S2).

Figure S1. Killing impact of 200 nM CQ on NF54 CQ-S parasite line.

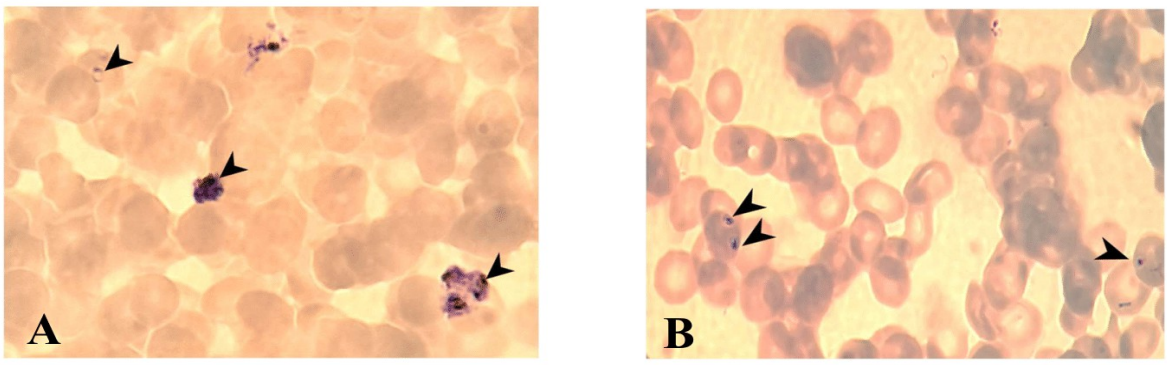

Panel A. Presence of asexual blood-stages (rings, trophozoites and schizonts) (black arrows).
Panel B. Presence of dead or pyknotic parasites (black arrows).

Table S1. Origin, year of collection and genotypes in Pfkelch13, Pfcrt and Pfmdr-1 of the parasite lines.

Strain ID	Origin	Year	*Kelch13*	*Pfcrt*	*Pfmdr-1*
NF54	Africa	-	Wild type	CVMNKTHFIMCGT	NYSND
3D7	Africa	-	Wild type	CVMNKTHFIMCGT	NYSND
$3D7^{C580Y}$	Africa	-	C580Y	CVMNKTHFIMCGT	NYSND
$PL1^{C580Y}$	Pailin	2010	C580Y	CVIETTHFIMCGT	NFSND
$PL2^{C580Y}$	Pailin	2010	C580Y	CVIETTHFIMCGT	NFSND
$PL3^{WT}$	Pailin	2010	Wild type	CVIETTHFIMCGT	NFSND

Position of amino acid corresponds to codons 72, 73, 74, 76, 93, 97, 145, 218, 343, 350, 353 and 356 for pfcrt, to codons 86, 184, 1034, 1042 and 1246 for pfmdr-1.

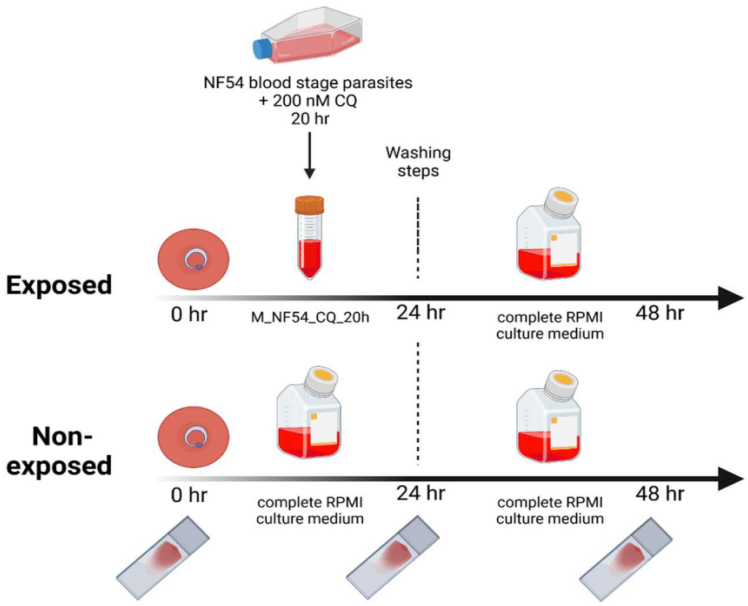

Figure S2. Schematic representation of the experimental design.

Early 0-3 hpi ring-stage parasites treated with M_NF54_CQ20h showed a decrease *in vitro* susceptibility to DHA.

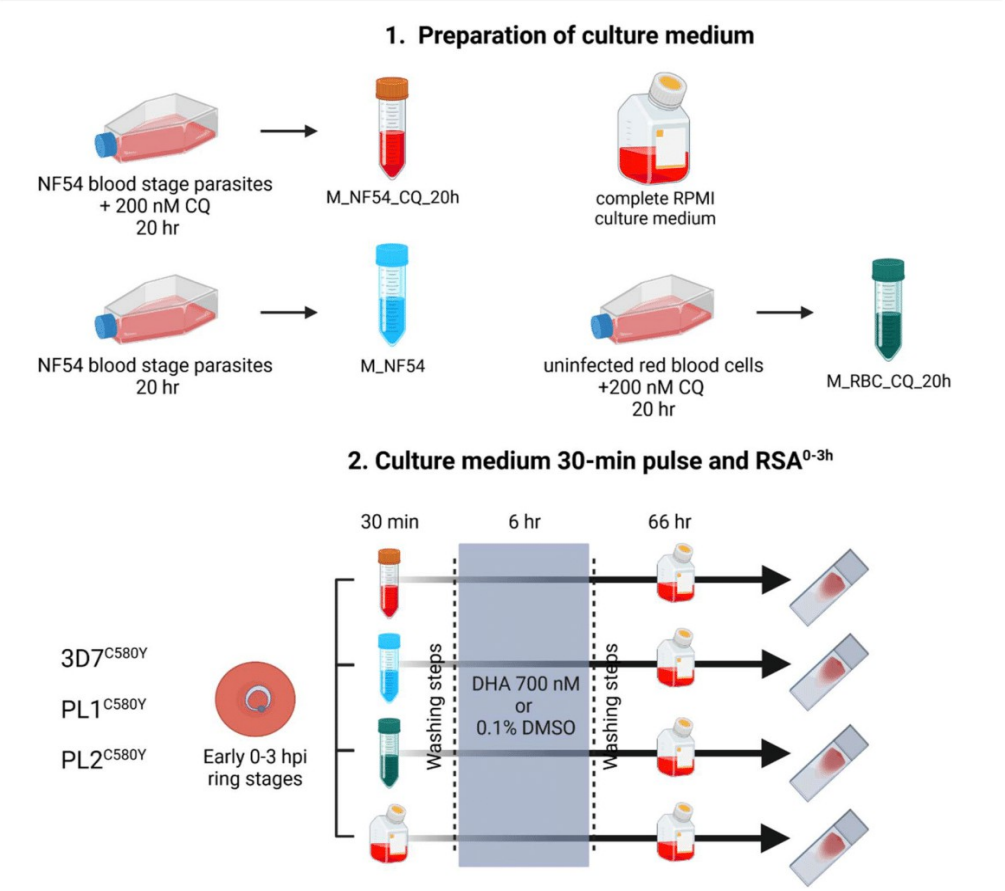

Figure S3. Schematic representation of the experimental design.

Dilutions of the M_NF54_CQ20h medium restore gradually the original *in vitro* susceptibility to DHA of the *P. falciparum* parasite lines.

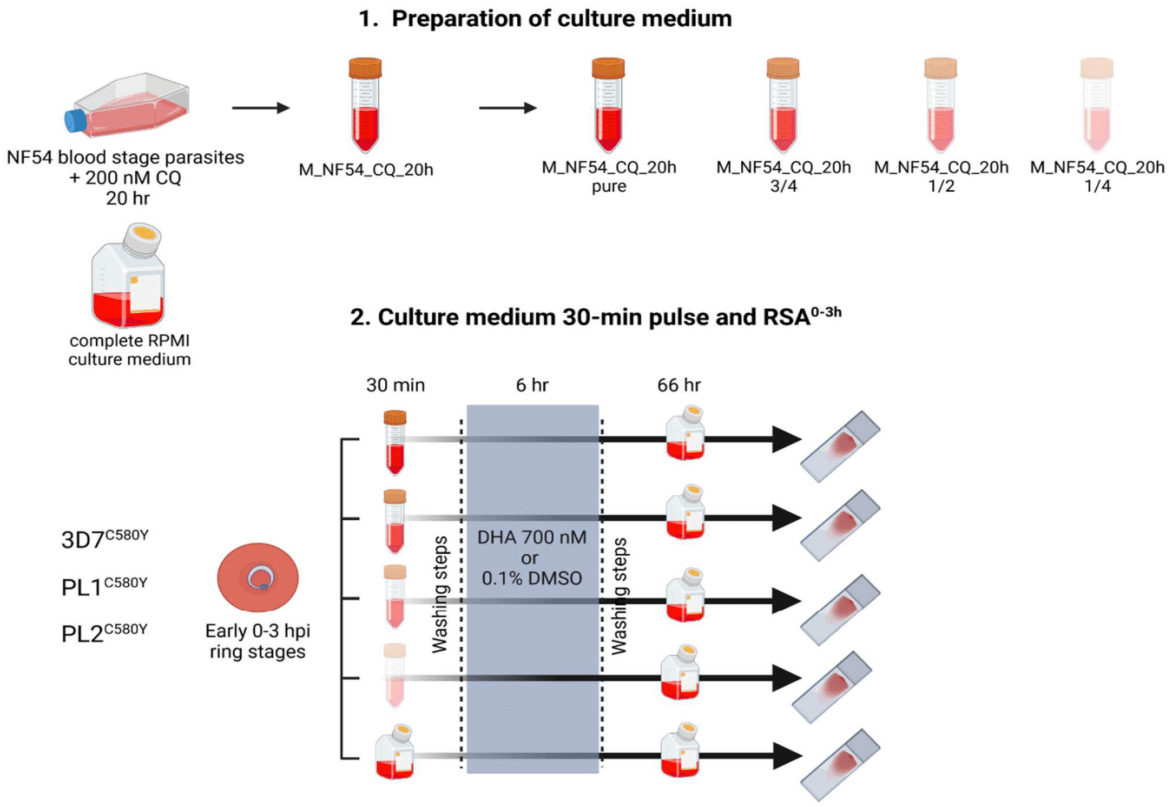

Figure S4. Schematic representation of the experimental design.

To prepare the dilution of M_NF54_CQ20h medium, complete RPMI culture medium was used to dilute M_NF54_CQ20h medium to ¾ (3 volumes M_NF54_CQ20h medium and 1 volume complete RPMI culture medium), to ½ (1 volume M_NF54_CQ20h medium and 1 volume complete RPMI culture medium) and to ¼ (1 volume M_NF54_CQ20h medium and 3 volumes complete RPMI culture medium). Diluted M_NF54_CQ20h medium were kept at 37°C in water bath until used.

The ring-stage delayed growth and reduced *in vitro* DHA susceptibility induced by the CQ-killed parasite medium are mediated by several molecules of different molecular weight, independent of the *Pfkelch13* genotype.

Centricon® filtration. M_NF54_CQ20h medium was centrifuged (2000 rpm, 5 min), collected in a 50 mL tube and stored at 37°C in water bath. Centricon filters (Merck Millipore) were sterilized with 70% ethanol solution and prepared according to the manufacturer instructions. We used four filter sizes to filtrate four independent M_NF54_CQ20h medium. The filter pore sizes were as following:100 kDa (pore diameter: 10 nm), 30 kDa (pore diameter: 3 nm), 10 kDa (pore diameter: 1 nm) and 3 kDa (pore diameter: 0.3 nm). Centrifugations parameters and volumes were prepared according to the manufacturer instructions.

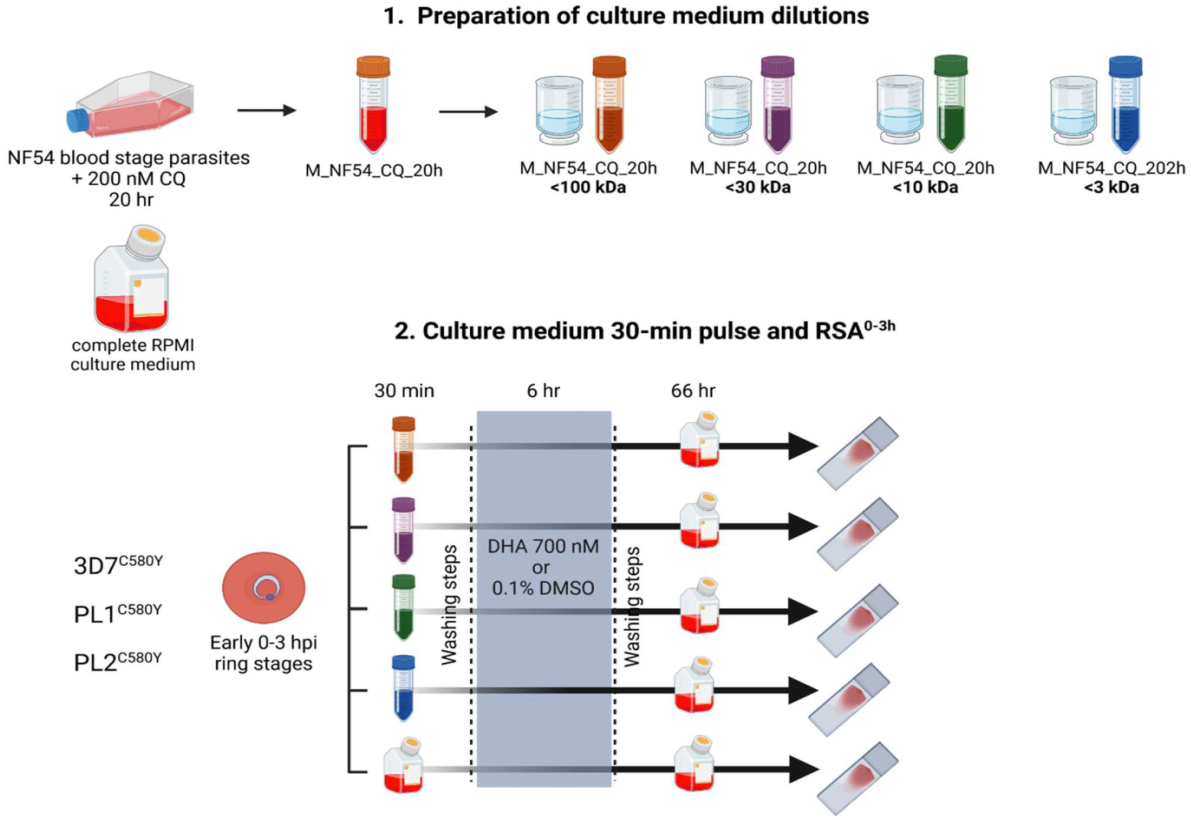

Figure S5. Schematic representation of the experimental design.

DHA-treated mature stage parasites release molecules into the culture medium that reduce the *in vitro* susceptibility of ring-stage parasites to DHA.

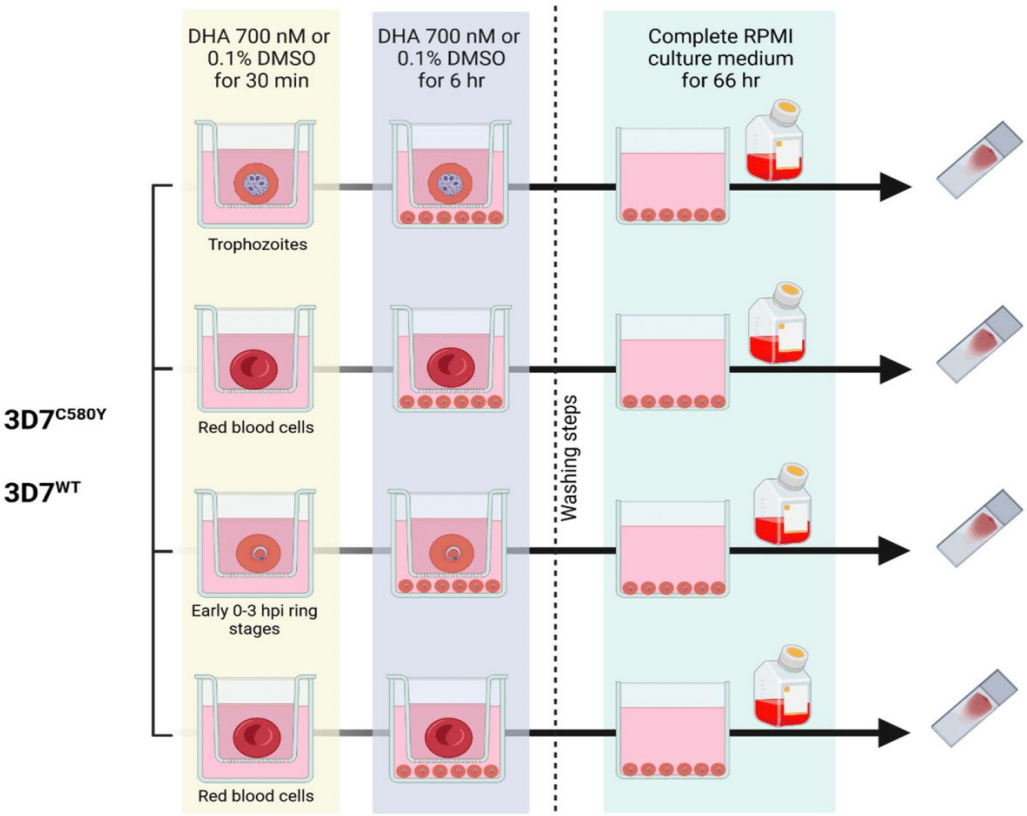

Figure S6. Schematic representation of the experimental design.

Acknowledgement

We thank the staff of the ICAReB platform at Institut Pasteur for providing the blood. We are also grateful to the BIHP staff (Biologie des Infections Hôtes-Parasites) unit led by Artur Scherf at Institut Pasteur for their advice and technical supports. We deeply thank Professor David Baker from the *London School of Hygiene and Tropical Medicine* for providing the ML10.

Authors contribution

LP performed the experiments, the data analysis and wrote the first draft of the manuscript redaction. DM was involved in the study design, the data analysis, the manuscript revision and the scientific supervision.

Competing interests

The authors declare they have no conflict of interest.

Materials & correspondence

All correspondence and material request shall be addressed to Didier Ménard at dmnenard@unistra.fr

References

1. World malaria report 2022; World Health Organization.

2. White, N. J. & Nosten, F. Artemisinin-Based Combination Treatment of Falciparum Malaria. *The American Journal of Tropical Medicine and Hygiene* 77, 181–192 (2007).

3. White, N. J. Clinical pharmacokinetics and pharmacodynamics of artemisinin and derivatives. *Transactions of the Royal Society of Tropical Medicine and Hygiene* 88, 41–43 (1994).

4. White, N. Antimalarial drug resistance and combination chemotherapy. *Phil. Trans. R. Soc. Lond. B* 354, 739–749 (1999).

5. Straimer, J. *et al.* K13-propeller mutations confer artemisinin resistance in *Plasmodium falciparum* clinical isolates. *Science* 347, 428–431 (2015).

6. Miotto, O. *et al.* Emergence of artemisinin-resistant *Plasmodium falciparum* with kelch13 C580Y mutations on the island of New Guinea. *PLoS Pathog* 16, e1009133 (2020).

7. Balikagala, B. *et al.* Evidence of Artemisinin-Resistant Malaria in Africa. *N Engl J Med* 385, 1163–1171 (2021).

8. Uwimana, A. *et al.* Emergence and clonal expansion of *in vitro* artemisinin-resistant *Plasmodium falciparum* kelch13 R561H mutant parasites in Rwanda. *Nat Med* 26, 1602–1608 (2020).

9. Mathieu, L. C. *et al.* Local emergence in Amazonia of *Plasmodium falciparum* k13 C580Y mutants associated with *in vitro* artemisinin resistance. *eLife* 9, e51015 (2020).

10. Witkowski, B. *et al.* Novel phenotypic assays for the detection of artemisinin-resistant

Plasmodium falciparum malaria in Cambodia: in-vitro and ex-vivo drug-response studies. *The Lancet Infectious Diseases* 13, 1043–1049 (2013).

11. Ariey, F. *et al.* A molecular marker of artemisinin-resistant Plasmodium falciparum malaria. *Nature* 505, 50–55 (2014).

12. Ménard, D. *et al.* A Worldwide Map of *Plasmodium falciparum* K13-Propeller Polymorphisms. *N Engl J Med* 374, 2453–2464 (2016).

13. Birnbaum, J. *et al.* A Kelch13-defined endocytosis pathway mediates artemisinin resistance in malaria parasites. *Science* 367, 51–59 (2020).

14. Yang, T. *et al.* Decreased K13 Abundance Reduces Hemoglobin Catabolism and Proteotoxic Stress, Underpinning Artemisinin Resistance. *Cell Reports* 29, 2917-2928.e5 (2019).

15. Wang, J. *et al.* Haem-activated promiscuous targeting of artemisinin in *Plasmodium falciparum*. *Nat Commun* 6, 10111 (2015).

16. Klonis, N. *et al.* Artemisinin activity against *Plasmodium falciparum* requires hemoglobin uptake and digestion. *Proc. Natl. Acad. Sci. U.S.A.* 108, 11405–11410 (2011).

17. Witkowski, B. *et al.* Increased Tolerance to Artemisinin in *Plasmodium falciparum* Is Mediated by a Quiescence Mechanism. *Antimicrob Agents Chemother* 54, 1872–1877 (2010).

18. Nakazawa, S., Kanbara, H., Aikawa, M. *Plasmodium falciparum*: Recrudescence of parasite in culture. *Experimental Parasitology* 81, 556-563 (1995).

19. Babbitt, S. E. *et al. Plasmodium falciparum* responds to amino acid starvation by entering into a hibernatory state. *Proc. Natl. Acad. Sci. U.S.A.* 109, (2012).

20. Singhaboot, Y. *et al.* Temperature Dependence of Plasmodium falciparum Erythrocytic Stage Development. *The American Journal of Tropical Medicine and Hygiene* 100, 1191–1195 (2019).

21. Kwiatkowski, D. Febrile temperatures can synchronize the growth of *Plasmodium falciparum in vitro*. *J. Exp. Med.* 169, 357-361 (1989).

22. Teuscher, F. *et al.* Artemisinin-Induced Dormancy in *Plasmodium falciparum* : Duration, Recovery Rates, and Implications in Treatment Failure. *J INFECT DIS* 202, 1362–1368 (2010).

23. Tripathi, J. *et al.* The artemisinin-induced dormant stages of *Plasmodium falciparum* exhibit hallmarks of cellular senescence and drug resilience. http://biorxiv.org/lookup/doi/10.1101/2023.01.29.526019 doi:10.1101/2023.01.29.526019. (2023)

24. Sharon, M. & Regev-Rudzki, N. Cell communication and protein degradation: All in one parasitic package. *Journal of Extracellular Vesicles* 10, (2021).

25. Klonis, N. *et al.* Altered temporal response of malaria parasites determines differential sensitivity to artemisinin. *Proc. Natl. Acad. Sci. U.S.A.* 110, 5157–5162 (2013).

26. Brancucci, N. M. B. *et al.* Lysophosphatidylcholine Regulates Sexual Stage Differentiation in the Human Malaria Parasite *Plasmodium falciparum*. *Cell* 171, 1532-1544.e15 (2017).

27. Mutai, B. K. & Waitumbi, J. N. Apoptosis stalks *Plasmodium falciparum* maintained in continuous culture condition. *Malar J* 9, S6 (2010).

28. Chou, E. S. *et al.* A high parasite density environment induces transcriptional changes and cell death in *Plasmodium falciparum* blood stages. *FEBS J* 285, 848–870 (2018).

29. Rojas, F. *et al.* Oligopeptide Signaling through TbGPR89 Drives Trypanosome Quorum Sensing. *Cell* 176, 306-317.e16 (2019).

30. Duvalsaint, M. & Kyle, D. E. Phytohormones, Isoprenoids, and Role of the Apicoplast in Recovery from Dihydroartemisinin-Induced Dormancy of *Plasmodium falciparum*. *Antimicrob Agents Chemother* 62, e01771-17 (2018).

31. Regev-Rudzki, N. *et al.* Cell-Cell Communication between Malaria-Infected Red Blood Cells via Exosome-like Vesicles. *Cell* 153, 1120–1133 (2013).

32. Mantel, P.-Y. *et al.* Malaria-Infected Erythrocyte-Derived Microvesicles Mediate Cellular Communication within the Parasite Population and with the Host Immune System. *Cell Host &*

Microbe 13, 521–534 (2013).

33. Babatunde, K. A. *et al.* Malaria infected red blood cells release small regulatory RNAs through extracellular vesicles. *Sci Rep* 8, 884 (2018).

34. Sampaio, N. G. *et al.* Extracellular vesicles from early stage *Plasmodium falciparum* -infected red blood cells contain PfEMP1 and induce transcriptional changes in human monocytes. *Cellular Microbiology* 20, e12822 (2018).

35. Mbagwu, S. I., Lannes, N., Walch, M., Filgueira, L. & Mantel, P.-Y. Human Microglia Respond to Malaria-Induced Extracellular Vesicles. *Pathogens* 9, 21 (2019).

36. Ofir-Birin, Y. *et al.* Malaria parasites both repress host CXCL10 and use it as a cue for growth acceleration. *Nat Commun* 12, 4851 (2021).

37. Wu, Y. *et al.* An external sensing system in *Plasmodium falciparum*-infected erythrocytes. *Malar J* 15, 103 (2016).

38. Ghorbal, M. *et al.* Genome editing in the human malaria parasite *Plasmodium falciparum* using the CRISPR-Cas9 system. *Nat Biotechnol* 32, 819–821 (2014).

39. Lambros, C. & Vanderberg, J. P. Synchronization of *Plasmodium falciparum* Erythrocytic Stages in Culture. *The Journal of Parasitology* 65, 418 (1979).

40. Ressurreição, M. *et al.* Use of a highly specific kinase inhibitor for rapid, simple and precise synchronization of *Plasmodium falciparum* and *Plasmodium knowlesi* asexual blood-stage parasites. *PLoS ONE* 15, e0235798. https://doi.org/10.1371/journal.pone.0235798 (2020).

Travail expérimental : Mise en évidence de l'hétérogénéité transcriptionnelle du stade ring dans une population phénotypiquement homogène de *P. falciparum*.

Le travail présenté ci-après visait à explorer le profil transcriptionnel des stades rings en arrêt de croissance après exposition à un environnement extracellulaire stressant. L'objectif de ces expériences était de définir des biomarqueurs spécifiques de la dormance (profil d'expression des gènes) parmi des parasites synchronisés en stade ring 0-3h de fonds génétiques différents (*Pfkelch13-WT* et *Pfkelch13-C580Y*) exposés à un stress cellulaire. Pour cela, nous avons conduit une approche basée sur le séquençage ARN en single-cell sur 10 000 cellules. Ces données préliminaires, basées sur une population de jeunes rings phénotypiquement homogène, nous ont permis d'identifier 975 transcrits définissant 9 sous-populations. Ce travail a été réalisé en collaboration avec les plateformes Biomics et CBUtech ainsi que le hub bio-informatique de l'Institut Pasteur.

Matériel et Méthode

Culture de P. falciparum. Les souches de référence 3D7 (*Pfkelch13-WT*) et 3D7-580 (*Pfkelch13-C580Y*) ont été cultivées en flasque T50 (Falcon®) dans du milieu RPMI 1640 (Gibco®) supplémenté avec 10% d'Albumax (Gibco®), 0,2 nM d'hypoxanthine, et 4 µg/mL de gentamycine (Merck®). Les cultures ont été maintenues à 1% de parasitémie (4% d'hématocrite). Le sang des donneurs sains a été fourni par la plateforme Icareb de l'Institut Pasteur. Le milieu de culture a été changé toutes les 2 jours. Les parasites ont été incubés en atmosphère humide à 37°C dans un incubateur trigaz (90% diazote, 5% dioxygène et 5% dioxyde de carbone).

Synchronisation des stades rings 0-3h. Les parasites ont été cultivés jusqu'à une parasitémie de 1% puis synchronisés en stade ring jeune (~0-12h post invasion) par traitement au sorbitol 5% (Lambros *et al.*, 1979). Après quelques heures de culture, les parasites au stade trophozoïtes 20-32h ont été traités avec 200 nM de ML10 pour bloquer l'éclosion des schizontes (Ressurreiçao *et al.*, 2020). Les parasites 37-49h ont ensuite été centrifugés (8 minutes, 600g, sans frein) dans une solution de Percoll 75% afin d'isoler les schizontes. Les schizontes ont été recueillis, lavés dans 10 mL de RPMI puis centrifugés 2 minutes à 2000 rpm pour éliminer le ML10 et le percoll résiduel. Le culot de parasite a été remis en suspension dans 10 mL de milieu RPMI complet et incubé en flasque T50 avec agitation pendant 3h à 37°C (90% diazote, 5% dioxygène et 5% dioxyde de carbone). Un contrôle a été réalisé par frottis sanguin coloré au Giemsa pour valider la présence de ring 0-3h. Finalement, les cultures ont été synchronisées par traitement au Sorbitol 5% afin

d'éliminer les formes matures résiduelles. La parasitémie des stades ring 0-3h a été calculée par lecture en microscopie sur frottis coloré au Giemsa.

Production du surnageant de parasite stressé (SCS). La souche de référence NF54 a été cultivée en flasque T50 (Falcon®) dans du milieu RPMI 1640 (Gibco®) supplémenté avec 10% d'Albumax (Gibco®), 0,2 nM d'hypoxanthine, et 4 µg/mL de gentamycine (Merck®). Les cultures ont été maintenues à une parasitémie de 1% et un hématocrite de 4%. Les parasites asynchrones ont été traités pendant 20h avec 200 nM de Chloroquine (figure 1). La culture a été centrifugée pendant 5 minutes à 2000 rpm, le surnageant a été collecté en tubes 50 mL puis placé au bain-marie à 37°C jusqu'à utilisation.

Induction du stress et coloration des parasites. Les parasites synchronisés en ring 0-3h des souches 3D7 et 3D7-580 ont été transférés en plaque 48 puits et exposés 1h avec 1 mL de surnageant de culture stressée ou le milieu de culture RPMI complet et maintenu à 2% d'hématocrite. Les parasites ont été ensuite incubés avec 0,5 µL de fluorophore Vybrant Green (Thermofischer®) puis placés pendant 15 minutes dans l'obscurité à 37°C en incubateur trigaz. Les longueurs d'ondes d'excitations et d'émissions du Vybrant Green sont de 488 nm et 520 nm respectivement. Ce fluorophore a été choisi en raison de sa faible cytotoxicité et de l'absence d'interférence avec la transcription cellulaire.

Tri cellulaire et séquençage ARN single-cell. Les stades rings 1-4h préalablement marqués ont été dilués dans 1 mL de PBS à une concentration finale de $1x10^6$ cellules par mL. Le tri cellulaire a été réalisé par cytométrie (laser bleu, 488 nm) avec un FACS Aria Fusion (BD Biosciences®). Nous avons utilisé des paramètres de tri très sélectif pour éliminer les globules rouges polyinfectés. Au final, nous avons recueilli 60 000 cellules par échantillon. Nous avons ensuite mis en pratique le protocole d'extraction Chromium Next GEM Single Cell 3' Reagent Kits v3.1 (10X Genomics®) préalablement adapté pour 10 000 cellules (le maximum possible selon les instructions du fabricant). La préparation des ADNc et des banques a été réalisée en accord selon les instructions du fabricant. Le séquençage des ADNc a été réalisé par un séquenceur Illumina® NextSeq500 en utilisant une flow cell Hight Output (figure 1).

Analyse bio-informatique. Les données de séquençage de chaque échantillon ont été traitées avec le pipeline 10X CellRanger v7.0.0. Les séquences ont été alignées sur les génomes concaténés de la souche de référence 3D7 de *P. falciparum* et du génome humain. Le traitement par CellRanger a

permis de conserver environ 10 000 cellules par échantillon contenant le plus d'UMIs (40 000 cellules au total). Les données de séquençage ont été ensuite annotées sur la base des jeux de données du Malaria Cell Atlas (https://www.malariacellatlas.org/).

Le contrôle qualité des cellules a été réalisé avec le programme Seurat (Stuart *et al*., 2019). Un objet Seurat a été créé basé sur la fonction Read10X. Les cellules ont été filtrées selon les critères suivants : nombre d'UMIs par cellule >100 ; fraction des UMIs alignés sur le génome de *P. falciparum* 3D7 >50%. Le jeu de donnée contenait 3669 cellules total (844 à 969 cellules par échantillon) pour un total de 5336 gènes détectés (exprimés dans au moins 1 cellule). Pour obtenir des types cellulaires putatifs, les données sont intégrées au pipeline Seurat v3 avec les paramètres par défaut. Nous avons utilisé les fonctions NormalizeData, FindVariableFeatures (conservant les 2000 gènes les plus variables), ScaleData et RunPCA. Pour la visualisation, nous avons utilisé FindNeighbors, FindClusters (résolution de 0,5) et RunUMAP sur les 10 premières composantes principales.

Nous avons réalisé une annotation préliminaire du jeu de donnée en utilisant MetaNeighbor (Crow *et al.*, 2018) comparé aux données du Malaria Cell Atlas (Reid *et al.*, 2018 ; Howick *et al.*, 2019 ; Real *et al.*, 2021). MetaNeighbor a permis de réaliser la correspondance entre le type de cellule et le profil d'expression sur la base d'un jeu de données servant de requête comparé à une référence. Nous avons sélectionné les jeux de données de référence contenant les stades du développement asexué de *P. falciparum*. Pour le lancement de MetaNeighbor, les données ont été converties en format SingleCellExperiment, la liste des transcrits a été extraite pour chaque échantillon, un score de similarité a été calculé et a permis la répartition des profils transcriptomiques de chaque cellule en sous-population.

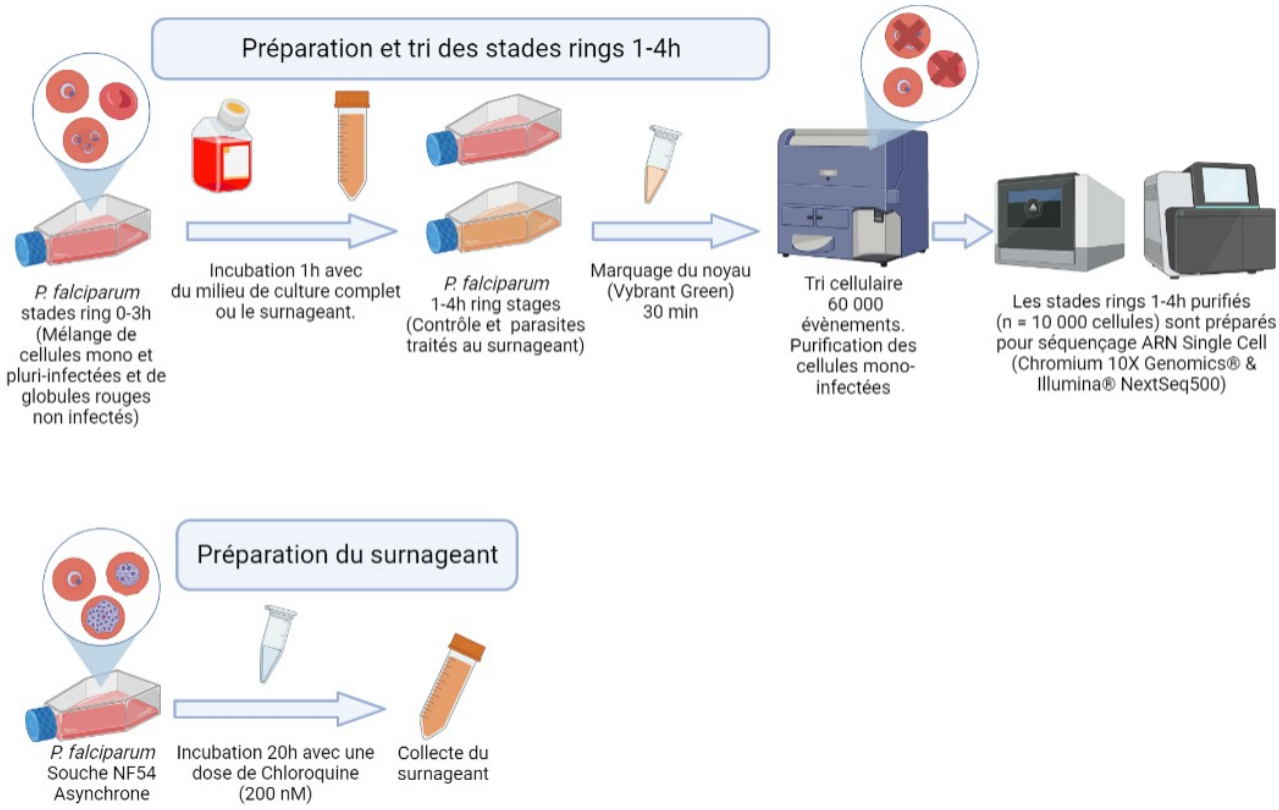

Figure 1 : Résumé du protocole expérimental de la préparation des parasites jusqu'au séquençage.

Résultats

Le stade ring 1-4h de P. falciparum exprime une diversité de profils transcriptomiques.

Bien qu'à un stade préliminaire, les données présentées apportent des informations intéressantes sur le transcriptome des stades rings 1-4h de *P. falciparum*. Après l'application de filtres (contrôle qualité), nous avons conservé les données de 952 cellules pour 3D7 *Pfkelch13-WT* RPMI, 969 cellules pour 3D7 *Pfkelch13-WT* SCS, 844 cellules pour 3D7 *Pfkelch13-C580Y* RPMI et 904 cellules pour *Pfkelch13-C580Y* SCS.

Les données obtenues ont été comparées aux jeux de données du Malaria Cell Atlas afin de pouvoir classer les cellules sur la base des profils d'expression de gènes associés aux stades asexués du parasite. Nous avons premièrement constaté que le transcriptome des rings 1-4h en condition physiologique (non stressé) était hétérogène (figure 2). En effet, nous avons constaté que les cellules séquencées ne formaient pas une seule population homogène d'un point de vue transcriptionnel, mais un ensemble de 9 sous-populations distinctes (figure 2). Les profils d'expressions de ces sous-populations correspondaient au développement temporel du parasite dans le cycle asexué. Toutes les sous-populations à l'exception de la sous-population 8 (colorée en vert) étaient présentes indépendamment du génotype *Pfkelch13* ou de l'exposition au SCS (figure 2).

Surprenamment, nous avons observé que la sous-population 8 était quasiment absente dans le jeu de données de la souche 3D7 *Pfkelch13-WT* (représentant seulement 0,5% et 0,8% de la population totale en condition RPMI et SCS respectivement) alors que cette sous-population était largement représentée dans le jeu de données de la souche mutée 3D7 *Pfkelch13-C580Y* (représentant 9,1% et 19,4% de la population totale en condition RPMI et SCS respectivement). Ces données suggèrent fortement l'existence d'une sous-population spécifique de la présence de la mutation C580Y chez la souche 3D7. Ces résultats étant issus de parasites synchronisés et de souches clonales, démontre également l'existence d'une hétérogénéité transcriptionnelle forte du stade ring 1-4h de *P. falciparum* en condition physiologique.

L'exposition au SCS provoque des changements dans la distribution des sous-populations transcriptionnelles.

Premièrement, nous avons constaté que l'exposition à 1h au SCS induit une augmentation de la proportion de cellules de la sous-population 9 (colorée en orange foncée); de l'ordre de 70% pour la souche 3D7 *Pfkelch13-WT* et de 40% pour la souche 3D7 *Pfkelch13-C580Y* (figure 2). En second lieu, nous avons observé que la sous-population 8 (colorée en vert), spécifique à la souche mutée *Pfkelch13-C580Y* était également enrichie d'un facteur 2 après exposition au surnageant de parasite stressé. Les sous-populations 1 à 7 étaient toujours présentes indépendamment des conditions expérimentales ou du génotype *Pfkech13*, indiquant que la diversité transcriptionnelle du stade ring 1-4h de *P. falciparum* est une propriété innée (figure 2). Ces observations laissent supposer que l'exposition à un environnement extracellulaire stressant provoque une réponse transcriptionnelle d'une partie de la population des stades rings 1-4h de *P. falciparum*. Finalement, nous pouvons admettre que l'exposition au SCS induit deux types de réponses transcriptionnelles différentes. Premièrement, l'enrichissement de la sous-population 8 observé chez les deux souches 3D7 *Pfkelch13-WT* et 3D7 *Pfkelch13-C580Y*, indique qu'il s'agit d'une réponse indépendante de la présence de mutations dans *Pfkelch13* (figure 2). Deuxièmement, l'enrichissement de la sous-population 9 indique une réponse transcriptionnelle plus spécifique à la souche mutée *Pfkelch13-C580Y* (figure 2).

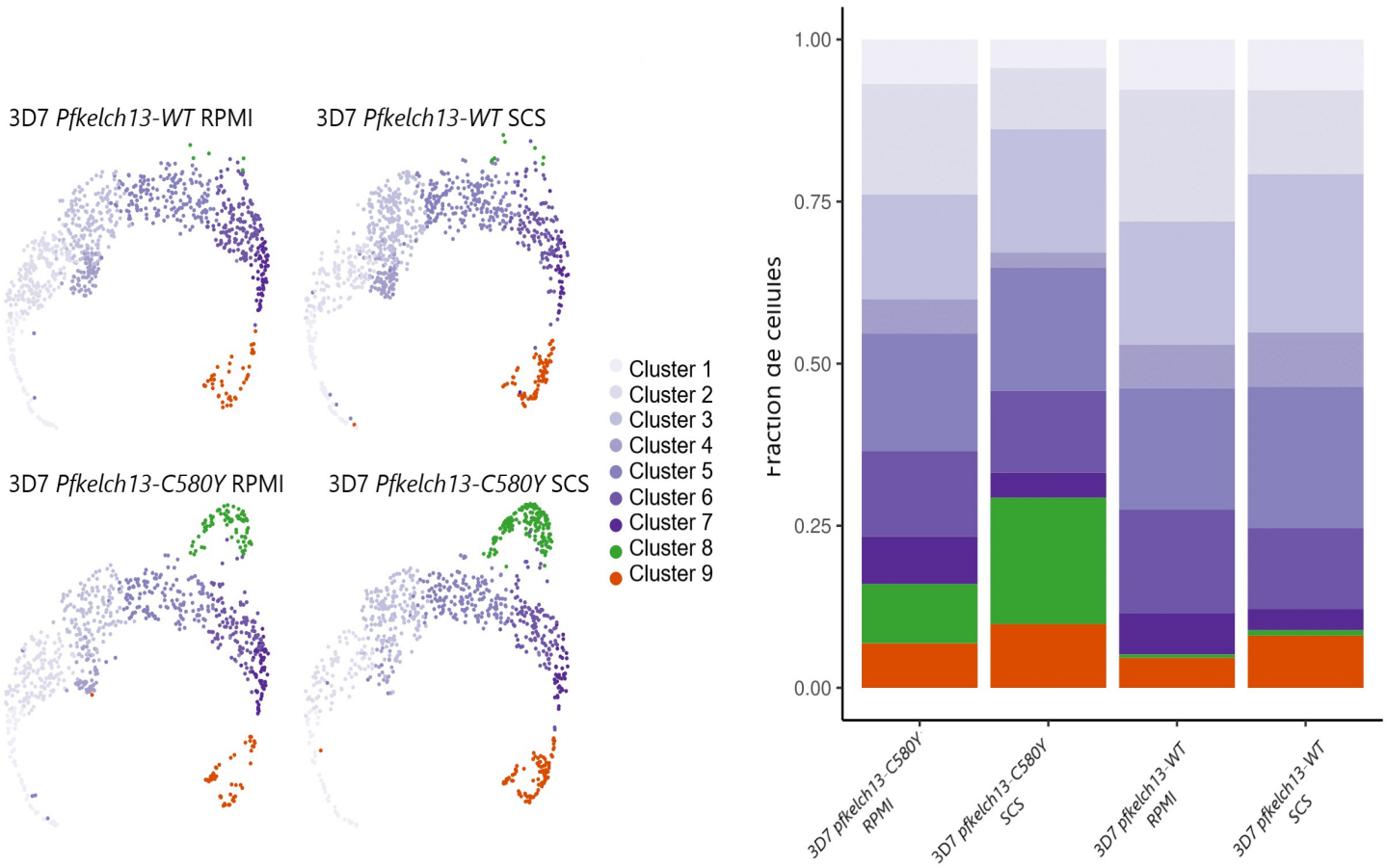

Figure 2 : Hétérogénéité transcriptionnelle chez les stades rings 1-4h synchronisés de *P. falciparum*. Visualisation en analyse par composante principale de la distribution des profils transcriptomiques des cellules séquencées. Chaque point représente le transcriptome d'une cellule dans un échantillon donné. Les cellules sont classées en sous-population sur la base de la similarité de leur profil d'expression avec les données de références du Malaria Cell Atlas. Chaque cluster est une sous-population de cellule ayant un profil d'expression spécifique.

- 3D7 *Pfkelch13-WT* RPMI : rings 0-3h de la souche 3D7 (*Pfkelch13-WT*) traités 1h avec du milieu complet.
- 3D7 *Pfkelch13-WT* SCS : rings 0-3h de la souche 3D7 (*Pfkelch13-WT*) traités 1h avec du SCS.
- 3D7 *Pfkelch13*-C580Y RPMI : rings 0-3h de la souche 3D7 (*Pfkelch13-C580Y*) traités 1h avec du milieu complet.
- 3D7 *Pfkelch13-C580Y* SCS : rings 0-3h de la souche 3D7 (*Pfkelch13-C580Y*) traités 1h avec du SCS.

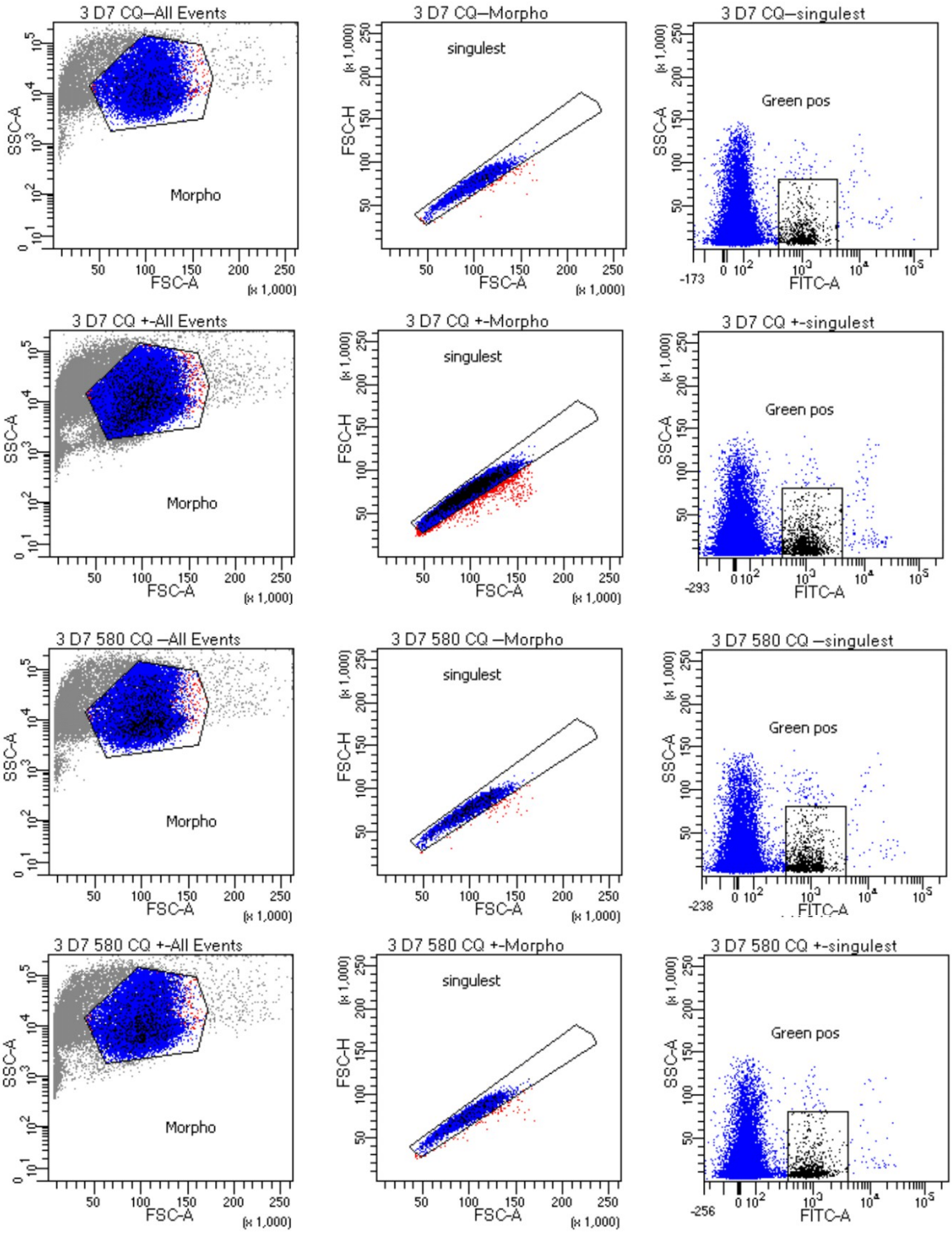

Figure 3 : Tri cellulaire des stades rings 1-4h des souches 3D7 et 3D7-580.

Les stades rings 1-4h des souches 3D7 (*Pfkelch13-WT*) et 3D7-580 (*Pfkelch13-C580Y*) marqués au Vybrant Green ont été triés (n = 60 000 par condition) sur un trieur Aria Fusion (laser bleu 488 nm). Les cellules sont triées selon les critères de taille (FSC) et de granulosité (SSC) afin de cibler les globules rouges. Seuls les événements singulets (une cellule par goutte) sont conservés. Le tri a été ajusté pour cibler les globules rouges monoinfectés (positif à la fluorescence, canal FITC-A).

- 3D7 CQ - = rings 1-4h de la souche 3D7 (*Pfkelch13-WT*) traités 1h avec du milieu complet.
- 3D7 CQ + = rings 1-4h de la souche 3D7-580 (*Pfkelch13-WT*) traités 1h avec du SCS.
- 3D7 580 CQ - = rings 0-3h de la souche 3D7-580 (*Pfkelch13-C580Y*) traités 1h avec du milieu complet.
- 3D7 580 CQ + = rings 0-3h de 3D7 (*Pfkelch13-C580Y*) traités 1h avec du SCS.

Discussion

Ces données préliminaires montrent l'existence d'une forte hétérogénéité transcriptionnelle constitutive au sein d'une population clonale et synchrone de jeunes stades ring de *P. falciparum* âgés de 1 à 4h. Neuf sous-populations ont pu être définies sur la base des profils transcriptionnels pour l'ensemble des conditions et des souches testées. Un enrichissement des sous-populations 8 et 9 a pu être constaté après exposition au SCS pendant 1h, supportant l'idée d'une réponse transcriptionnelle à des signaux de l'environnement extracellulaire. Plus précisément, l'enrichissement de la sous-population 8 après exposition au SCS indique une réponse transcriptionnelle indépendante du génotype *Pfkelch13* (figure 2) alors que l'enrichissement de la sous-population 8 correspond à une seconde réponse transcriptionnelle, spécifique de la présence de la mutation *Pfkelch13-C580Y.* Collectivement, ces données préliminaires apportent des éclaircissements sur la diversité du transcriptome du stade ring 1-4h de *P. falciparum*, et mettent en évidence la grande plasticité transcriptionnelle des formes jeunes du parasite.

Nous avons pris un maximum de précaution sur le plan technique concernant la purification et le séquençage du transcriptome des stades rings 1-4h afin d'éviter les artefacts et les faux positifs. Après ré invasion, les rings 0-3h ont été traités au Sorbitol 5% afin d'éliminer les formes matures résiduelles (Lambros *et al.*, 1979). L'absence de formes matures a pu être confirmée par un examen microscopique des frottis sanguin des rings 0-3h et par cytométrie en flux (figure 3). Nous avons pour cela utilisé le Vybrant Green, décrit comme préservant la viabilité des parasites, évitant des interférences potentielles dans l'expression des gènes (Philipp *et al.*, 2012). Le protocole appliqué pour le tri des stades rings 1-4h en cytométrie a été ajusté pour minimiser le risque de recueillir des globules rouges polyinfectés, et ainsi d'éliminer une source de biais potentiels (figure 3). La qualité des séquences a pu être validée par l'outil Seurat (Stuart *et al.*, 2019). Le principal avantage de notre approche single cell a été de s'affranchir du bruit de fond généré par le transcriptome de parasites morts. Il est toutefois possible que des globules rouges non infectés aient pu être intégrés à nos échantillons durant le tri cellulaire. Cependant, les seuils de similarités utilisés pour l'annotation de nos séquences durant l'analyse bio-informatique ont permis de retirer spécifiquement toutes les séquences d'origine humaine du jeu de donnée.

Ces données préliminaires suggèrent donc l'existence d'un profil transcriptomique hétérogène des jeunes stades ring de *P. falciparum*. Le stade ring de *P. falciparum* apparaît ainsi être hautement plastique du point de vu transcriptionnel. Ces observations sont à mettre en relation avec les données d'une précédente étude révélant une diversité de profils d'expressions de parasites prélevés *in vivo* où il a été observé que le stade ring prédominait parmi les populations parasitaires circulant dans le sang de patients infectés (Daily *et al.*, 2007). L'étude détaillée des profils d'expression des sous-populations 8 et 9 est en cours d'investigation, avec pour priorité l'identification de biomarqueurs spécifiques de ces sous-populations.

Discussion et conclusion générale

L'ensemble de ce travail de thèse, mené au cours de ces trois dernières années apporte une contribution significative dans notre connaissance sur la résistance de *P. falciparum* à l'artémisinine par une approche originale combinant santé publique, technique et recherche fondamentale.

Approche santé publique. Le travail réalisé en Érythrée montre l'émergence locale de cas de paludisme à *P. falciparum* résistant à l'artémisinine. En effet, nous avons constaté que le nombre d'échecs thérapeutique, caractérisé par le nombre de patients positifs à *P. falciparum* à J+3 post traitement TCA, était en augmentation, passant de 0,4% en 2016 à 4,2% en 2019. Une augmentation du nombre de patients porteur de parasites possédant la mutation *Pfkelch13-R622I* a également été constatée, passant de 8,6% en 2016 à 21% en 2019. Nous avons pu ensuite confirmer *in vitro* que cette mutation était capable de conférer une résistance partielle à l'artémisinine, dans une moindre mesure cependant que la mutation *Pfkelch13-C580Y* présente chez les souches en Asie du Sud-Est (Straimer *et al.*, 2015). Cette observation est conforme à une précédente étude révélant que le génotype *Pfkelch13* entraîne une variation significative du taux de survie des parasites résistants à l'artémisinine (Stokes *et al.*, 2021).

Une seconde découverte importante a porté sur la proportion importante (16,9%) de parasites possédant des délétions dans les gènes *Pfhrp2* et *Pfhrp3* en plus de la mutation *Pfkelch13-R6221*. Les protéines HRP2 et HRP3 du parasite sont utilisées comme biomarqueurs dans les tests de diagnostic rapide réalisés sur le terrain pour le dépistage du paludisme. Ces mutants HRP2/HRP3 étant indétectables par ces tests, il est possible que le nombre de cas de paludisme soient actuellement sous-estimé en Érythrée, dû à des faux négatifs. Nos données suggèrent donc que des souches résistantes à l'artémisinine et difficilement détectable par les tests de diagnostic rapides circulent actuellement dans la Corne de l'Afrique.

Il est possible que l'émergence de ces souches soit dû à une combinaison de facteurs. En effet, les stratégies de lutte anti-vectorielle et de prise en charge des patients en Érythrée ont permis une diminution importante de la morbidité et de la mortalité des cas de paludisme au cours de la dernière décennie. En conséquence, la diminution de la prévalence de *P. falciparum* a pu entraîner une diminution de l'immunité acquise dans la population, et un plus grand recours aux antipaludiques par la population, favorisant ainsi l'émergence de résistances (Scott *et al.*, 2018).

La principale inquiétude que soulève ce travail est le fort risque de diffusion de ces parasites résistants dans les pays voisins, ce qui aurait des conséquences catastrophiques sur les populations.

Il est donc prioritaire de mener une surveillance génomique renforcée dans les zones de pré élimination où les stratégies de luttes antipaludiques sont largement implémentées. La surveillance de la résistance à la drogue partenaire utilisée dans les TCA doit également être renforcée. Ce travail décrit pour la première fois l'émergence de la résistance à l'artémisinine en Afrique de l'Est. Nos résultats s'inscrivent dans un contexte d'émergence à l'échelle du continent africain entier, où la résistance à l'artémisinine a également été rapportée en Ouganda (Balikagala *et al.*, 2021) et au Rwanda (Uwimana *et al.*, 2020).

Approche technique. L'approche technique au cours de cette thèse s'est focalisée sur l'optimisation du test RSA. Le RSA reste à ce jour la technique de référence pour la détection de la résistance à l'artémisinine chez *P. falciparum* (Witkowski *et al.*, 2013). Cette technique possède toutefois certaines limites, car il s'agit d'un protocole long et laborieux, nécessitant l'utilisation de stades rings 0-3h finement synchronisés. Cela exige de connaître précisément la durée du cycle sanguin de la souche testée, qui peut varier entre 36 à 54 heures (Smith *et al.*, 2020 ; Wockner *et al.*, 2020). Ces variations de temps de croissance d'origine génétique rendent difficile l'application du test RSA quand plusieurs souches sont simultanément testées.
Nous avons ainsi pu optimiser le test RSA en incorporant une étape supplémentaire utilisant l'inhibiteur de kinase ML10 (Ressurreiçao *et al.*, 2020). Ce composé entraîne une inhibition réversible de l'éclosion des schizontes et permet donc après plusieurs lavages, d'obtenir un maximum de schizontes matures de souches présentant des fonds génétiques différents. Nos données présentées indiquent que les concentrations de ML10 utilisées, allant de 50 à 200 nM, n'ont pas d'effet cytotoxique notable. Ainsi, l'utilisation d'une seule dose de ML10 permet un enrichissement significatif en schizontes chez toutes les souches testées, d'un facteur 3 à 16, indépendamment de la concentration de ML10 utilisée. Nos données montrent qu'une exposition à 200 nM de ML10 pendant 17h à 20h permet d'obtenir une proportion maximum de schizontes viables. Enfin, l'incorporation du ML10 dans le protocole RSA n'a pas eu d'effet significatif sur les taux de survie des parasites *Pfkelch13-WT* (DHA sensible) et *Pfkelch13-C580Y* (DHA résistant), indiquant que le ML10 peut être ajouté à la procédure sans crainte d'impacter le résultat final. Dans le cadre de cette thèse, ce nouveau protocole a été largement mis en pratique avec succès.

Approche recherche fondamentale. L'approche fondamentale de la thèse s'est principalement concentrée sur l'étude de la dormance induite par les drogues (DID) et la résistance à l'artémisinine des stades ring de *P. falciparum*, d'un point de vue métabolomiques, signalétiques et transcriptomiques.

L'analyse du profil métabolique des stades ring en dormance a été réalisée par une approche métabolomique non ciblée en spectrométrie de masse. L'ensemble de ces travaux ont été menés sur des souches 3D7 éditées par la technique CRISPR-Cas9 (Ghorbal *et al.*, 2014), permettant d'obtenir les génotypes *Pfkelch13-WT* (DHA sensible), *Pfkelch13-C580Y* et *Pfkelch13-Y493H* (DHA résistante).

Le principal défi technique abordé dans ce travail a été de mettre au point une méthode permettant de supprimer le bruit de fond généré par les globules rouges non infectés tout en isolant les stades rings viables. Cette technique associait une lyse à la Streptolysine-O (SLO) des globules rouges non infectés suivie d'une purification des cellules infectées par centrifugation différentielle en gradient de Percoll. Après validation, cette technique baptisée SLOPE (Streptolysine-O et Percoll) a été mise en pratique pour enrichir les échantillons en stade rings pour une application en spectrométrie de masse.

L'hypothèse de départ était que, durant une exposition à la DHA, les parasites porteurs de mutations *Pfkelch13* conférant une résistance à l'artémisinine avaient un profil métabolique différent de celui des parasites sauvages. Les parasites en dormance ont été obtenus en incubant les stades rings 0-3h avec une dose de DHA (700 nM) pendant 6h, considérant que la culture était constituée d'un mélange de parasites morts et de rings dormants après l'exposition.

Nos données nous ont indiqué que les parasites dormants issus des souches résistantes (*Pfkelch13-C580Y* et *Pfkelch13-Y493H*) subissaient des changements métaboliques importants durant l'exposition à la DHA. Ainsi, le métabolisme énergétique basé sur la glycolyse et le cycle de Krebs s'orientait vers un métabolisme basé sur le catabolisme des acides aminés comme source d'énergie. En effet, l'α-cetoglutarate, métabolite à l'interface entre les voies métaboliques des acides aminés (acide glutamique notamment) et le cycle de Krebs, était significativement enrichi chez les rings traités à la DHA. La diminution de la glycolyse et l'enrichissement en α-cetoglutarate suggéraient que les parasites traités à la DHA catabolisent activement les acides aminés pour la production d'énergie. Ces données étaient cohérentes avec de précédentes études montrant que *P. falciparum* est capable d'utiliser les sucres et les acides aminés comme substrat énergétique (Kumar *et al.*, 2020).

Le glutathion était également significativement plus abondant chez les rings en dormance après une exposition à la DHA. Le glutathion est en effet un métabolite antioxydant impliqué dans la réponse au stress oxydatif durant l'exposition à la DHA de souches résistantes de *P. falciparum* (Siddiqui *et al.*, 2017). Nos données suggéraient que le parasite dormant produit activement du glutathion, possiblement pour se protéger de l'effet oxydant des radicaux libres induit par l'activation de la DHA.

Phénotypiquement, les rings exposés à la DHA présentaient une progression dans le cycle asexué

ralentie, avec un allongement d'environ 6h du stade ring, données cohérentes avec un métabolisme énergétique ralenti et une inhibition du catabolisme de l'hémoglobine (Cobbold *et al.*, 2016). Ce ralentissement du métabolisme énergétique associé au rallongement du stade ring semblent permettre au parasite d'échapper à la toxicité de la DHA, du fait du temps de demi-vie court de la drogue, et de la faible activation de la DHA liée à l'inhibition du catabolisme de l'hémoglobine.
Ces résultats apparaissent cohérents avec d'autres résultats mettant en évidence une surexpression de EXP1, transporteur impliqué dans l'importation d'acides aminés depuis le sérum de l'hôte chez les parasites résistants *Pfkelch13* mutés (Mesen-Ramirez *et al.*, 2021). Il apparaît donc intéressant d'explorer en détail le rôle de EXP1 dans l'importation d'acides aminés chez le ring dormant, afin d'en faire une cible thérapeutique potentielle. Ainsi, l'ensemble de ces données permet d'établir le profil métabolique des stades ring en dormance et de comprendre comment cette adaptation permet aux mutants résistants *Pfkelch13* de *P. falciparum* de survivre à l'artémisinine par un métabolisme énergétique alternatif.

Les mécanismes d'induction de la dormance ont également été abordés durant cette thèse par notre travail sur la communication entre les parasites. En effet, nous souhaitions explorer une possible relation entre dormance induite et signaux extracellulaires de l'environnement où évolue le stade ring. En effet, de nombreuses publications ont montré que *P. falciparum* était capable d'émettre et de recevoir des signaux extracellulaires. On peut citer, à titre d'exemple, l'implication du lysophosphatidylcholine, molécule de l'hôte et sa capacité à provoquer la différenciation de stades asexués en stades sexués (gamétocyte) (Carter et Miller, 1979 ; Brancucci *et al.*, 2017). D'autres études ont également mis en évidence le rôle des vésicules extracellulaires émises par le parasite dans le milieu extracellulaire, et leur capacité à manipuler la réponse immunitaire de l'hôte (Regev-Rudzki *et al.*, 2013 ; Mantel *et al.*, 2013 ; Sampaio *et al.*, 2018 ; Mbagwu *et al.*, 2019). Enfin, des travaux ont suggéré que *P. falciparum* était capable de réguler sa population par quorum sensing, en induisant l'apoptose lorsque la parasitémie *in vitro* est trop élevée (Mutai *et al.*, 2010 ; Chou *et al.*, 2018). De plus, concernant la dormance induite, il a été mis en évidence que des phytohormones étaient capables de provoquer le réveil des parasites dormants après traitement à la DHA (Duvalsaint et Kyle, 2018).
Basé sur ces données, notre hypothèse de départ était donc que la DID est un mécanisme potentiellement induit par des signaux extracellulaires. Pour tester cette hypothèse, nous avons mis au point un protocole *in vitro* permettant de produire de manière reproductible un environnement extracellulaire défavorable. Succinctement, des parasites de la souche NF54 ont été exposés pendant 20h à 200 nM de chloroquine afin d'induire un stress cellulaire et la mort des parasites. Le

surnageant de culture stressée (SCS) a été recueilli et utilisé pour exposer des jeunes rings 0-3h de souches résistantes à la chloroquine. L'objectif ici était de tester si le SCS contenait des facteurs ou des molécules solubles capable d'induire la dormance des parasites exposés et/ou de modifier le taux de survie des parasites possédant différents génotypes *Pfkelch13* après traitement à l'artémisinine.

Les données que nous avons pu obtenir montraient qu'un traitement de 24h avec le SCS induisait un arrêt de croissance réversible de l'ordre de 24h chez toutes les souches testées. Ces observations ont pu être reproduites avec des souches sensibles (*Pfkelch13-WT*) et résistantes (*Pfkelch13-C580Y*) à la DHA. Ces données laissent supposer que le parasite est capable de bloquer de manière réversible sa progression dans le cycle asexué en absence de DHA, et indépendamment du génotype *Pfkelch13*.

Dans la mesure où la majorité des parasites exposés au SCS pendant 24h était au stade ring, nous avons pu en déduire que la dégradation de l'hémoglobine était ralentie durant cet arrêt de croissance temporaire. Pour faire le lien entre l'arrêt de croissance temporaire après exposition au SCS et la résistance à l'artémisinine, nous avons prétraités des stades rings 0-3h pendant 30 min au SCS suivi d'une exposition à la DHA (700 nM) pendant 6h. Le taux de survie des parasites mesuré par RSA était significativement plus élevé chez les parasites prétraités au SCS pour toutes les souches testées, suggérant que cette augmentation de survie après exposition à la DHA était causée par un arrêt de croissance temporaire induit par des facteurs ou molécules solubles présents dans le SCS.

Pour confirmer cette hypothèse, nous avons exposé des rings 0-3h à des dilutions de SCS pendant 30 min puis avec une dose de 700 nM de DHA pendant 6h. Nous avons constaté qu'une dilution du SCS au 1/2 suffisait à ramener le taux de survie RSA au taux initial observé chez toutes les souches testées en condition RPMI (sans incubation préalable avec le SCS). Ceci indiquait que l'augmentation de la survie était bien associée à des facteurs extracellulaires relargués par les parasites morts, et qu'une concentration seuil de ces facteurs était nécessaire pour produire un arrêt de croissance et une capacité augmentée à survivre en présence de DHA.

Pour caractériser ces facteurs extracellulaires ou molécules solubles, nous avons ensuite cherché à définir leurs tailles moléculaires. Le SCS a donc été filtré sur filtre Centricon®, permettant d'exclure les molécules de tailles supérieures à 100 kDa, 30 kDa, 10 kDa et 3 kDa. Suivant le même protocole, nous avons observé que l'ensemble des SCS filtrés induisaient une augmentation significative du taux de survie par rapport aux parasites non traités. Cependant, nous avons constaté que les parasites traités avec les filtrats < 10 kDa et < 3 kDa avaient une survie significativement plus faible que les parasites traités avec le SCS non filtré ou les filtrats < 100 kDa et < 30 kDa, suggérant que la dormance était principalement induite par un groupe de molécules de taille inférieure à 30 kDa. Enfin, nous avons pu mesurer une augmentation significative du taux de survie

des rings 0-3h sensibles (*Pfkelch13-WT*) et résistants (*Pfkelch13-C580Y*) à l'artémisinine après prétraitement au SCS^{3kDa} (filtré par < 3kDa), suggérant que la dormance serait un mécanisme indépendant des mutations *Pfkelch13*. Collectivement, nos données soutiennent l'idée que la dormance serait un mécanisme de survie innée chez *P. falciparum* et indépendant de *Pfkelch13*. La dormance serait induite par des facteurs ou des molécules solubles extracellulaires inférieurs à 30 kDa, de nature et de concentration actuellement inconnue. Pour déterminer la nature de ces facteurs, nous envisageons d'analyser le métabolome par une approche non ciblée en spectrométrie de masse sur des échantillons des différents filtrats de SCS.

Même si la caractérisation des facteurs ou molécules contenus dans le SCS est en cours d'investigation, nos données permettent cependant d'exclure certaines hypothèses. En effet, le SCS ne peut pas contenir de vésicules extracellulaires dans notre approche expérimentale. Les filtres 100 kDa, 30 kDa, 10 kDa et 3 kDa permettent le passage d'éléments inférieurs à 10 nm, 3 nm, 1 nm et 0,3 nm respectivement, tandis que les vésicules extracellulaires ont une taille variant de 30 à 500 nm (Sharon et Rudzki, 2021). L'induction de la dormance est donc nécessairement dépendante de petites molécules diffusibles. Des données chez *Trypanosoma* indiquent que des polypeptides extracellulaires servent à la communication entre les parasites notamment dans le choix de leur différenciation (Rojas *et al.*, 2019). Il serait donc intéressant d'explorer cette piste chez *P. falciparum*. On peut également éliminer une possible implication de la chloroquine contenue dans le SCS qui aurait pu fausser nos résultats. Tout d'abord, nous avons traité des rings 0-3h avec le SCS pendant 30 min, or, la chloroquine n'est uniquement active que sur les stades matures, par l'inhibition de la cristallisation de l'hème (Slater et Cerami, 1992 ; Sullivan *et al.*, 2017). Il est donc peu probable que la chloroquine ait pu induire un stress chez les stades rings 0-3h. De plus, les souches exposées au SCS sont hautement résistantes à la chloroquine (allèle CVIET au sein du gène *Pfcrt*). Il est donc raisonnable de considérer que nos observations soient bien dues à des facteurs ou des molécules solubles contenus dans le SCS.

Nos données suggèrent donc que la dormance et la résistance à l'artémisinine médiée par les mutations *Pfkelch13* sont deux mécanismes différents. Le dénominateur commun entre la dormance et la résistance à l'artémisinine conférée par les mutations *Pfkelch13* est la dégradation de l'hémoglobine, caractéristique de la progression dans le cycle asexué du parasite. Dans le cas de parasites mutants *Pfkelch13*, l'augmentation de la survie est due à une diminution de l'endocytose de l'hémoglobine, et une diminution de l'activation de l'artémisinine (Klonis *et al.*, 2011 ; Wang *et al.*, 2015 ; Birnbaum *et al.*, 2020). Dans le cas de la dormance, l'arrêt de croissance temporaire induit par le SCS seul suppose que le stade ring est capable de bloquer le catabolisme de l'hémoglobine, indépendamment du génotype *Pfkelch13* et de la présence d'artémisinine. En conclusion, nous

pouvons émettre l'hypothèse de l'existence de deux mécanismes distincts permettant aux stades ring de survivre à une exposition à la DHA : d'une part, par la capacité des rings à stopper leur progression vers le stade mature, c'est-à-dire en relation avec à une dormance innée présente chez tous les parasites mais dont l'induction est dépendante de la concentration en facteur ou molécules solubles d'un milieu extracellulaire défavorable ; et de l'autre part du fait de la présence de mutations *Pfkelch13*, entraînant une instabilité et un turnover augmentée de la protéine K13 et par la même une diminution de la capacité d'endocytose de l'hémoglobine et de l'activation de la DHA. Ces deux mécanismes semblent donc distincts mais complémentaires, pour augmenter la capacité de survie des stades rings après exposition à la DHA.

La dormance semble être une réponse universelle face à un stress environnemental. D'autres études ont également décrit des arrêts de croissance temporaires de *P. falciparum* dans différents contextes comme la privation d'acides aminés (Babbitt *et al.*, 2012) ou en présence d'antipaludiques comme l'atovaquone et le proguanil (Thapar *et al.*, 2005).

En prenant en compte ces études et nos résultats, il apparaît que le concept de DID (dormance induite par les drogues) est réducteur, dans la mesure où la dormance est une stratégie de réponse face à une situation stressante au sens large (incluant les antipaludiques). La "dormance induite par le stress" (DIS) semble un terme plus approprié. Reste maintenant à caractériser les facteurs ou molécules solubles présentes dans le milieu extracellulaire et médiant la cascade de signalisation impliquée dans l'induction de la dormance. Le travail que nous avons mené sur l'induction de la dormance par le SCS peut donc servir de base à de futures recherches sur le 'quorum quenching', c'est-à-dire la capacité à perturber la communication entre les parasites, avec pour application l'inhibition de l'induction de la dormance des stades rings.

Pour terminer, l'exploration du transcriptome du stade ring à l'échelle de la cellule a pu être réalisée durant la thèse. L'analyse des données obtenues n'en est encore qu'à un stade préliminaire, elle nous suggère cependant l'importance de la diversité transcriptionnelle observée chez le stade ring 1-4h des souches 3D7 *Pfkelch13-WT* et 3D7 *Pfkelch13-C580Y* de *P. falciparum*. Au total, 9 sous-populations distinctes ont pu être détectées par notre approche. Les sous-populations 1 à 7 et 9 sont communes aux deux souches testées alors que la sous-population 8 est spécifique à la souche mutée 3D7 *Pfkelch13-C580Y.* Cela semble indiquer que la présence de la mutation *Pfkelch13-C580Y* induit un profil d'expression spécifique d'une partie des stades rings 1-4h. Nous avons également observé que l'exposition des stades ring au SCS provoque des changements transcriptionnels notables, avec un enrichissement des sous-populations 8 et 9, suggérant qu'un environnement extracellulaire défavorable est susceptible de médier une réponse transcriptionnelle

chez le stade ring 1-4h spécifique. Deux réponses transcriptionnelles après exposition au SCS semblent se dégager de nos données, avec une réponse spécifique de la souche mutée 3D7 *Pfkelch13-C580Y* avec l'enrichissement de la sous-population 8 ; et une réponse indépendante du génotype *Pfkelch13*, avec l'enrichissement de la sous-population 9, communes aux deux souches testées.

L'hétérogénéité du transcriptome des rings observé, notamment en condition physiologique, suppose que ce stade est vraisemblablement un carrefour de différenciation de *P. falciparum*. Les changements transcriptionnels observés chez les rings 1-4h incubés avec le SCS concordent avec les résultats d'une précédente étude rapportant des changements importants du transcriptome de parasites en état de stress *in vivo* chez les patients (Daily *et al.*, 2007). De plus, nous savons qu'un environnement extracellulaire dense en parasite entraîne chez *P. falciparum* l'induction de l'apoptose et des changements de profils d'expressions (Mutai *et al.*, 2010 ; Chou *et al.*, 2018). Ces travaux sont donc cohérents avec nos observations et semblent confirmer que le stade ring 1-4h est capable d'intégrer des signaux de son environnement et d'adapter ses profils d'expressions. L'ensemble de ces données nous permet de supposer que les parasites de la sous-population 9 correspondent à des parasites en arrêt de croissance puisque l'exposition au SCS induit un phénotype d'arrêt de croissance temporaire des stades ring de *P. falciparum*, indépendamment du génotype *Pfkelch13*, et que cette sous-population est enrichie de manière significative après exposition au SCS. On peut donc formuler l'hypothèse que la sous-population 9 serait constituée de rings dormants, et serait enrichie après exposition à un stress. Pour démontrer cette hypothèse, la purification spécifique des cellules de la sous-population 9 et leur mise en culture est nécessaire afin d'évaluer leur progression dans le cycle asexué. Des analyses supplémentaires sur les biomarqueurs spécifiques des sous-populations détectées sont en cours.

Conclusion générale.

En conclusion de cette thèse, l'étude de la résistance de *P. falciparum* à l'artémisinine a été abordée par des approches transversales associant santé publique, diagnostic et recherche fondamentale visant à explorer la biologie cellulaire du parasite au niveau métabolique, signalétique et transcriptionnel.

Il en ressort que le stade ring de *P. falciparum* apparaît comme une cellule particulièrement plastique tant sous les aspects phénotypiques (arrêt temporaire de croissance), métaboliques (alternance entre métabolisme des sucres ou des acides aminés pour la production d'énergie) et transcriptomiques (hétérogénéité des transcrits parmi une population phénotypiquement homogène). Le stade ring a donc un haut potentiel de résilience et d'adaptation aux différentes conditions

auxquelles le parasite est confronté, notamment sa capacité à ‘sentir’ l’environnement et à détecter les signaux de stress dans le milieu extracellulaire. Les données produites nous ont donc permis de mieux caractériser la dormance du stade ring comme une stratégie de survie innée chez *P. falciparum*, indépendante mais complémentaire de la résistance à l'artémisinine conférée par les mutations *Pfkelch13*. L'induction de la dormance par des facteurs extracellulaires de nature et de concentration inconnues nécessite maintenant d’être explorée plus en détail.

Bilan personnel de la thèse

Je suis dans l'ensemble, satisfait d'avoir pu réaliser cette thèse "hybride", abordant sous trois approches différentes une même problématique. Ces travaux, le suivi par mon directeur de thèse, l'école doctorale et mon comité attitré m'ont permis d'acquérir de nouvelles compétences, d'avoir un recul critique sur mon travail et le monde de la recherche en général. De plus, j'ai beaucoup appris sur la vie du chercheur, avec la méthodologie de rédaction des publications, des projets, et sur la manière de présenter les résultats. Je suis satisfait d'avoir pu terminer ce travail malgré un contexte difficile dû au COVID-19, mais aussi aux déménagements de l'équipe dans les locaux de Pasteur, aux lourdeurs administratives et finalement à la dissolution de l'unité. Je ne regrette cependant rien, j'estime que tout ceci fait partie du jeu, et je suis heureux d'avoir pu apporter ma contribution à la recherche sur un pathogène d'intérêt mondial tel que *P. falciparum*.

Références bibliographiques

- Ressources numériques :
- https://www.who.int/teams/global-malaria-programme/reports/world-malaria-report-2022
- https://plasmodb.org/plasmo/app
- https://www.malariacellatlas.org/
- https://malariaatlas.org/fr/

- Articles & revues (Par ordre d'apparition dans le texte)

1. Laveran, C. L. A., Kean, B. H., Mott, K. E. & Russell, A. J. A Newly Discovered Parasite in the Blood of Patients Suffering from Malaria. Parasitic Etiology of Attacks of Malaria. *Reviews of Infectious Diseases* **4**, 908–911 (1982).

2. Gardner, M. J. *et al.* Genome sequence of the human malaria parasite *Plasmodium falciparum*. *Nature* **419**, 498–511 (2002).

3. Rosenberg, R., Wirtz, R. A., Schneider, I. & Burge, R. An estimation of the number of malaria sporozoites ejected by a feeding mosquito. *Transactions of the Royal Society of Tropical Medicine and Hygiene* **84**, 209–212 (1990).

4. Mazier, D. *et al.* Complete Development of Hepatic Stages of *Plasmodium falciparum in Vitro*. *Science* **227**, 440–442 (1985).

5. Trager, W. & Bradbury, P. C. The Fine Structure of *Plasmodium falciparum* and its Host Erythrocytes in Natural Malarial Infections in Man.

6. Raventos-Suarez, C., Kaul, D. K., Macaluso, F. & Nagel, R. L. Membrane knobs are required for the microcirculatory obstruction induced by *Plasmodium falciparum*-infected erythrocytes. *Proc. Natl. Acad. Sci. U.S.A.* **82**, 3829–3833 (1985).

7. Lanzer, M., Wickert, H., Krohne, G., Vincensini, L. & Braun Breton, C. Maurer's clefts: A novel multi-functional organelle in the cytoplasm of *Plasmodium falciparum*-infected erythrocytes. *International Journal for Parasitology* **36**, 23–36 (2006).

8. Moore, L. R. *et al.* Hemoglobin degradation in malaria-infected erythrocytes determined from live cell magnetophoresis. *FASEB j.* **20**, 747–749 (2006).

9. Rosenthal, P. Hemoglobin catabolism and iron utilization by malaria parasites. *Molecular and Biochemical Parasitology* **83**, 131–139 (1996).

10. Pagola, S., Stephens, P. W., Bohle, D. S., Kosar, A. D. & Madsen, S. K. The structure of malaria pigment $_{NL}$-haematin. **404**, (2000).

11. Trager, W. & Jensen, J. B. Human Malaria Parasites in Continuous Culture. *Science* **193**, 673–675 (1976).

12. Bruce, M. C., Alano, P., Duthie, S. & Carter, R. Commitment of the malaria parasite *Plasmodium falciparum* to sexual and asexual development. *Parasitology* **100**, 191–200 (1990).

13. Maier, A. G., Matuschewski, K., Zhang, M. & Rug, M. *Plasmodium falciparum*. *Trends in Parasitology* **35**, 481–482 (2019).

14. Beier, J. C. Malaria parasite development in mosquitoes. *Annu. Rev. Entomol.* **43**, 519–543 (1998).

15. Kappe, S. H. I. *et al.* Exploring the transcriptome of the malaria sporozoite stage. *Proc. Natl. Acad. Sci. U.S.A.* **98**, 9895–9900 (2001).

16. Young, J. A. *et al.* The *Plasmodium falciparum* sexual development transcriptome: A microarray analysis using ontology-based pattern identification. *Molecular and Biochemical Parasitology* **143**, 67–79 (2005).

17. Smith, L. M. *et al.* An intrinsic oscillator drives the blood stage cycle of the malaria parasite *Plasmodium falciparum*. *Science* **368**, 754–759 (2020).

18. World malaria report 2022. (2022).

19. Sinka, M. E. *et al.* A global map of dominant malaria vectors. *Parasites Vectors* **5**, 69 (2012).

20. Coulibaly, D. *et al.* Spatio-temporal analysis of malaria within a transmission season in Bandiagara, Mali. *Malar J* **12**, 82 (2013).

21. Christiansen-Jucht, C., Parham, P. E., Saddler, A., Koella, J. C. & Basáñez, M.-G. Temperature during larval development and adult maintenance influences the survival of *Anopheles gambiae* s.s. (2014).

22. Ménard, D. *et al.* A Worldwide Map of *Plasmodium falciparum* K13-Propeller Polymorphisms. *N Engl J Med* **374**, 2453–2464 (2016).

23. Gething, P. W. *et al.* Climate change and the global malaria recession. *Nature* **465**, 342–345 (2010).

24. Joshi, Y. K., Tandon, B. N., Acharya, S. K., Babu, S. & Tandon, M. Acute hepatic failure due to *Plasmodium falciparum* liver injury. *Liver* **6**, 357–360 (2008).

25. Kochar, D. K. *et al.* Hepatocyte dysfunction and hepatic encephalopathy in *Plasmodium falciparum* malaria. *QJM* **96**, 505–512 (2003).

26. Parroche, P. *et al.* Malaria hemozoin is immunologically inert but radically enhances innate responses by presenting malaria DNA to Toll-like receptor 9. *Proc. Natl. Acad. Sci. U.S.A.* **104**, 1919–1924 (2007).

27. Dostert, C. *et al.* Malarial Hemozoin Is a Nalp3 Inflammasome Activating Danger Signal. *PLoS ONE* **4**, e6510 (2009).

28. Idro, R., Jenkins, N. E. & Newton, C. R. Pathogenesis, clinical features, and neurological outcome of cerebral malaria. *The Lancet Neurology* **4**, 827–840 (2005).

29. White, M. & Watson, J. Age, exposure and immunity. *eLife* **7**, e40150 (2018).

30. Rodriguez-Barraquer, I. *et al.* Quantification of anti-parasite and anti- disease immunity to malaria as a function of age and exposure.

31. Alebie, G., Urga, B. & Worku, A. Systematic review on traditional medicinal plants used for the treatment of malaria in Ethiopia: trends and perspectives. *Malar J* **16**, 307 (2017).

32. Cock, I. E., Selesho, M. I. & van Vuuren, S. F. A review of the traditional use of southern African medicinal plants for the treatment of malaria. *Journal of Ethnopharmacology* **245**, 112176 (2019).

33. Slater, A. F. G. & Cerami, A. Inhibition by chloroquine of a novel haem polymerase enzyme activity in malaria trophozoites. *Nature* **355**, 167–169 (1992).

34. Combrinck, J. M. *et al.* Insights into the Role of Heme in the Mechanism of Action of Antimalarials. *ACS Chem. Biol.* **8**, 133–137 (2013).

35. Olafson, K. N., Ketchum, M. A., Rimer, J. D. & Vekilov, P. G. Mechanisms of hematin crystallization and inhibition by the antimalarial drug chloroquine. *Proc. Natl. Acad. Sci. U.S.A.* **112**, 4946–4951 (2015).

36. Sullivan, D. J. Quinolines block every step of malaria heme crystal growth. *Proc. Natl. Acad. Sci. U.S.A.* **114**, 7483–7485 (2017).

37. Costa, E. A. *et al.* New Insights into the Mechanism of Action of the Drug Chloroquine: Direct Interaction with DNA and Cytotoxicity. *J. Phys. Chem. B* **126**, 3512–3521 (2022).

38. Camarda, G. *et al.* Antimalarial activity of primaquine operates via a two-step biochemical relay. *Nat Commun* **10**, 3226 (2019).

39. Peters, P. J., Thigpen, M. C., Parise, M. E. & Newman, R. D. Safety and Toxicity of Sulfadoxine/Pyrimethamine: Implications for Malaria Prevention in Pregnancy using Intermittent Preventive Treatment. *Drug Safety* **30**, 481–501 (2007).

40. Peterson, D. S., Walliker, D. & Wellems, T. E. Evidence that a point mutation in dihydrofolate reductase-thymidylate synthase confers resistance to pyrimethamine in *falciparum* malaria. *Proc. Natl. Acad. Sci. U.S.A.* **85**, 9114–9118 (1988).

41. Basco, L. K., de Pécoulas, P. E., Wilson, C. M., Le Bras, J. & Mazabraud, A. Point mutations in the dihydrofolate reductase-thymidylate synthase gene and pyrimethamine and cycloguanil resistance in *Plasmodium falciparum*. *Molecular and Biochemical Parasitology* **69**, 135–138 (1995).

42. Mather, M. W. *et al.* Uncovering the Molecular Mode of Action of the Antimalarial Drug Atovaquone Using a Bacterial System. *Journal of Biological Chemistry* **280**, 27458–27465 (2005).

43. Wong, W. *et al.* Mefloquine targets the *Plasmodium falciparum* 80S ribosome to inhibit protein synthesis. *Nat Microbiol* **2**, 17031 (2017).

44. Sheridan, C. M., Garcia, V. E., Ahyong, V. & DeRisi, J. L. The *Plasmodium falciparum* cytoplasmic translation apparatus: a promising therapeutic target not yet exploited by clinically approved anti-malarials. *Malar J* **17**, 465 (2018).

45. White, N. J. & Nosten, F. Artemisinin-Based Combination Treatment of *Falciparum* Malaria. *The American Journal of Tropical Medicine and Hygiene* **77**, 181–192 (2007).

46. Ying-Zi, Y., Little, B. & Meshnick, S. R. Alkylation of proteins by artemisinin. *Biochemical Pharmacology* **48**, 569–573 (1994).

47. Klonis, N. *et al.* Artemisinin activity against *Plasmodium falciparum* requires hemoglobin uptake and digestion. *Proc. Natl. Acad. Sci. U.S.A.* **108**, 11405–11410 (2011).

48. Wang, J. *et al.* Haem-activated promiscuous targeting of artemisinin in *Plasmodium falciparum*. *Nat Commun* **6**, 10111 (2015).

49. Veiga, M. I. *et al.* Globally prevalent PfMDR1 mutations modulate *Plasmodium falciparum* susceptibility to artemisinin-based combination therapies. *Nat Commun* **7**, 11553 (2016).

50. Fidock, D. A. *et al.* Mutations in the *P. falciparum* Digestive Vacuole Transmembrane Protein PfCRT and Evidence for Their Role in Chloroquine Resistance. *Mol Cell* 6(4): 861–871. (2000).

51. Witkowski, B. *et al.* A surrogate marker of piperaquine-resistant *Plasmodium falciparum*

malaria: a phenotype–genotype association study. *The Lancet Infectious Diseases* **17**, 174–183 (2017).

52. Duru, V. *et al. Plasmodium falciparum* dihydroartemisinin-piperaquine failures in Cambodia are associated with mutant K13 parasites presenting high survival rates in novel piperaquine *in vitro* assays: retrospective and prospective investigations. *BMC Med* **13**, 305 (2015).

53. Ross, L. S. *et al.* Emerging Southeast Asian *PfCRT* mutations confer *Plasmodium falciparum* resistance to the first-line antimalarial piperaquine. *Nat Commun* **9**, 3314 (2018).

54. Dhingra, S. K., Small-Saunders, J. L., Ménard, D. & Fidock, D. A. *Plasmodium falciparum* resistance to piperaquine driven by *PfCRT*. *The Lancet Infectious Diseases* **19**, 1168–1169 (2019).

55. Wilson, C. M. ; Serrano A. E. ; Wasley A. ; Bogenschutz M. P. ; Shankar A. H. ; Wirth D. F. Amplification of a Gene Related to Mammalian *mdr* Genes in Drug-Resistant *Plasmodium falciparum*. *Science* **244**. (1989)

56. Price, R. N. *et al.* Mefloquine resistance in *Plasmodium falciparum* and increased *pfmdr1* gene copy number. *The Lancet* **364**, 438–447 (2004).

57. Srivastava, I. K., Morrisey, J. M., Darrouzet, E., Daldal, F. & Vaidya, A. B. Resistance mutations reveal the atovaquone-binding domain of cytochrome b in malaria parasites. *Mol Microbiol* **33**, 704–711 (1999).

58. Korsinczky, M. *et al.* Mutations in *Plasmodium falciparum* Cytochrome *b* That Are Associated with Atovaquone Resistance Are Located at a Putative Drug-Binding Site. *Antimicrob Agents Chemother* **44**, 2100–2108 (2000).

59. Fisher, N. *et al.* Cytochrome b Mutation Y268S Conferring Atovaquone Resistance Phenotype in Malaria Parasite Results in Reduced Parasite bc1 Catalytic Turnover and Protein Expression. *Journal of Biological Chemistry* **287**, 9731–9741 (2012).

60. Cowman, A. F., Morry, M. J., Biggs, B. A., Cross, G. A. & Foote, S. J. Amino acid changes linked to pyrimethamine resistance in the dihydrofolate reductase-thymidylate synthase gene of

Plasmodium falciparum. *Proc. Natl. Acad. Sci. U.S.A.* **85**, 9109–9113 (1988).

61. Wang, P. *et al.* Resistance to antifolates in *Plasmodium falciparum* monitored by sequence analysis of dihydropteroate synthetase and dihydrofolate reductase alleles in a large number of field samples of diverse origins. *Molecular and Biochemical Parasitology* **89**, 161–177 (1997).

62. Plowe, C. V. *et al.* Mutations in *Plasmodium falciparum* Dihydrofolate Reductase and Dihydropteroate Synthase and Epidemiologic Patterns of Pyrimethamine-Sulfadoxine Use and Resistance. *J INFECT DIS* **176**, 1590–1596 (1997).

63. Nzila, A. M. *et al.* Towards an Understanding of the Mechanism of Pyrimethamine-Sulfadoxine Resistance in *Plasmodium falciparum*: Genotyping of Dihydrofolate Reductase and Dihydropteroate Synthase of Kenyan Parasites. *Antimicrob Agents Chemother* **44**, 991–996 (2000).

64. Noedl, H. *et al.* Evidence of Artemisinin-Resistant Malaria in Western Cambodia. *N Engl J Med* **359**, 2619–2620 (2008).

65. Dondorp, A. M. *et al.* Artemisinin Resistance in *Plasmodium falciparum* Malaria. *N Engl J Med* **361**, 455–467 (2009).

66. Uwimana, A. *et al.* Emergence and clonal expansion of *in vitro* artemisinin-resistant *Plasmodium falciparum* kelch13 R561H mutant parasites in Rwanda. *Nat Med* **26**, 1602–1608 (2020).

67. Balikagala, B. *et al.* Evidence of Artemisinin-Resistant Malaria in Africa. *N Engl J Med* **385**, 1163–1171 (2021).

68. Ariey, F. *et al.* A molecular marker of artemisinin-resistant *Plasmodium falciparum* malaria. *Nature* **505**, 50–55 (2014).

69. Straimer, J. *et al.* K13-propeller mutations confer artemisinin resistance in *Plasmodium falciparum* clinical isolates. *Science* **347**, 428–431 (2015).

70. Witkowski, B. *et al.* Increased Tolerance to Artemisinin in *Plasmodium falciparum* Is Mediated

by a Quiescence Mechanism. *Antimicrob Agents Chemother* **54**, 1872–1877 (2010).

71. Witkowski, B. *et al.* Reduced Artemisinin Susceptibility of *Plasmodium falciparum* Ring Stages in Western Cambodia. *Antimicrob Agents Chemother* **57**, 914–923 (2013).

72. Tilley, L., Straimer, J., Gnädig, N. F., Ralph, S. A. & Fidock, D. A. Artemisinin Action and Resistance in *Plasmodium falciparum*. *Trends in Parasitology* **32**, 682–696 (2016).

73. Yang, T. *et al.* Decreased K13 Abundance Reduces Hemoglobin Catabolism and Proteotoxic Stress, Underpinning Artemisinin Resistance. *Cell Reports* **29**, 2917-2928.e5 (2019).

74. Birnbaum, J. *et al.* A Kelch13-defined endocytosis pathway mediates artemisinin resistance in malaria parasites. *Science* **367**, 51–59 (2020).

75. Ross, L. S. & Fidock, D. A. Elucidating Mechanisms of Drug-Resistant *Plasmodium falciparum*. *Cell Host & Microbe* **26**, 35–47 (2019).

76. Coppée, R., Jeffares, D. C., Miteva, M. A., Sabbagh, A. & Clain, J. Comparative structural and evolutionary analyses predict functional sites in the artemisinin resistance malaria protein K13. *Sci Rep* **9**, 10675 (2019).

77. Gnädig, N. F. *et al.* Insights into the intracellular localization, protein associations and artemisinin resistance properties of *Plasmodium falciparum* K13. *PLoS Pathog* **16**, e1008482 (2020).

78. Mok, S. *et al.* Artemisinin-resistant K13 mutations rewire *Plasmodium falciparum*'s intra-erythrocytic metabolic program to enhance survival. *Nat Commun* **12**, 530 (2021).

79. Iwagami, M. *et al.* Heterogeneous distribution of k13 mutations in *Plasmodium falciparum* in Laos. *Malar J* **17**, 483 (2018).

80. Witkowski, B. *et al.* Novel phenotypic assays for the detection of artemisinin-resistant *Plasmodium falciparum* malaria in Cambodia: in-vitro and *ex-vivo* drug-response studies. *The Lancet Infectious Diseases* **13**, 1043–1049 (2013).

81. Davis, S. Z. *et al.* The extended recovery ring-stage survival assay provides a superior association with patient clearance half-life and increases throughput. *Malar J* **19**, 54 (2020).

82. Amaratunga, C., Neal, A. T. & Fairhurst, R. M. Flow Cytometry-Based Analysis of Artemisinin-Resistant *Plasmodium falciparum* in the Ring-Stage Survival Assay. *Antimicrob Agents Chemother* **58**, 4938–4940 (2014).

83. Wockner, L. F. *et al.* Growth Rate of *Plasmodium falciparum*: Analysis of Parasite Growth Data from Malaria Volunteer Infection Studies. *The Journal of Infectious Diseases* jiz557 (2019) doi:10.1093/infdis/jiz557.

84. Teuscher, F. *et al.* Artemisinin-Induced Dormancy in *Plasmodium falciparum* : Duration, Recovery Rates, and Implications in Treatment Failure. *J INFECT DIS* **202**, 1362–1368 (2010).

85. Peatey, C. *et al.* Dormant *Plasmodium falciparum* Parasites in Human Infections Following Artesunate Therapy. *The Journal of Infectious Diseases* **223**, 1631–1638 (2021).

86. Bigger, J. W. Treatment of Staphylococcal infections with Penicillin by intermitent sterilisation. *The Lancet* 497-500 (1944).

87. Li, B. & Foley M. F. Genetic and molecular control of seed dormancy. *Trends in plant science* 2(10) 384-389 (1997).

88. Soltani, A. *et al.* The genetics and physiology of seed dormancy, a crucial trait in common bean domestication. *BMC Plant Biol* **21**, 58 (2021).

89. Cochrane, V. W. Dormancy in Spores of Fungi. *Transactions of the American Microscopical Society* **93**, 599 (1974).

90. Tommerup, I. C. Spore dormancy in vesicular-arbuscular mycorrhizal fungi. *Transactions of the British Mycological Society* **81**, 37–45 (1983).

91. Lewis, K. Persister Cells. *Annu. Rev. Microbiol.* **64**, 357–372 (2010).

92. Diniz, D. F. A., de Albuquerque, C. M. R., Oliva, L. O., de Melo-Santos, M. A. V. & Ayres, C. F. J. Diapause and quiescence: dormancy mechanisms that contribute to the geographical expansion of mosquitoes and their evolutionary success. *Parasites Vectors* **10**, 310 (2017).

93. Li, L. & Bhatia, R. Stem Cell Quiescence. *Clinical Cancer Research* **17**, 4936–4941 (2011).

94. Recasens, A. & Munoz, L. Targeting Cancer Cell Dormancy. *Trends in Pharmacological Sciences* **40**, 128–141 (2019).

95. Kaprelyants, A. S., Gottschal, J. C. & Kell, D. B. Dormancy in non-sporulating bacteria. *FEMS Microbiology Letters* **104**, 271–286 (1993).

96. Kim, S. B., Lyou, S. E., Kim, M. S., Lee, T. K. Bacterial Resuscitation from Starvation-Induced Dormancy Results in Phenotypic Diversity Coupled with Translational Activity Depending on Carbon Substrate Availability. *Microbial Ecology* (2022)

97. Née, G., Xiang, Y. & Soppe, W. J. The release of dormancy, a wake-up call for seeds to germinate. *Current Opinion in Plant Biology* **35**, 8–14 (2017).

98. Lemons, J. M. S. *et al.* Quiescent Fibroblasts Exhibit High Metabolic Activity. *PLoS Biol* **8**, e1000514 (2010).

99. Vega, N. M., Allison, K. R., Khalil, A. S. & Collins, J. J. Signaling-mediated bacterial persister formation. *Nat Chem Biol* **8**, 431–433 (2012).

100. Keroack, C. D. & Duraisingh, M. T. Molecular mechanisms of cellular quiescence in apicomplexan parasites. *Current Opinion in Microbiology* **70**, 102223 (2022).

101. Lyons, R. E., McLeod, R. & Roberts, C. W. Toxoplasma gondii tachyzoite–bradyzoite interconversion. *Trends in Parasitology* **18**, 198–201 (2002).

102. Krotoski, W. A. Discovery of the hypnozoite and a new theory of malarial relapse. *Transactions of the Royal Society of Tropical Medicine and Hygiene* **79**, 1–11 (1985).

103. Deye, G. A. *et al.* Use of a Rhesus *Plasmodium cynomolgi* Model to Screen for Anti-Hypnozoite Activity of Pharmaceutical Substances. *The American Journal of Tropical Medicine and Hygiene* **86**, 931–935 (2012).

104. Pasini, E. M. *et al.* An improved Plasmodium cynomolgi genome assembly reveals an unexpected methyltransferase gene expansion. *Wellcome Open Res* **2**, 42 (2017).

105. Habtewold, T. *et al. Plasmodium* oocysts respond with dormancy to crowding and nutritional stress. *Sci Rep* **11**, 3090 (2021).

106. Richter, J., Franken, G., Mehlhorn, H., Labisch, A. & Häussinger, D. What is the evidence for the existence of *Plasmodium ovale* hypnozoites? *Parasitol Res* **107**, 1285–1290 (2010).

107. LaCrue, A. N., Scheel, M., Kennedy, K., Kumar, N. & Kyle, D. E. Effects of Artesunate on Parasite Recrudescence and Dormancy in the Rodent Malaria Model *Plasmodium vinckei*. *PLoS ONE* **6**, e26689 (2011).

108. Nakazawa, S., Kanbara, H., Aikawa, M. *Plasmodium falciparum* : Recrudescence of parasite in culture. *Experimental Parasitology* **81**, 556-563 (1995).

109. Cheng, Q., Kyle, D. E. & Gatton, M. L. Artemisinin resistance in *Plasmodium falciparum*: A pocess linked to dormancy? *International Journal for Parasitology: Drugs and Drug Resistance* **2**, 249–255 (2012).

110. Grobler, L., Chavchich, M., Haynes, R. K., Edstein, M. D. & Grobler, A. F. Assessment of the Induction of Dormant Ring Stages in *Plasmodium falciparum* Parasites by Artemisone and Artemisone Entrapped in Pheroid Vesicles *In Vitro*. *Antimicrob Agents Chemother* **58**, 7579–7582 (2014).

111. Peatey, C. L. *et al.* Mitochondrial Membrane Potential in a Small Subset of Artemisinin-Induced Dormant *Plasmodium falciparum* Parasites *In Vitro*. *J Infect Dis.* **212**, 426–434 (2015).

112. Gray, K.-A. *et al.* Correlation between Cyclin Dependent Kinases and Artemisinin-Induced Dormancy in *Plasmodium falciparum* . *PLoS ONE* **11**, e0157906 (2016).

113. Holmes, M. J., Augusto, L. da S., Zhang, M., Wek, R. C. & Sullivan, W. J. Translational Control in the Latency of Apicomplexan Parasites. *Trends in Parasitology* **33**, 947–960 (2017).

114. Reyser, T. *et al.* Identification of compounds active against quiescent artemisinin-resistant *Plasmodium falciparum* parasites via the quiescent-stage survival assay (QSA). *Journal of Antimicrobial Chemotherapy* **75**, 2826–2834 (2020).

115. Connelly, S. V. *et al.* Restructured mitochondrial-nuclear interaction in *Plasmodium falciparum* dormancy and persister survival after artemisinin exposure. http://biorxiv.org/lookup/doi/10.1101/2020.09.28.314435 (2020) doi:10.1101/2020.09.28.314435.

116. Chen, N. *et al.* Fatty Acid Synthesis and Pyruvate Metabolism Pathways Remain Active in Dihydroartemisinin-Induced Dormant Ring Stages of *Plasmodium falciparum*. *Antimicrob Agents Chemother* **58**, 4773–4781 (2014).

117. Duvalsaint, M. & Kyle, D. E. Phytohormones, Isoprenoids, and Role of the Apicoplast in Recovery from Dihydroartemisinin-Induced Dormancy of *Plasmodium falciparum*. *Antimicrob Agents Chemother* **62**, e01771-17 (2018).

118. Babbitt, S. E. *et al. Plasmodium falciparum* responds to amino acid starvation by entering into a hibernatory state. *Proc. Natl. Acad. Sci. U.S.A.* **109**, (2012).

119. Andrade, C. M. *et al.* Increased circulation time of *Plasmodium falciparum* underlies persistent asymptomatic infection in the dry season. *Nat Med* **26**, 1929–1940 (2020).

120. Stuart, T. *et al.* Comprehensive Integration of Single-Cell Data. *Cell* **177**, 1888-1902.e21 (2019).

121. Crow, M., Paul, A., Ballouz, S., Huang, Z. J. & Gillis, J. Characterizing the replicability of cell types defined by single cell RNA-sequencing data using MetaNeighbor. *Nat Commun* **9**, 884 (2018).

122. Real, E. *et al.* A single-cell atlas of *Plasmodium falciparum* transmission through the mosquito. *Nat Commun* **12**, 3196 (2021).

123. Reid, A. J. *et al.* Single-cell RNA-seq reveals hidden transcriptional variation in malaria parasites. *eLife* **7**, e33105 (2018).

124. Howick, V. M. *et al.* The Malaria Cell Atlas: Single parasite transcriptomes across the complete *Plasmodium* life cycle. *Science* **365**, eaaw2619 (2019).

125. Lambros, C. & Vanderberg, J. P. Synchronization of *Plasmodium falciparum* Erythrocytic Stages in Culture. *The Journal of Parasitology* **65**, 418 (1979).

126. Philipp, S., Oberg, H.-H., Janssen, O., Leippe, M. & Gelhaus, C. Isolation of erythrocytes infected with viable early stages of *Plasmodium falciparum* by flow cytometry. *Cytometry* **81A**, 1048–1054 (2012).

127. Ressurreição, M. *et al.* Use of a highly specific kinase inhibitor for rapid, simple and precise synchronization of *Plasmodium falciparum* and *Plasmodium knowlesi* asexual stage parasites. http://biorxiv.org/lookup/doi/10.1101/2020.04.24.059493 (2020) doi:10.1101/2020.04.24.059493.

128. Daily, J. P. *et al.* Distinct physiological states of *Plasmodium falciparum* in malaria-infected patients. *Nature* **450**, 1091–1095 (2007).

129. Stokes, B. H. *et al. Plasmodium falciparum* K13 mutations in Africa and Asia impact artemisinin resistance and parasite fitness. *eLife* **10**, e66277 (2021).

130. Scott, N. *et al.* Implications of population-level immunity for the emergence of artemisinin-resistant malaria: a mathematical model. *Malar J* **17**, 279 (2018).

131. Ghorbal, M. *et al.* Genome editing in the human malaria parasite *Plasmodium falciparum* using the CRISPR-Cas9 system. *Nat Biotechnol* **32**, 819–821 (2014).

132. Kumar, M., Skillman, K. & Duraisingh, M. T. Linking nutrient sensing and gene expression in *Plasmodium falciparum* blood-stage parasites. *Mol Microbiol* **115**, 891–900 (2021).

133. Siddiqui, G., Srivastava, A., Russell, A. S. & Creek, D. J. Multi-omics Based Identification of Specific Biochemical Changes Associated With Pfkelch13-Mutant Artemisinin-Resistant

Plasmodium falciparum. *The Journal of Infectious Diseases* **215**, 1435–1444 (2017).

134. Cobbold, S. A. *et al.* Metabolic Dysregulation Induced in *Plasmodium falciparum* by Dihydroartemisinin and Other Front-Line Antimalarial Drugs. *J Infect Dis.* **213**, 276–286 (2016).

135. Mesén-Ramírez, P. *et al.* The parasitophorous vacuole nutrient channel is critical for drug access in malaria parasites and modulates the artemisinin resistance fitness cost. *Cell Host & Microbe* **29**, 1774-1787.e9 (2021).

136. Carter, R. & Miller, L. H. Evidence for environmental modulation of gametocytogenesis in *Plasmodium falciparum* in continuous culture. *Bulletin of the World Health Organization* **57**, 37-52 (1979)

137. Brancucci, N. M. B. *et al.* Lysophosphatidylcholine Regulates Sexual Stage Differentiation in the Human Malaria Parasite *Plasmodium falciparum*. *Cell* **171**, 1532-1544.e15 (2017).

138. Regev-Rudzki, N. *et al.* Cell-Cell Communication between Malaria-Infected Red Blood Cells via Exosome-like Vesicles. *Cell* **153**, 1120–1133 (2013).

139. Mantel, P.-Y. *et al.* Malaria-Infected Erythrocyte-Derived Microvesicles Mediate Cellular Communication within the Parasite Population and with the Host Immune System. *Cell Host & Microbe* **13**, 521–534 (2013).

140. Sampaio, N. G. *et al.* Extracellular vesicles from early stage *Plasmodium falciparum* infected red blood cells contain PfEMP1 and induce transcriptional changes in human monocytes. *Cellular Microbiology* **20**, e12822 (2018).

141. Mbagwu, S. I., Lannes, N., Walch, M., Filgueira, L. & Mantel, P.-Y. Human Microglia Respond to Malaria-Induced Extracellular Vesicles. *Pathogens* **9**, 21 (2019).

142. Mutai, B. K. & Waitumbi, J. N. Apoptosis stalks *Plasmodium falciparum* maintained in continuous culture condition. *Malar J* **9**, S6 (2010).

143. Chou, E. S. *et al.* A high parasite density environment induces transcriptional changes and cell

death in *Plasmodium falciparum* blood stages. *FEBS J* **285**, 848–870 (2018).

144. Sharon, M. & Regev-Rudzki, N. Cell communication and protein degradation: All in one parasitic package. *Journal of Extracellular Vesicles* **10**, (2021).

145. Rojas, F. *et al.* Oligopeptide Signaling through TbGPR89 Drives Trypanosome Quorum Sensing. *Cell* **176**, 306-317.e16 (2019).

146. Thapar, M. M., Gil, J. P. & Björkman, A. *In vitro* recrudescence of *Plasmodium falciparum* parasites suppressed to dormant state by atovaquone alone and in combination with proguanil. *Transactions of the Royal Society of Tropical Medicine and Hygiene* **99**, 62–70 (2005).